GEORGIA INSTITUTE OF TECHNOLOGY — OFFICE OF CONTRACT ADMINISTRATION

PROJECT ADMINISTRATION DATA SHEET

[x] ORIGINAL [ ] REVISION NO. _____

Project No. E-16-660 * DATE 12/11/81

Project Director: Dr. B. T. Zinn School/Lab Aerospace Engineering

Sponsor: Air Force Office of Scientific Research (AFOSR); Bolling AFB, D.C. 20332

Type Agreement: Contract F49620-82-C-0013

Award Period: From 11/27/81 To 9/30/~~82~~ 83 (Performance) _____ (Reports)

Sponsor Amount: $62,919 (E-16-660 only) ** Contracted through:

Cost Sharing: $13,705 (E-16-364) GTRI/~~GIT~~

Title: Investigation of Unsteady Burning Characteristics of Solid Propellants (TASK I)

ADMINISTRATIVE DATA

OCA Contact Leamon R. Scott

1) Sponsor Technical Contact:

AFOSR/NA
Director of Aerospace Sciences
Building 410
Bolling AFB, D.C. 20332
202-767-4937

2) Sponsor Admin/Contractual Matters:

ISAF. AFSC
Air Force Office of Scientific Research
Building 410
Bolling AFB, D.C. 20332
Buyer: C.R. Arnold/bls/PKD/202-767-4994

Defense Priority Rating: DOC-9

Security Classification: N/A

RESTRICTIONS

See Attached government Supplemental Information Sheet for Additional Requirements.

Travel: Foreign travel must have prior approval – Contact OCA in each case. Domestic travel requires sponsor approval where total will exceed greater of $500 or 125% of approved proposal budget category.

Equipment: Title vests with GIT. Authorization granted to acquire equipment required for performance and which have acquisition cost of less than $1K.

COMMENTS:

* Co-project with E-16-690/Hubbartt/Jagoda/Strahle; E-16-691/Price/Sigmon; and E-16-692/Strahle.

** Total Contract amount is $280,000.

COPIES TO:

Administrative Coordinator
Research Property Management
Accounting
Procurement/EES Supply Services
Research Security Services
~~Reports Coordinator~~ (OCA)
Legal Services (OCA)
Library
EES Public Relations (2)
Computer Input
Project File
Other _____

GEORGIA INSTITUTE OF TECHNOLOGY — OFFICE OF CONTRACT ADMINISTRATION

PROJECT ADMINISTRATION DATA SHEET

[x] ORIGINAL [ ] REVISION NO. _____

Project No. E-16-692* DATE 12/14/81

Project Director: W. C. Strahle School/Lab Aerospace Engineering

Sponsor: Air Force Office of Scientific Research (AFOSR); Bolling AFB, D.C. 20332

Type Agreement: Contract F49620-82-C-0013

Award Period: From 11/27/81 To 9/30/~~82~~ 83 (Performance) _____ (Reports)

Sponsor Amount: $36,949 (E-16-692 only) ** Contracted through:

Cost Sharing: $8,046 (E-16-367) GTRI/~~GTRC~~

Title: Rocket Motor Aeroacoustics (Task IV)

ADMINISTRATIVE DATA

OCA Contact Leamon R. Scott

1) Sponsor Technical Contact:

AFOSR/NA
Director of Aerospace Sciences
Building 410
Bolling AFB, D.C. 20332
202-767-4937

2) Sponsor Admin/Contractual Matters:

USAF, AFSC
AIR FORCE OFFICE OF SCIENTIFIC RESEARCH
BUILDING 410
BOLLING AFB, D.C. 20332
Buyer; C.R. Arnold/b1s/PKD/202-767-4994

Defense Priority Rating: DO C-9

Security Classification: N/A

RESTRICTIONS

See Attached government Supplemental Information Sheet for Additional Requirements.

Travel: Foreign travel must have prior approval — Contact OCA in each case. Domestic travel requires sponsor approval where total will exceed greater of $500 or 125% of approved proposal budget category.

Equipment: Title vests with GIT. Authorization granted to acquire equipment required for performance and which have acquisition cost of less than $1K.

COMMENTS:

* Co-project with E-16-660/Zinn; E-16-690/Jagoda/Hubbartt/Strahle and E-16-691/Price/Sigman.

** Total Contract Amount is $280,000.

COPIES TO:

Administrative Coordinator
Research Property Management
Accounting
Procurement/EES Supply Services
Research Security Services
~~Reports Coordinator~~ (OCA)
Legal Services (OCA)
Library
EES Public Relations (2)
Computer Input
Project File
Other _____

FORM OCA 4:781

GEORGIA INSTITUTE OF TECHNOLOGY — OFFICE OF CONTRACT ADMINISTRATION

PROJECT ADMINISTRATION DATA SHEET

[x] ORIGINAL [ ] REVISION NO. _____

Project No. E-16-691 * DATE 12/14/81

Project Director: E. W. Price & R. K. Sigman School/Lab Aerospace Engineering

Sponsor: Air Force Office of Scientific Research (AFOSR); Bolling AFB, D.C. 20332

Type Agreement: Contract F49620-82-C-0013

Award Period: From 11/27/81 To 9/30/~~82~~ 83 (Performance) _____ (Reports)

Sponsor Amount: $73,760 (E-16-691 only) ** Contracted through:

Cost Sharing: $10,064 (E-16-366) GTRI/GIT

Title: Behavior of Aluminum in Solid Propellant Combustion (Task III)

ADMINISTRATIVE DATA

OCA Contact Leamon R. Scott

1) Sponsor Technical Contact:

AFOSR/NA
Director of Aerospace Sciences
Building 410
Bolling AFB, D.C. 20332
202-767-4937

2) Sponsor Admin/Contractual Matters:

USAF, AFSC
AIR FORCE OFFICE OF SCIENTIFIC RESEARCH
BUILDING 410
BOLLING AFB DC 20332
Buyer: C.R. Arnold/bls/PKD/202-767-4994

Defense Priority Rating: DO C-9

Security Classification: _____

RESTRICTIONS

See Attached government Supplemental Information Sheet for Additional Requirements.

Travel: Foreign travel must have prior approval — Contact OCA in each case. Domestic travel requires sponsor approval where total will exceed greater of $500 or 125% of approved proposal budget category.

Equipment: Title vests with GIT. Authorization granted to acquired equipment required for performance and which have acquisition cost of less than $1K.

COMMENTS:

* E-16-660/Zinn; E-16-690/Price/Sigman and E-16-692/Strahle.

** Total Contract amount is $280,000.

COPIES TO:

Administrative Coordinator
Research Property Management
Accounting
Procurement/EES Supply Services
Research Security Services
~~Reports Coordinator~~ (OCA)
Legal Services (OCA)
Library
EES Public Relations (2)
Computer Input
Project File
Other _____

FORM OCA 4:781

GEORGIA INSTITUTE OF TECHNOLOGY — OFFICE OF CONTRACT ADMINISTRATION

PROJECT ADMINISTRATION DATA SHEET

[x] ORIGINAL [ ] REVISION NO. _____

Project No. E-16-690 * DATE 12/14/81

Project Director: J.I. Jagoda, J.E. Hubbart, W.C. Strahle School/Lab Aerospace Engineering

Sponsor: Air Force Office of Scientific Research (AFOSR); Bolling AFB, D.C. 20332

Type Agreement: Contract F49620-82-C-0013 83

Award Period: From 11/27/81 To 9/30/~~82~~ (Performance) _____ (Reports)

Sponsor Amount: $106,372 (E-16-690 only) ** Contracted through:

Cost Sharing: $23,168 (E-16-365) GTRI/~~GIT~~

Title: Heterogeneous Diffusion Flame Stabilization (Task II)

ADMINISTRATIVE DATA OCA Contact Leamon R. Scott

1) Sponsor Technical Contact:
AFOSR/NA
Director of Aerospace Sciences
Building 410
Bolling AFB, D.C. 20332
202-767-4937

2) Sponsor Admin/Contractual Matters:
USAF, AFSC
AIR FORCE OFFICE OF SCIENTIFIC RESEARCH
BUILDING 410
BOLLING AFB, D.C. 20332
BUYER; C.R. Arnold/b1s/PKD/202-767-4994

Defense Priority Rating: DO C-9 Security Classification: N/A

RESTRICTIONS

See Attached government Supplemental Information Sheet for Additional Requirements.

Travel: Foreign travel must have prior approval — Contact OCA in each case. Domestic travel requires sponsor approval where total will exceed greater of $500 or 125% of approved proposal budget category.

Equipment: Title vests with GIT. Authorization granted to acquire equipment required for performance and which have acquisition cost of less than $1K.

COMMENTS:

E-16-660/Zinn; E-16-691/Price/Sigman and E-16-692/Strahle.

** Total Contract Amount is $280,000.

COPIES TO:

Administrative Coordinator
Research Property Management
Accounting
Procurement/EES Supply Services
Research Security Services
~~Reports Coordinator~~ (OCA)
Legal Services (OCA)
Library
EES Public Relations (2)
Computer Input
Project File
Other _____

FORM OCA 4:781

GEORGIA INSTITUTE OF TECHNOLOGY — OFFICE OF CONTRACT ADMINISTRATION

REVISED*

PROJECT ADMINISTRATION DATA SHEET

[x] ORIGINAL [ ] REVISION NO. _____

Project No. E-16-614* DATE 9/10/82

Project Director: Strahle/Jagoda School/~~XXX~~ A.E.

Sponsor: Air Force Office of Scientific Research (AFOSR); Bolling AFB, D.C.

Type Agreement: Contract F49620-82-C-0013 (P00002)

Award Period: From 11/27/81 To 9/30/82 (Performance) 11/30/82 (Reports)

Sponsor Amount: $83,000 (E-16-614 only) ** Contracted through:

Cost Sharing: $39,905 (E-16-318 GTRI/~~XXX~~

Title: Laser Raman Scattering System

ADMINISTRATIVE DATA

OCA Contact _____

1) Sponsor Technical Contact:

AFOSR/NA
Director of Aerospace Sciences
Building 410
Bolling AFB, D.C. 20332
Phone: (202) 767-4937

2) Sponsor Admin/Contractual Matters:

USAF, AFSC
Air Force Office of Scientific Research
Building 410
Bolling AFB, D.C. 20332

Defense Priority Rating: DO C-9

Security Classification: N/A

RESTRICTIONS

See Attached AFOSR Supplemental Information Sheet for Additional Requirements.

Travel: Foreign travel must have prior approval — Contact OCA in each case. Domestic travel requires sponsor approval where total will exceed greater of $500 or 125% of approved proposal budget category.

Equipment: Title vests with Gov't. Authorization granted to acquire or fabricate equipment listed in ? (Provision 16); * Title vests with Govt. Authorization granted to acquire equipment required performance & which have acquisition cost of less than $1K.(Provision 15); Title vests with

COMMENTS:

* Co-project with E-16-660/Zinn; E-16-690/Jagoda/Hubbartt/Strahle; E-16-691/Price/Sigman; and E-16-692/Strahle

** Total Contract Amount is $363,000

COPIES TO: RAN

~~Administrative Coordinator~~
Research Property Management
Accounting
Procurement/EES Supply Services
Research Security Services
Reports Coordinator (OCA)
Legal Services (OCA)
Library
EES Public Relations (2)
Computer Input
Project File
Other GTRI

FORM OCA 4-781

GEORGIA INSTITUTE OF TECHNOLOGY OFFICE OF CONTRACT ADMINISTRATION

SPONSORED PROJECT TERMINATION/CLOSEOUT SHEET

Date April 19, 1985

Project No. E-16-614/W.C. Strahle, J.I. Jagoda; E-16-660/B.T. Zinn; E-16-690/J.I. Jagoda, School/~~XXX~~ AE

~~Include Subproject No(s)~~ J.F. Hubbartt, W.C. Strahle; E-16-691/E.W. Price, R.K. Sigman; E-16-692/W.C. Strahle

Project Director(s) Noted above GTRC / ~~GXX~~

Sponsor Air Force Office of Scientific Research

Title Investigation of Unsteady Burning Characteristics of Solid Propellants(Task I)

Effective Completion Date: (Performance) (Reports)

Grant/Contract Closeout Actions Remaining:

- [ ] None
- [ ] Final Invoice or Final Fiscal Report
- [X] Closing Documents
- [X] Final Report of Inventions
- [X] Govt. Property Inventory & Related Certificate - Include all five projects listed above.
- [ ] Classified Material Certificate
- [ ] Other

NOTE: A single final report was submitted referencing E-16-660 covering all of the co-projects listed above. One final invoice consolidating all final projects listed above has been received.

Continues Project No. Continued by Project No.

COPIES TO:

Project Director
Research Administrative Network
Research Property Management
Accounting
Procurement/GTRI Supply Services
Research Security Services
Reports Coordinator (OCA)
Legal Services

Library
GTRC
Research Communications (2)
Project File
Other Heyser
Jones

FORM OCA 69.285

SCIENTIFIC REPORT

BEHAVIOR OF ALUMINUM IN SOLID PROPELLANT COMBUSTION

By

E. W. Price, R. K. Sigman, J. K. Sambamurthi and C. J. Park

Prepared for

AIR FORCE OFFICE OF SCIENTIFIC RESEARCH
BOLLING AIR FORCE BASE, DC 20332

Under

Contracts AFOSR F 49620–78–C–0003
and AFOSR F 49620–82–C–0013

June 1982

GEORGIA INSTITUTE OF TECHNOLOGY
A UNIT OF THE UNIVERSITY SYSTEM OF GEORGIA
SCHOOL OF AEROSPACE ENGINEERING
ATLANTA, GEORGIA 30332

UNCLASSIFIED

SECURITY CLASSIFICATION OF THIS PAGE *(When Data Entered)*

REPORT DOCUMENTATION PAGE		READ INSTRUCTIONS BEFORE COMPLETING FORM
1. REPORT NUMBER	2. GOVT ACCESSION NO.	3. RECIPIENT'S CATALOG NUMBER
4. TITLE *(and Subtitle)* BEHAVIOR OF ALUMINUM IN SOLID PROPELLANT COMBUSTION		5. TYPE OF REPORT & PERIOD COVERED SCIENTIFIC REPORT 1 Oct. 1977 - 28 Feb. 1982 6. PERFORMING ORG. REPORT NUMBER
7. AUTHOR(s) E. W. Price, R. K. Sigman, J. K. Sambamurthi and C. J. Park		8. CONTRACT OR GRANT NUMBER(s) AFOSR F49620-78-C-0003 AFOSR F49620-82-C-0013
9. PERFORMING ORGANIZATION NAME AND ADDRESS GEORGIA INSTITUTE OF TECHNOLOGY SCHOOL OF AEROSPACE ENGINEERING ATLANTA, GA 30332		10. PROGRAM ELEMENT, PROJECT, TASK AREA & WORK UNIT NUMBERS N/A
11. CONTROLLING OFFICE NAME AND ADDRESS AIR FORCE OFFICE OF SCIENTIFIC RESEARCH/NA BLDG. 410 BOLLING AIR FORCE BASE, DC 20332		12. REPORT DATE June 1982 13. NUMBER OF PAGES 91
14. MONITORING AGENCY NAME & ADDRESS *(if different from Controlling Office)*		15. SECURITY CLASS. *(of this report)* UNCLASSIFIED 15a. DECLASSIFICATION/DOWNGRADING SCHEDULE N/A

16. DISTRIBUTION STATEMENT *(of this Report)*

Approved for public release; distribution unlimited

17. DISTRIBUTION STATEMENT *(of the abstract entered in Block 20, if different from Report)*

18. SUPPLEMENTARY NOTES

19. KEY WORDS *(Continue on reverse side if necessary and identify by block number)*

SOLID PROPELLANT COMBUSTION,
ALUMINUM AGGLOMERATION,
ALUMINUM COMBUSTION.

20. ABSTRACT *(Continue on reverse side if necessary and identify by block number)*

This report is concerned with achieving improved combustion of the aluminum ingredient in solid propellant. The approach is to clarify understanding of the complex detailed processes exhibited by aluminum and relate them to control of propellant burning rate, combustion stability, combustion efficiency and two phase flow behavior in the motor. A series of experiments were contrived to elucidate the microscopic details of aluminum behavior and their relation to microscopic details of the propellant, and to behavior of the other propellant ingredients.

DD FORM 1 JAN 73 1473 EDITION OF 1 NOV 65 IS OBSOLETE

UNCLASSIFIED

SECURITY CLASSIFICATION OF THIS PAGE *(When Data Entered)*

ACKNOWLEDGEMENT

The research summarized in this report was sponsored by the Air Force Office of Scientific Research. Technical monitor of the project is Dr. L. H. Caveny. The authors are grateful for the opportunity to pursue this research in the depth necessary to unravel the controlling details of a very complex combustion process.

TABLE OF CONTENTS

INTRODUCTION

Metal powders are used as fuel components in solid propellants because of their high density, and high heat release when burned. The metals have other benefits as well, such as suppression of combustion instability, modification of burning rate, reduction of sensitivity to detonation, favorable supply, etc. These advantages are not all applicable to all metals in all rocket motors in all applications. Indeed, for rocket motor applications, only aluminum powder has seen widespread use. Even aluminum has been considered disadvantageous in some applications, particularly those in which the smoky exhaust trail of aluminized propellants compromises system effectiveness too severely. However, aluminum (and possibly other metals) is a highly desirable ingredient in many applications, and is the second most plentiful ingredient in roughly 50% of all propellant manufactured.

The advantages and disadvantages of aluminum, both real and potential, depend to a significant degree on the details of combustion of the aluminum. Combustion behavior is in turn relatively complex compared to other propellant ingredients, a circumstance resulting from the low volatility of the metal and its oxide. The fine metal particles go through a complex accumulation-concentration-agglomeration on the propellant burning surface, yielding relatively large and slow-burning droplets. The combustion behavior, and nature of the oxide products, are sensitive to details of the propellant and motor, and are difficult to predict in advance of testing the all-up system. Because of this, a number of efforts have been mounted in the past to achieve better understanding and/or engineering characterization of aluminum behavior in propellant combustion, and its effect on system performance. The present study has been aimed at understanding the detailed processes that determine the behavior of aluminum in the rocket motor, using methods that provide information at the microscopic level of the aluminum particles, agglomerates and oxide product droplets. Such understanding provides the basis for more rational "design" of propellant formulation, prediction of performance, and manipulation of design to achieve best performance.

In the interests of perspective, the combustion "metabolism" of aluminum is outlined in Fig. 1, which shows the routes by which ingredient aluminum particles in propellants can progress to their final reaction products (the figure is based on the usual case where the products are molten Al_2O_3). For any given propellant,there is

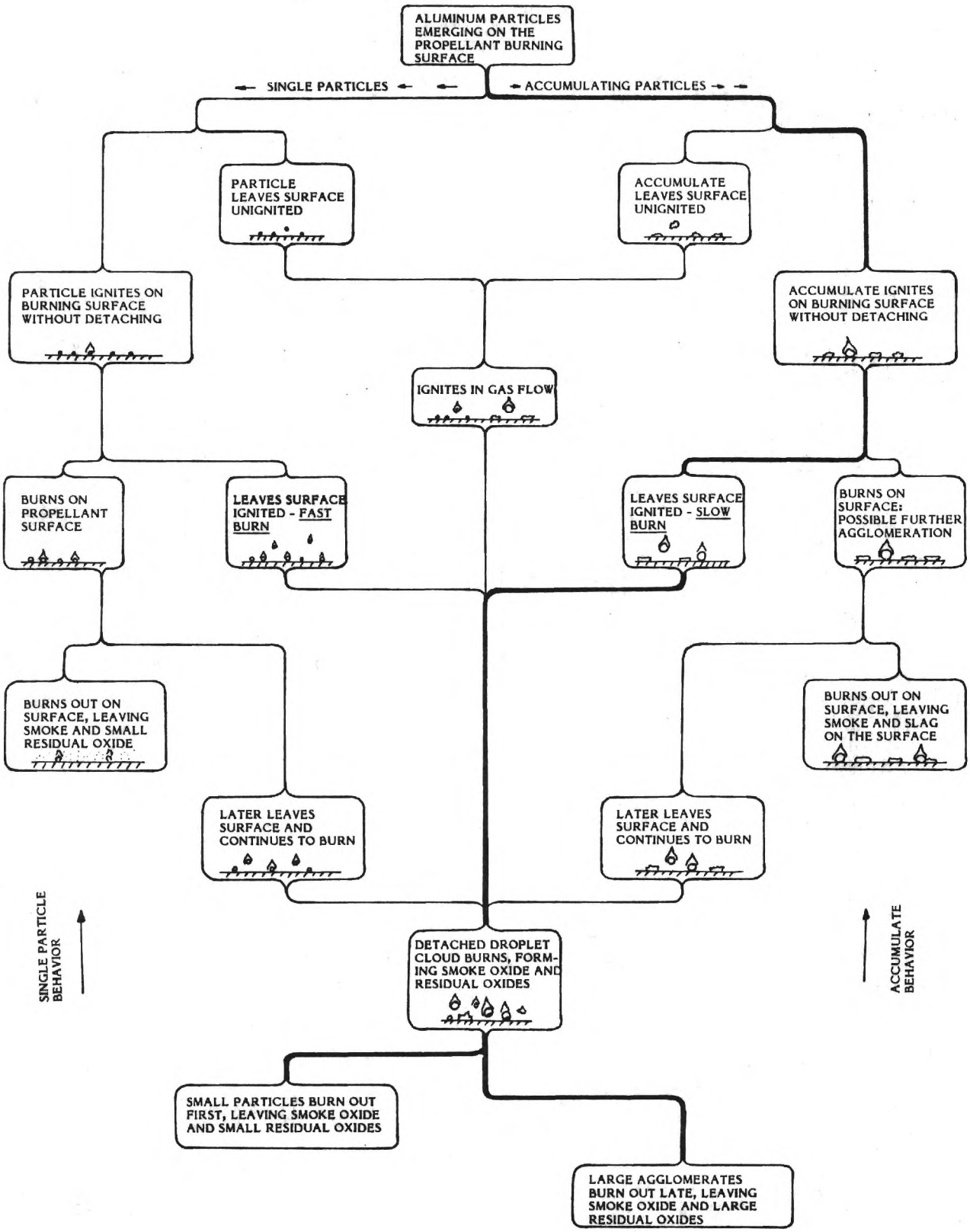

Fig. 1 Alternative paths of aluminum behavior in the combustion zone. The path emphasized by the heavy line is most typical with ammonium perchlorate-hydrocarbon binder propellants.

a "most typical" route, but some of the particles follow other routes, giving a statistical array of behavior. However under most conditions, aluminum concentrates on the burning surface (Fig. 2); agglomerates, ignites and detaches from the surface as a single complex event (Fig. 3); burns as 50 - 300 μm diameter agglomerates while moving away from the burning surface (Fig. 4); forms a fine Al_2O_3 smoke (< 2 μm) in a flame envelope about the agglomerate (Fig. 5); concurrently accumulates oxide on the surface of agglomerates that ends up as "residual" oxide droplets in the 5 - 100 μm range when the agglomerates burn out (Fig. 6). This sequence is noted by the heavy lines in Fig. 1.

It is this detailed behavior that determines the effect of aluminum on such combustion variables as

propellant burning rate
combustion stability
combustion efficiency
combustion quenching
aluminum slag residue

and such oxide product effects as

two-phase flow in the combustor and nozzle
thrust efficiency
component erosion
damping of combustor oscillations
oxide slag residue.

The combustion studies seek to understand the accumulation-concentration-agglomeration-ignition-detachment-agglomerate combustion sequence by studies that clarify these individual steps. This involves consideration of the original distribution of aluminum particles in the propellant microstructure; the relative dimensions of the combustion zone and the particulate ingredients; the forces conducive to retention and concentration of aluminum; the conditions that delay ignition during concentration; the processes that connect accumulated particles and set the stage for coalescence; the conditions that eventually break down sintered surface accumulations and cause agglomeration, ignition and detachment from the

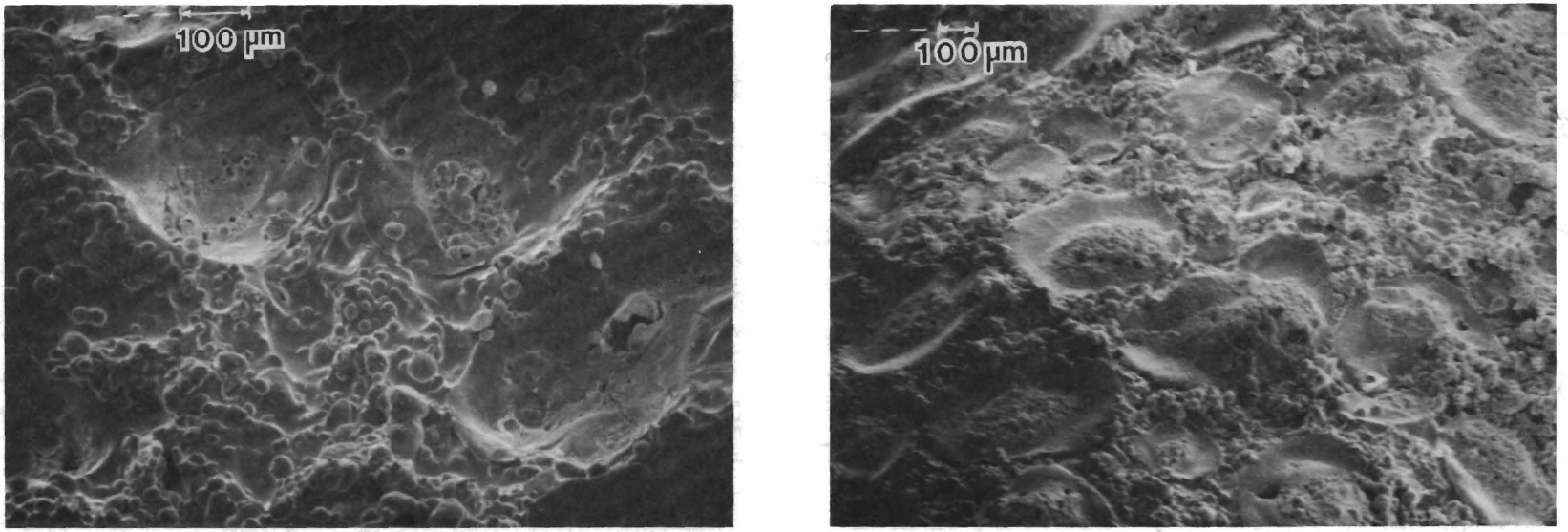

Fig. 2 Aluminum concentration on the burning surface. Scanning electron microscope pictures of surfaces quenched by rapid depressurization.

a) Aluminum concentration in a "pocket", with relatively visible evidence of binder melt (from 6.9 MPA test).

b) General pattern of aluminum concentration, selected to show also an example of relatively dry sintering of accumulated aluminum (from 0.7 MPa test).

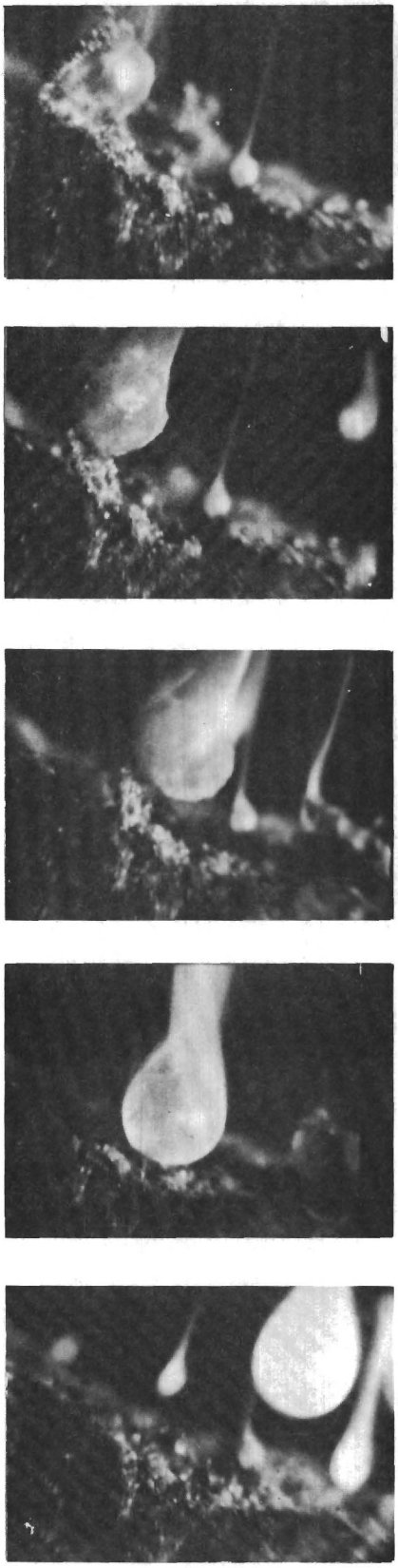

Fig. 3 Formation of an agglomerate from a surface accumulation of aluminum particles (from high speed motion pictures by D. Zurn, Naval Weapons Center).

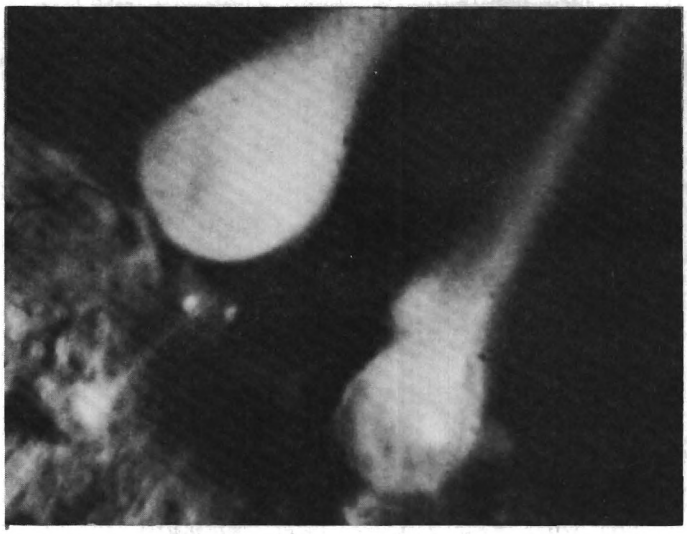

Fig. 4 Burning agglomerates, shortly after leaving the propellant burning surface.

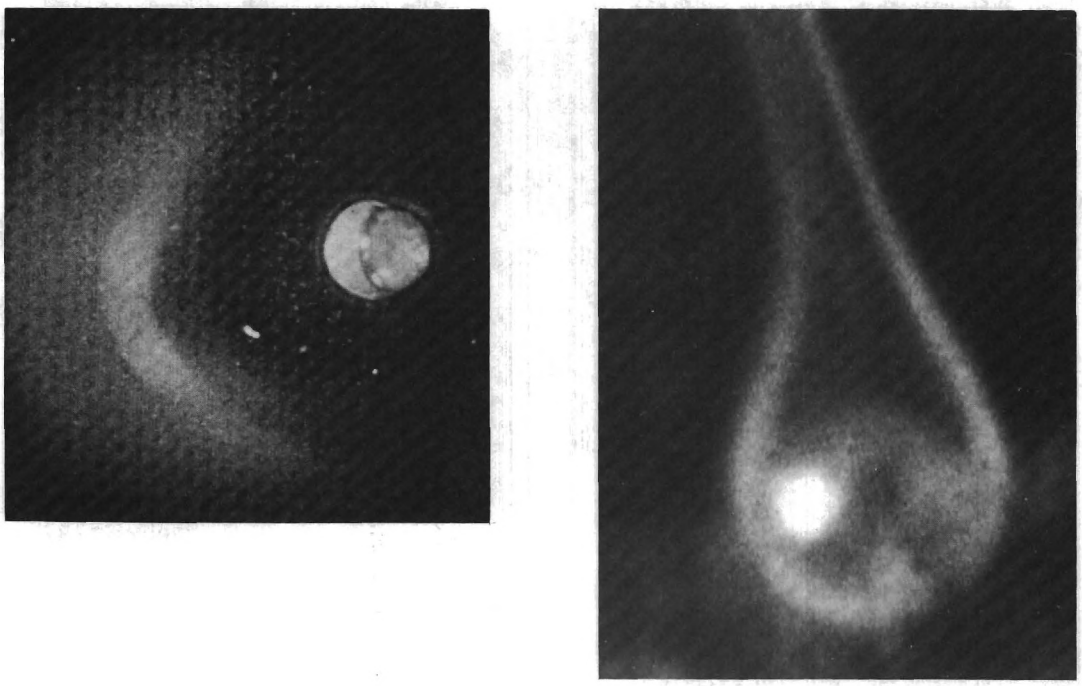

Fig. 5 Illustration of smoke oxide formation in the detached flame around the agglomerate.
a) Aluminum droplet with oxide lobe and smoke cloud deposited on a quench plate in an experiment burning single aluminum particles in air at 1 atm (photo by Prentice, NWC).
b) Burning aluminum agglomerate observed in high speed photography of propellant combustion.

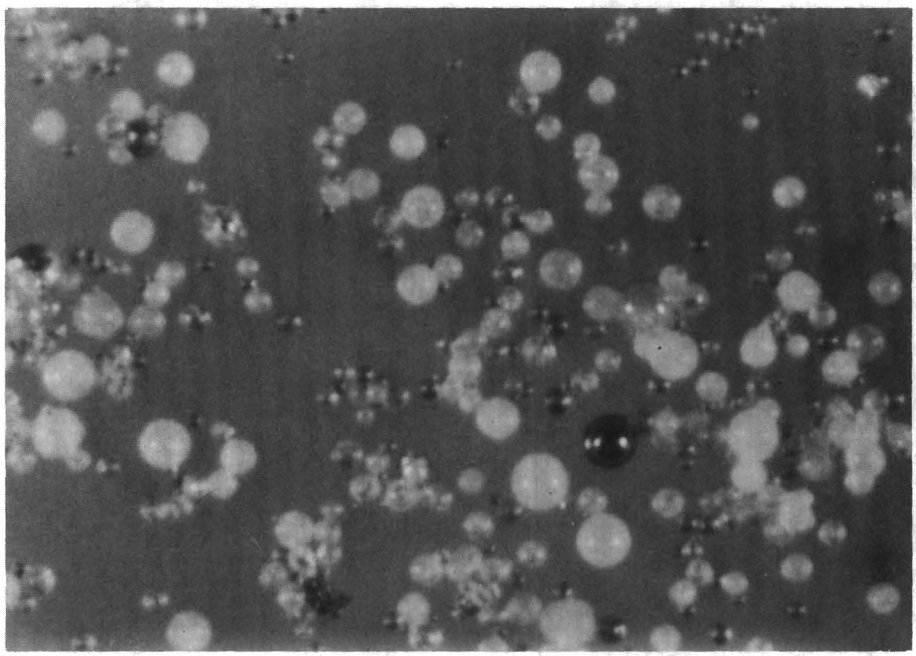

Fig. 6 Residual oxide, evolved from agglomerate oxide.

burning surface; and the combustion of agglomerates in the gas flow field. While it is not practical to seek complete understanding of all these complex processes, it is also not practical to ignore any of them because they are "branch points" for the alternative paths in Fig. 1, and each branch point can exercise decisive effects on combustion. The present investigations have sought to clarify these branch points, establish their roles at the microscopic level in real propellant combustion, and thus provide the basis for understanding the relation between conventional propellant variables (composition, particle size) and macroscopic combustion behavior (burning rate, stability, combustion efficiency, etc.). The discussion in the following seeks (in the first sections) to develop the arguments and summarize past results into a connected account of how aluminum behaves as it "moves through" the combustion wave. These sections are followed by accounts of several supporting studies that have not been reported previously. These studies were carried out as part of the basic study, and in part to explore potentially useful ideas emerging from the study (e.g., modifications of aluminum powder to control agglomeration, and use of high aluminum-content propellants).

PROPELLANT MICROSTRUCTURE

Typical composite propellants are made with oxidizer as a primary particulate ingredient (70 - 75% by weight for aluminized propellants), with particles ranging from 6 - 600 μ m (mass average 100 μm). Aluminum particles are typically 16% by weight, in the size range 5 - 40 μm. The balance of the mass (10 - 15%) is typically a polymeric material. In order to achieve a near-stoichiometric mixture, the binder content is made as low as possible consistent with acceptable processing characteristics and physical properties of the propellant. To achieve this, the size distribution of the particulate ingredients is normally chosen rather carefully so as achieve dense particle packing and minimize packing voids that that yield locally high concentrations of binder. On the other hand, it is required that the surface of all particles be "wetted" by binder in order to get acceptable mechanical properties, so all particles are surrounded by binder. In meeting all these requirements, propellant processors have to limit the "smallness" of particles (total surface area) to avoid processing problems (e.g., viscosity of the uncured mix). The net result is reflected in the typical figures noted above, but with oxidizer particle blends involving two to four different sizes, a substantial portion being in the coarse component (e.g., 200 - 400).

Given the foregoing practical realities and trade practices, a typical propellant looks like that shown in Fig. 7. An aggregate of coarse oxidizer particles is set in a "sponge" of binder and finer oxidizer and aluminum particles. In a low burning rate propellant, the coarse particles will be more densely packed (and possibly larger), with the "sponge" being correspondingly more tenuous and containing less fine oxidizer. Because the aluminum particles are normally relatively small in both size and total volume, they can be pictured as being part of the sponge. Thus the aluminum is not homogeneously distributed on the dimensional scale of the oxidizer particles, being located in that 30 - 50% of the volume occupied by the sponge. That volume is very fuel rich, containing only about 30% of the oxidizer in a propellant that is already fuel rich in overall formulation.

When a propellant burns, a burning front propagates through the matrix, with

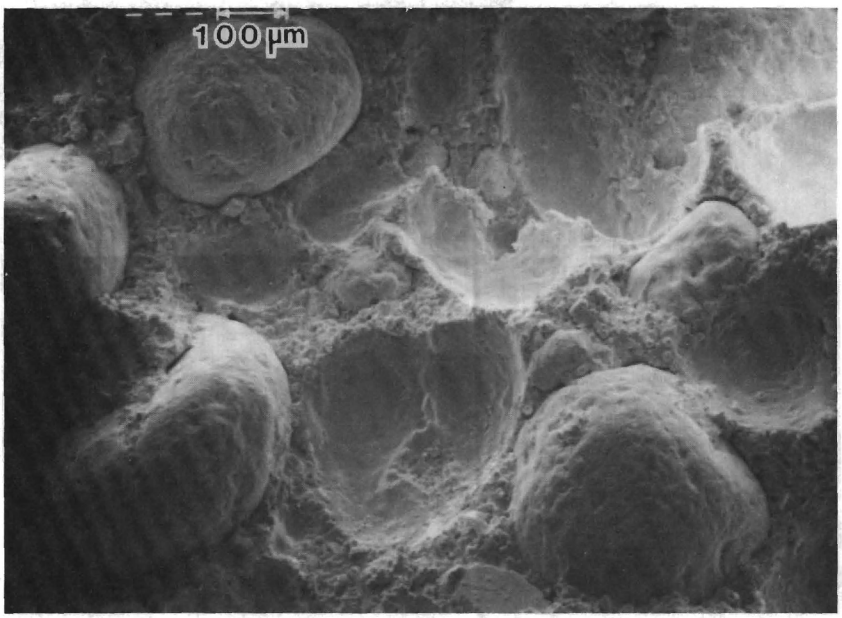

Fig. 7 Illustration of propellant microstructure. Scanning electron microscope picture of a surface produced by breaking the propellant (to show structure).

the burning surface representing a sort of "cross section" of the propellant microstructure (Fig. 8). Oxidizer particles are readily visible, as is the "cross section" of the sponge (in Fig. 8 a nonaluminized propellant was used to enhance the visibility of sponge structure). The binder area of the surface is revealed as a tenuous, interconnected structure with occasional patches of larger dimensions corresponding to voids or "pockets" in the packing pattern of the larger oxidizer particles. These pockets may contain smaller oxidizer particles, which are often difficult to distinguish. A similar structure is revealed with aluminized propellants, but the sponge pattern is usually dominated on the burning surface by aluminum particles (Fig. 9). The aluminum presents an appearance of an interconnected array, which to some extent is a reflection of its actual distribution in the propellant (i.e., as part of the sponge). However, the distribution of the aluminum is critically dependent on its particle size relative to the coarser AP particles. Very fine aluminum can be uniformly dispersed in the sponge, but coarser aluminum particles will be isolated from each other because they will not fit in the thinner elements of the sponge structure. Thus aluminum may be localized in the thicker sponge components corresponding to oxidizer packing voids (referred to in this report as "binder pockets"). The degree of interconnectedness between these aluminum concentrations will depend on the size of aluminum particles and their corresponding ability to "fit" in the connective structure of the sponge between pockets. These circumstances are important because they affect the continuity of the aluminum's array on the burning surface, which in turn affects the opportunity for coalescence between pocket concentrations of aluminum.

As noted earlier, oxidizer is usually present as a blend of particle sizes. The smaller fraction typically has a particle size of the same order as the aluminum (this was the case for the propellant in Fig. 9). Thus arguments regarding the distribution of aluminum particles in the sponge apply also to the finer part of the oxidizer particle population. As noted earlier, this means that the aluminum containing part of the sponge contains also oxidizer, yielding a very fuel-rich propellant (which will ordinarily not burn unaided). Obviously the distributions of fine oxidizer and aluminum in the sponge are amenable to some delicate tailoring by careful particle size tailoring, but the size distributions ordinarily available are too broad for such "fine tuning" of microstructure, and the effects on combustion are consequently unevaluated.

In the present work, particle size has been one of the principal variables in experiments. The foregoing description of microstructure was evolved as a

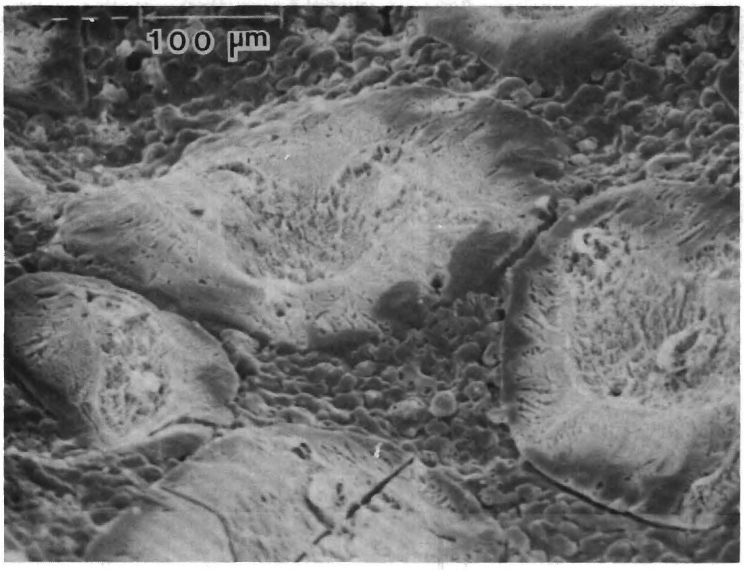

Fig. 8 Illustration of distribution of binder in a heterogeneous propellant. Scanning electron microscopc picture of a quenched surface (non aluminized sample used to enhance visibility of binder; test pressure 6.9 MPa; propellant contains fine AP, visible in the binder).

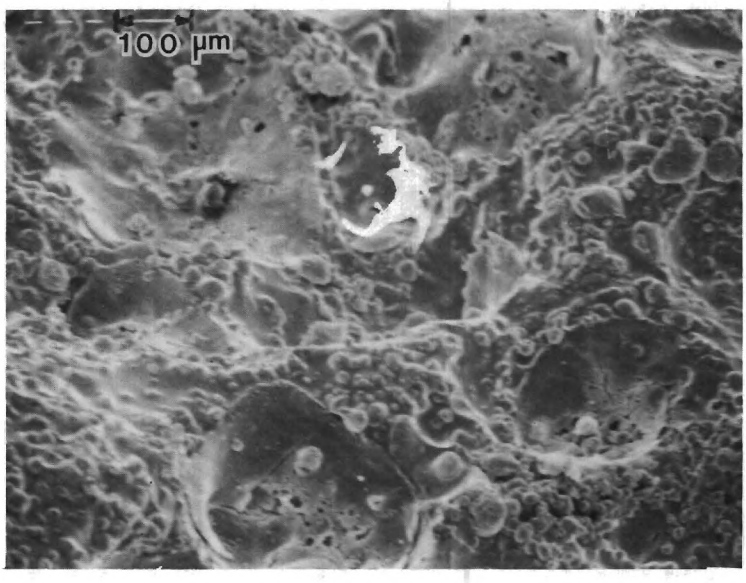

Fig. 9 Illustration of distribution of aluminum on the burning surface. SEM picture of a sample quenched from 6.9 MPa.

consequence of efforts to understand results of tests, and as a basis for design of test experiments. In hindsight, the description is fairly obvious, and a key element of the description (the concept of pockets) was presented by one of the authors earlier (Ref. 1). The more elaborate description presented here is designed to accomodate a more detailed understanding of aluminum behavior described in the following.

PRE-AGGLOMERATION BEHAVIOR OF ALUMINUM*

There is very little controversy over the thesis that aluminum forms agglomerates near the propellant burning surface, but there have been a variety of proposals as to what processes lead to agglomeration. These different proposals do not represent a controversy so much as divergent efforts to produce tractable idealized modeling schemes from which agglomeration behavior can be calculated (Ref. 2-4). The experimental evidence is largely in the form of combustion photography (which doesn't get published), and more controlled studies of response of aluminum powders to heating (available in diverse sources (Ref. 5)). In addition, some idea of intermediate steps leading to agglomeration can be gained from examination of quenched burning surfaces. These methods have all been used in one or more of past studies and the present study. The general interpretation is relatively unambiguous, and is summarized in the following.

Aluminum is seen to accumulate on the propellant burning surface, often residing there for much longer times than required for the burning surface to recede past the particles. In other words, particles typically adhere to the surface. Mobility is typically low, consistent with an "adhesive" surface retention. Knowing the propellant microstructure, it is evident that most adhering particles on a receding surface will be joined by underlying particles. This in turn implies that accumulation and concentration of aluminum particles will normally occur, an implication supported by countless observations by combustion photography and quenched sample studies. Low volatility of the metal, protective nature of the oxide skin, and initially low local concentration of oxidizing species prevent ignition of the metal during this surface accumulation (as seen later in this report, such accumulation occurs without ignition even on the burning surface of AP oxidizer). Finally, it is an observed fact that the accumulating particles eventually coalesce into agglomerates, implying that concentration proceeds to the point of contact between particles. Presence of relatively rigid structures of aluminum particles is manifested in combustion photography and quench tests; thus it is evident that particle contact progresses to a state of sintering, similar to that resulting from controlled heating of aluminum powder in oxidizing atmospheres. Indeed, acid etching of recovered accumulates shows them to consist of an

---

* This section is condensed from Ref. 7. See that reference for more extensive illustrations of relevant experimental results.

interconnected oxide shell structure filled with aluminum (Ref. 5 - 7).

In view of chaotic microstructure of the heterogeneous propellants, it is to be expected that some diversity and intermittency of behavior would occur. Some aluminum particles leave the surface without evident interaction with others. All aluminum eventually leaves the surface, and the extent of prior concentration and sintering can only be fully described with the aid of statistical language. Recalling the earlier discussion of the implications of propellant microstructure, the statistical language of accumulation, sintering and detachment must be linked to the statistical language of propellant microstructure, and concepts such as "pockets", "bridging" between pockets, and formation of "sintered filigrees" are terms used to connect propellant microstructure to the state of connectedness of accumulated aluminum on the burning surface. The ultimate size of an accumulate is thus dictated to some extent by the original concentration of aluminum in the propellant microstructure (pockets) and to some extent by the spatially nonuniform conditions that cause sintered structures to adhere to the propellant surface without ignition. Finally, ignition may precipitate detachment, and the ultimate size of the accumulate will in that case be determined by conditions necessary for ignition. Recalling the earlier reference to the reluctance of aluminum to ignite in the AP flame, it must be anticipated that ignition termination of surface accumulation may be as dependent on propellant microstructure as is the pattern of accumulation. This will be so when the ignition is induced by the local oxidizer-binder flamelets associated with oxidizer-binder interfacial regions of the burning surface microstructure. It is in or beyond these flamelets that high enough temperatures are reached to achieve ignition of sintered aluminum accumulates. The process of ignition and concurrent agglomeration is described in the following.

THE AGGLOMERATION EVENT

Agglomeration takes place when the progressive state of an accumulate reaches a point where the oxide containment of the molten aluminum breaks down. At this point, two processes come precipitously into dominance. The surface tension of the molten aluminum causes the metal to draw into a spherical configuration. Since the breakdown of the oxide containment does not occur simultaneously throughout the accumulate, this spheroidization is progressive. The second process that comes concurrently into dominance is the oxidation rate of the aluminum as it escapes the containment of the existing oxide shell. Thus it is typical in combustion photography, under conditions favorable for good resolution, to see areas of spheroidization in a surface accumulate, accompanied by onset of evidence of associated aluminum vapor flame and telltale oxide smoke trail.

The agglomeration event can be so rapid that it is not resolved in photography at a few thousand frames per second, or it can be fairly protracted and easy to observe (large accumulates at low pressure). The progressive nature of the event is obvious under favorable viewing conditions. Initiation appears to start at locations where the accumulate is best exposed to the high temperature of the diffusion flame elements (AP-binder flame). That region of the accumulate glows brightly, spheroidizes and develops darker reflective areas that are apparently molten metal. The smoke veil and trail develops over these areas when they appear. At this point, the oxide residue from the spheroidized portion is visible (at least in part) as a white glowing film over parts of the sphere, presumably molten. This is accompanied by increasing brightness of the neighboring portions of the accumulate. The molten portion starts to coalesce progressively into the rest of the accumulate, at the same time exhibiting a loss of any other attachment to the propellant surface. Under the conditions that give good resolution of these progressive features, the surface accumulation of aluminum is usually widely interconnected, so that the propagative aspect of a coalescence is relatively visible. Indeed, some investigators who observed the behavior without aid of the external illumination used to show the nonluminous part of the accumulate have interpreted the behavior as indicating a freely rolling droplet on the propellant surface (without accompanying rationale for the long delay before "lift-off" from the surface). In any case, the flaming agglomerate eventually burns itself free of surface attachment and moves away in a near spherical condition (Fig. 4), typically

showing burning metallic areas; bright molten oxide areas; and often darker or orange irregular areas of not yet melted material at the last point of contact of the droplet with the propellant surface. This is in effect the birth of an agglomerate, whose individual identity remains until burnout somewhere in the flow field. Such an agglomerate is typically 10 times the diameter of the original ingredient aluminum particles, implying an agglomeration of 1000 particles.

The foregoing description is based on interpretation of combustion photography, aided by a good deal of prior knowledge of the nature of surface accumulates, the propellant combustion zone, and aluminum combustion. It is basically a visualization of the agglomeration, seen from the outside. What's happening inside the coalescing mass, how does it affect the process, and what is the end effect on the fully developed agglomerate? This can be inferred from the nature of the situation, properties of materials involved, and the externally observable behavior.

When the accumulate first starts to break down and coalesce, it is a nonuniformly preheated structure consisting of an intricate solid oxide encasement of liquid aluminum. The metal of the original aluminum particles is probably mostly still unconnected, any contact points having oxidized to form the connected accumulate structure. Any localized breakdown of the oxide leading to onset of coalescence is initially insulated from the overall accumulate by the rigidity and low thermal conductivity of the oxide containment structure. However, the rise in local heat release due to the flame around the coalescing aluminum at the initial breakdown point melts the oxide locally, assuring continued and spreading reaction of aluminum.

As the oxide shell structure breaks down, it is swept up by the coalescing aluminum in the form of thin (sub micron) solid and melting sheets with varying degree of connectedness. Insoluble in the liquid aluminum, the oxide will be partly trapped in the interior of the agglomerate, and partly left as melting surface aggregations remaining after withdrawal of coalescing aluminum (Fig. 10 a). The quenched agglomerate in Fig. 10 b shows the tendency of the aluminum to spheroidize when the accumulate is not yet fully molten in the interior. Fig. 3 shows the tendency for much of the initial oxide to be left as a melting aggregate on the agglomerate surface. This external residue is the source of part of the oxide typically present as an oxide lobe on a fully burning agglomerate (Fig. 4). Acid etching of such agglomerates after quench-collection reveals the presence of a complex interior oxide structure (Fig. 11), probably evolved from the accumulate

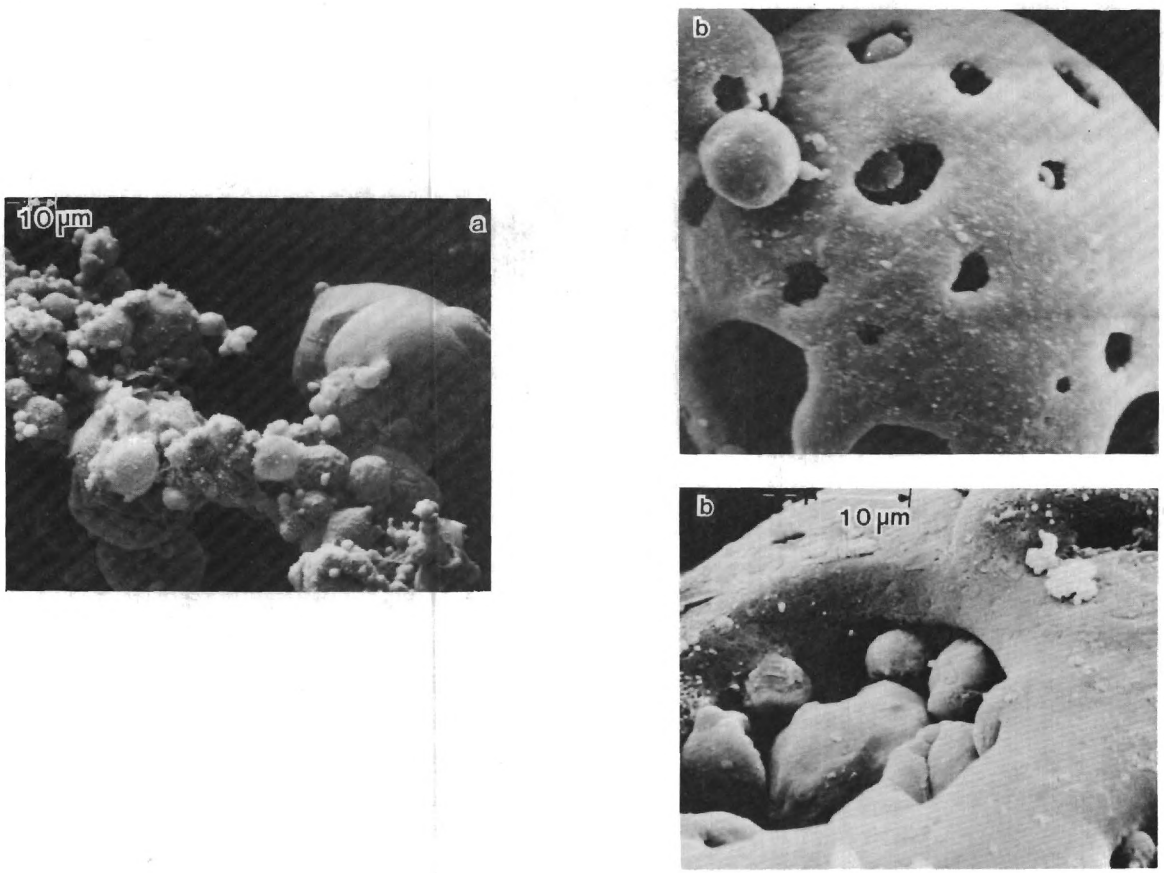

Fig. 10 Transition from accumulate to agglomerate.
a) Accumulate with sites where coalescence, burning and oxide lobe formation have occurred.
b) Spheroidization is largely complete, but not all original oxide has yet melted.

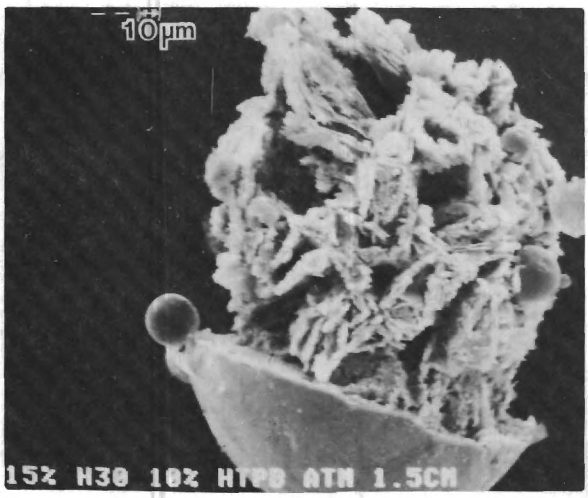

Fig. 11 Flake oxide in the interior of the aluminum portion of an agglomerate (revealed by acid etching). (From ethanol plume quench test at 1 atm.)

oxide that was trapped in the agglomerate during coalescence of the accumulate. Since the temperature of the burning agglomerates is above the melting point of the oxide, that oxide in the interior presumably survived as liquid sheets that solidified to the form in Fig. 11 during quenching. There is some evidence that the amount and structure of interior oxide is dependent on the abruptness of the agglomeration event, suggesting that the aluminum coalescence would exclude the oxide if it were completely free to flow. Thus agglomerates formed in the argon atmosphere in a hot stage microscope have little or no oxide trapped in the interior (Ref. 7,8). Combustion-produced agglomerates are observed in the present studies to have more interior oxide if formed in high pressure burning. The differences are conspicuous when one tries to cut the quenched agglomerate: "high pressure" agglomerates are brittle and give ragged cut surfaces, while "low pressure" agglomerates are soft, and cut smoothly. Thus it seems clear that the agglomeration is a dynamic event that yields a product that is dependent on a large complex of conditions. Indeed, the agglomerate may contain also carbon, nitrogen and/or chlorine and their compounds, probably only in small quantities.

A point of particular interest regarding the agglomeration event is its relation to ignition of the aluminum. Under most conditions, agglomerates are already burning at the moment of detachment from the propellant surface. When ingredient aluminum particles of agglomerate size are used in a propellant, they usually ignite some distance from the burning surface (and in some laboratory experiments, fail to ignite at all). This point may seem unimportant, since ingredient aluminum particles of a size comparable to that of typical agglomerates are usually not used in practical situations. The importance lies in the demonstration that the agglomeration process is an exothermic process, occurring in a loosely connected filigree on the propellant burning surface. Further, it is the initiation point of the sustained burning of the aluminum. Its responsiveness to combustor flow conditions (Ref. 9) and gas flow oscillations (Ref. 10) is likely to be a factor in erosive burning, g-force effects (Ref. 11), slag retention, combustor stability, propellant quench limits, combustion efficiency, and product oxide droplet size role in two-phase losses.

NATURE AND COMBUSTION OF AGGLOMERATES

The foregoing sections have described how aluminum agglomerates are formed in the propellant combustion. Much of that information was drawn from earlier research on this and other projects. A substantial part of recent effort on this project has been on the nature of the agglomerates and their combustion and (next section) on the nature of the oxide droplets formed during combustion. This work was reported in Ref. 7, and is presented here in summary form.

Test Methods

Experimental studies were based on analysis of samples collected in the outflow from the burning surface of real and model propellants. Collection was accomplished by directing the flow from the burning surface into a pool of ethanol. The method quenches burning agglomerates, and collects most of the condensed material in the flow except the fine oxide smoke formed in the flame envelope of the burning agglomerates (mass of that smoke is calculated from mass and composition of the original sample and collected sample). The collected samples were subjected to a variety of analyses, including: particle size analysis; determination of unreacted aluminum content; microscopic examination; and determination of interior structure by cleaving, breaking, acid etching and heat treatment. Such studies were made as a function of distance from the propellant surface, pressure, and propellant formulation variables. The objective was to reconstruct from quench sample data the combustion history of agglomerates.

Trends of Agglomerate Populations

When samples are quench-collected close to the propellant burning surface (1.5 cm), and washed to remove smoke oxide (i.e., $< 2\ \mu m$), they are mostly aluminum agglomerates (low pressure tests), consisting of a wide size range of agglomerates with small transparent oxide lobes. At greater distances from the propellant surface, the oxide lobe portion of each agglomerate becomes relatively large (Fig. 12), and a variety of small residual oxide particles appear in the collected samples (remnants of burnout of the initially small agglomerates). Figure 13 shows a typical sequence of agglomerate mass size distributions corresponding to quenches at increasing distances from the burning surface. The area under the curves is indicative of the total weight of the agglomerates in the quench sample

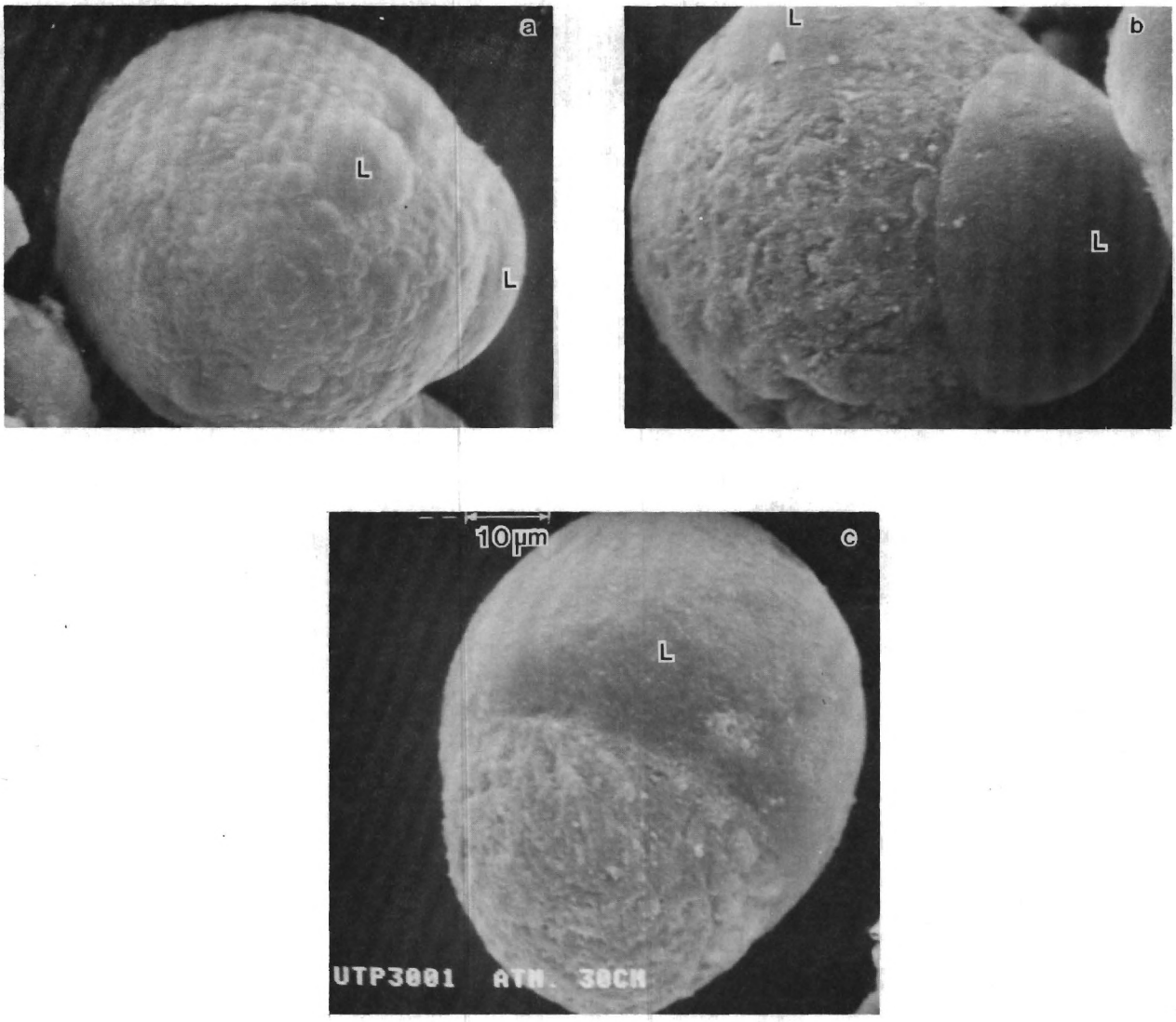

Fig. 12 Comparison of agglomerates at different quench distances, illustrating growth of relative size of the oxide lobe (test pressure 1 atm). The smooth lobe (denoted by L) is oxide. a) 1.5 cm; b) 10 cm; c) 30 cm.

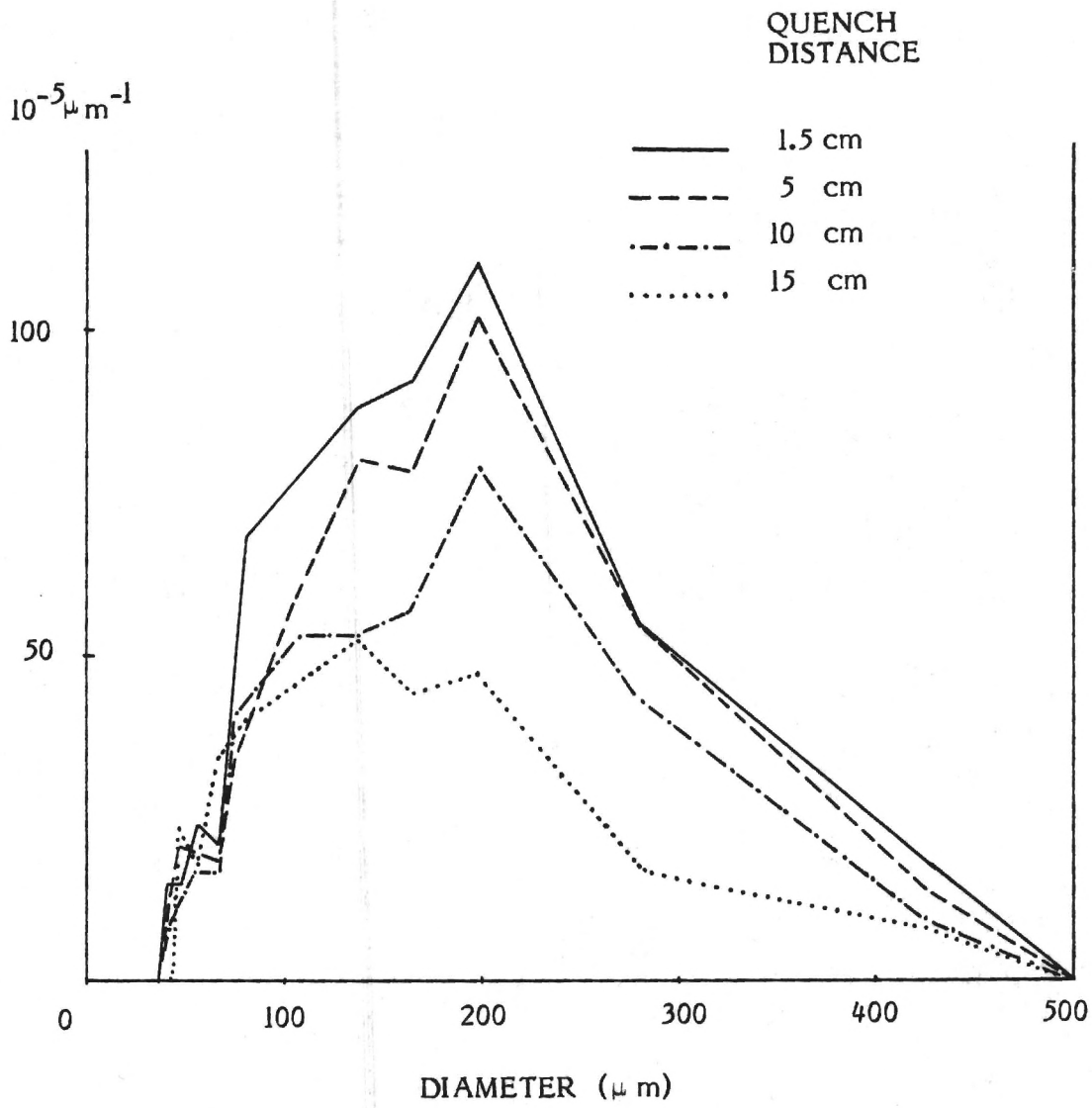

Fig. 13 Mass size distribution of agglomerates at four different quench distances (Thiokol 1780-1, 0.7 MPa test). The ordinate scale is mass per micron per initial aluminum mass.

(including oxide on the agglomerates, but excluding oxide particles). It is interesting to note that the size distribution curves don't change much with burning distance, although each particle is getting smaller and the total mass is decreasing. This relatively constant size distribution of the agglomerate population was noted earlier in an analytical study of burning agglomerate populations (Ref. 12), and is due in part to the nature of the original size distribution, and in part to the fact that some of the burned aluminum is retained on the agglomerate in oxide form, with weight gain due to the oxygen uptake. Some idea of agglomerate burning rate can be obtained from the curves in Fig. 13, in which the total agglomerate sample weight at a quench distance of 1.5 cm is about 32% of the original aluminum weight. Allowing for the weight of the oxide on the agglomerates in the sample, this corresponds to a combustion efficiency of about 78% at a distance of 1.5 cm from the propellant surface (0.7 MPa test). From estimates of flow velocity, this corresponds to 0.005 sec of burning, assuming the agglomerates started burning when they left the burning surface.

The actual aluminum combustion rate was determined by chemical analysis of the quenched samples obtained at different quench distances. The samples were analyzed for free aluminum content by dissolution in dilute HCl followed by a titration process to determine the aluminum content in the resulting solution. This measurement was made for several quench distances and for two propellants, and the results are shown in Fig. 14. These results are similar to those in previous reports on this study (Ref. 7, 13), but are considered to be more accurate because of a more accurate method for analysis of aluminum content, and elimination of igniter residue present in earlier tests. For completeness, the results of the previous tests are presented in Fig. 15 and 16. While results in these latter figures indicate an artificially high free aluminum content, the error is only about 20% of the indicated values, and the error is relatively insensitive to other test variables. The results thus provide valid trends with pressure and formulation variables. Systematic testing of the effect of relevant variables is continuing, using the improved method of Fig. 14. The collected results to date (Fig. 13 - 16) indicate:

1. An initially rapid decrease in unburned aluminum (high aluminum consumption rate), which presumably reflects burn-up of the smaller agglomerates and unagglomerated particles.
2. A drop-off in combustion rate, to a rather low rate by 10 cm from the burning surface, reflected in quenched samples consisting of agglomerates

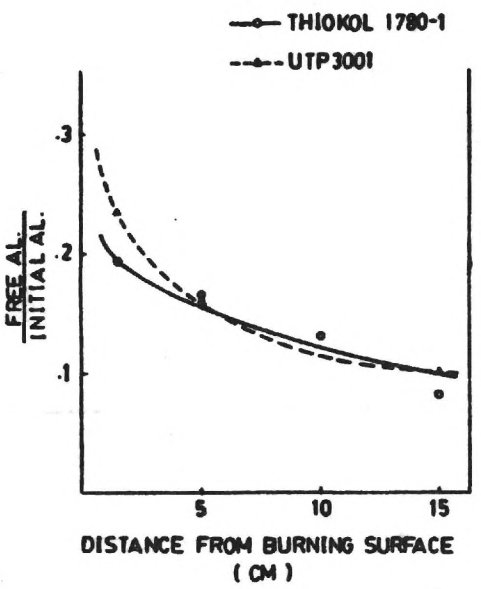

Fig. 14 Unreacted aluminum remaining at various quench distances. Tests using titration method of aluminum analysis and "clean" ignition. The ordinate is fraction of original aluminum remaining.

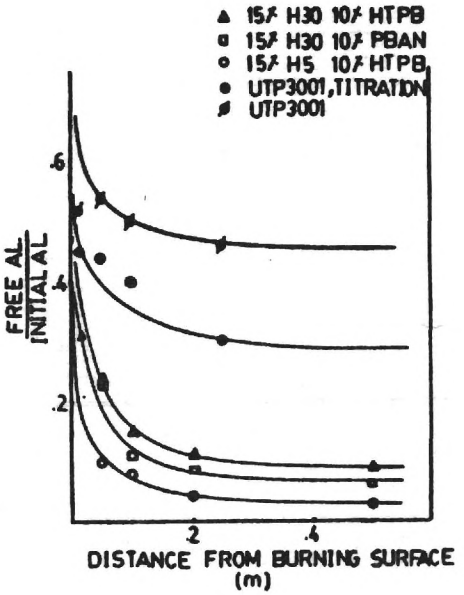

Fig. 15 Unreacted aluminum remaining at various quench distances with various propellants. Atmospheric pressure tests. Lower three curves are for propellants with 10% binder; 15% Al; 75%, 100 μm AP. All tests in this figure used ignition and chemical analysis procedure that gave a positive error in aluminum content of about 20%.

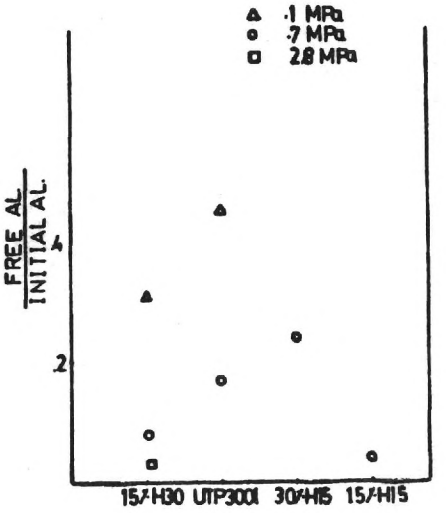

Fig. 16 Unreacted aluminum remaining at 1.5 cm for different propellants and pressures. Propellants are 10% HTPB binder; 15% Al; 75%, 100 μm AP; except as noted. Results include bias described in Fig. 15.

that now have relatively large oxide lobes.

3. A significant dependence of the observed aluminum level on propellant and test variables (Fig. 15,16).

Discussion of Chemical Analyses Results, and Outstanding Issues Regarding Agglomerate Population

The foregoing results are qualitatively consistent with the agglomerate size distribution effects in Fig. 13 and with earlier calculations of burning of droplet populations (Ref. 12). However, the results raise a number of questions that are the objects of continued study. Some of the questions relate to combustion mechanisms, and some relate to available experimental methods, which are only marginally adequate for quantitative work. These questions merit some discussion.

On the fundamental side, relatively little is known about the roles of the various oxidizing species present in the propellant combustion environment, and how they affect aluminum combustion. This means that the relevance of much past research on aluminum combustion is uncertain. Likewise, relatively little is known about the combustion of aluminum droplets with the large oxide accumulation typically present in the latter part of burning of agglomerates (e.g., beyond 5 cm quench distance in Fig. 14). Little is known about combustion of any aluminum droplets in the fuel-rich, high temperature conditions present in the propellant combustion environment at locations where the larger oxide-loaded agglomerates complete their burning. These conditions of oxide-burden and low oxidizer concentration are not very favorable for burnup of large agglomerates, and this is no doubt a factor in the "tail-off" of the curves in Fig. 14. It is also the key to the question of aluminum combustion efficiency in motors, since it is this prolonged phase of combustion that might not go to completion in a rocket motor. In this connection, one would anticipate that the outcome in the rocket motor would be quite sensitive to such variables as aluminum agglomeration, propellant stoichiometry, pressure, convective flow situations and motor stay time. These trends are implied by results of the present experiments, and generally recognized by developers of high performance motors.

Regarding the adequacy of the quenching experiment, the more serious limitations are most manifest in the same "tail-off" region that controls combustion efficiency. At low pressures, experiments are appreciably non-adiabatic and the temperature tends to drop off in the flow away from the

propellant surface even while the aluminum is still burning (Ref. 14). This is presumably due in part to the very effects one is anxious to study; retardation of reaction rate by depletion of oxidizing species and encroachment of oxide on the agglomerate surfaces. Under some conditions, the agglomerate temperature apparently falls below the oxide freezing point, a situation that virtually arrests agglomerate burning. At this point in the laboratory experiment the simulation of the nearly adiabatic rocket motor environment is totally broken down. This situation appears to have happened in the case of atmospheric pressure tests on UTP 3001 propellant shown in Ref. 7 and Fig. 15, in which combustion of aluminum seems to have ceased at about 55% burned (top curve). Visual examination of samples in this particular test sequence shows little change in appearance of agglomerates beyond 5 cm. In an earlier study (Ref. 14) of this same propellant in a similar, but larger, experimental apparatus (lower proportional heat loss), the agglomerate combustion rate at atmospheric pressure was also low, but did not appear to be arrested. Likewise, there is no evidence of arrested burning of agglomerates at higher pressure (Fig. 14), or in the service rocket motor. Thus the apparent cessation of agglomerate burning in the atmospheric pressure tests on UTP 3001 propellant seems to reflect poor simulation of rocket motor behavior late in agglomerate burning, aggravated in this case by the low pressure of these tests and relatively poor stoichiometry of this particular propellant (16% binder). As can be seen in Fig. 14, the combustion efficiency is much better at 0.7 MPa (100 psi), and a similar pressure dependence is evident with the other propellants noted in Fig. 16.

In the determinations of unreacted aluminum in the quench samples, the procedure was revised part way through the studies summarized in Fig. 14-16. Also a change was made in sample ignition method that affected results somewhat. While tests are now being re-run with the improved procedures, some of the results (most of Fig. 15 and all of Fig. 16) are based on tests by the "old" method. The trends in those tests are valid, but indicate artificially high aluminum content (and incorrect characterization of oxide products, as noted later). The original procedure for aluminum analysis was to dissolve the aluminum in HCl, wash it away, and compare dry sample weights before and after aluminum removal. It was later decided that this procedure was removing some of the oxide as well (see later), giving an indicated aluminum content higher than the true value. A further source of error resulted from use of an igniter paste on the propellant samples that

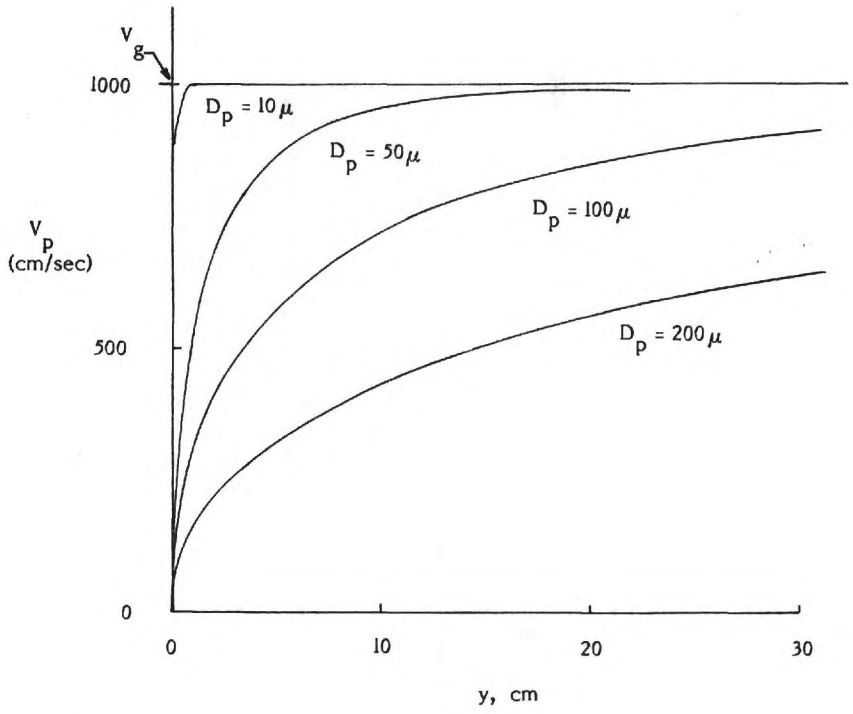

Fig. 17 Agglomerate velocity vs distance from the burning surface (calculated, see Ref. 12).

contained titanium and boron. The data in Fig. 15 and 16 are affected by these error sources, but were included because the error is only about 10-20%, and the repeat tests were not completed at report time. The tests summarized in Fig. 14 used a nonmetalized igniter paste, and an improved method of determining free aluminum content that measured the amount of aluminum directly rather than by weight differencing.

One further experimental problem, applicable particularly to short quench distances and fast-burning samples, is related to determination of the actual time-to-quench. As noted in Ref. 12, large agglomerates do not come up to speed as fast as small ones when they leave the propellant surface. (Fig. 17 shows the result from Ref. 12, which is for an upward flowing plume.) Further, the actual distance to quench depends on undetermined details of the alcohol behavior during the test. Finally, at higher pressures, the burning rate increases producing a higher mass flux in the tube. Correspondingly, the density and velocity of the gas flow change. Thus even small particles which convect at the gas velocity would experience different burning times if quenched at the same distance at different pressures. The problem of nonuniform, nonconstant velocity near the propellant surface is common to all quench experiments; but could be circumvented by use of

complementary combustion photography tests if deemed sufficiently important. The problem of uncertainty about the site and details of the quench event is being attacked by a modified design of the experiment that controls the location of the alcohol surface. In the present work, testing at high pressure would have been more extensive if these problems could have been resolved. Regardless of quantitative problems, such tests did provide comparative results at different pressures, and provided information on pressure effects on the detailed nature of agglomerates and oxide products, described in the following.

Nature of Agglomerates

In discussing combustion of aluminum agglomerates, it is often assumed for convenience that they are aluminum droplets, or aluminum droplets with oxide lobes. Experimental investigators are generally aware that the agglomerates are much more complex (Ref. 14, 15). These added complexities may not be important during much of the burning period of the agglomerate, but they merit study for at least two reasons. First, they provide information about how agglomerates are formed. Second, the complexities become important in the later, slow burning part of the agglomerate burning history, and the transition to residual oxide droplets.

The external appearance of quenched agglomerates was shown in Fig. 12. The trend with burning time is qualitatively independent of the initial agglomerate size, pressure, and propellant formulation, except under marginal conditions noted before, when the agglomerate droplet temperature drops low enough to allow flame collapse and oxide freezing. Examination of the interior of normal agglomerates reveals a relatively complex structure (Ref. 7). Cleaved agglomerates show voids, of non-characteristic shape, size and location (Fig. 18). Voids are larger in low pressure tests and early in burning, and usually include one under the oxide lobe (making it somewhat like a bubble early in burning). Agglomerates from atmospheric pressure tests are fairly soft, while agglomerates from tests at higher pressure are brittle and don't cut easily. These trends have not been studied thoroughly (e.g., as a function of propellant composition). Void volume was generally less than 15% of agglomerate volume, except in atmospheric pressure tests.

Another feature of the interior of the aluminum lobe of the agglomerate is revealed by careful acid etching to remove the aluminum. It is found that the interior contains an intricate structure of oxide flakes (See Fig. 11.). These

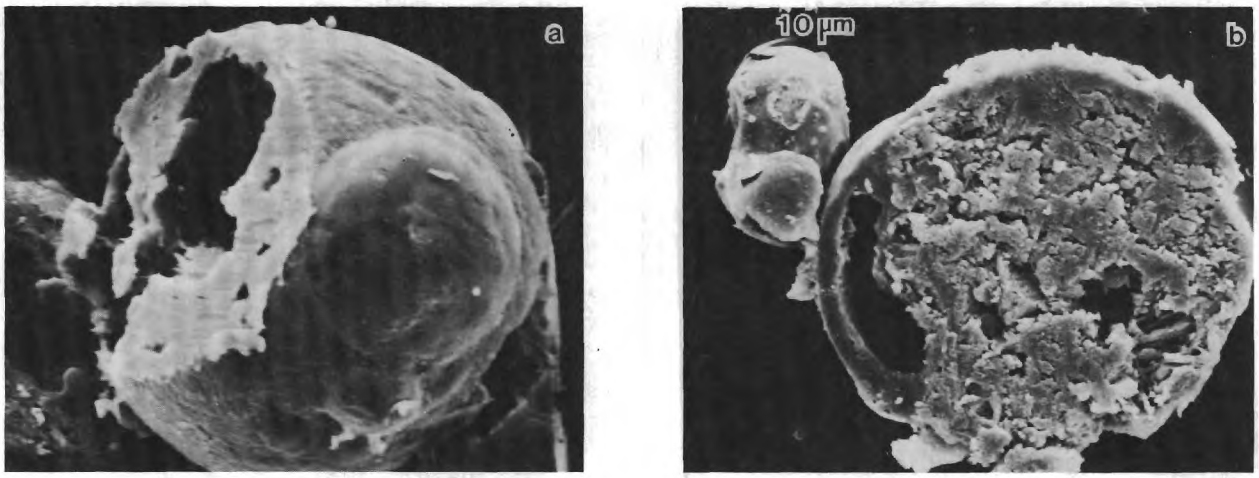

Fig. 18 Agglomerates cleaved to show interior.
a) Soft agglomerate from atmospheric pressure test.
b) Brittle agglomerate from test at 2.8 MPa.

structures are not recognizable in cleaved samples, but are evidently responsible for the brittle quality of agglomerates from quench tests at elevated pressure. The flake structure is much more extensive in agglomerates from tests at elevated pressure.

The inhomogeneous nature of the aluminum section of the agglomerate poses two practical questions suggested above. First, does the inhomogeneity have any significant effect on combustion? Is it telling us something about formation of agglomerates? The answers are speculation at present. As indicated in Fig. 9-11, the agglomeration event involves the melt-down and coalescence of a very complex structure, under the influence of surface tension forces of the molten aluminum. It seems likely that this event would trap some solid oxide shell structures in the interior of the agglomerate, and that this insoluble oxide would change during inflamation, into thin molten films in the interior of the agglomerate. If the melt-down and coalescence of the accumulate is gradual enough (e.g., at low pressure), the aluminum probably withdraws into a sphere with the oxide changing from a solid aggregation on the surface to a molten oxide lobe. At higher pressure, coalescence is more abrupt, and more oxide aggregate is trapped inside the

agglomerate. The test results suggest that trapped aggregate is first converted to very thin oxide sheets, insoluble in the molten aluminum, which become concentrated as the aluminum evaporates away. If the agglomerate is quenched, the films apparently freeze into the flake arrays noted above and in Fig. 11. It seems likely that it is these flakes that make agglomerates brittle.

Regarding the voids in the agglomerates, there is no direct evidence as to their source. They may be blown by aluminum vapor, or possibly formed by gas entrapment during coalescence as suggested by agglomerates frozen during coalescence (Fig. 10). Given the complexity of the accumulate, the coalescence event and the gaseous environment, there is no shortage of hypotheses. There is no clear evidence that the voids affect burning, except as they affect agglomerate surface area to mass ratio. They will cause agglomerates to weigh less than would be judged on the basis of visual (motion picture) observations of diameter.

The aluminum agglomerate is typically characterized as an aluminum droplet with an oxide lobe as in Fig. 12. Actual characterization of the oxide lobe has proven to be difficult because its character changes during burning, is different at different pressures, and depends on the propellant. In general, the oxide lobe appears to be more well defined in low pressure tests. This is very likely due to greater pre-ignition oxidation of accumulates at low pressure, and more complete coalescence of the oxide into a lobe (as opposed to formation of flakes in the aluminum lobe) at low pressure. The oxide lobes increase in size during agglomerate burning at low pressure, and tend to change from transparent to white as burnout is approached (inferred from agglomerate size distribution trends and detailed agglomerate features). The data at higher pressure are too sparse to identify trends, but oxide lobes on agglomerates are less conspicuous, suggesting that more of the oxide is inside the agglomerate and/or that less oxide is formed or retained on the agglomerate.

It is relevant to raise the question of final fate of an agglomerate that is near burnout, and dominated by the oxide lobe (Fig. 19). During burning, the flake oxide is concentrated in the contracting aluminum lobe, and may concurrently be reduced to lower oxides and/or flow into the oxide lobe (or neither). During this burnout stage, the state of the droplet's flame envelope is a matter of speculation. The fragmentation events observed in many studies in non-propellant environments apparently do not consistently occur, because oxide droplets continue to be added to the population in sizes comparable to the residual oxide in the agglomerate that are burning out. This will be examined in greater detail in the next section.

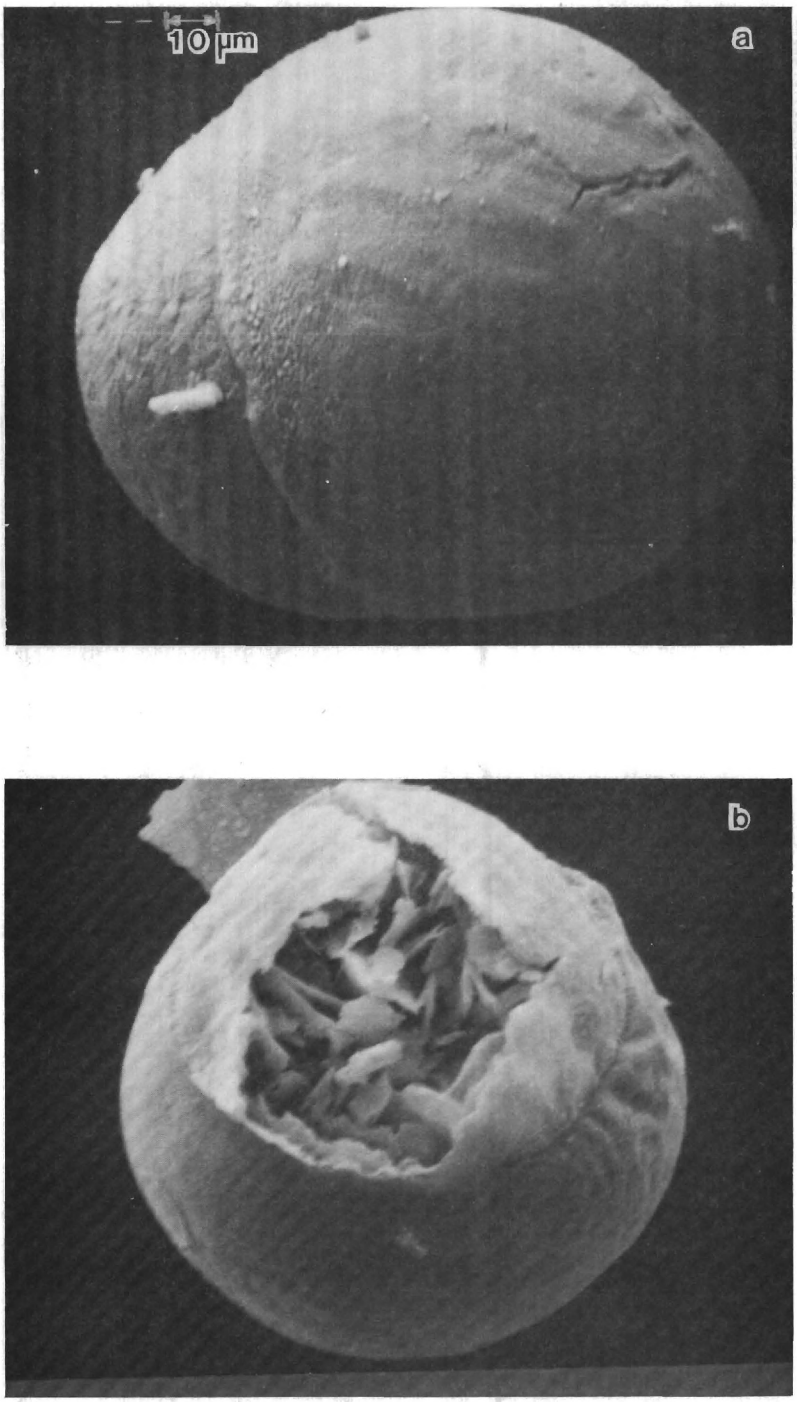

Fig. 19 Agglomerates quenched near burnout. Atmospheric pressure tests.
a) As quenched.
b) Acid-etched.

PRODUCT ALUMINUM OXIDE PARTICLES

It has often been noted (Ref. 16-18) that burning of aluminum droplets leads to two kinds of oxide product droplets, i.e., "smoke" formed in the flame envelope of the aluminum droplet, and "residual oxide" droplets left over when the agglomerates burn out. These are two entirely different populations of droplets, the former being generally less than two microns in diameter and the latter being substantially larger. Being governed by different formation processes, their size distributions are subject to entirely different constraints. In particular, the residual oxide droplet size distribution is linked to the agglomerate size distribution, and hence to all the processes discussed above that govern agglomerate size.

The importance of the combustion-generated size distributions was noted earlier. The effects on combustor stability, component erosion, thrust loss, etc., depend on the details of the size distribution. The effects cannot be fully characterized in practice without consideration of subsequent population changes in the combustor and nozzle flow, a subject beyond the scope of the present study. However, calculations of populations in the flow field cannot be made properly without use of correct starting populations, which are the combustion-generated ones discussed here. Particular attention was paid here to the residual oxide droplet population because, although it represents only 5-20% of the total oxide, its role in motor performance problems is relatively large, relatively unpredictable, and closely related to other aspects of the present study.

Kinds of Oxide Particles and Size Trends

Quenched samples yield a variety of particles other than agglomerates. After all the smoke particles are washed away (separated from the larger particles by repeated sedimentation-decanting operations), the remaining particles consist of white oxide spheres, transparent oxide spheres, and various debris originating from igniter materials and carbonaceous binder residue. In previous reports (Ref. 7, 13), reference was made to black shiny spheres thought to represent a burnout transition state between agglomerates and white oxide spheres. These have been found to be a product of igniter paste, used in those tests, that contained titanium and boron. While black shiny product spheres have been reported in the past from tests that did not use such igniter materials, none have been obtained in recent

tests on this project using a nonmetallic igniter paste.

In this report, the combination of white and transparent oxide particles and of oxide contained on and inside agglomerates is referred to collectively as "residual oxide", because it consists of that oxide that is believed to be converted to relatively large "non-smoke" oxide when agglomerates burn out. White and transparent oxide particles are the product of those agglomerates that are already burned out. Their external appearance is illustrated in Fig. 20. The transparent oxide particles represent a relatively small portion of the residual oxide. They are generally less than 35 μm, and of smaller average size than the white oxide particles. The size distributions of the oxide particles is illustrated by Fig. 21. These results correspond to the agglomerate size distributions in Fig. 13. The ordinate in Fig. 21 is normalized by a mass corresponding to complete oxidation of all of the aluminum in the propellant sample, referred to below as "ultimate" oxide. Thus, the curves corresponding to longer quench distance have larger ordinates; the area under each curve is indicative of mass fraction (of ultimate oxide) in the particular sample. The jagged nature of the curves is due to the rather crude method of determining the mass in different size intervals. The method consists of sieve-sizing the test samples, weighing the size fractions, and visually determining the relative number of agglomerates vs oxide particles in each size interval. No correction was made for difference in density of particles.

From the particle size distributions, it appears that particles on the small end of the distribution (transparent oxides, typically 20-25 μm continue to be formed as the flow moves away from the burning surface. This suggests that the small transparent oxide particles are not simply the residue of burnout of the smaller aluminum droplets (in fact very few oxide particles are present in samples quenched 1.5 cm from the burning surface). Since the transparent oxide particles continue to be formed further downstream, they can presumably be produced from the initially large agglomerates remaining further downstream, possibly by expulsion during burnout, or by fragmentation. At the same time, increasingly larger oxide particles (white oxide) are added further downstream, indicating that the initially large agglomerates that burn out further downstream make larger residual oxide droplets as well. At this point it is not determined whether the continued growth of both ends of the size distribution is a consequence of alternative modes of agglomerate burnout, or a mode of burnout that typically produces both kinds of oxide particles.

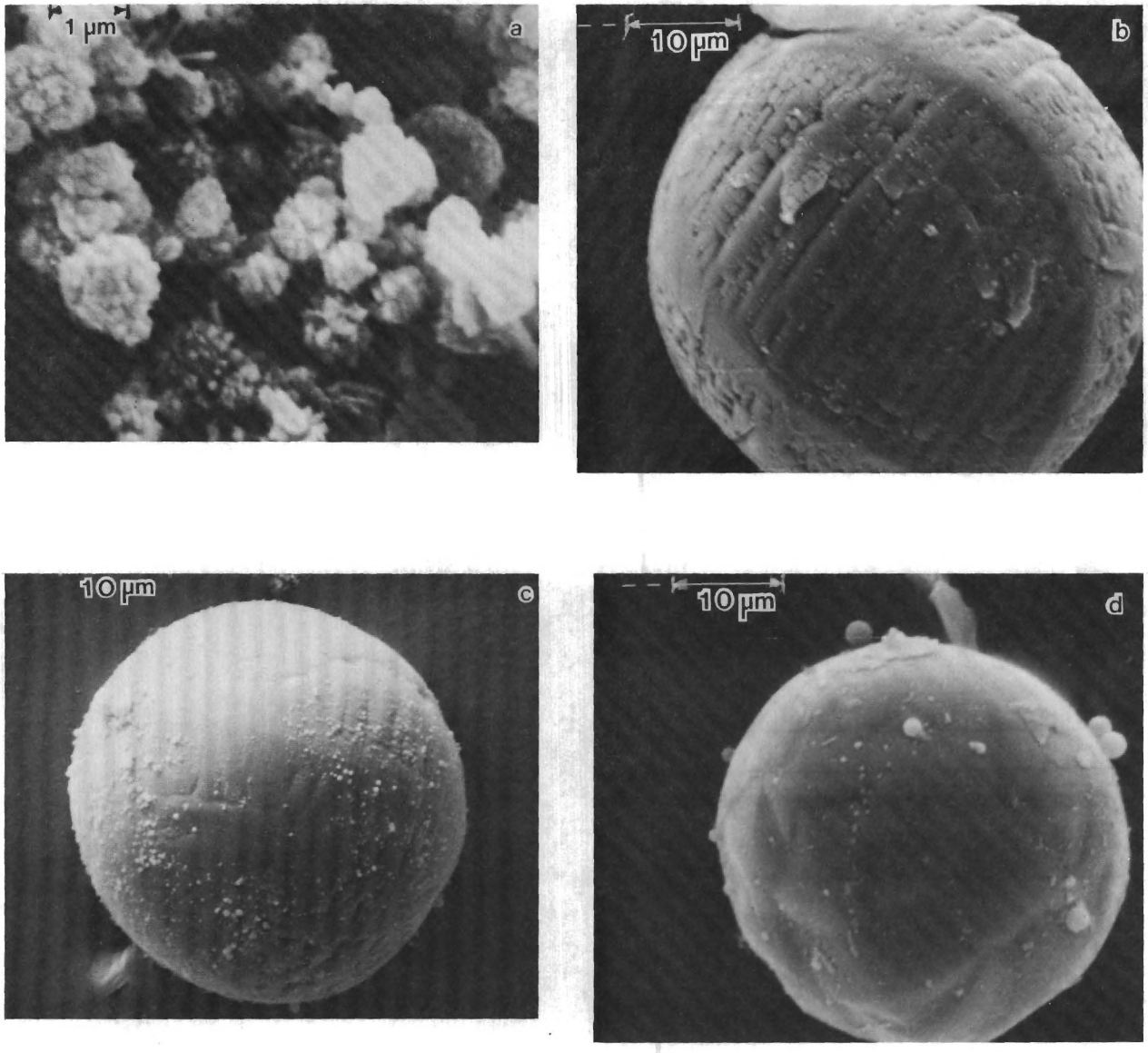

Fig. 20 Exterior appearance of oxide particles.
a) Smoke oxide (2.8 MPa test).
b) White oxide (atmospheric test).
c) White oxide (2.8 MPa test).
d) Transparent oxide (2.8 MPa test).

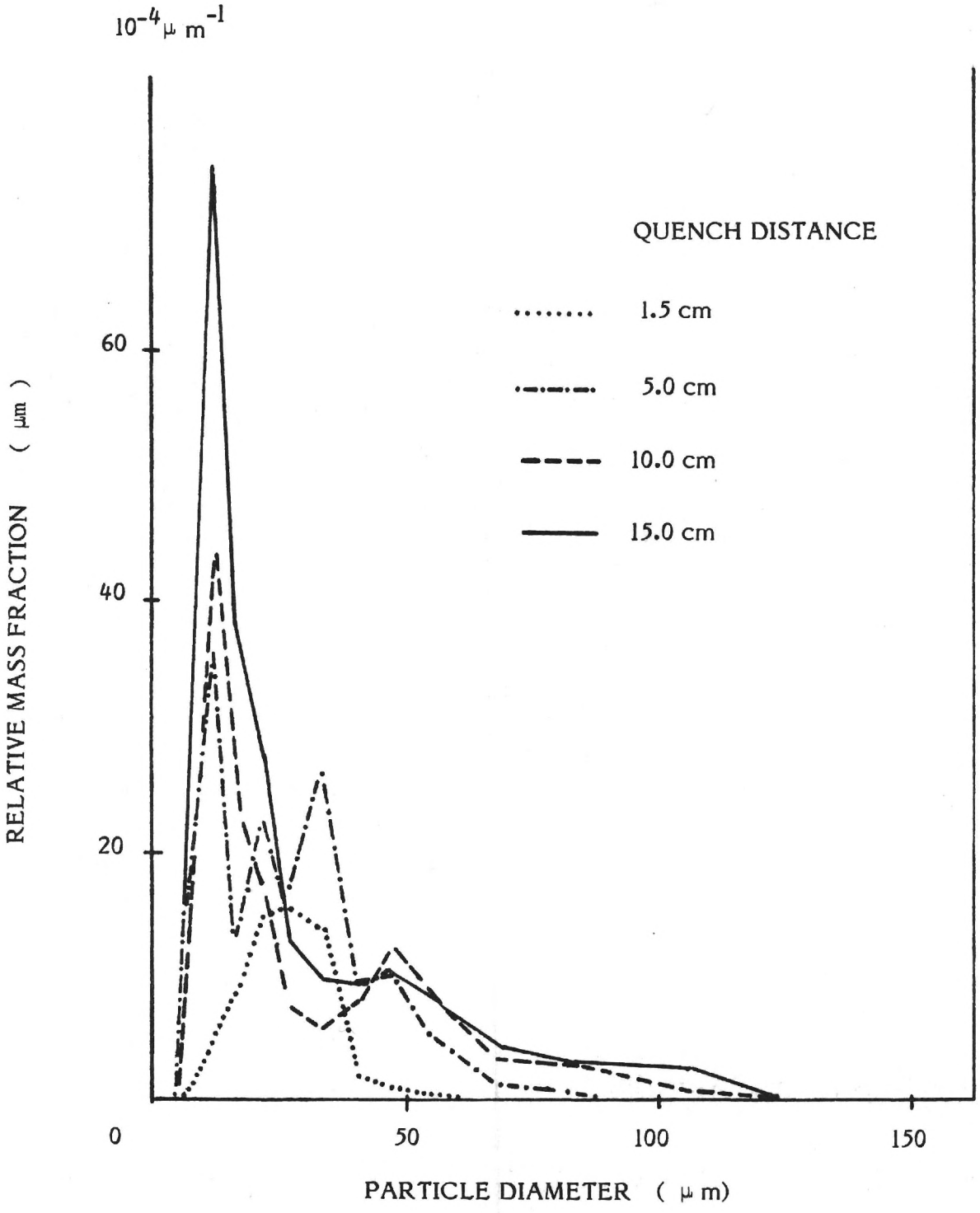

Fig. 21 Oxide particle size distribution; Thiokol batch 1780-1, test pressure 0.7 MPa. (Smoke "oxide" was removed from samples. Mass fraction is based on mass compared to oxide that would result from conversion of all original aluminum.)

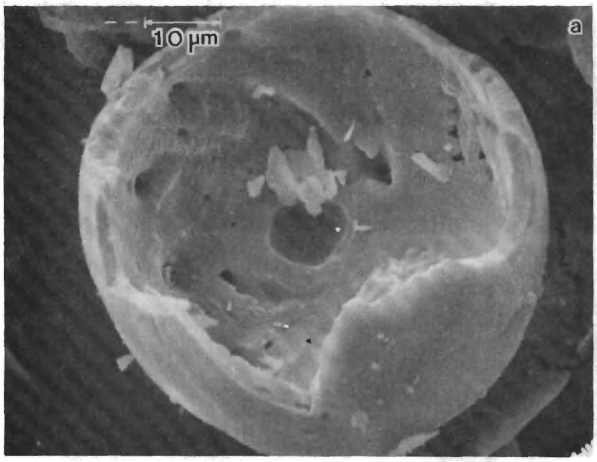

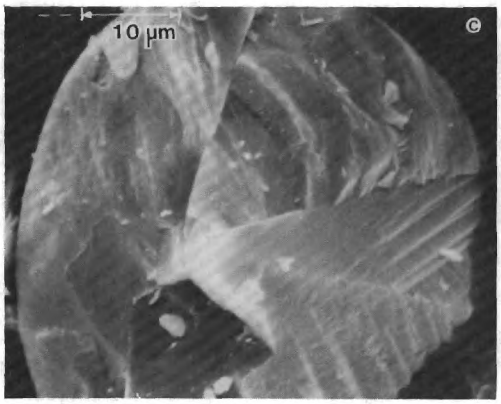

Fig. 22 Interior of oxide particles.
a) White oxide (atm).
b) White oxide (2.8 MPa).
c) Transparent oxide (2.8 MPa).

Detailed Nature of Oxide Particles

The nature of oxide particles was examined by microscopic study of the exterior surface, and of the interior as revealed by broken particles. Particles were subjected to acid etching and to observation during heating to 1200°C. The exterior appearance of the particles is shown in Fig. 6 and 20. White oxides are nearly spherical, but show surface striations suggestive of crystallization patterns (especially at atmospheric pressures). In an optical microscope, transparent oxides look like glassy spheres, but SEM's show them to be slightly irregular in shape.

The interior nature of transparent oxide particles is glassy and void free (Fig. 22). The interiors of white oxide particles are extraordinarily complex (Fig. 22), with a typically sponge-like structure. White oxide particles recovered from atmospheric pressure tests are often hollow with nearly 40% void. The appearance

is believed to be a consequence of conversion of the oxide-capped, flake-containing agglomerates during the slow burning and burnout phase of the agglomerates. The oxide lobe and flake oxide apparently do not coalesce completely into a homogeneous droplet, even though surface tension seems to close the exterior surface. This interpretation of the origin of white oxides is consistent with the appearance of agglomerates captured in the late stage of burning.

The oxide particles show no reactivity when placed in 3% HCl in water for prolonged periods of time. The particles show no change when heated to 1200°C in argon or oxygen.

Relative Mass of Different Forms of Oxide

In the present studies, the oxide reaction products have been classified as either "smoke" or "residual". The former constitutes the majority of the oxide, is in particle sizes under 2 μm, and is produced in the detached flame envelope around the burning agglomerates. In the experiments reported here, these particles were not subjected to detailed study. They are only partially captured in the quench experiment and were removed from the sample to facilitate study of the agglomerates and residual oxide. The total weight of smoke oxide could be determined by mass balance, since all other weights were measured. Smoke masses so determined are reported in the following.

The term "residual oxide" refers to all the oxide remaining in the sample after the repeated washing (sedimentation and decanting) operations. This includes transparent oxides, white oxides, and oxide on and in the agglomerates. The oxide on and in the agglomerates consists of the oxide lobes, flake oxide, and surface oxide (surface oxide probably is minimal except under adverse burning conditions). In a previous section, it was noted that the mass of unreacted aluminum was determined by a solution-titration method. The mass of residual oxide was taken to be the difference between the initial weight of the washed sample and the unreacted aluminum weight so determined. The smoke oxide mass was then determined as the difference between the total oxide (based on the mass of aluminum consumed) and the residual oxide weight. Fig. 23 shows the trend of residual and smoke oxide with quench distance for several test conditions (masses have been normalized by dividing by the mass of the total oxide that would result from oxidation of all of the aluminum in the test sample). Also shown is the ratio of residual oxide to smoke oxide for the tests reported. The trend of oxide masses

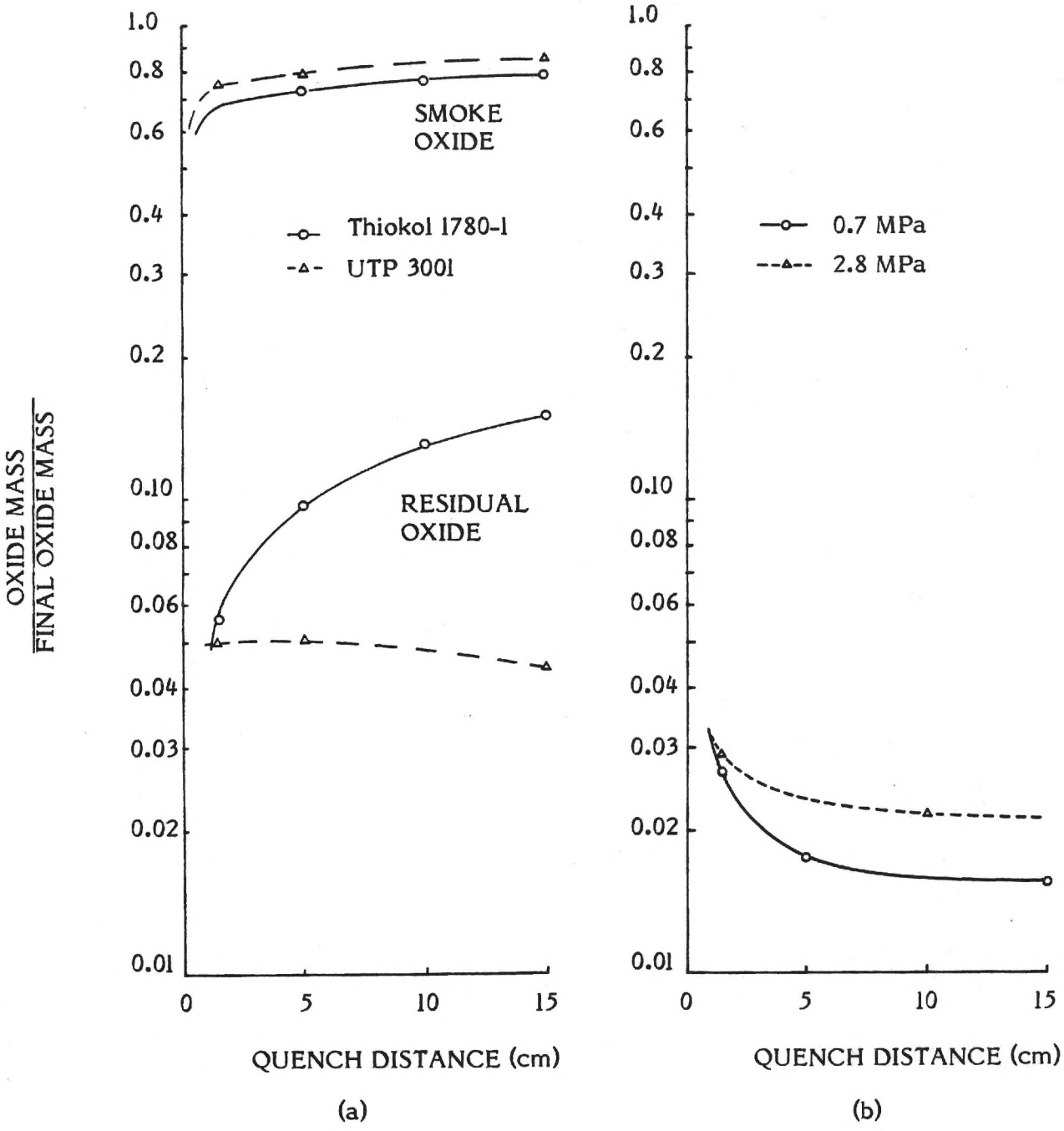

Fig. 23 Oxide mass fractions vs quench distance.
a) Smoke and residual oxide for UTP 3001 propellant and Thiokol batch 1780-1, test pressure 0.7 MPa.
b) Mass fraction of residual oxide in flake form for UTP 3001 propellant at two pressures.

with quench distance simply reflects the consumption of aluminum shown in Fig. 14 and 15. The trend at large distances is pressure and propellant dependent, but indicates that final residual oxide totals 5-15% of oxide formed and smoke 95-85%. The ratios of residual oxide to smoke oxide are slightly dependent on pressure and quench distances, although it appears that the nature of agglomerate combustion is not critically sensitive to time during agglomerate burning or other conditions. On the other hand, it is clear from collected results that instances of rapid consumption of aluminum correspond to conditions that produce small initial agglomerate size, and that the size of the white oxide particles is then correspondingly small.

One further aspect of the quenched samples was examined by determinations of mass fraction, i.e., the relative amount of residual oxide in flake form, and in consolidated (i.e., oxide particles and lobe) forms. It was found that the structure of the oxide flake was so delicate that it would break up during acid etching of agglomerates and as a result could be carried away in the washing operation. Oxide samples remaining were weighed, and the mass was compared with the higher total residual oxide masses indicated by the acid dissolution-titration method. The difference in the two masses was assumed to correspond to the mass of flakes removed in the acid etch-washing operation. While this method gives somewhat erratic results for flake mass, some useful results are evident. In interpreting results, it should be remembered that the flake oxide is distinguishable only when it is still dispersed in the aluminum lobes of agglomerate particles, becoming an indistinguishable part of the residual oxide particles upon burnout. In the plume, flake oxide is thus progressively converted to residual oxide as the smaller agglomerates burn out. At a quench distance of 1.5 cm, the indicated amount of flake oxide is roughly 1-4% of the "ultimate" oxide, suggesting that the mass of accumulated oxide engulfed during agglomerate formation is of this same order. This is an estimate of pre-agglomeration oxidation of aluminum on the propellant burning surface (the estimate is somewhat low, because even at 1.5 cm quench distance, some of the smaller agglomerates have burned out and converted their flake oxide to residual oxide). The argument that flake oxide is progressively converted to residual oxide by agglomerate burnouts is affirmed by the decreasing trend in flake oxide with increasing quench distance (Fig. 23). Flake mass also appears to depend on propellant composition and pressure, but present data are not sufficient to establish quantitative trends. A possible exception is the trends for

UTP 3001 propellant, which has shown unusually slow combustion of aluminum in the plume (Fig. 15). This propellant also shows low sensitivity of flake oxide mass to quench distance, and lower flake mass at higher pressure, probably both attributable to slow agglomerate combustion rate, improving with increasing pressure.

COMBUSTION OF DRY-PRESSED MIXTURES OF ALUMINUM AND AMMONIUM PERCHLORATE POWDERS

Combustion of the aluminum ingredient in composite hydrocarbon binder propellants is a consequence of the availability of oxidizing species provided by decomposition of the solid oxidizer. However, the detailed accumulation-agglomeration-metal ignition process is substantially determined by events other than molecular level oxidation. In order to unravel the roles of different steps in the propellant combustion process, it is helpful to determine just how much of the aluminum "metabolism" is due purely to interaction with the ammonium perchlorate oxidizer. It had been established before that aluminum could survive the environment on the surface of burning ammonium perchlorate for an appreciable time (Ref. 19, 20) without ignition, while there are some recent conflicting claims that intermediate reaction products of AP (present primarily in the AP decomposition-flame zone) might be particularly important to ignition of aluminum (Ref. 21). Previous work on the present project had confirmed a substantial body of literature (e.g., Ref. 22-24) concerning the protective character of the oxide "skin" on aluminum particles. Those collected results had indicated that temperatures in the range 1200 to 2030°C might be required to ignite particles. The AP flame would thus be marginal as an ignition source. However, the ignition requirements referred to in Ref. 22 to 24 were not determined in chemical environments typical of an AP deflagration wave, nor on assemblages of aluminum particles typical of propellant burning surfaces. Thus it was important to determine whether accumulating aluminum on an AP burning surface would adhere there (as implied by results in Ref. 11, 19, 25 and elsewhere), and if it would, whether it would sinter, ignite, and agglomerate.

In order to resolve these questions, combustion tests were run on hard-pressed (175 MPa) samples of Al/AP powder mixes. Tests consisted of interrupted burning by rapid depressurization, and combustion cinemicrophotography. Tests were run with different mixture ratios of Al and AP, different particle size combinations, different kinds of aluminum powder, and different pressures. A summary of test conditions is shown in Table 1, and a description and interpretation of results was reported in Ref. 20. These results indicated the following critical points about aluminum behavior and Al-AP interactions:

Table 1
Summary of Tests on Dry-Pressed AP/Al Mixtures*

Sample / Pressure		85% 10 μm AP 15% 5 μm Al (H-5)	85% 60 μm AP 15% 30 μm Al (H-30)	85% 100 μm AP 15% 30 μm Al (H-30)			85% 100 μm AP 15% 95 μm Al (H-95)		
MPa	PSI	Movie	Movie	dp/dt Quench	Movie Hi Mag	Movie Lo Mag	dp/dt Quench	Movie Hi Mag	Movie Lo Mag
4.2	600			✓✓✓ ✓			✓✓✓ ✓		
5.5	800			✓	35	38		5, 9, 13	c
6.9	1000	55	57	✓✓✓	33	4	✓✓✓	1,10,14	

* Check marks denote tests. Number identify the pertinent film.

1. Aluminum particles do not ingite in the AP deflagration zone (propellant-ingredient-size particles).
2. Aluminum adheres to the deflagrating AP surface, and under most conditions accumulates there. Accumulation is very limited where the aluminum particles are comparable in size to the oxidizer particles; those (large) aluminum particles do linger on the surface, but the spacing of the particles is now large enough to reduce chances of a surface particle being joined by underlying particles as occurs with small Al particles.
3. Accumulation of aluminum on the AP surface leads to rigid assemblages on the burning surface that eventually break up and detach. Break-away is usually followed by local inflamation of the accumulate. This appears to occur at break points in the detaching crust, followed by spread into the rest of the crust.
4. The spreading inflamation leads to formation of several large agglomerates, that appear to burn thereafter much in the manner observed with propellants.

The foregoing observations were based on the motion picture tests. Quench tests yielded relatively little evidence of surface accumulation of aluminum, which apparently detached during the depressurization quench.

The test results are interpreted as follows, in the light of earlier tests on behavior of aluminum powders during heating (Ref. 5, 8, 26). Upon being reached by the receding surface of the sample, an aluminum particle adheres to the surface, which is generally believed to consist of a froth layer at a temperature of about 600°C. The particle probably proceeds to higher temperature under the influence of the nearby AP flame, while continuing to reside on the surface. Underlying aluminum particles emerge and join the original ones, concentrating into contacting arrays. The oxide skin on each particle apparently limits aluminum oxidation to a continuing build up of surface oxide. This includes sintering of the particles to each other when they are contacting. As the sintered layer becomes more dense and more heavily oxidized, it becomes resistant to flow of gas from the underlying AP, and also resistant to heat flow from the AP flame to the AP surface. Under these conditions, the layer would be expected to be above the aluminum melting point, and the structural strength would be due to the sintered solid oxide structure that encases the aluminum. This structure in turn is stressed by the gas through

flow, and the stage is set for break-up of the sintered accumulation.

Break-up of the accumulation implies local break up of the oxide that has been "protecting" the aluminum, which promptly increases its oxidation rate and locally heats the sintered structure. Under favorable heat-flow conditions, this can lead to progressive breakdown of adjoining sintered structure, i.e., inflamation. Alternately, aluminum exposed in a break may simply be covered over by new solid oxide, which the AP flame is unable to melt. Both alternatives apparently occur, sometimes in the same test. The inflamation alternative is believed to proceed as follows. A breaking section of the accumulate with exposed molten aluminum self heats due to oxidation of exposed aluminum. This is aided and sustained by limited flow of aluminum under surface tension forces, with associated continual mechanical degradation of any newly forming oxide skin. Heat release goes primarily to heat-up of those particles that are actually reacting, which are insulated from their colder, unignited neighbors by the very oxide that sinters them together. Local self heating melts the protective oxide locally, permitting local coalescence of aluminum "particles" (Fig. 10a), retraction of insoluble oxide from the metal surface, and establishment of a high temperature aluminum vapor flame (photographically manifested by rapidly increased brightness and establishment of the characteristic luminous smoke trail). This state is sometimes reached at more than one site in large accumulates, and leads to a rapid propagative heat-up, oxide melt-down, and inflamation of the accumulate and transformation to one or more burning agglomerates.

While the foregoing scenario is very complex, the observed combustion behavior is hardly amenable to a simple explanation. The interpretation rests on a great deal of information about the real behavior, including not only the combustion of AP/Al samples, but also on behavior of single aluminum particles and powders. The scenario explains why larger unsintered particles don't ignite (no means to break down the oxide skin); why heavier sintering and non-ignition can occur at lower pressure (low oxidizer concentration and poor heating from the oxidizer flame permit protective oxidation of break-up surfaces); and why vigorous combustion can occur when typically reluctant ignition is finally achieved (transition to vapor phase burning). The scenario also has major implications for aluminum behavior in propellant combustion:

1. Ignition of accumulating aluminum will generally depend on exposure to high temperature flames resulting from AP-Binder interaction (i.e., the AP flame alone is not enough). Conditions that delay this AP-Binder flame exposure will yield prolonged accumulation and large agglomerates.

2. Vigorous inflamation of accumulates on or near the burning surface is favored by large specific surface of aluminum (small particles), because the eventual breakup and coalescence of the accumulates at the surface is then a highly exothermic event. Large single aluminum particles ignite further from the surface because the protective oxide won't break down at temperatures near the burning surface, even when the particles linger long enough to heat up to surrounding temperature.

3. The size of agglomerates in propellant combustion is generally recognized to be strongly affected by the degree of segregation of aluminum particles in the propellant microstructure, with local concentrations ("pockets") of aluminum tending to form single agglomerates. It is also recognized that this criterion for agglomerate size is modified by the susceptibility of the accumulating aluminum to ignition, which event usually causes the accumulated aluminum to detach from the propellant surface. In this context it is important to keep in mind that the AP flame will not cause ignition, a fact that accounts for the massive accumulations on the surface of AP/Al samples. Under adverse ignition conditions, accumulated aluminum on the burning surface of propellants may also end up on the surface of oxidizer particles of the propellant and remain during all or part of the burning of the oxidizer particle. Under some conditions (notably low pressure), delayed ignition can even give rise to interconnection ("bridging") of local accumulations to give the more massive accumulations observed with AP/Al samples. In that case, correspondingly large agglomerates may be formed.

STUDY OF THE ACCUMULATION-AGGLOMERATION PROCESS USING AP-BINDER SANDWICHES WITH ALUMINUM FILLED BINDER

One of the primary problems in the study of accumulation and agglomeration of aluminum in a propellant is the chaotic nature of the propellant on the dimensional scale of the relevant processes. In effect, it is impossible to describe what was tested or what happened. On the other hand, some success had been achieved in a companion project to the present one, through testing sandwiches of AP and binder. A sandwich consists of two layers of pre-pressed sheets of ammonium perchlorate (oxidizer) with a layer of binder (fuel) of controlled thickness cured between the sheets. Such systems do not provide the intermittency of microstructure present with granular mixes but they simplify the geometry of the combustion zone and separate the ingredients of the propellant into precisely definable regions providing a better understanding of the flame structure and greater resolution by experimental methods. Using aluminum in the binder lamina provides a means to conduct controlled accumulation-sintering-agglomeration experiments in a combustion environment simulating critical aspects of real propellants.

The investigation of aluminum combustion in sandwiches consisted of preparing sandwiches with various combinations of binder, aluminum and oxidizer in the fuel lamina; edge burning the sandwiches at various pressures; and observing combustion behavior by photography and by microscopic study of quenched samples (quenched by rapid depressurization). Fig. 24 gives the matrix of test conditions used. Only a limited number of tests with photography were run, but quench tests were run at all the indicated conditions, and two tests were run at some test conditions to determine reproducibility.

Results of Sandwich Quench Tests

All test results described below were for binder lamina thickness between 60 and 90 μm. With pure binder laminated sandwiches, it is observed on quenched samples that the binder is slightly recessed at low pressure (1.4 MPa) and is protruding at high pressures (6.9 MPa) (Fig. 25) (Ref. 19, 27, 28). The AP burning rate adjacent to the binder is retarded, with the maximum regression of the surface occuring at about 100 μm from the interface. There are bands of relatively smooth AP surface running along the edges of the interfaces in all samples. These features

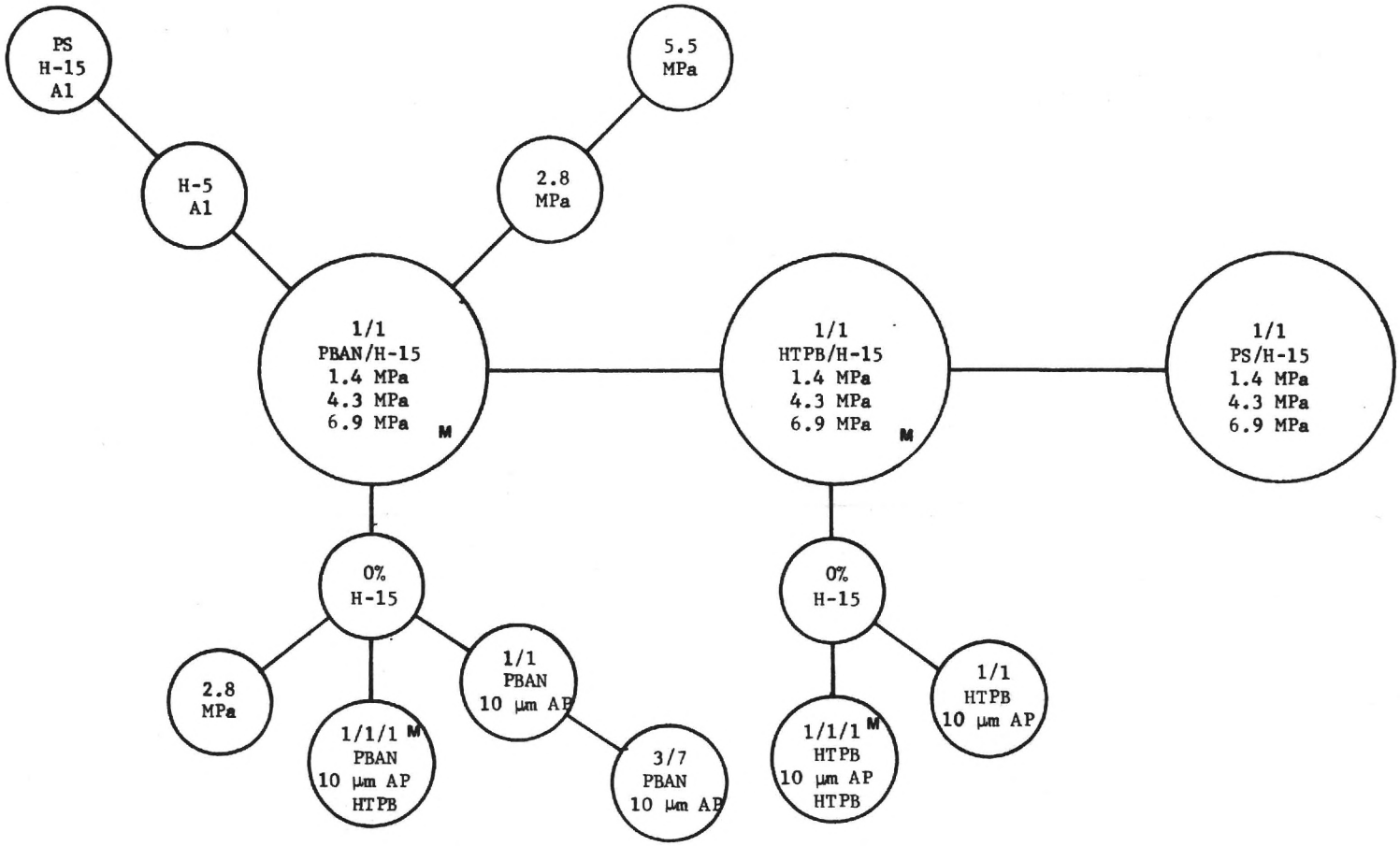

Fig. 24 Summary of conditions for sandwich burning tests (large circles denote primary burning tests (large circles denote primary conditions, small circles denote variants on primary conditions). (M denotes combustion photography.)

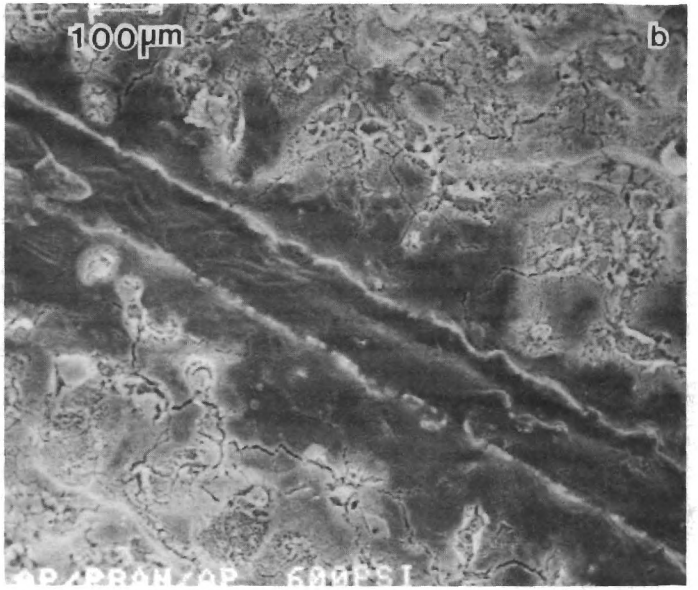

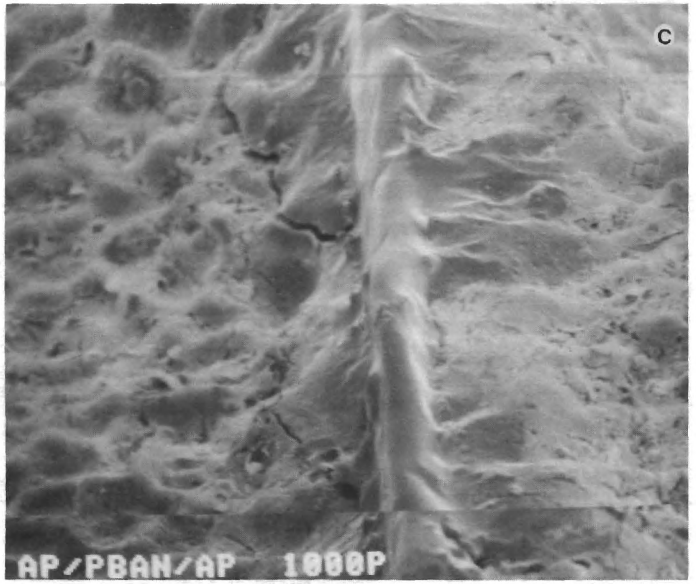

Fig. 25 Examples of quenched AP/PBAN sandwiches.
a) 1.4 MPa, b) 4.1 MPa, c) 6.9 MPa.

did not change with type of binder except that polysulfide has a drier appearance.

The general effect of addition of aluminum to the binder lamina is illustrated in Fig. 26 by samples with a 1/1, PBAN/H-15 Al lamina. The accumulated aluminum is visible on the binder lamina, and has the appearance of being wetted by molten binder. The volumetric loading of aluminum in the lamina is less than 50%, but the surface generally appears to have a higher concentration of aluminum. As noted later, some test conditions lead to occasional presence of dry accumulates and occasional agglomerates on the quenched surface, and some conditions lead to small accumulates or single aluminum particles on the oxidizer surface. In the example shown, the binder lamina is slightly recessed. The smooth bands on the AP surface adjoining the AP-binder interfaces are equally evident with aluminized laminae, and were present under all test conditions in this study. A tendency for the leading edge of the AP surface to be at a location some distance from the interface (i.e., interface AP protruding) was noted above for unaluminized sandwiches, and occurs also with aluminized binder (all tests with binder-Al, all pressures). Use of aluminized binder increased the burning rate in some tests (increased in the case in Fig. 26). In the following, the effect of various test variables are described in terms of the features noted above for aluminized PBAN sandwiches.

a) Effect of Pressure

In the sample case used in Fig. 26 (1/1, PBAN/H-15, at 4.1 MPa), increasing the pressure reduced the amount of distinguishable aluminum on the binder surface, as well as the amount scattered on the AP surface (almost none at 6.9 MPa). The wetted appearance of the aluminum concentrated on the binder lamina is evident at all pressures, with occasional areas of dry-sintered particles at low pressure. The surface profiles of the aluminized PBAN sandwiches (i.e., details near the fuel laminae) were alike over the pressure range 1.4 - 6.9 MPa, and similar to the unaluminized PBAN sandwiches at lower pressures. The trend of the nonaluminized laminae to protrude at higher pressure (Fig. 25) did not occur for the aluminized PBAN sandwiches (Fig. 27). In general, the overall sandwich burning rate appeared to be higher with aluminized PBAN sandwiches, a feature reflected in the overall sandwich profiles, which have more "Vee" shaped profiles.

The above observations of pressure dependence do not all apply for other binders, or other additions to the binder, as noted later.

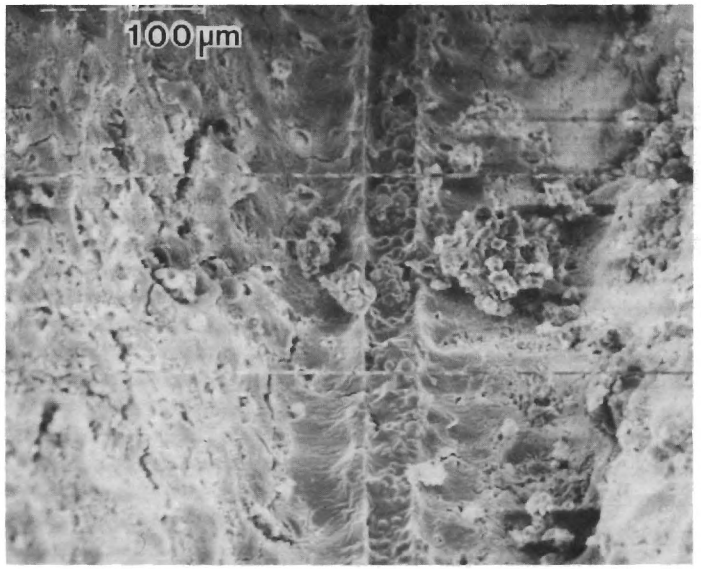

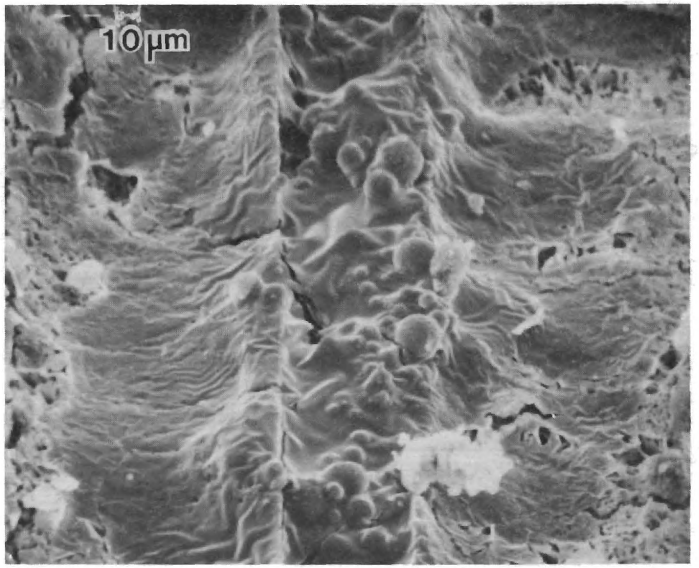

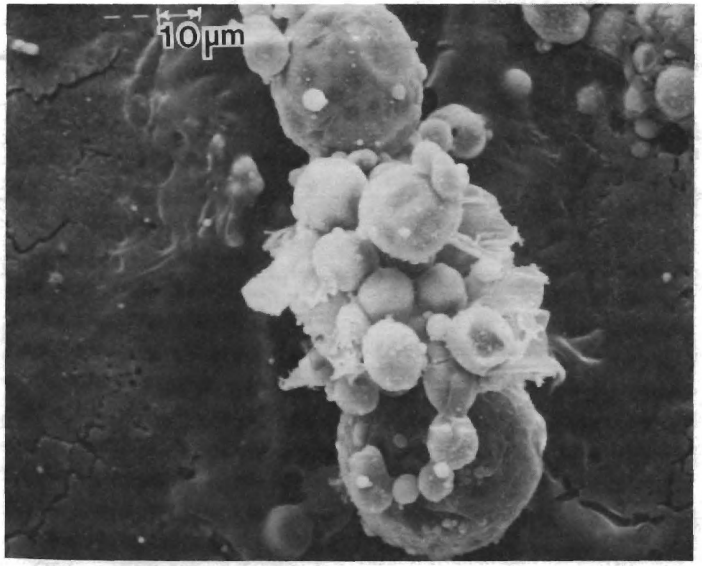

Fig. 26 Examples of quenched sandwich similar to Fig. 25b, but with fuel lamina 1/1, PBAN/H-15 Al, 4.1 MPa.

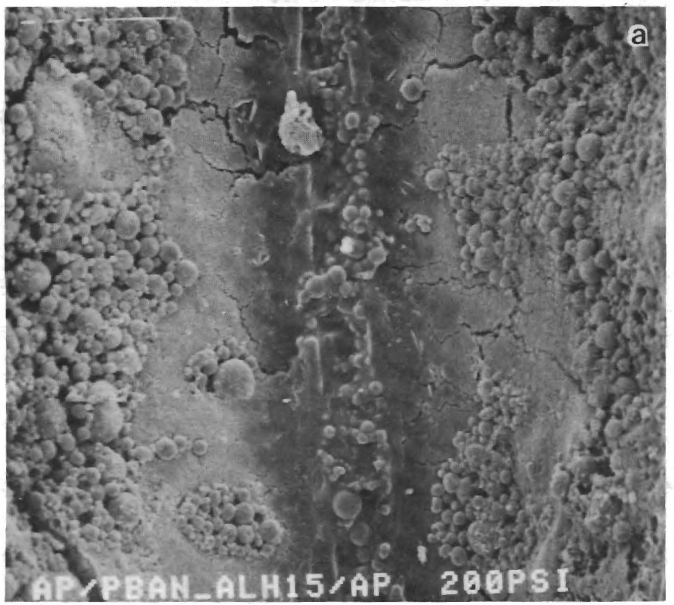

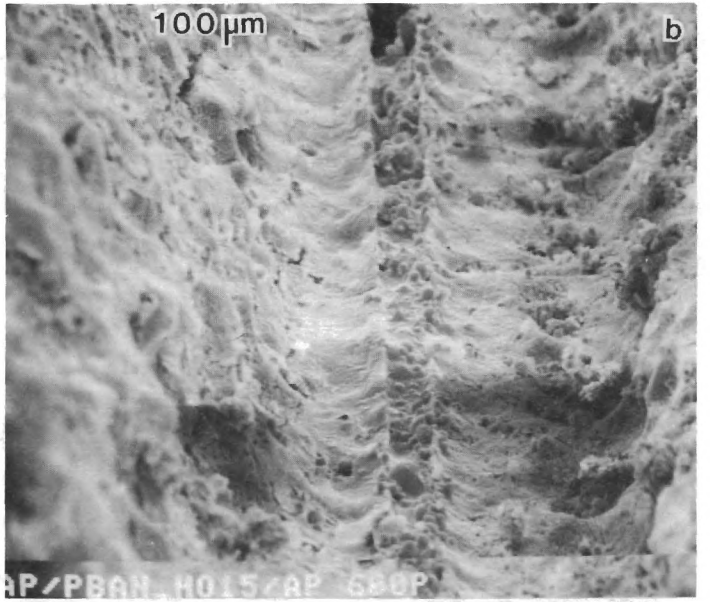

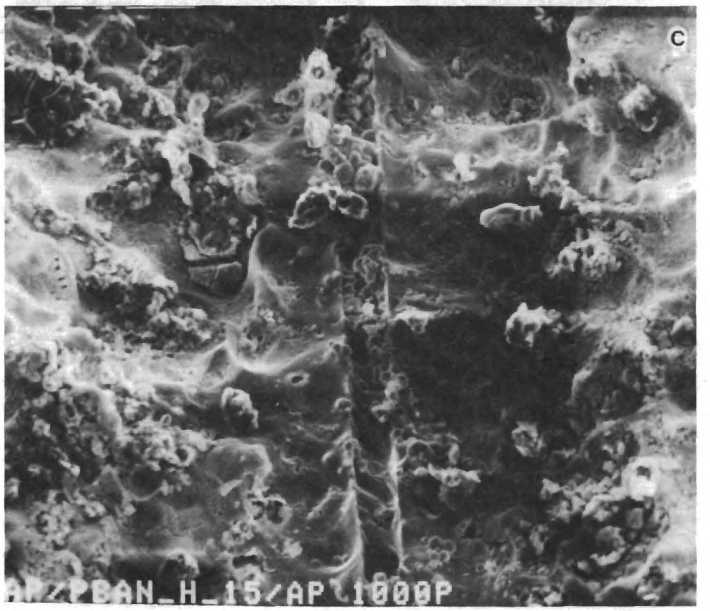

Fig. 27 Effect of pressure on quenched surfaces for sandwiches with 1/1, PBAN/H-15 Al fuel laminae.
a) 1.4 MPa, b) 4.1 MPa, c) 6.9 MPa.

b) Effects of Aluminum Variations

Changes in aluminum (with PBAN binder) had only moderate effect on quenched samples. Use of pre-stretched H-15 in place of as received H-15 (1/1, Binder/Al) produced no effect (although a substantial change was evident in the combustion photography tests described later).

Reducing the aluminum loading to 3/7, Al/Binder resulted in a somewhat lower aluminum concentration on the binder surface, and gave a somewhat smaller enhancement over the non-aluminized burning rate at pressures > 3.5 MPa (as compared to 1/1 Binder/Al).

Use of finer aluminum particles (H-5) in place of H-15 increased the level of accumulation at all pressures.

c) Effect of Binder

Changes in binder resulted in unexpectedly large effects on aluminized sandwiches. At low pressure these differences from PBAN sandwiches were not conspicuous, except for a drier, denser looking aluminum accumulation with polysulfide binder. Above 3.5 MPa, the effect of binder was more conspicuous, as shown in Fig. 28. In particular, the sandwiches with HTPB binder had aluminum accumulation that appeared to be flooded with binder melt. The HTPB/Al lamina and immediately adjoining AP protruded conspicuously at 6.9 MPa. The protrusion was significantly larger than observed in the tests with PBAN/Al fuel laminae or binder laminae alone.

d) Effect of AP in Binder

Introduction of 10 μm AP into a pure PBAN lamina in a 1 to 1 ratio (replacement of Al by AP) resulted in a binder surface that still looked wet, but irregular on a scale comparable to the oxidizer particle dimensions. No distinguishable AP particle surfaces were evident. The binder laminae were recessed slightly at all pressures (Fig. 29), as in the case of aluminized PBAN laminae, and pure PBAN binder at lower pressures. The very localized protrusion of AP immediately adjoining the fuel laminae (Fig. 25-28) is absent with the PBAN/AP lamina (Fig. 29). Instead, at a high pressure there is a wider plateau-like region of protruding AP unique to these samples (Fig. 29 b, c) and the AP/Al/Binder samples noted in the next section. The extent of protrusion of this region was more than with pure binder laminae for PBAN binder, less for HTPB

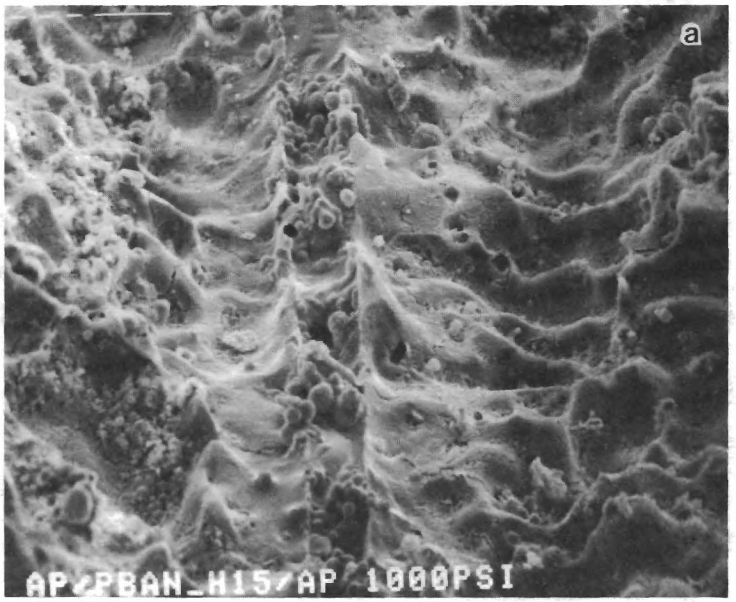

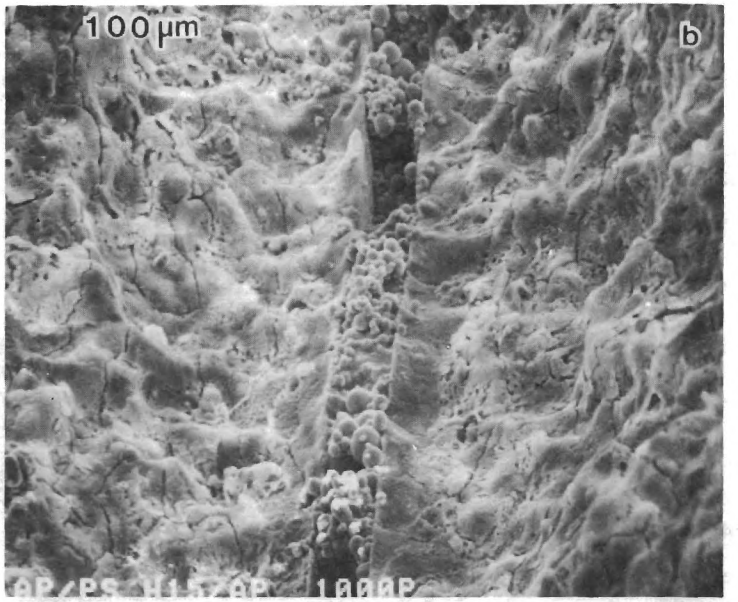

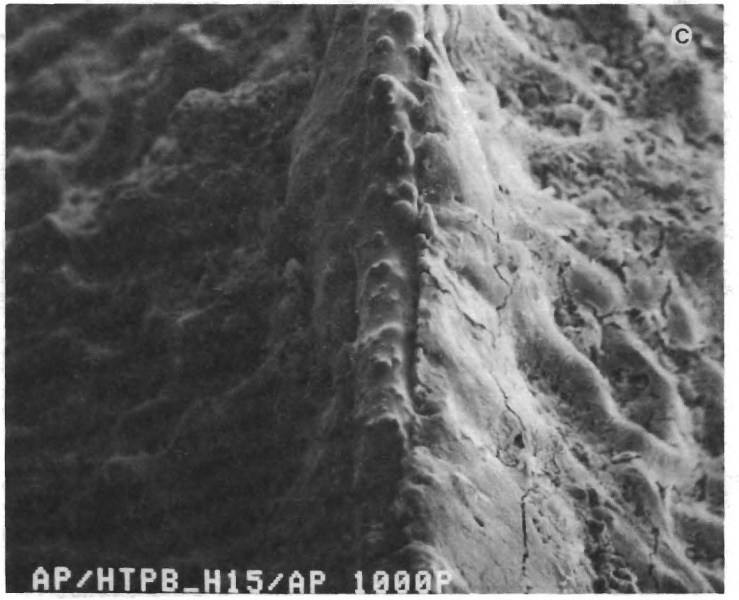

Fig. 28 Effect of type of binder on quenched aluminized sandwiches at 6.9 MPa (1/1, Binder/H-15 Al).
a) PBAN, b) PS, c) HTPB. Compare with Fig. 25c.

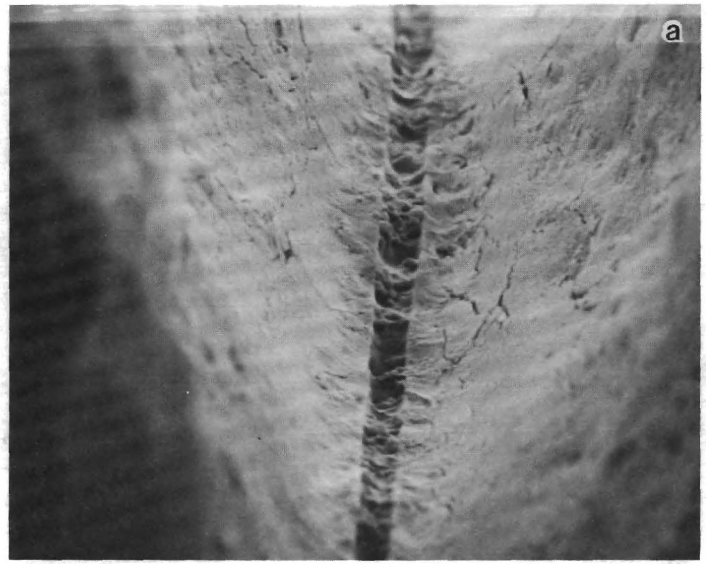

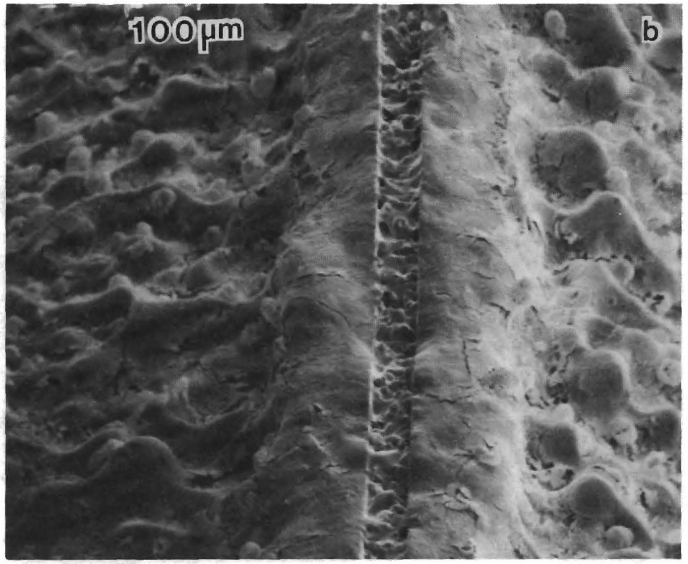

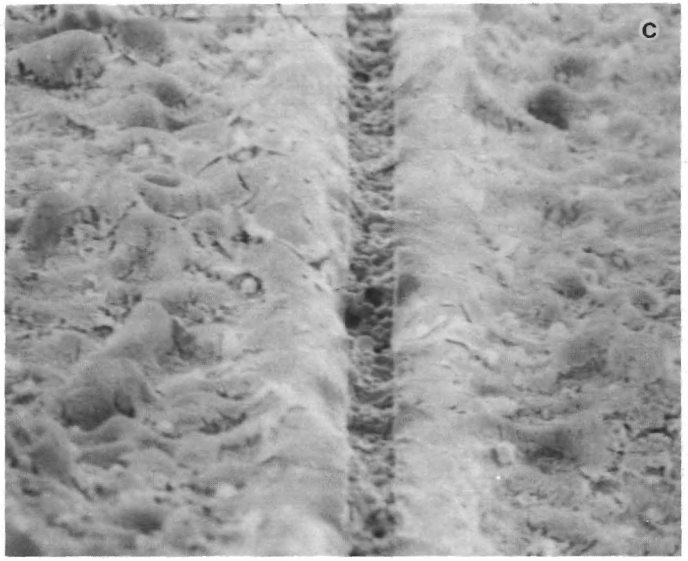

Fig. 29 Effect of introduction of 10 µm ammonium perchlorate in the binder lamina (Compare with Fig. 25.)
a) 1/1, PBAN/AP, 1.4 MPa.
b) 1/1, PBAN/AP, 6.9 MPa.
c) 3/7, PBAN/AP, 6.9 MPa

binder (Fig. 30). The test with a 7/3, AP/PBAN sandwich at high pressure exhibited less overall protrusion of the interfacial regions, and the interface was no longer the most protruding point in the interface region of the profile (Fig. 29c, not shown in Fig. 30).

e) Effect of Al and AP on the Binder

When a 1/1/1; Binder/AP/Al filled lamina was used, the lamina surface had less accumulated aluminum compared to the one with no fine AP at all pressures. The aluminum still had a wet appearance with both binders. But at 6.9 MPa with HTPB binder, the singular protruding feature of the lamina region with only aluminum (Fig. 28c) was absent when fine AP was added too. In general, the Binder/AP/Al sandwiches gave surface profiles closely resembling those obtained with sandwiches having 1/1 Binder/fine AP filled lamina.

Combustion Photography

The test conditions for which combustion photography was used are denoted by the symbol "M" in Fig. 24. From these few tests it was evident that aluminum left the surface primarily as ignited particles and agglomerates (6.9 MPa). Agglomerates were larger, and fewer original particles were present with HTPB binder than with PBAN binder. Addition of fine AP resulted in a reduction of agglomerate size, but did not seem to change the amount of unagglomerated aluminum leaving the surface. There was an appearance of distinguishable diffusion flame sheets or flamelet arrays extending from each AP/Binder interface. It is judged that these are smoke (carbon) trails from the true flames. Aluminum ignition tends to occur in these (presumably hot) regions, in the manner noted by previous investigators (Ref. 19). However, this was not completely systematic in these thin binder sandwiches. Some agglomerates appeared to form up and ignite while straddling the fuel lamina. Such agglomerates are probably of a size comparable to the lamina width. In the case of the HTPB/Al sandwiches at 6.9 MPa, the protruding lamina was easily visible and the top edge appeared to sway locally from one side to the other. In this situation, most of the aluminum emerged burning from one side or the other, not from the tip of the lamina.

In general, the photographic tests were too limited to make generalizations except for the following points:

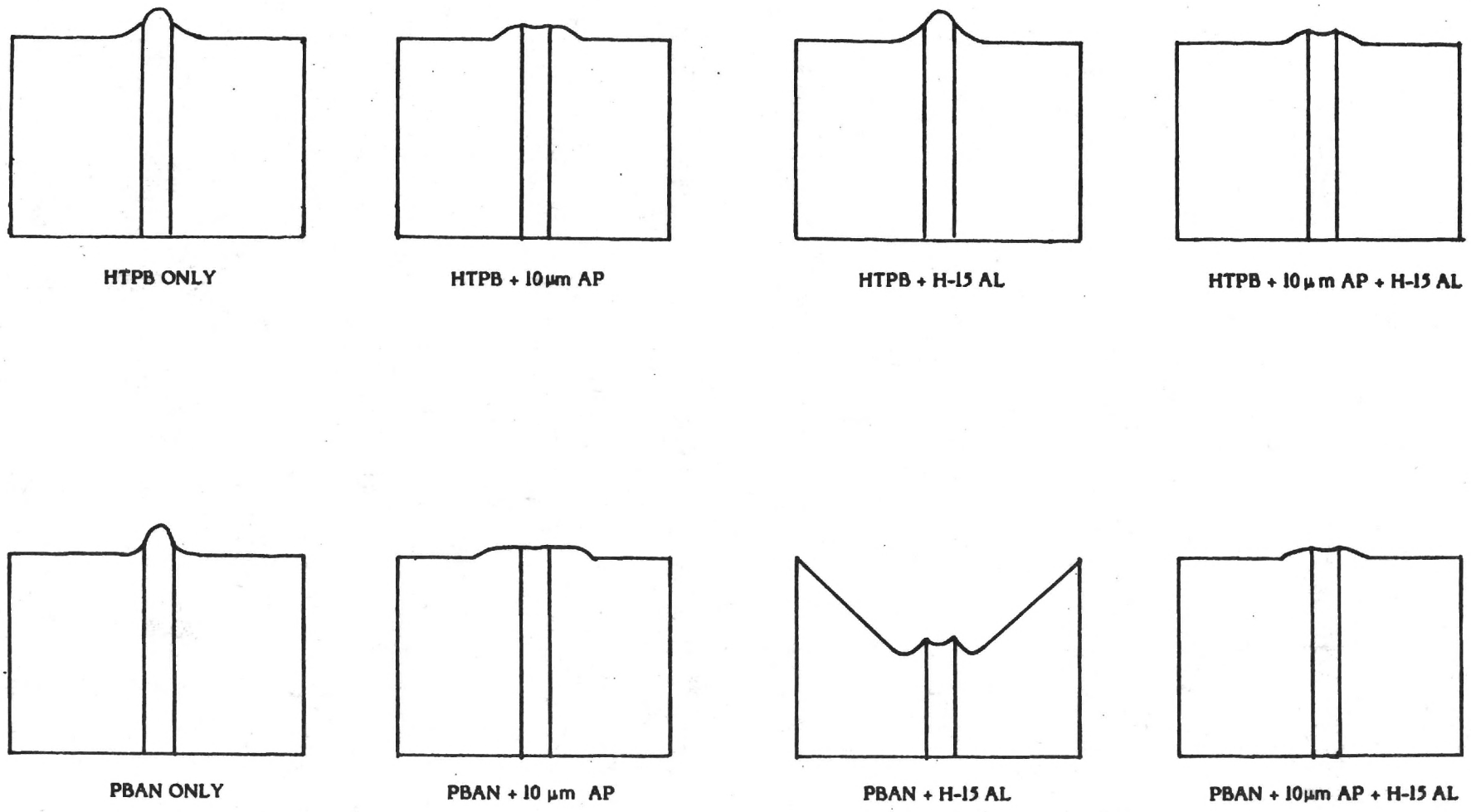

Fig. 30 Sandwich surface profiles for two binders and different combinations of AP and/or Al in the binder laminae.

a) There was extensive agglomerate formation at the sandwich surface. No unignited material was evident leaving the surface.

b) Agglomerates were smaller with PBAN binder than with HTPB binder.

c) Replacement of a 1/1, PBAN/Al lamina by a 1/1/1 PBAN/Al/AP lamina resulted in smaller agglomerates.

d) Separate AP/Binder flame sheets were evident for the two AP-fuel interface planes of the sandwiches, manifested by fluctuating smoke sheets.

e) Ignition of aluminum was favored in proximity of the AP/Binder flame, but with thin sandwiches the agglomerates were of comparable size to the fuel laminae and sometimes ignited and detached from a symmetrical position relative to the fuel lamina.

f) The test in which "pre-stretched" aluminum was used in place of as-received aluminum (H-15) exhibited substantial reduction in size of agglomerates.

Discussion of Sandwich Tests

The original objective of the aluminized binder sandwich tests was to provide a more controlled experiment for observation of aluminum accumulation, sintering, agglomeration and ignition. In particular, it was desired to examine the condition of the aluminum on the burning surface of thin binder lamina, a critical aspect of the behavior that had received only limited attention in a previous study (Ref. 18). Relative to this behavior, the principal result was the notable difference in appearance of the accumulated aluminum with different binders. HTPB binder resulted in a binder-flooded appearance; PBAN binder resulted in obvious aluminum accumulation, with appearance of wetting of particle surfaces and bridging between particles by binder melt; PS binder resulted in a dry-looking accumulation of aluminum. These results, observed on quenched samples, did not provide clues to subsequent development of agglomerates, except in the context of photographic observations of burning. The motion pictures showed that the size of agglomerates was greater with the "flooded look" of the HTPB sandwiches. Since HTPB appears to be the more thermally stable of the binders tested (Ref. 8,29), this suggests that the binder melt plays an important role in protecting the aluminum from ignition while it is concentrated and heated on the burning surface. The fact that use of sintering-resistant pre-stretched aluminum reduces agglomeration suggests that concentration and heat-up of the aluminum do not assure agglomeration, i.e., that a

final particle-to-particle sintering step is necessary for agglomeration. Likewise, the reduction of agglomeration by addition of fine AP to the aluminized binder lamina suggests that improvement of ignition conditions can block agglomeration. These speculations are consistent with propellant experience; additional combustion photography tests are needed to fully interpret the quenched surface observations.

The original plan for the sandwich tests covered only the study of aluminized binder lamina samples. However, the conspicuous effect of binder type on both surface profiles and aluminum wetting led to a series of tests on nonaluminized sandwiches, to determine to what extent the presence of aluminum was involved. The tests with fine AP additions were then conducted because of observations of the effect of fine AP in propellant testing (Ref. 11, 21, 30). Interpretation of the results of these further tests cannot be made yet, but the key results regarding surface profiles of the whole series of sandwich tests merit recapitulation.

1. Surface profiles with and without aluminum were similar with PBAN binder, except that the mildly protruding binder at higher pressure was changed to a mildly recessed profile when aluminum was added. A corresponding increase in sample burning rate resulted, accompanied by a corresponding "V" shaped overall sample profile.

2. With HTPB binder the effect of addition of aluminum had the opposite effect at high pressure. The extent of protrusion of the fuel lamina and adjoining AP was conspicuously increased (compared to nonaluminized HTPB sandwiches). The enhancement of sample burning rate observed with PBAN binder was absent with HTPB binder.

3. Addition of fine AP to PBAN binder laminae resulted in mildly recessed binder laminae at all pressures, as with the addition of aluminum. The corresponding increase in burning rate at higher pressure did not occur. Instead, the usually narrow region of protruding AP adjoining the lamina interfaces was widened. Similar effects were observed with HTPB binder.

4. Addition of both fine AP and aluminum to the binder laminae produced profiles similar to those with only AP added. The primary difference from sandwiches with aluminized binder was the widened region of AP protrusion at 6.9 MPa, and reduction of the unique height of protrusion of the lamina region with HTPB binder.

MODIFICATION OF ALUMINUM TO CONTROL AGGLOMERATION

Background

In view of the obvious importance of the role of the oxide skin on aluminum particles in controlling the onset of sintering, agglomeration and ignition of aluminum, it is reasonable to seek beneficial modification of the oxide. A method explored by Kraeutle (Ref. 31) was to enhance the oxide by further oxidation, by holding powders at elevated temperature in oxidizing atmospheres. This modification method was called "pre-oxidation", and was conducted at temperatures below the aluminum melting point.

A method explored earlier in the present project (Ref. 20,32) was called "pre-stretching" the oxide, by heating particles through the aluminum melting point. The oxide skin deforms to accomodate the relatively greater thermal expansion and phase change expansion of the aluminum. The oxide deformation is presumably by both inelastic stretching and cracking. In the presence of a low concentration of oxygen, the cracked areas will close rapidly by further oxidation. Upon cooling, the particles shrink, the oxide skin wrinkles or exhibits depressions (Ref. 32), but the oxide surface area is believed to remain sufficient to enclose the aluminum when the particle later melts in the combustion zone. This argument was developed from growing understanding of ignition behavior of aluminum powder, and was evaluated earlier in the project using the hot stage microscope to produce and test the pre-stretched oxide particles (Ref. 32). In those tests the tendency of aluminum powders to sinter and agglomerate when heated was sharply reduced by pre-stretching the oxide.

In subsequent combustion studies on this program, modified aluminum has been carried as one of the test variables, thus giving a systematic demonstration of the potential of modificiation of the oxide skin as a means of controlling agglomeration. For those combustion studies aluminum with pre-stretched oxide was produced in greater quantity by heating the powder in a half open quartz tube to 700^{o}C, using a tube furnace flushed with a nitrogen flow (with some entrained air). The "pre-stretched" aluminum was subsequently sieved to eliminate any large agglomerates or sintered accumulates formed during the "pre-stretching" process. Since the smallest sieve mesh is 37 μ, it is probable that some small accumulates were included, but the mean particle diameter was not significantly altered.

The "pre-stretched" aluminum was compared with as received, and pre-

oxidized aluminum in a series of "propellant" formulations. The formulations included dry pressed AP/Al, and AP/Al/Wax samples. Sandwiches were also prepared consisting of an aluminum filled PBAN lamina between AP slabs. The results of some of these tests have been reported in interim reports (Ref 28, 32), but will be repeated here for completeness.

Combustion of AP/Al Samples

Samples were prepared from mixturs of AP and Al powders by dry pressing mixtures of 85%, 100 μm AP and 15% Alcoa 123 Al to pressure of 170 MPa for 20 minutes. Similar samples were made with pre-stretched Alcoa 123 Al, and samples with pre-oxidized Alcoa 123 Al (provided by Karl Kraeutle of Naval Weapons Center). Tests were run at 6.9 MPa (1000 psi), and observations were made by combustion photography.

Tests on the samples with untreated aluminum exhibited massive accumulation and sintering of aluminum on the burning surface, with ignition occurring only during break-up of detaching accumulate layers. Very large agglomerates formed. Results with the pre-oxidized and with the pre-stretched aluminum were alike. In the tests with pre-stretched aluminum, only small accumulates were evident, with more or less continual detachment of small fragments. Aluminum ignition was only occasional. This result supports the mechanistic argument that led to "pre-stretching" experiments (Ref. 20,32), and suggests a means of controlling accumulate size, using a modification of aluminum powder that is economically viable in production, possibly by simply changing process control variables in the original powder manufacture. The observation of only limited ignition of the pre-stretched aluminum supports the earlier argument that conditions in the AP flame are not conducive to ignition of aluminum unless some mechanical breakage of the hot sintered accumulate exposes aluminum, and thus provides the opportunity for localized exothermic reaction.

Combustion of AP/Al-Binder/AP Sandwiches

Sandwiches were prepared using the usual method (Ref. 27, 28) of laminating a thin layer of binder between two AP slabs. In this case the binder was a 1/1 mixture of PBAN and Valley Met H-15 aluminum. Samples were prepared using as received and pre-stretched H-15, and combustion tests were run at a pressure of 6.9 MPa (1000 psi) and observed by high speed cinephotography. The sandwiches

prepared with as-received H-15 burned with large slow moving agglomerates, and the ignition and detachment of agglomerates was noticably intermittent, almost periodic. The sample with pre-stretched aluminum burned with small agglomerates and single ignited particles that left the surface in a more or less continuous manner. In this test the pre-stretched aluminum was shown to substantially reduce agglomeration thus improving the combustion behavior of the aluminum. In contrast to the tests on dry-pressed AP/Al samples, use of pre-stretched aluminum in sandwich tests led to improved aluminum ignition, presumably because ignition is induced by the hot AP-Binder flame instead of by aluminum exposure during accumulate break-up.

Combustion of AP/Al/Wax Samples

A set of propellant samples were prepared by dry pressing 30% Valley Met H-30 aluminum, 7% carnauba wax, and 63% 100 μ AP. One sample was prepared using as received H-30, a second sample used pre-stretched H-30, and a third sample used "pre-oxidized" H-30. A fourth sample was prepared in a manner that illustrated the differences in aluminum behavior more graphically in a single motion picture, by using as-received and pre-stretched aluminum in different parts of the same sample. As in the AP/Al tests, dry pressed samples are prepared by mixing the ingredients, pouring the ingredients into a die and pressing the mixture in a hydraulic press to obtain a compact disc of propellant. The fourth sample was prepared by using a piece of card stock to divide the die into two halves. One half of the die was loaded with the mixture containing as received aluminum while the other half contained the mixture with pre-stretched H-30. The mixture was carefully tamped down and the card separator was carefully removed. The sample was then hydraulically pressed to obtain a disc of propellant. After careful cutting, a 10 mm x 6 mm x 1.6 mm sample was obtained, one half containing as-received H-30 and one half with pre-stretched H-30. Motion pictures of these "half and half" propellants are comparable to split frame motion pictures, i.e., a direct comparison of the combustion behavior of the aluminum is possible.

Motion pictures were filmed for each of the samples burning at 6.9 MPa (1000 psi). The sample with as received H-30 exhibited relatively unfavorable Al combustion characteristics. The surface was covered with large filigrees, aluminum ignition was sporadic, and moderately large to large agglomerates were formed. Significant improvement was seen with the samples with pre-stretched

and pre-oxidized H-30. The surface was rough but fewer filigrees were evident. The aluminum left the surface (ignited) in small agglomerates or single particles. Viewing the "half and half" sample was quite convincing. In any single frame, the region above the half of the sample with as-received aluminum was dark with two or three large burning agglomerates. The region over the other half of the sample surface (pre-stretched aluminum) was nearly a continuous white field of burning particles (Fig. 31).

Combustion of the samples prepared with "pre-oxidized" H-30 was indistinguishable from the "pre-stretched". Both modifications of the aluminum resulted also in higher sample burning rates.

Summary of Aluminum Modification Tests

Combustion photography was used to compare aluminum behavior in tests on three kinds of samples:

Dry-pressed mixtures of AP and Al powders.

Dry-pressed mixtures of AP, Al, and Carnauba wax powders.

Sandwiches with aluminum in the binder lamina.

Both pre-oxidation and pre-stretching treatments of aluminum particles resulted in reduction of accumulation of aluminum on the burning surface, and major reduction of the size of aggregates leaving the surface. In those tests where an AP-hydrocarbon flame was present, the changes resulting from use of modified aluminum led to more prompt ignition of accumulating aluminum and to correspondingly smaller agglomerates. In the tests on AP/Al samples (no hydrocarbon fuel), aluminum ignition was not improved, apparently because conditions in the combustion zone of the AP are not conducive to ignition of the aluminum. In general, the results are consistent with those obtained earlier by Boggs, et al (Ref. 33), with pre-oxidized aluminum, although detailed comparison cannot be made of the two aluminum modifications because of differences in other test sample variables.

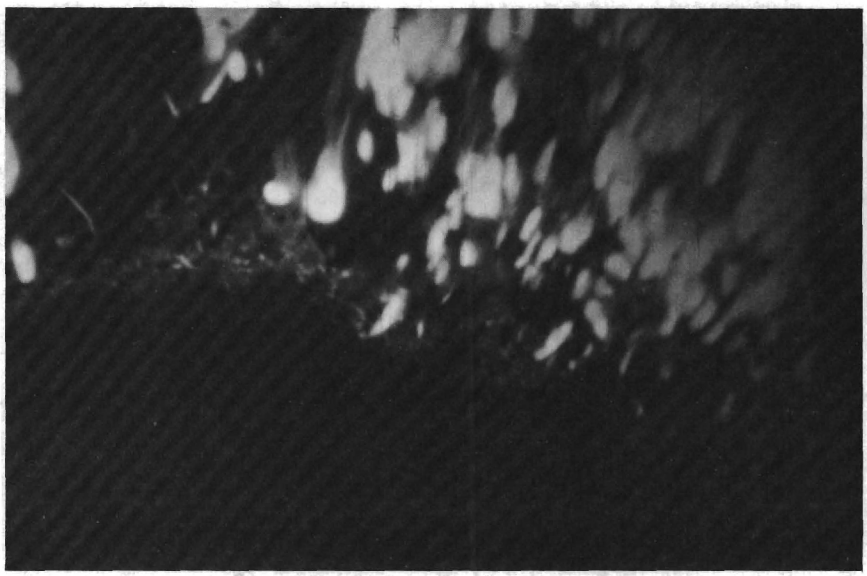

Fig. 31 Comparison of aluminum combustion with dry pressed AP/Al/Wax samples: pre-stretched on the right and as-received aluminum on the left.

STUDIES OF A FAMILY OF PROPELLANTS PREPARED AT THIOKOL-ELKTON

Background

Variation of composition and ingredient particle sizes is probably the most critical factor available in conduct of propellant combustion research. The high cost of preparation of propellant mixes, unfortunately, tends to limit the systematic use of this critical variable as an investigative tool in research and often forces the use of samples prepared by improvised means of unevaluated relevance (e.g., use of samples prepared by dry pressing powder mixes). During the present study, a family of samples became available, which has a systematic variation of composition, prepared by state-of-the-art method (Ref. 34). These same formulations were studied by the suppliers (Ref. 11, 34) using a variety of combustion experiments. In the present program this series of propellants was studied by combustion photography, and by scanning electron microscope analysis of sample surfaces quenched by rapid depressurization. The objectives were three-fold: first, it was desired to establish a basis of comparison of test results on conventional propellants with work on the present program using samples prepared by various improvised methods; second, it was desired to take advantage of the available range of systematic variations of formulations; and third, it was desired to provide an independent set of test results that could be compared with those of the propellant supplier (for reproducibility or possible mutual improvement of experimental methods). In the following, information regarding the propellants, tests, results, and interpretation is summarized.

Propellant Formulations

The range of test variables covered in this investigation is given in Table 2. The actual composition of the propellants can be obtained from Ref. 11 and 34; they are high solids HTPB propellants with variations on a baseline propellant having 18% aluminum and a trimodal AP blend. One or two variables were changed at a time to study the effect of these variations on the combustion behavior of the propellant. All the propellants studied are low burning rate composite propellants. The sample designated 1780-1 was used here as a baseline formulation. Not all the formulations in the supplier's original program were available, and not all those supplied were tested in the present investigation. Choices were based in part on anticipated results, and in part on supplier's test results.

Table 2

Range of Major Propellant Variables Investigated

HTPB BINDER	
LEVEL:	9 to 14%
ALUMINUM	
LEVEL:	18 to 22.4 %
SIZE:	7.5 to 84 μm
AMMONIUM PERCHLORATE	
LEVEL:	55 to 71%
SIZE:	6 to 400 μm
MODALITY:	
Bimodal:	400/fine
Trimodal:	400/200/fine
HMX	
LEVEL:	0 to 15%
SIZE:	6 and 9 μm
ALTERNATIVE:	RDX

Experimental Procedures

Combustion Photography: The experimental set up and the procedure are similar to those described in Ref. 35. The sample dimensions were 10 mm x 6 mm x 1.6 mm. Ektachrome 7241 high speed color film was used for motion pictures. The film framing rates and the aperture f-stop setting varied with test pressure, and are given in Table 3. The samples were externally illuminated by a Xenon lamp under all test conditions. Test conditions are tabulated in Table 4.

Quench Procedure: Quenching was accomplished by rapid depressurization of the combustion vessel by diaphragm rupture. The experimental set up and technique are described in Ref. 36. The sample dimensions were maintained the same as in combustion photography for ease of comparison of results. The quenched samples were then prepared for study under a scanning electron microscope. Quench test conditions are tabulated in Table 5.

Results

Combustion Photography: Combustion photography provides details regarding the combustion efficiency, nature of accumulates on the burning surface, size of agglomerates leaving the surface, burning rate, etc.. The combustion photographs were initially compiled into edited motion pictures for three different pressures and then spliced together into one picture for easy comparison of combustion of different samples. The results of combustion photography allow a comparison of combustion behavior as a function of size of aluminum, % binder, size of AP particles, addition of HMX, usage of DDI curative in propellant and pressure. The pictures were examined for:

(a) Degree of accumulation of aluminum on the surface.

(b) Duration of retention of accumulated aluminum on the surface.

(c) Qualitative estimate of the size range of agglomerates leaving the burning surface.

(d) Ignition characteristics of agglomerates.

(e) Burning rate of sample.

(f) Brightness of field of view which in turn is a measure of the vigorousness of combustion.

(g) Qualitative estimate of unignited aluminum leaving the burning surface.

Behavior in each test was ranked in Table 6, and can be interpreted by comparison with behavior of the baseline propellant No. 1780-1 as described below, in terms of

Table 3

High Speed Camera Settings for Combustion Photography

Pressure MPa (psi)	Film Speed f/sec	F-Stop
1.4 (200)	3000	5.6
3.45 (500)	3400	8.0
6.9 (1000)	4000	11.0

Table 4

Test Conditions for Combustion Photography

PRESSURE / FORMULATION	1.4 MPa (200 psi)	2.62 MPa (350 psi)	3.45 MPa (500 psi)	6.9 MPa (1000 psi)
BASELINE	X	X	X	X
AL EFFECT (SIZE)				
Fine Al	X		X	X
Coarse Al	X		X	X
BINDER EFFECT				
High Binder	X		X	
DDI	X		X	
Catalyst Fe_2O_3			X	
AP SIDE EFFECTS				
400/200/71	X		X	
400/71			X	
400/41			X	
HMX	X		X	X

Table 5

Conditions for Quench Tests of Propellants

1.	6.9 MPa Quenches of all formulations.
2.	Quenches of baseline formulation at progressively lower pressures of 6.9, 5.2, 3.45, 2.42, 1.41, 0.7 MPa.
3.	Quenches of 400/200/71 (no fine AP) at the same series of pressures as in 2.
4.	Quenches of DDI curative propellant at the same series of pressures as in 2.

accumulating insight into the aluminum behavior and the observed results ranked in the table.

At a pressure of 1.4 MPa (200 psi) the combustion of the baseline formulation is as follows. As the burning surface recedes, the ingredient aluminum particles accumulate on the surface due to the concentration of the surface aluminum particles with the underlying particles, and retention on the surface by the surface tension forces of the molten binder, in the absence of favorable ignition conditions. The accumulation is moderate in the case of the baseline propellant. Past studies (Ref. 6, 33, 37, 38) indicate that as this accumulation progresses, a sintered filigree of particles forms and as accumulation progresses further, a part of the filigree is eventually exposed to the hot diffusion flame. This results in local breakdown of the sintered oxide skin of the filigree, followed by a spreading inflamation and coalescence into an agglomerate. In the case of the baseline propellant of the present study, most of the accumulated aluminum ignites on the propellant surface and ignition-coalescence is rapid. Some of the burning agglomerates reside on the burning surface for a short time before being swept away by the gas flow. The agglomerates leaving the burning surface range in size from single particles to about 350 μm. The field of view is moderately bright both close to the burning surface and in the far field, with a moderate amount of smoke in the combustion zone. No unignited aluminum is evident leaving the burning surface. To the extent possible in still photographs, the foregoing details are illustrated in Fig.32.

The propellant combustion behavior is not significantly different at 3.45 MPa except that the degree of accumulation is less and hence smaller agglomerates leave the burning surface.

The results of all tests are tabulated in comparative terms in Table 6 a (1.4 MPa tests) and Table 6 b (3.45 MPa). The numbers 1 - 5 used in these tables rank the indicated combustion behavior on a scale of 1-5.

It is observed from the analysis of this combustion photography that the general trend is for a bright combustion field, short residence time, smaller agglomerates, and high burning rate to go together. Conditions which favor this complex of behavior are:

a) Small (i.e., < 15 μm) aluminum particle size: Relatively fine aluminum provides more surface area and finer sintered structure of accumulates, which results in more vigorous inflamation at the moment of accumulate breakdown. However, under adverse ignition conditions, the large surface area can lead to more

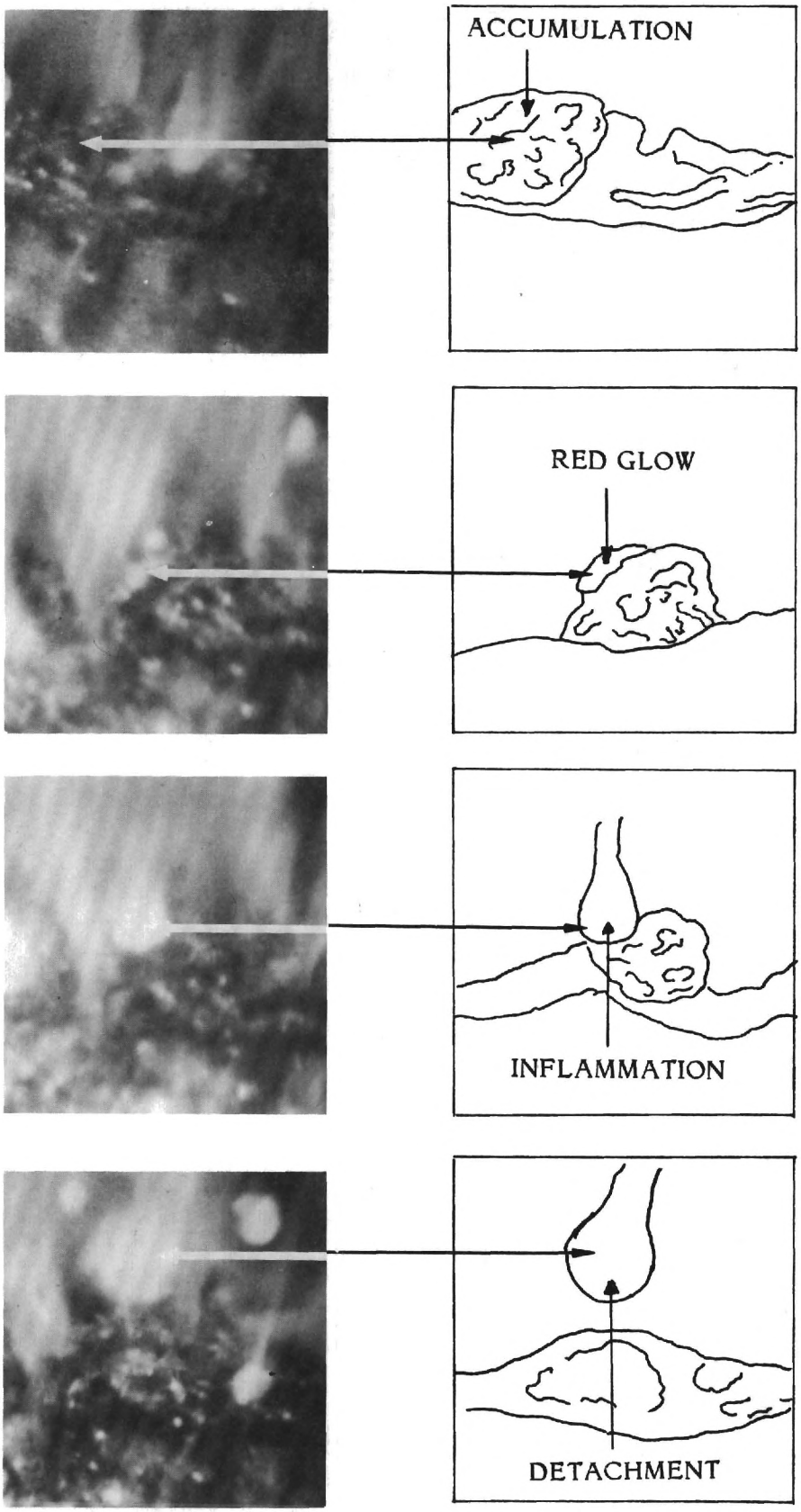

Fig. 32 Combustion field for sample 1780-1 at 1.4 MPa.

Table 6a

Comparative Results of Tests Run at 1.4 MPa

CHARACTERISTICS / FORMULATION	Degree of Accumulation	Retention on Burning Surface	Ignition		Aggl. Size		Brightness		Smoke	Burning Rate	Unburned Aluminum Leaving Surface
			Surface or Gas	Quick or Slow	Range	Avg. Size	Near Field	Far Field			
BASELINE	3	2	S	Q	3	3	2	2	2	--	1
AL EFFECT											
Fine Al	3*	2	S	S & Q Crusts	3	2	3	3	2	Higher	1
Coarse Al	5	3	S & G	S	2	2	1	1	3	Smaller	2
BINDER EFFECT											
High % Binder	4	3	S	S	4	4	1	1	3	Lower	1
DDI Curative	3	2	S	Q	3	2	2	2	2	Lower	1
AP SIDE EFFECT											
400/200/90 μm AP	2	1	S	Q	2	1	1	--	2		1
HMX	3	2	S	Q	3	2	1	1	2	Higher	1

* (Crusting occasionally)

Table 6b

Comparative Results of Tests Run at 3.45 MPa

CHARACTERISTICS / FORMULATION	Degree of Accumulation	Retention on Burning Surface	Ignition		Aggl. Size		Brightness		Smoke	Burning Rate	Unburned Aluminum Leaving Surface
			Surface or Gas	Quick or Slow	Range	Avg. Size	Near Field	Far Field			
BASELINE	3	2	S	Q	3	3	2	2	2	--	1
AL EFFECT											
Fine Al	3*	2	S	Q	3	2	3	3	2	Higher	1
Coarse Al	4	3	S & G	S	2	2	1	1	3	Lower	2
BINDER EFFECT											
High % Binder	4	3	S	S	4	4	1	1	3	Lower	1
DDI Curative	2	2	S	Q	3	2	2	2	2	Lower	1
Fe_2O_3 Catalyst	3	2	S	Q	3	2	3	2	2	Higher	1
AP SIDE EFFECT											
600/200/90 μm	2	1	S	Q	2	2	3	2	2	Higher	1
400/90 μm	2	1	S	Q	1	1	3	--	2	Lower	1
400/50	3	2	S	Q	2	2	2	2	2	Higher	1
HMX	3	2	S	Q	3	3	1	1	2	Higher	1

* (Crusting occasionally)

extensive sintering and larger agglomerates, as observed here with the finest aluminum particle size.

b) Low binder to oxidizer ratio: The "bright burning" complex is apparently favored by the more oxidizer-rich environment and perhaps even more by the less prolonged surface retention and protection from oxidizing species, due to reduced binder presence in the surface accumulates.

c) Close proximity of the oxidizer-binder flame to the accumulating aluminum: Whether due to higher pressure or to propellant microstructure, proximity to these high temperature flamelets appears to precipitate early ignition of aluminum, and hence less accumulation and agglomeration and more vigorous combustion.

SEM Studies of Quenched Burning Surfaces

The general appearance of quenched surfaces is illustrated by the series in Fig. 33 for 1780-1 formulation at 5 pressures. The coarser oxidizer particles are conspicuous at lower pressures, with the intervening areas showing a binder surface that looks like it was a melt prior to quench. The aluminum concentrated in the binder is evident at lower pressure, while the fine oxidizer particles are either not evident, or not distinguishable from aluminum particles. The larger oxidizer particles generally have concave surfaces, especially at high pressure. The profiles of the oxidizer surfaces have a close resemblance to the profiles obtained in aluminized sandwich burning tests. The region adjoining the binder is protruding and has a smooth surface. Further from the interface, the sloping surface flattens out and transitions to a central area that has a frothy surface appearance, sometimes raised (low pressure). Under some conditions (low pressure), collections of aluminum particles were contained in the central froth region (Fig. 34). At pressures higher than 3.45 MPa the surfaces of the oxidizer particles were deeply concave and exhibited no froth or aluminum. In general, the array of accumulated aluminum on the burning surface reflected its original distribution in the propellant microstructure. The fine oxidizer did not manifest its presence. "Pocket" concentrations of aluminum occurred in spite of the presence of the fine AP. These trends were generally true over the whole pressure range, but the aluminum concentration became flooded with binder melt at higher pressure.

The principal effects of propellant variations on samples quenched at 6.9 MPa were the following:

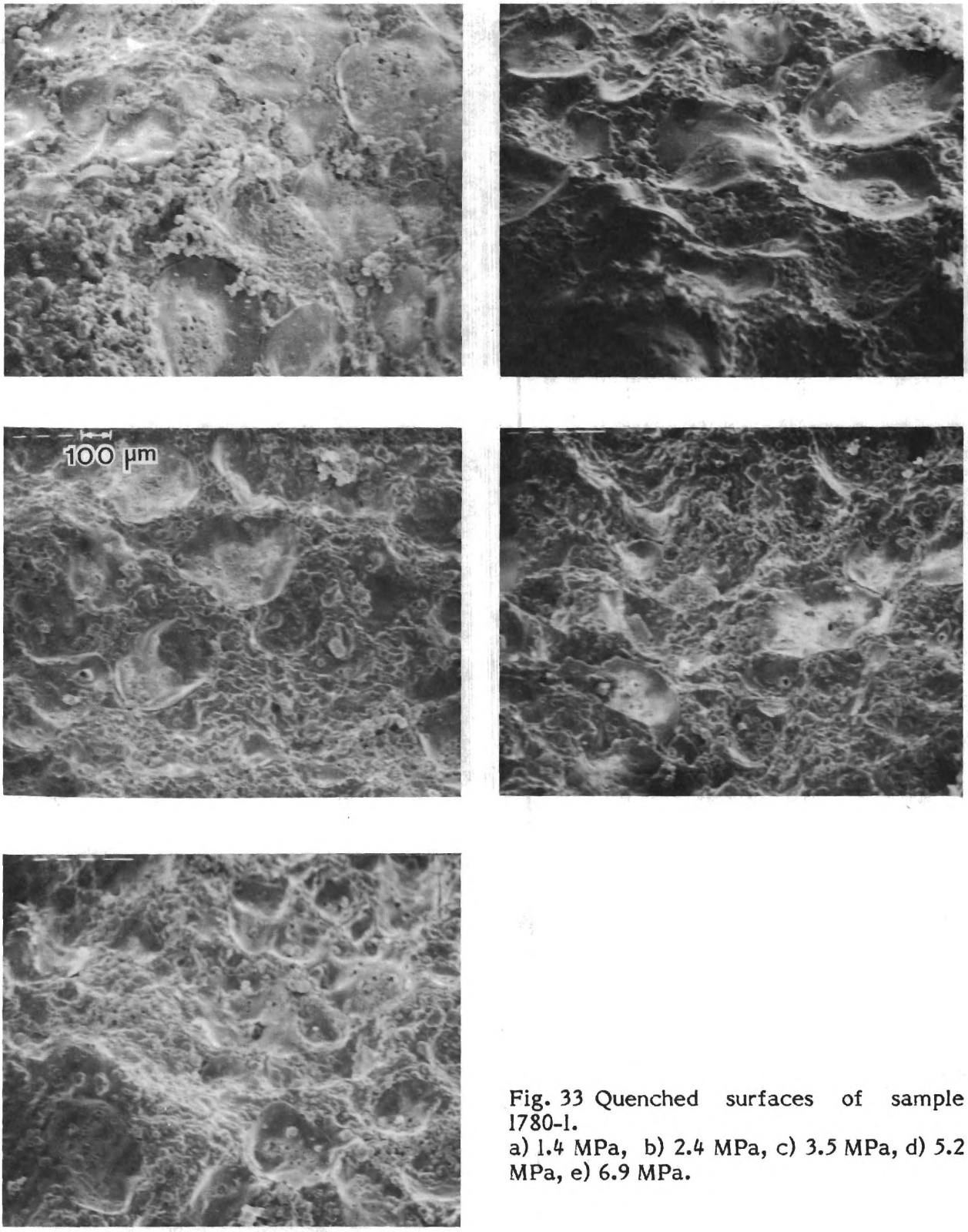

Fig. 33 Quenched surfaces of sample 1780-1.
a) 1.4 MPa, b) 2.4 MPa, c) 3.5 MPa, d) 5.2 MPa, e) 6.9 MPa.

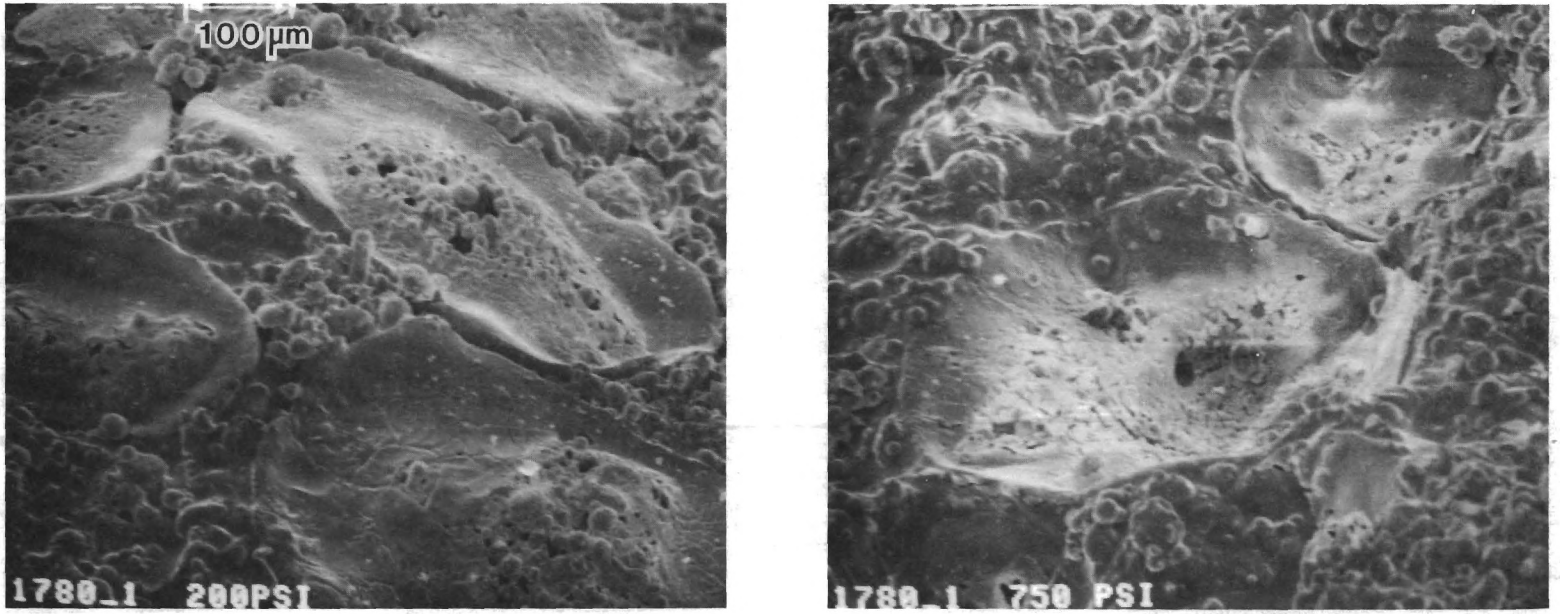

Fig. 34 Aluminum accumulation on the surface of an oxidizer particle, sample 1780-1.
a) Heavy at 1.4 MPa, b) not at 5.2 MPa.

a) Replacement of fine AP by an intermediate size resulted in a surface accumulation of aluminum that was of a filigree nature. This result is a consequence of the fact that pockets in the propellant microstructure were eliminated by being filled with the intermediate size AP particles, leaving the relatively finer aluminum particles in less concentrated clumps. The aluminum looked appreciably less flooded.

b) The sample with fine aluminum showed local areas of formation of aluminum crust, larger than typical pocket accumulations.

c) The samples with a moderate amount of HMX tended to give a more wet looking binder surface, with very small holes in the binder surface.

d) The sample with coarse aluminum showed very little accumulated aluminum on the surface, localized only to individual pockets, containing 4 - 10 particles.

The reader is reminded that the description of the sample surface may reflect changes that took place during quench. It seems likely that the drier aluminum accumulates may detach during quench, and the binder may experience some local flow of the molten surface. The holes in the binder with HMX may be blown during quench, and the froth on the oxidizer surface may be disrupted. These are all believed to be of only moderate importance to surface appearance, except for the possible detachment of accumulates in transition (which limits their observation to the relatively poor resolution obtainable from the combustion photography).

Discussion

The results indicate the relevance of the early comments on propellant microstructure to the formation of surface accumulates and agglomerates. Pocket-forming oxidizer particle blends form agglomerates of pocket size. In this respect, the presence of a moderate amount of fine AP does not prevent pocket size accumulates, but apparently aids ignition of aluminum enough to give somewhat more vigorous inflamation and burning. Using fine aluminum seems to have aided sintering, which in turn led to some very large agglomerates, a behavior that was not prevented by presence of fine oxidizer. The presence of aluminum accumulations in the middle of oxidizer burning surfaces has been observed in previous studies (Ref. 11, 25, 37), and is believed to result from a failure of the pocket accumulation to ignite at the time of transition as the underlying surface passes from binder to an underlying oxidizer particle. This is consistent with

observations reported in earlier sections regarding survival of accumulates on oxidizer surfaces. In general, this type of behavior is more common under the unfavorable ignition conditions at low pressure. Of particular importance is the effect of filling the "pockets" with oxidizer particles large enough to displace the aluminum into thinner "sponge" elements of binder, oxidizer particles large enough to deflagrate on the surface like the larger particles. This leads to a more tenuous filigree of aluminum accumulation, that forms in close proximity with hot oxidizer-binder flamelets. The result is relatively small and vigorously burning agglomerates.

COMBUSTION OF HIGH ALUMINUM CONTENT SOLID PROPELLANTS

Most rocket propellants with aluminum as a fuel ingredient contain 12 - 18% aluminum. Motor performance calculations generally indicate that optimum performance would be obtained at a higher aluminum content, and particularly so in volume-limited applications where high propellant density is also advantageous. In addition, there is some indication that high aluminum content reduces susceptibility to detonation. However, there are problems with high aluminum content that reduce its actual performance, problems that would have to be minimized before increased aluminum would be advantageous. However, the seriousness of these problems (low combustion efficiency and high two-phase flow losses in the nozzle flow) has remained substantially unevaluated, as have the possibilities of reducing the problems by better "design" of combustion. Results and methods of the present research offered the means to achieve improved combustion and control of product oxide droplet size distribution, and an exploratory study was made. This work was reported in Ref. 39 and is summarized here.

Three types of experiments were conducted on propellants containing 5 - 35% aluminum. These consisted of high speed cinemicrophotography; microscopic studies of quenched burning surfaces; and microscopic and chemical analysis of the efflux from the burning surface (quench-collected in ethanol at various distances from the burning surface). In order to permit a large range of propellant formulations, the propellant was simulated by one of two different processes.

1. Dry-pressing powder mixtures in which polymeric binder is replaced by carnauba wax powder.
2. Hand mixing small samples of conventional ingredients, followed by pressing and then curing.

The modifications in formulation that were tested are shown in the test summaries in Fig. 35 to 37. The charts show a central reference formulation and test pressure, and sequences of values of different variables, changed one at a time from the central reference condition. At least one test was run for each condition in the charts.

A motion picture sequence is available summarizing the combustion photography. The effects of test variables on combustion characteristics are

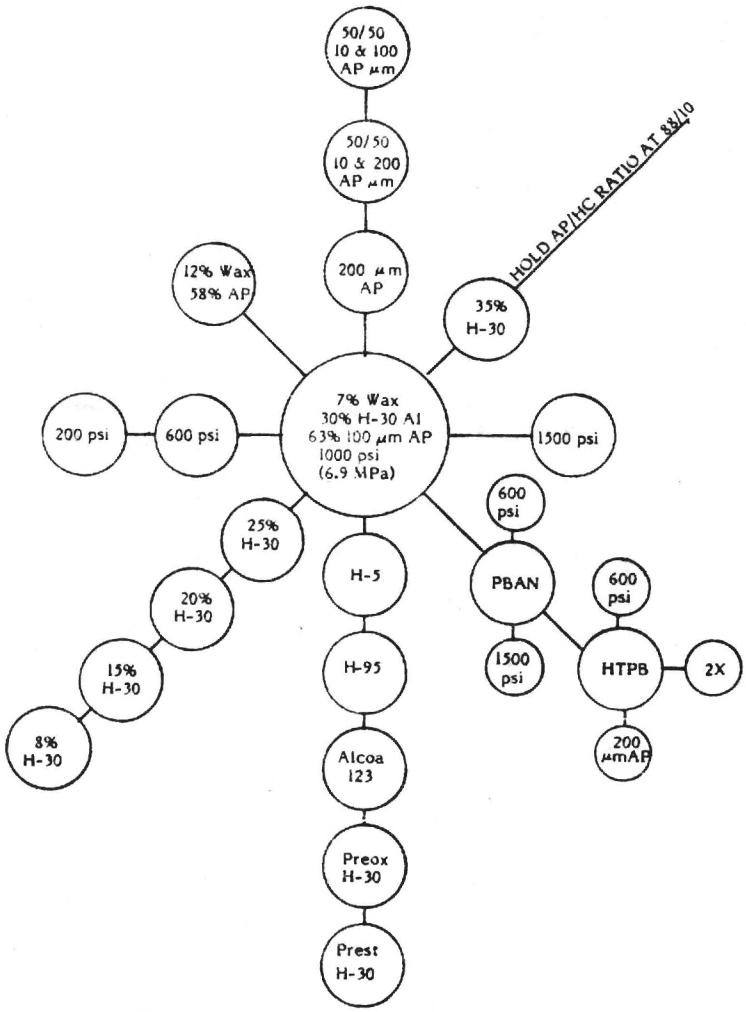

Fig. 35 Test conditions for combustion photography: AP-Wax-Al, "dry pressed" samples. Each small circle indicates one or more tests with indicated modification of test conditions relative to the "reference state" inside the large circle.

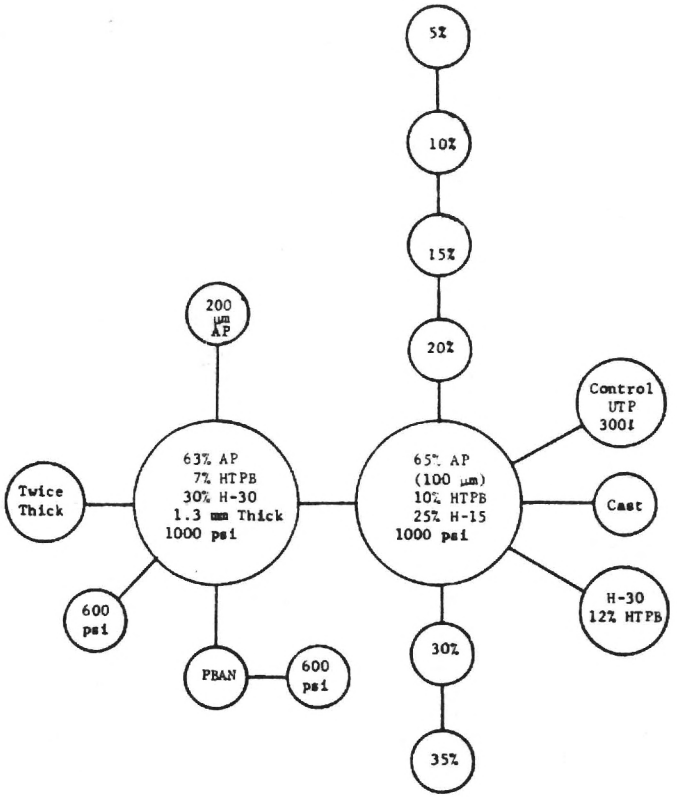

Fig. 36 Test conditions for combustion photography: AP-HTPB-Al, "wet pressed" samples.

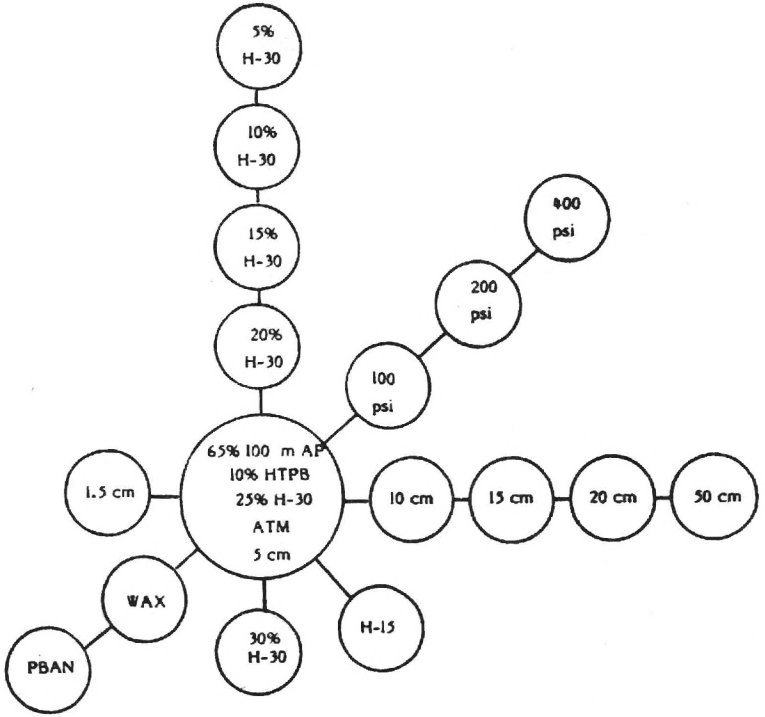

Fig. 37 Test conditions for plume quench samples.

tabulated in Table 7. Fig. 38 shows the effect of aluminum content on the burning surface as revealed by microscopic examination of quenched samples. Fig. 39 shows typical size distribution of aluminum agglomerates from plume quench tests and Fig. 40 shows amounts of unreacted aluminum remaining in plume quench samples for various test conditions (indicative of combustion efficiency). These and other results are presented in more detail in Ref. 39. From the combined results, the following conclusions were drawn regarding high aluminum content propellants.

1. Combustion efficiency of aluminum remains high to 25% aluminum. It is pressure-dependent in the range tested, and would apparently be better at typical rocket motor pressures than in the tests reported here.
2. Burning rate tends to a maximum around 18% aluminum, and the brightness of the combustion field peaks at about the same aluminum content.
3. The size of aluminum agglomerates (and degree of agglomeration) increase with aluminum content, especially above 25% aluminum. Other indicators of slow combustion also follow this trend (burning rate, brightness of field, combustion efficiency at 5 cm).
4. Several measures for improving combustion were found to be effective, including: treatment of aluminum powder to minimize agglomeration; choice of relative size of AP and Al particles so as to isolate groupings of accumulating aluminum particles on the burning surface from each other; choice of propellant and motor conditions conducive to aluminum ignition (particle size control, low binder content, high pressure).
5. An accompanying study (summarized elsewhere in this report and in Ref. 7) shows that the oxide products of burned agglomerates consist of about 85% smoke particles (< 2 μm) and 15% burnout residuals of agglomerates. The size of the latter depends on the size of the parent agglomerate, and increases with % aluminum. The size range is 5 - 80 μm. With a 25% aluminum propellant, the size could probably be kept around 10 -25 μm by appropriate choices of aluminum powder and of ingredient particle size distribution (this is a "projection"). Flow effects may modify the combustion-generated sizes.
6. Combustion behavior appears to be significantly dependent on propellant binder type, content, and/or distribution in the matrix. However,

Table 7
Summary of Effect of Test Variables on Combustion Behavior
As Indicated by Combustion Photography

Behavior / Variables	Accumulation on Surface	Accumulate Attachment to Surface	Ignition of Agglomerate	Size of Agglomerate
Effect of Increase in % Aluminum	Increases	Effect not clearly visible from movie; seems to be no effect. Oscillating sintered Al increases.	More agglomerates ignite on surface and remain longer on surface.	Increases
Effect of Increase in Pressure	Decreases but the effect is not significant between 1000 & 1500 psi.	At low pressure stays attached and glows red. Effect vanishes with pressure.	No significant variation. Mostly surface ignition.	Decreases, but not significantly between 1000 & 1500 psi.
Effect of Increase in Aluminum Particle Size	Increases	Stays attached to the surface longer; and with 95 μm particle intensively.	Ignition in the gas phase to surface ignition mostly.	Increases, but with 95 μm particle very little agglomeration.
Effect of Pre-treatment of Al (pre-oxidizing & pre-stretching)	Decreases considerably	Residence time on surface is reduced.	Ignition mostly in gas phase.	Decreases significantly.
Effect of Increase in Oxidizer Particle Size	Increases	Could not be detected very well.	No significant difference except with 200 μm AP Al agglomerates were spewed in all directions.	Increases
Effect of Addition of Fine AP	Decreases	No significant difference, but spewing of Al in 200 μm AP sample was absent.	No noticable difference.	Decreases
Wet Pressed Effect of Binder				
(a) PBAN	Decreases compared to wax.	Not observable.	Mostly surface ignition.	Decreases compared to wax.
(b) HTPB	Sample did not burn to completion (thickness effect) and sample burned almost like PBAN sample when made twice as thick.			
Second Series Effect of % Al Increase in HTPB Series.	Not observable because of bright field of view in all tests.		Ignition mostly after leaving surface in all samples.	Increases gradually.

Table 7 (Continued)
Summary of Effect of Test Variables on Combustion Behavior
As Indicated by Combustion Photography

Behavior Variables	Burning Rate	Brightness Near Burning Surface	Additional Remarks
Effect of Increase in % Aluminum	Peaks between 15 & 20% Al loading.	Peaks at 15 and 20% Al loading.	Amount of unburned Al leaving surface increases.
Effect of Increase in Pressure	Increases gradually.	Increases	Amount of unburned Al decreases, but not very significantly.
Effect of Increase in Aluminum Particle Size	Decreases	Decreases	Amount of unburned particle increases and is considerable with H-95.
Effect of Pre-treatment of Al (pre-oxidizing & pre-stretching)	Increases	Increases. Pre-oxidized gives higher burning rate.	Very little unburned Al leaving surface.
Effect of Increase on Oxidizer Particle Size	Decreases	Decreases	More unburned Al leaving surface.
Effect of Addition of Fine AP	Increases	Increases	Less unburned Al leaving the burning surface.
Wet-Presssed Effect of Binder (a) PBAN	Increases	Increases considerably.	Less unburned Al leaving surface.
(b) HTPB	Sample did not burn to completion (thickness effect), and sample burned almost like PBAN sample when made twice as thick.		
Second Series Effect of % Al Increase in HTPB Series	Peaks between 15 & 20% Al loading.	Peaks about 20% Al loading.	Very little unburned Al leaving the surface.

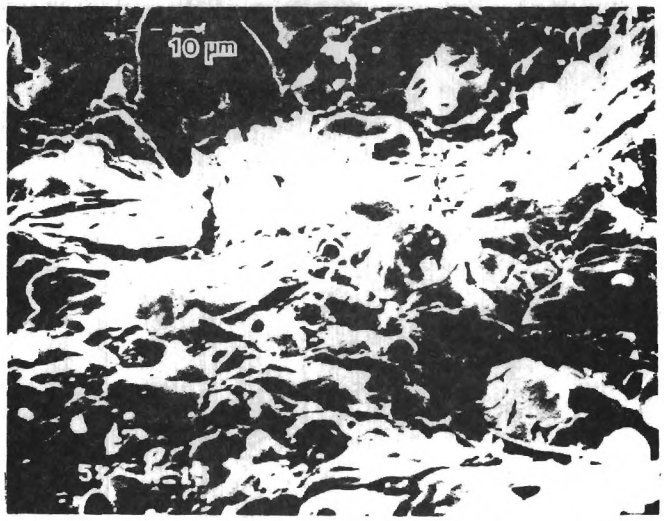

a

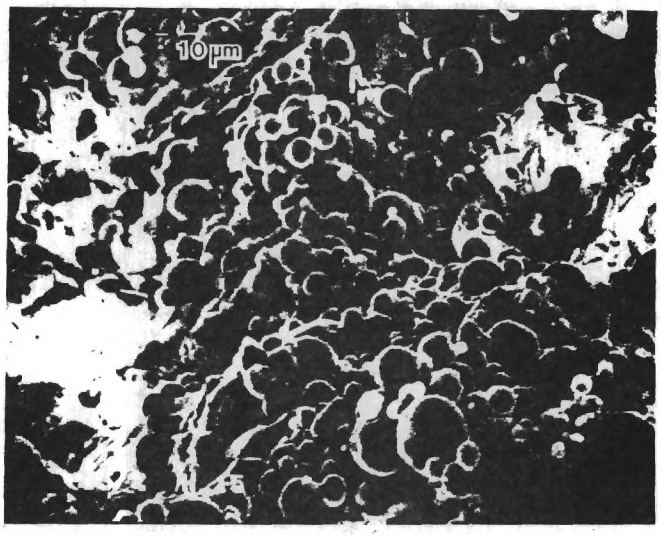

b

Fig. 38 Aluminum accumulation on the burning surface of AP-HTPB-Al sample quenched by rapid depressurization at 6.9 MPa. (a) Low % aluminum (5%). (b) High % aluminum (35%).

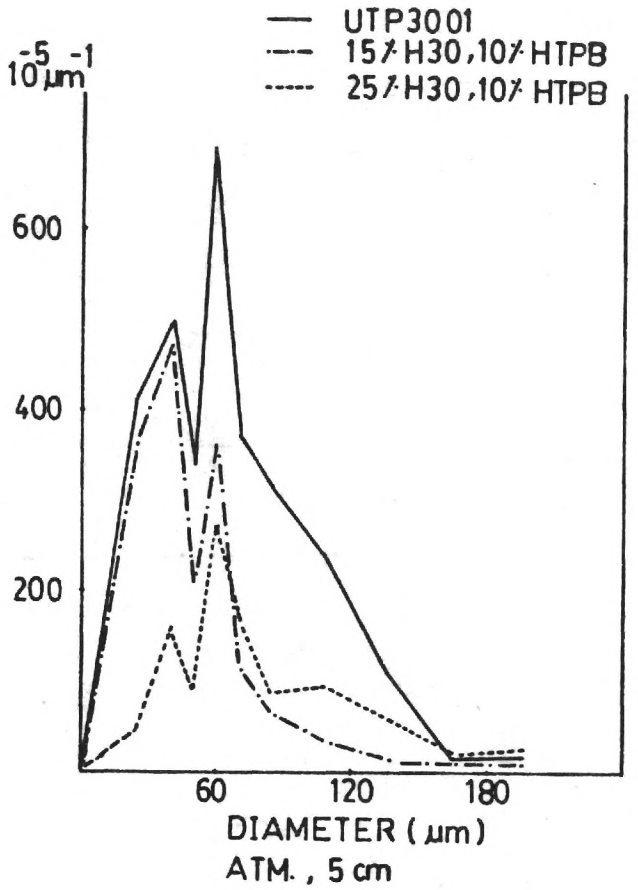

Fig. 39 Size distribution of particles in plume quench samples. Atmospheric pressure tests, quench distance = 5 cm.

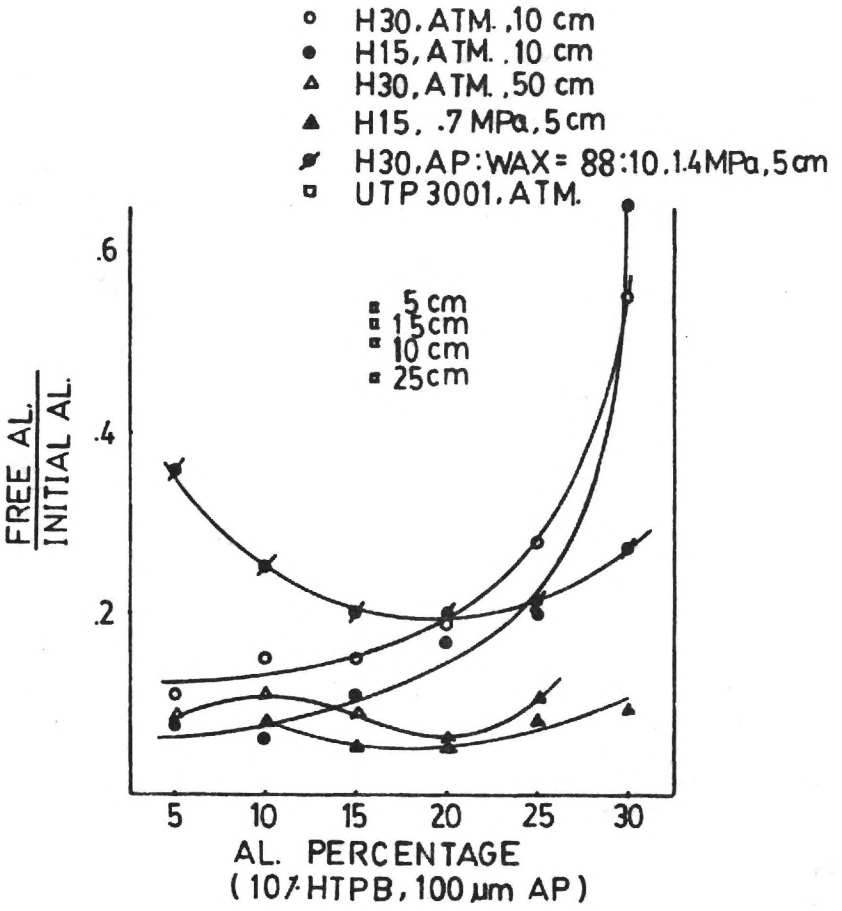

Fig. 40 Mass fraction of unreacted aluminum in plume quench samples (weight difference method of Al determination).

this variable was not adequately evaluated because of the improvised methods for propellant processing available in the study.

In general, the results suggest that combustion efficiency can be held to conventional levels with aluminum contents up to about 25%, provided propellant ingredients are tailored for that purpose. In the process, combustion-generated aluminum oxide size distributions can be kept comparable to present ones. This conclusion needs further support by tests on propellants with conventional binders and processing.

REFERENCES

1. Price, E. W., et al, "Combustion of Solid Propellants and Low Frequency Combustion Instability," NOTS TP 4244, June 1967.
2. Povinelli, L. A., and R. A. Rosenstein, "Alumina Size Distributions from High-Pressure Composite Solid Propellant Combustion," AIAA J., Vol. 2, No. 10 (1964), pp. 1754-1760.
3. Miller, R. R., "Some Factors Affecting the Combustion of Aluminum in Solid Propellants," ICRPG 2nd Combustion Conference, CPIA Publication 105, Vol. I, May 1966, p. 331-335.
4. Cohen, N. S., "A Pocket Model for Aluminum Agglomeration in Composite Propellants," AIAA/SAE/ASME 17th Joint Propulsion Conference, AIAA Paper 81-1585.
5. Price, E. W., "Combustion of Aluminum in Solid Propellant Flames," 53rd Meeting of AGARD Propulsion and Energetics Panel, 1979, AGARD-CP-259, pp. 14-1-14-15.
6. Hubbartt, J. E., E. W. Price, W. C. Strahle and B. T. Zinn, "Rocket Research at Georgia Tech," AFOSR Interim Scientific Report, November 1978.
7. Price, E. W., C. J. Park, R. K. Sigman and J. K. Sambamurthi, "The Nature and Combustion of Agglomerates," 18th JANNAF Combustion Meeting, CPIA Publication 347, October 1981.
8. Price, E. W., and R. K. Sigman, "Behavior of Aluminum in Solid Propellant Combustion," AFOSR-TR-77-0050, November 1976.
9. Caveny, L. H., and A. Gany, "Aluminum Combustion Under Rocket Motor Conditions," 53rd Meeting of the AGARD Propulsion and Energetics Panel, 1979, AGARD-CP-259, pp.13-1-13-13.
10. Price, E. W., "Relevance of Analytical Models for Perturbation of Combustion of Solid Propellants," AIAA J., Vol. 7, No. 1, (1969), pp. 153-154.
11. Brundige, W. N., and L. H. Caveny, "Combustion of Low-Burn-Rate HTPB Propellants in an Acceleration Field - Part III," 18th JANNAF Combustion Meeting, CPIA Publication 347, October 1981.
12. Price, E. W., et al, "The Fire Environment of a Solid Rocket Propellant Burning in Air," AFWL-TR-78-34, March 1979.
13. Price, E. W., W. C. Strahle, B. T. Zinn, J. E. Hubbartt, R. K. Sigman and B. R. Daniel, "Rocket Research at Georgia Tech," AFOSR Final Technical Report,

Georgia Institute of Technology, November 1981.

14. Price, E. W., E. A. Powell and R. K. Sigman, "Further Studies of the Fire Environment of a Solid Rocket Propellant Burning in Air," AFWL-TR-79-55, April 1980.
15. Micheli, P. L., and W. G. Schmidt, "Behavior of Aluminum in Solid Rocket Motors, Vol. I" AFRPL-TR-77-29, December 1977.
16. Kraeutle, K. J., and H. H. Bradley, Jr., "Combustion of Aluminized Propellants: The Influence of Pressure and Propellant Combustion on Formation of Aluminum Combustion Residue," 14th JANNAF Combustion Meeting, CPIA Publication 292, Vol. I, December 1977, pp. 209-219.
17. Price, E. W., J. E. Crump, H. C. Christensen and R. Sehgal, "Comments on 'Alumina Size Distributions from High-Pressure Composite Solid-Propellant Combustion'," AIAA J., Vol. 3, No. 9 (1965), pp. 1790-1791.
18. Brzustowski, T. A., and I. Glassman, "Vapor-Phase Diffusion Flames in the Combustion of Magnesium and Aluminum: I. Analytical developments, and II. Experimental observations in oxygen atmospheres," AIAA Progress in Astronautics and Aeronautics: Heterogeneous Combustion, edited by H. G. Wolfhard, I. Glassman, and L. Green, Jr., Academic Press Inc., New York, 1964, Vol. 15, pp. 75-158.
19. Boggs, T. L., D. E. Zurn, W. C. Strahle, J. C. Handley and T. T. Milkie, "Mechanisms of Combustion," NWC-TP-5514, July 1973.
20. Price, E. W., W. C. Strahle, B. T. Zinn, J. E. Hubbartt, D. H. Neale, R. K. Sigman and B. R. Daniel, "Rocket Research at Georgia Tech," AFOSR Interim Scientific Report, November 1979.
21. Schmidt, W., and R. Poynter, "Zirconium/Aluminum Combustion," AFRPL-TR-80-8, March 1980.
22. Mellor, A. M., and I. Glassman, "Augmented Ignition Efficiency for Aluminum," Combust. Sci. Technol., Vol. 1, No. 6 (1970), pp. 437-447. (See also: same title, Princeton University, Dept. of Aerospace Sciences Technical Report No. 791, 1967.)
23. Frolov, Yu. V., P. F. Pokhil, and V. S. Logachev, "Ignition and Combustion of Powdered Aluminum in High-Temperature Gaseous Media and in a Composition of Heterogeneous Condensed Systems," Fizika Goreniya i Vzryva, Vol. 8, No. 2 (1973), pp. 213-236.

24. Glassman, I., "Combustion of Metals: Physical Considerations," ARS Progress in Astronautics and Rocketry, Vol. 1, Solid Propellant Rocket Research, Academic Press, New York, 1960, pp. 253-258.

25. Boggs, T. L., et al, "Combustion of Solid Propellants and Low Frequency Combustion Instability," Progress Report, 1 October 1967-1 Novemberl968, NWC-TP-4749, June 1969.

26. Prentice, J. L., and K. J. Kraeutle, "Metal Particle Combustion," Progress Report, 1 May 1967-30 September 1968, NWC-TP-4658, January 1969.

27. Price, E. W., J. C. Handley, R. R. Panyam, R. K. Sigman, and A. Ghosh, "Combustion of Ammonium Perchlorate-Polymer Sandwiches," AIAA J., Vol. 19, No. 3, (1981), pp. 380-386.

28. Price, E. W., R. K. Sigman and R. R. Panyam, "Combustion Mechanisms of Solid Propellants," Annual Technical Report 1 August 1979-31 July 1980 for Office of Naval Research, Georgia Institute of Technology, September 1981.

29. Cohen, N. S., R. W. Fleming, and R. L. Derr, "Propellants and Combustion -- I, Role of Binder in Solid Propellant Combustion," AIAA/SAE 8th Joint Propulsion Specialist Conference, AIAA Paper 72-1121. (See also: AIAA J., Vol. 12, No. 2 (1974), pp. 212-218.

30. Miller, R. R., M. T. Donohue, R. A. Young, and J. R. Martin, "Control of Solids Distribution in HTPB Propellants," AFRPL-TR-78-14, April 1978.

31. Kraeutle, K. J., "The Behavior of Aluminum During Subignition Heating and Its Dependence on Environmental Conditions and Particle Properties," 9th JANNAF Combustion Meeting, CPIA Publication 231, December 1972, pp. 325-340.

32. Price, E. W., W. C. Strahle, B. T. Zinn, J. E. Hubbartt, R. K. Sigman, and B. R. Daniel, "Rocket Research at Georgia Tech," AFOSR Interim Scientific Report, Georgia Institute of Technology, November 1980.

33. Boggs, T. L., K. J. Kraeutle, and D. E. Zurn, "The Combustion of As-Received and Preoxidized Aluminum in Sandwich and Propellant Configurations," 9th JANNAF Combustion Meeting, CPIA Publication 231, December 1972, pp. 341-345.

34. Brundige, W. N., "Space Motor Combustion Technology, Phase I. Data Base Development," AFRPL-TR-80-52, December 1980.

35. Boggs, T. L., J. E. Crump, K. J. Kraeutle, and D. E. Zurn, "Cinephotomicrography and Scanning Electron Microscope as Used To Study

Solid Propellant Combustion at the Naval Weapons Center," NWC-TP-5944, May 1977.

36. Varney, A. M., "An Experimental Investigation of the Burning Mechanisms of Ammonium Perchlorate Composite Solid Propellants," Ph.D. Thesis, Georgia Institute of Technology, 1970.
37. Price, E. W., K. J. Kraeutle, R. K. Sigman, J. E. Crump,T. L. Boggs, D. E. Zurn, "Behavior of Aluminum in Solid Propellant Combustion, NWC-TP-6120, in press.
38. Crump, J. E., J. L. Prentice, and K. J. Kraeutle, "Role of Scanning Electron Microscope in the Study of Solid Propellant Combustion: II. Behavior of Metal Additives," Combust. Sci. Technol., Vol. 1 (1969), pp. 205-223.
39. Price, E. W., J. K. Sambamurthi, R. K. Sigman and C. J. Park, "Combustion of High Aluminum Content Solid Propellants," 18th JANNAF Combustion Meeting, CPIA Publication 347, October 1981.

DISTRIBUTION LIST

	Copies
Aerojet Solid Propulsion Company P. O. Box 13400, Bldg. 2019/Dept. 4350 Sacramento, CA 95813 Attn: Mr. Michael J. Ditore	1
Aerojet Strategic Propulsion Co. P. O. Box 15699C Sacramento, CA 95813 Attn: Dr. R. L. Lou Dr. Wilfred Schmidt	2
Aerospace Corporation P. O. Box 92957 Los Angeles, CA 90045 Attn: Ellis M. Landsbaum	1
U. S. Air Force Academy FJSRL/NC USAF Academy, CO 80840 Attn: Dr. John S. Wilkes, Jr.	1
AFATL Code DLDL Eglin AFB, FL 32542 Attn: Mr. Otto K. Heiney	1
Air Force Office of Scientific Research Directorate of Aerospace Sciences Bolling Air Force Base Washington, DC 20332 Attn: Dr. L. H. Caveny	10
Air Force Office of Scientific Research Directorate of Chemical Sciences Bolling Air Force Base Washington, DC 20332 Attn: Mr. Donald L. Ball	10
AFRPL Code PACC Edwards AFB, CA 93523 Attn: Mr. W. C. Andrepont Mr. Wayne Roe	2
AFRPL Code MKP/MS24 Edwards AFB, CA 93523 Attn: Mr. R. Geisler	1

	Copies
AFRPL Code DYSC Edwards AFB, CA 93523 Attn: Mr. Daweel George	1
AFRPL Code LK Edwards AFB, CA 93523 Attn: LTC B. Loving	1
AFRPL Code CA Edwards AFB, CA 93523 Attn: Dr. R. R. Weiss	1
Aeropropulsion Laboratory Wright-Patterson AFB Fairborn, Ohio Attn: Dr. F. D. Stull	1
Army Ballistic Research Labs ARRADCOM Code DRDAR-BLI Aberdeen Proving Ground, MD 21005 Attn: Mr. J. M. Frankle Dr. Ingo W. May Mr. L. A. Watermeier	3
Army Ballistic Research Labs ARRADCOM Code DRDAR-BLP Aberdeen Proving Ground, MD 21005 Attn: Dr. A. W. Barrows	1
Army Ballistic Research Labs ARRADCOM Code DRDAR-BLT Aberdeen Proving Ground, MD 21005 Attn: Dr. Philip Howe	1
Army Frankford Arsenal Bridge & Tacony Streets Philadelphia, PA 19137 Attn: J. Lannon	1
HQ US Army Material Development Readiness Command Code DRCDE-DW 5011 Eisenhower Avenue Room 8N42 Alexandria, VA 22333 Attn: Mr. S. R. Matos	1

	Copies
Army Missile Command Code DRSMI-R Redstone Arsenal, AL 35898 Attn: Dr. R. G. Rhoades	1
Army Missile Command Code DRSMI-RKL Redstone Arsenal, AL 35898 Attn: Dr. W. W. Wharton	1
Army Research & Development Command ARRADCOM Code LCWSL Dover, NJ 07802 Attn: Mr. C. Lenchitz	1
Army Research & Development Command ARRADCOM Code DRDAR-SCA-PE Dover, NJ 07802 Attn: Mr. L. Stiefel	1
U. S. Army Research Office P. O. Box 12211, Research Triangle Park, NC 27709 Attn: D. Squires	2
Atlantic Research Corp. 5390 Cherokee Ave. Alexandria, VA 22314 Attn: Dr. C. B. Henderson Dr. Merrill K. King Dr. W. Waesche	3
Brigham Young University Provo, UT 84601 Attn: Dr. Merrill W. Beckstead	1
British Embassy Munitions Directorate Propellants and Explosives Defence Equipment Staff 3100 Massachusetts Ave. Washington, DC 20008 Attn: Dr. T. Sinden	1

	Copies
Case Western Reserve Univ. Dept. of Mechanical & Aerospace Engineering Cleveland, Ohio 44106 Attn: James S. T'ien	1
California Institute of Tech. 204 Karman Lab 1201 E. California St. Pasadena, CA 91109 Attn: Fred E. C. Culick	1
California Institute of Tech. Jet Propulsion Laboratory 4800 Oak Grove Drive Pasadena, CA 91103 Attn: Leon D. Strand	1
Mr. Norman Cohen 858-A Pine Ave. Redlands, CA 92373	1
Defense Technical Information Center Code DTIC-DDA-2 Cameron Station Alexandria, VA 22314	12
Georgia Institute of Tech. School of Aerospace Eng. Atlanta, GA 30332 Attn: Prof. Edward Price	1
Hercules Inc. Aerospace Division Alleghany Ballistic Lab P. O. Box 210 Washington, DC 21502 Attn: Dr. Rocco C. Musso Dr. R. R. Miller	2
Hercules Inc. Bacchus Works P. O. Box 98 Magna, UT 84044 Attn: Dr. E. H. Debutts Dr. James H. Thacher Dr. K. McCarty	3

DISTRIBUTION LIST

	Copies
Hercules Inc. Eglin Code AFATL/DLDL Eglin AFB, FL 32542 Attn: Dr. Ronald L. Simmons	1
Institute for Defense Analyses 400 Army-Navy Drive Arlington, VA 22202 Attn: R. C. Oliver	1
Johns Hopkins University APL Chemical Propulsion Info. Agency Johns Hopkins Road Laurel, MD 20810 Attn: Mr. Thomas W. Christian Mr. Theodore M. Gilliland	2
Lawrence Livermore Laboratory University of California Code L-324 Livermore, CA 94550 Attn: Dr. R. McGuire	1
Los Alamos Scientific Lab Code NSP/DOD, MS-245 P. O. Box 1663 Los Alamos, NM 87545 Attn: Dr. B. G. Craig	1
Los Alamos Scientific Lab Mail Stop 920 Los Alamos, NM 87545 Attn: Ms. Joan L. Janney	1
Los Alamos Scientific Lab Code WX-2 P. O. Box 1663 Los Alamos, NM 87545 Attn: Dr. R. Rogers	1
Los Alamos Scientific Lab P. O. Box 1663 Los Alamos, NM 87545 Attn: Dr. J. M. Walsh	1
NASA/George C. Marshall Space Flight Center Code EP 25 Huntsville, AL 35812 Attn: J. Q. Miller	1
NASA/George C. Marshall Space Flight Center Code EP 24 Huntsville, AL 35812 Attn: Robert J. Richmond	1
NASA/HQ Code RP 600 Independence Ave., SW, Rm. 625 Washington, DC 20546 Attn: Frank W. Stephenson, Jr.	1
Scientific Advisor Commandant of the Marine Corps Code RD-1 Washington, DC 20380 Attn: Dr. A. L. Slafkosky	1
Office of Naval Research Code 413 Arlington, VA 22217 Attn: Dr. Richard S. Miller	1
Office of Naval Research Western Office 1030 East Green Street Pasadena, CA 91106 Attn: Dr. R. J. Marcus	1
Naval Air Systems Command Code 330 Washington, DC 20361 Attn: Mr. R. Brown	1
Naval Air Systems Command Code 03P25 Washington, DC 20360 Attn: Mr. B. Sobers	1
Naval Air Systems Command Code NAIR-954-Tech Library Washington, DC 20361	1
Naval Explosives Dev. Engineering Department Assistant Director Naval Weapons Station Yorktown, VA 23691 Attn: Dr. L. R. Rothstein	1
Naval Explosive Ordnance Disposal Tech Center Code D Indian Head, MD 20640 Attn: Dr. Lionel Dickinson	1
Naval Materiel Command Strategic Systems Project Office Department of the Navy Room 901 Washington, DC 20376 Attn: Dr. J. F. Kincaid	1
Naval Material Command Strategic Systems Project Office Propulsion Unit Code SP 2731 Department of the Navy Washington, DC 20376	1
Naval Material Command Strategic Systems Project Office Department of the Navy Room 1048 Washington, DC 20376 Attn: Mr. E. L. Throckmorton	1
Naval Ordnance Station CM PM4 Indian Head, MD 20640 Attn: Mr. C. L. Adams	1
Naval Ordnance Station Code 5253 Indian Head, MD 20640 Attn: Mr. S. Mitchell	1
Naval Ordnance Station Indian Head, MD 20640 Attn: Mr. Peter L. Stang	1
Naval Postgraduate School Dean of Research Monterey, CA 93940 Attn: Dr. William Tolles	1
Naval Postgraduate School Physics & Chemistry Dept. Monterey, CA 93940 Attn: Prof. Richard A. Reinhardt	1
Naval Postgraduate School Department of Aeronautics Monterey, CA 93940 Attn: Mr. David W. Netzer	1
Office of Naval Research Mechanics Program Code 432 Arlington, VA 22217 Attn: Dr. N. L. Basdekas	1
Naval Research Lab. Code 6100 Washington, DC 20375	1
Naval Research Lab. Code 6510 Washington, DC 20375 Attn: Dr. J. Schnur	1
Naval Sea Systems Command Code SEA 64E Washington, DC 20362 Attn: Mr. R. Beauregard	1
Naval Sea Systems Command Code 62R2 Washington, DC 20362 Attn: Mr. J. Murrin Mr. R. Cassell	2
Naval Ship Engineering Center Materials Branch Philadelphia, PA 19112 Mr. John Boyle	1
Naval Ship Research & Development Center Applied Chemistry Division Annapolis, MD 21401 Attn: Dr. G. Bosmajian	1

DISTRIBUTION LIST

	Copies
Naval Surface Weapons Center Commander Silver Spring, MD 20910 Attn: Mr. G. B. Wilmot	1
Naval Surface Weapons Center Code R10 White Oak Laboratory Silver Spring, MD 20910 Attn: Dr. S. J. Jacobs	1
Naval Surface Weapons Center Code R11 White Oak Laboratory Silver Spring, MD 20910 Attn: Dr. H. G. Adolph	1
Naval Surface Weapons Center Code R13 White Oak Laboratory Silver Spring, MD 20910 Attn: Dr. R. Bernecker	1
Naval Surface Weapons Center Code R16 Indian Head, MD 20640 Attn: Dr. T. D. Austin	1
Office of Naval Technology Chief MAT Code 0716 Washington, DC 20360 Attn: Dr. A. Faulstich	1
Office of Naval Technology Chief MAT Code 0712 Washington, DC 20360 Attn: LCDR J. Walker	1
Naval Underwater Systems Center Energy Conversion Dept. Code 5B331 Newport, RI 02840 Attn: Mr. Robert S. Lazar	1
Naval Weapons Center Code 385 China Lake, CA 93555 Attn: Dr. A. Amster	1

	Copies
Naval Weapons Center Code 388 China Lake, CA 93555 Attn: Mr. T. L. Boggs Dr. R. L. Derr Dr. R. Reed, Jr.	3
Naval Weapons Center Code 3205 China Lake, CA 93555 Attn: Mr. Lee N. Gilbert Dr. L. Smith Dr. C. Thelen	3
Naval Weapons Center Code 3272 China Lake, CA 93555 Attn: Mr. R. McCarten	1
Pennsylvania State University Dept. of Mechanical Engineering University Park, PA 16802 Attn: Prof. Kenneth Kuo	1
Princeton Combustion Research Laboratories, Inc. 1041 U. S. Highway One North Princeton, NJ 08540 Attn: Dr. Martin Summerfield	1
Princeton University School of Engineering and Applied Sciences Dept. of Mech. Eng. & Aero Eng. The Engineering Quadrangle Princeton, NJ 08544 Attn: Dr. Forman A. Williams	1
Purdue University School of Mechanical Engineering TSPC Chaffee Hall West Lafayette, IN 47906 Attn: Mr. John R. Osborn	1
Rockwell International Corp. Rocketdyne Division BA08 6633 Canoga Ave. Canoga Park, CA 91304 Attn: Mr. Joseph E. Flanagan	1

	Copies
Rohm and Haas Company Huntsville, AL 35801 Attn: Dr. H. Shuey	1
Sandia Laboratories Division 2513 P. O. Box 5800 Albuquerque, NM 87185 Attn: Dr. S. Sheffield	1
Science Applications, Inc. Suite 423 20335 Ventura Blvd. Woodland Hills, CA 91364 Attn: Mr. R. B. Edelman	1
Space Sciences, Inc. 135 Maple Avenue Monrovia, CA 91016 Attn: Dr. M. Farber	1
Southwest Research Institute Institute Scientist P. O. Drawer 28510 San Antonio, TX 78228 Attn: Mr. William H. McLain	1
Thiokol Corporation Elkton Division P. O. Box 241 Elkton, MD 21921 Attn: Mr. W. Brundige	1
Thiokol Corporation Government Systems Group Technical Director P. O. Box 9258 Ogden, UT 84409 Attn: Dr. T. F. Davidson	1
Thiokol Corporation Huntsville Division Huntsville, AL 35807 Attn: Dr. D. A. Flanigan Mr. G. F. Mangum Mr. J. D. Byrd	3

	Copies
Thiokol Corporation Wasatch Division P. O. Box 524 Brigham City, UT 84302 Attn: Dr. J. C. Hinshaw Mr. John A. Peterson Dr. G. Thompson	3
United Technologies Corp. Chemical Systems Division P. O. Box 358 Sunnyvale, CA 94088 Attn: Dr. Robert S. Brown Dr. C. M. Frey Dr. R. Hermsen	3
University of Illinois AE Dept. Transportation Building, Room 105 Urbana, IL 61801 Attn: Dr. Herman Krier	1
University of Southern California Mechanical Engineering Dept. OHE 200 Los Angeles, CA 90007 Attn: Dr. M. Gerstein	1
University of Utah Salt Lake City, UT 84112 Attn: Dr. G. A. Flandro	1
University of Waterloo Dept. of Mechanical Engineering Waterloo, Ontario CANADA Attn: Dr. Clarke E. Hermance	1
Whittaker Corporation Bermite Division 22116 W. Soledad Canyon Road Saugus, CA 90024 Attn: Mr. L. Bloom	1

AFOSR INTERIM SCIENTIFIC REPORT

AFOSR–TR–82

COMBUSTION DYNAMICS IN ROCKETS

Co-Principal Investigators

B. R. Daniel
J. E. Hubbartt
J. I. Jagoda
E. W. Price
R. K. Sigman
W. C. Strahle
R. E. Walterick
B. T. Zinn

Prepared for

AIR FORCE OFFICE OF SCIENTIFIC RESEARCH
AEROSPACE SCIENCES DIRECTORATE
BOLLING AIR FORCE BASE, D. C.

Under

Contract No. F49620–82–C–0013

November 1982

GEORGIA INSTITUTE OF TECHNOLOGY
A UNIT OF THE UNIVERSITY SYSTEM OF GEORGIA
SCHOOL OF AEROSPACE ENGINEERING
ATLANTA, GEORGIA 30332

AFOSR INTERIM SCIENTIFIC REPORT

AFOSR-TR-82

COMBUSTION DYNAMICS IN ROCKETS

Co-Principal Investigators

B. R. Daniel
J. E. Hubbartt
J. I. Jagoda
E. W. Price
R. K. Sigman
W. C. Strahle
R. E. Walterick
B. T. Zinn

Prepared for

AIR FORCE OFFICE OF SCIENTIFIC RESEARCH
AEROSPACE SCIENCES DIRECTORATE
BOLLING AIR FORCE BASE, D. C.

Contract No. F49620-82-C-0013

November 1982

GEORGIA INSTITUTE OF TECHNOLOGY
School of Aerospace Engineering
Atlanta, Georgia 30332

Unclassified

SECURITY CLASSIFICATION OF THIS PAGE *(When Data Entered)*

REPORT DOCUMENTATION PAGE		READ INSTRUCTIONS BEFORE COMPLETING FORM
1. REPORT NUMBER AFOSR-TR-82	2. GOVT ACCESSION NO.	3. RECIPIENT'S CATALOG NUMBER
4. TITLE *(and Subtitle)* Combustion Dynamics in Rockets		5. TYPE OF REPORT & PERIOD COVERED INTERIM 1 Oct. 81 - 30 Sept 82 6. PERFORMING ORG. REPORT NUMBER
7. AUTHOR*(s)* B. R. Daniel, J. E. Hubbartt, J. I. Jagoda, E. W. Price, R. K. Sigman, W. C. Strahle, R. E. Walterick, B. T. Zinn		8. CONTRACT OR GRANT NUMBER*(s)* AFOSR F49620-82-C-0013
9. PERFORMING ORGANIZATION NAME AND ADDRESS Georgia Institute of Technology School of Aerospace Engineering Atlanta, Ga 30332		10. PROGRAM ELEMENT, PROJECT, TASK AREA & WORK UNIT NUMBERS
11. CONTROLLING OFFICE NAME AND ADDRESS Air Force Office of Scientific Research/NA Bldg. 410 Bolling Air Force Base, D. C. 20332		12. REPORT DATE Nov. 1982 13. NUMBER OF PAGES
14. MONITORING AGENCY NAME & ADDRESS*(if different from Controlling Office)*		15. SECURITY CLASS. *(of this report)* Unclassified 15a. DECLASSIFICATION/DOWNGRADING SCHEDULE

16. DISTRIBUTION STATEMENT *(of this Report)*

Approved for public release; distribution unlimited

17. DISTRIBUTION STATEMENT *(of the abstract entered in Block 20, if different from Report)*

18. SUPPLEMENTARY NOTES

19. KEY WORDS *(Continue on reverse side if necessary and identify by block number)*

Solid Propellant Combustion; Unsteady Combustion; Aluminum; Noise; Turbulence; Vibration; Ramjets

20. ABSTRACT *(Continue on reverse side if necessary and identify by block number)*

Progress is reported on four distinct projects which are administered as a group. The projects are identified as tasks. A summary for each task follows:

Task I. In the first phase of this program the previously developed impedance tube setup was utilized to determine the dependence of solid propellants pressure coupled response functions and associated gas phase

DD FORM 1 JAN 73 1473 EDITION OF 1 NOV 65 IS OBSOLETE

SECURITY CLASSIFICATION OF THIS PAGE *(When Data Entered)*

20. Cont'd

losses upon the aluminum content of the propellant. Tests over the 400-1000 Hz frequency range showed that increasing the aluminum content of the propellant increases both the propellant driving and associated gas phase losses. Furthermore, it shifts the frequency at which maximum driving occurs. In the second phase of this task, the modified impedance tube setup has been utilized in the investigation of the characteristics of the velocity coupled response factor. The status of this investigation is summarized in this report.

Task II. The cold flow test facility, which will be used in the first phase of modeling flows in the flame stabilization region, and the two-component LDV system, which will be the main tool for velocity measurements, have been developed and tested to verify that performance is satisfactory and to acquire skills. Also, it has been determined that Rayleigh scattering will be used for measuring species concentration in cold flows and Raman scattering will be used for measuring both species concentrations and temperatures in the combustion tests which come later. The Rayleigh scattering system has been developed and preliminary tests have been completed in order to eliminate problems and develop techniques. Testing in the cold flow facility is being initiated now. In addition, a computer code that uses the k- method to model turbulence has been acquired, tested extensively via numerical experiments, and improved. Further checks and improvements, as required, will be made as cold flow data becomes available.

Task III. Studies of aluminum agglomeration-combustion in AP/Al/HC binder systems were continued, including refinement and extension of experimental methods, extension of the range of test variables, and consolidation of results into a comprehensive qualitative theory of aluminum behavior and summary of experimental results. A family of propellants was contrived to provide a critical test of key elements of agglomeration theory. Test results support the theory.

Task IV. Progress continued in the comparison between theory and experiment in the problem of pressure fluctuation prediction given the state of turbulence in rocket-like interior flows. A breakthrough was made in the prediction of the non-propagational, hydrodynamic component of pressure and the acoustic component continues to be predictable. Four configurations have now been tested, varying length to diameter ratio and side wall impedance. Future tests will concentrate on mass flow and mass flow distribution variations.

TABLE OF CONTENTS

TASK I

INVESTIGATION OF THE PRESSURE AND VELOCITY COUPLED RESPONSE FUNCTIONS OF ALUMINIZED AND NON ALUMINIZED SOLID PROPELLANTS

BEN T. ZINN BRADY R. DANIEL

A. Research Objectives

The general objective of this study is the determination of the characteristics of the burn rates of different classes of solid propellants under various conditions simulating those observed in unstable solid propellant rocket motors. More specifically, the research conducted during the past year under this task was concerned with the determination of the dependence of propellant driving and damping upon the aluminum content of the propellant and the development of experimental capabilities for investigating the characteristics of velocity coupled response functions of solid propellants.

B. Status of Research

During the initial phase of this reporting period the previously developed impedance tube setup was utilized in the investigation of the effect of aluminum addition upon the response functions and gas phase losses associated with aluminized propellants. To isolate the effect of aluminum content, three different propellant formulations differing primarily in their aluminum content were tested over the 400-1000 Hz frequency range. The

tested propellants, UZ7, UZ8 and UZ9 had similar nonaluminized fractions and they contained 0,5 and 18 percent aluminum, respectively. Typical results obtained in these tests are provided in Fig. 1 where y_r, the real part of the admittance, describes the propellant driving and G the associated gas phase losses. Examination of Fig. 2 shows that increasing the aluminum content of the propellant (1) increases the driving capabilities of the propellant; (2) shifts the frequency at which maximum driving occurs; and (3) increases the gas phase damping. Since increasing both the propellant driving and the gas phase damping would exert countering effects on the stability of a rocket motor, one cannot determine the effect of aluminum addition upon a given rocket stability without conducting an analysis capable of properly accounting for the above indicated effects. Furthermore, it remains to establish that the observed effects are due to the aluminum addition only and not due to the slight differences in the compositions of the nonaluminized fractions of the tested propellants.

The experimental configuration developed for the determination of the velocity coupled response functions of solid propellants is shown in Fig. 2 along with the impedance tube wave equations. These equations are similar to those utilized in rocket motor axial stability analyses, the only difference being that in the latter case the length of the sidewall propellant sample is equal to the motor length. In an experiment, the "driver" propellant sample provides a stream of hot combustion products that moves past the "test" propellant samples in an attempt to simulate actual rocket flow conditions. The acoustic driver at the opposite end of the tube is used to excite a standing wave of a desired frequency inside the impedance tube and the

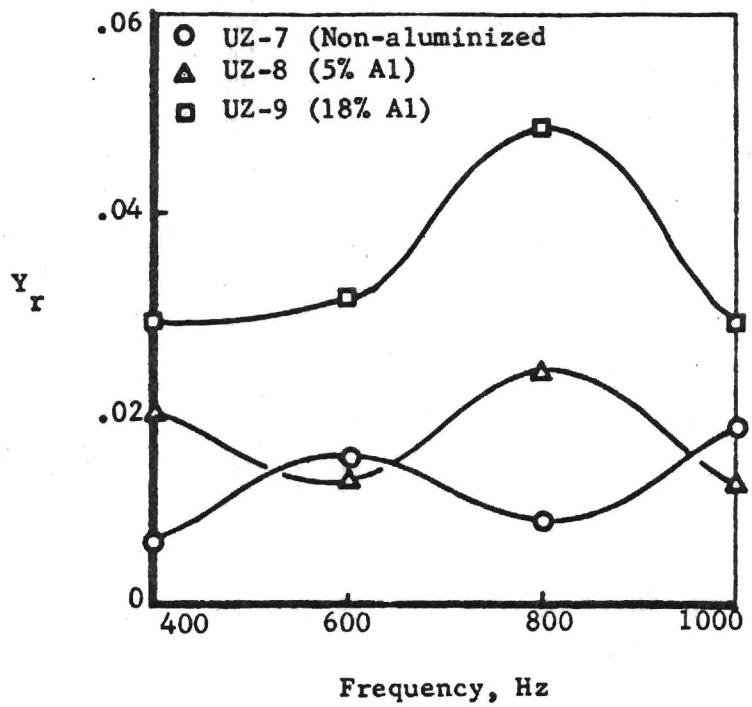

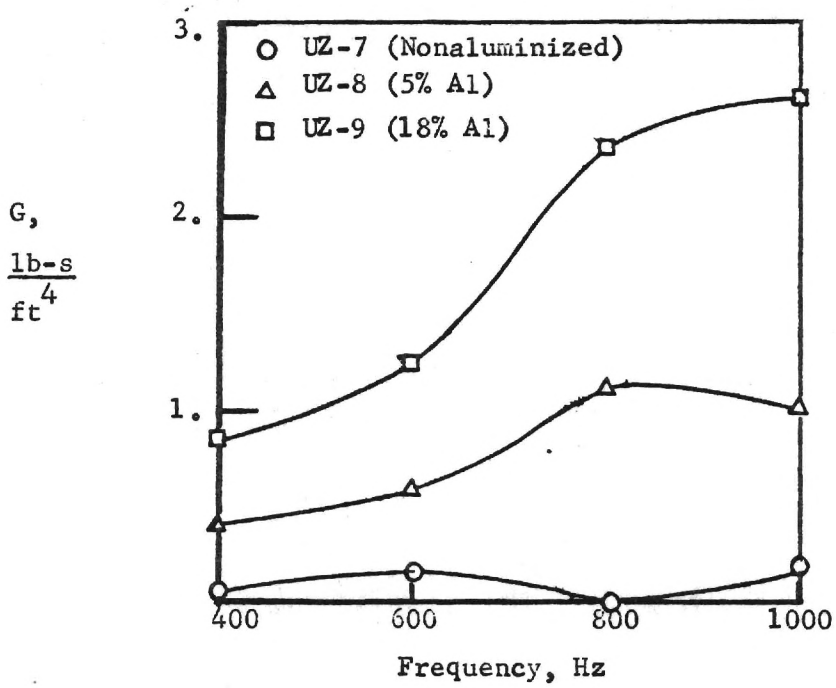

Fig. 1. Dependence of Propellant Driving, Y_r, and Associated Gas Phase Losses, G, upon Frequency and Propellant Aluminum Content.

IMPEDANCE TUBE WAVE EQUATIONS

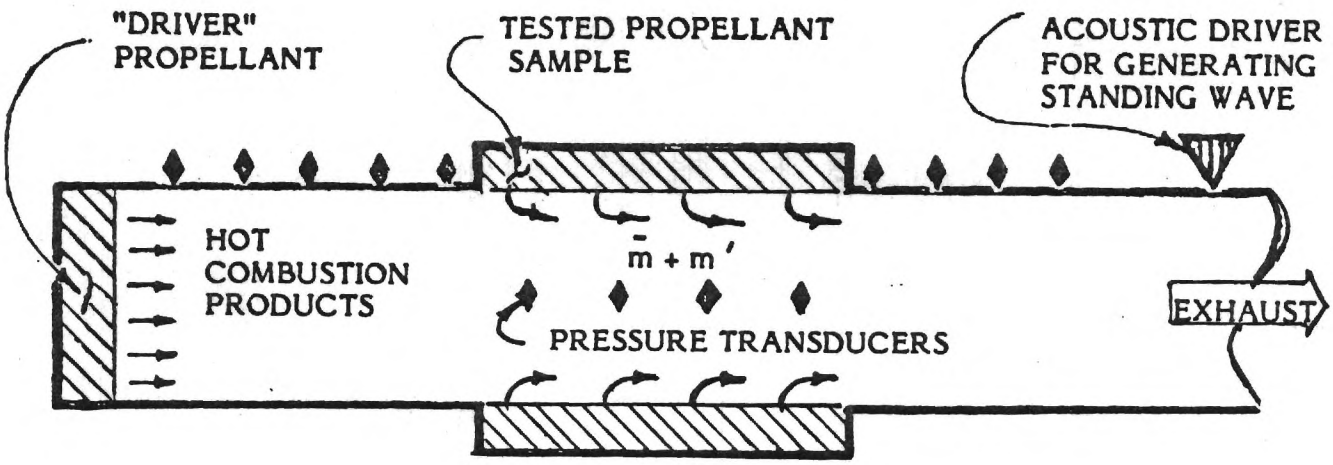

CONTINUITY: $$i\omega\rho' + \frac{d}{dx}(\bar{u}\rho' + \bar{\rho}u') = \frac{b}{A}m_b'$$

MOMENTUM: $$i\omega\bar{\rho}u' + \bar{\rho}\bar{u}\frac{du'}{dx} + \bar{\rho}\frac{d\bar{u}}{dx}u' + \frac{dp'}{dx} + \frac{b}{A}\bar{m}_b u' + F' = 0$$

ENERGY: $$i\omega p' + \bar{u}\frac{dp'}{dx} + \frac{d\bar{p}}{dx}u' + \gamma\bar{p}\frac{du'}{dx} + \gamma\frac{d\bar{u}}{dx}p' = \frac{b}{A}\bar{m}_b\bar{E}\left(\frac{E'}{\bar{E}} + \frac{m_b'}{\bar{m}_b}\right) + (\gamma-1)G\bar{u}u'$$

WHERE

$$E = \gamma RT_F + \gamma R\Delta T + (R/2C_v)(u^2 + u_b^2)$$

THE VELOCITY AND PRESSURE COUPLED RESPONSE FUNCTIONS ARE INTRODUCED BY LETTING

$$R_p = \frac{\left(\frac{E'}{\bar{E}} + \frac{m_b'}{\bar{m}_b}\right)}{\left(\frac{p'}{\bar{p}}\right)} \quad ; \quad R_v = \frac{\left(\frac{E'}{\bar{E}} + \frac{m_b'}{\bar{m}_b}\right)}{(u'/\bar{a})}$$

OR

$$\frac{m_b'}{\bar{m}_b} + \frac{E'}{\bar{E}} = R_p\frac{p'}{\bar{p}} + R_v\frac{u'}{\bar{a}}$$

Fig. 2. Set-up and Equations Utilized for the Determination of Velocity Coupled Response Functions.

tested propellant sample is placed in a region experiencing both pressure and axial velocity oscillations. The developed experimental setup permits locating the "test" propellants at any distance downstream of the "driver" propellant. Consequently, the response of the "test" propellants can be investigated at different acoustical environments along the standing wave (e.g., at a pressure node). A stepping motor is utilized to feed the "test" propellant samples inward at the propellant burning rate. This is done in order to maintain the burning "test" propellant surfaces flush with the impedance tube walls.

During a test, the acoustic pressure data are continuously fed, via an analog-to-digital converter, into a minicomputer-disc system for storage. The test duration is divided into a series of data acquisition periods, separated from each other by periods of data transfer. Each data acquisition period, called a block, can be programmed to acquire data over a period whose duration is a multiple of 12 cycles of the test signal.

After the test, the stored data are Fourier-analyzed to obtain the amplitudes and phases of the measured data at the test frequency. A study of the analyzed data shows the existence of ignition and extinguishment transients with a quasi-steady burning period in between. Data obtained during this quasi-steady period is used to evaluate the propellant response. The data reduction procedure developed for the velocity coupled case has been discussed in detail at the 18th JANNAF Combustion Meeting. It is to be noted, however, that the data-reduction procedure presumes a knowledge of the pressure coupled response and it determines only the velocity coupled

response function. Consequently, the pressure coupled response function needs to be determined in a separate experiment or by use of a reliable theory.

Since many of the acoustic pressure measurements are performed near the pressure node, the desired signal is often buried in noise from other sources. Signal averaging can be used to separate the signal from the noise. Since the available memory of the minicomputer limits the amount of data that can be recorded in a given block, an estimate of the minimum number of periods of the test signal over which the data should be averaged to sufficiently enhance the signal-to-noise ratio is required. This problem is currently being investigated by comparing data averaged over different numbers of cycles during the quasi-steady burning period.

The spatial amplitude and phase distributions, used to evaluate the velocity coupled response functions, were obtained by averaging the measured signals over 36 cycles. The needed pressure coupled response functions were measured by the use of the previously developed impedance tube method. A comparison between the computed standing wave pattern that provided the "best" agreement and the experimental data is presented in Fig. 2. The determined optimum value of R_v and the measured value of R_p that were used to predict the standing wave pattern are also indicated in the figure.

Examination of Fig. 2 indicates a reasonable agreement between the predicted and measured amplitude distributions. In contrast, some disagreement is noted in the compared phase distributions. These

discrepancies could be due to errors in measurements and/or data reduction procedure or due to shortcomings in the wave equations that are currently utilized (see Fig. 1) to model the axial instability problem. Specifically, a rigorous justification for the utilized definitions of R_p and R_v is lacking and there exists no proof that the utilized "one-dimensional" formulation is indeed capable of accounting for the multi-dimensional aspects of the problem where driving of the axial oscillations occurs on the side walls. These problems are currently under investigation under this program.

C. Publications

(1) Zinn, B. T., and Narayanaswami, L., "Application of the Impedance Tube Technique in the Measurement of Provided by Solid Propellants During Combustion Instabilities", Acta Astranautica, Vol. 9, 1982.

(2) Zinn, B. T., Baum, J. D. and Daniel, B. R., "Determination of Aluminized Solid Propellant Admittances by the Impedance Tube Method," AIAA Journal, Vol. 20, No. 3, pp. 417-421, March 1982.

(3) Zinn, B. T., and Narayanaswami, L., "Experimental Determination of the Velocity Coupled Response of Solid Propellants," Proceedings of the 18th JANNAF Combustion Meeting, Pasadena, CA, Oct. 1981.

(4) Sigman, R. K., and Zinn, B. T., "A Finite Element Approach for Predicting Nozzle Admittances," accepted for publication in the Journal of Sound and Vibrations.

D.Personnel

Principal Investigators - Ben T. Zinn and Brady R. Daniel.

Graduate Research Assistants - Lakshmanan Narayaraswami and Koorosh Madnia.

E Professional Activities

(1) Zinn, B. T., "Experimental Determination of the Velocity Coupled Response of Solid Propellants", presented at the 18th JANNAF Combustion Meeting, Jet Propulsion Laboratory, Pasadena, Calif., Oct. 19-23, 1981.

(2) Zinn, B. T., "Investigation of the Driving and Gas Phase Losses Associated with Different Aluminized and Nonaluminized Propellants," presented at the 19th JANNAF Combustion Meeting, NASA/Goddard Space Flight Center, Greenbelt, Md., October 4-7,1982.

(3) Zinn, B. T., "Investigation of the Velocity and Pressure Coupled Admittances of Aluminized and Nonaluminized Propellants", AFOSR Contractors' Meeting, Lancaster, Calif., March 1982.

(4) Member, U. S. Air Force Review Panel for the New Aero Propulsion Systems Test Facility (ASTF) in Tullahoma, Tenn.

TASK II

HETEROGENEOUS DIFFUSION FRAME STABILIZATION

WARREN C. STRAHLE JAMES E. HUBBARTT J. I. JAGODA

A. Research Objective

The overall objective of the program is to understand and be able to predict recirculatory turbulent reacting flows, flame stabilization limits, and fuel regression rates in a flame stabilization region like that for a solid fueled ramjet. The specific goals for the past year were to develop a cold flow test facility, develop the Laser Doppler Velocimeter, make plans and preparations for analysis and testing, and begin cold flow tests.

B. Status of research

During this past year substantial progress has been made toward the overall objective by way of completing preliminary tasks necessary before the integrated experimental and analytical studies. The tasks include the development of test equipment, diagnostic techniques, and analysis. The following paragraphs summarize the major accomplishments.

1. Test equipment. Design, fabrication, assembly, and check-out of the cold flow test facility has been completed. This facility will be used in the first phase of the progressive modeling of flows in flame stabilization zones. It has a rectangular cross-section and draws room air past a rearward facing step which simulates the flameholder with recirculation. The large scale test section is 43 cm long, 40.5 cm wide, and 10.5 cm high. The boundary layer thickness and step height are variable. Flow velocity is variable up to about 100 m/sec. Preliminary tests have shown that the mean flow in the test zone is two-dimensional and is the quality needed for evaluating and developing the analysis. The facility is equipped for making mean flow and turbulent velocity surveys using both Laser Doppler

Velocimeter (LDV) and hot wire anemometer techniques. Furthermore, mean velocity profiles can be evaluated using pressure probes and the surfaces are equipped with numerous static pressure taps for measuring pressure gradients.

Also, during this period, the second channel of the LDV has been acquired and assembled. In addition, the LDV actuator, with stepping motors and remote controller, has been developed. This portable actuator provides the capability of surveying over a total volume 30 x 48 x 70 cm. Finally, facilities for calibrating the LDV and hot wires have been developed.

2. Diagnostics. The program makes use of advanced laser diagnostic techniques for measuring instantaneous velocities, species concentration, and temperatures and for evaluating their spectra and correlations. This year, the work focused on considering and selecting techniques, developing equipment, and preliminary testing in simple flows. The testing has been necessary in order to develop procedures and skills, isolate and eliminate problems, and determine accuracies.

Testing with the two-channel LDV has uncovered serious problems with respect to the electronics, signal to noise ratio, flow seeding, and test section windows. Faulty electronic components have been repaired by the manufacturer. Also, as examples, it has been determined that the nominal diameter of seeding particles must be near 1μm for a satisfactory doppler signal and that the test section window must be clean and made of good quality glass rather than plexiglas to eliminate excessive noise. Now, it is thought that all serious problems have been resolved and that operator skills are adequate for final testing. Thus, testing will begin in the cold flow facility. In parallel, velocities will be measured with hot wires and pressure probes to check and complement the LDV data.

Rayleigh scattering (i.e., molecular scattering) has been selected as the technique for measuring species concentrations for the cold flow case with surface

blowing of foreign gases. Since velocity and concentration measurements are to be carried out simultaneously, the LDV beams will be used as the incident radiation for molecular scattering. The gases must be seeded for the LDV measurements and the intensity of light scattered from these seed particles is many orders of magnitude greater than that from molecules. Because this intense light will render the photomultiplier (PM) for Rayleigh scattering measurements inoperative for a long time, the PM must be gated off when particles are in the test volume. The gating circuit has been designed and assembled. Tests have shown that this circuit performs satisfactorily. However, the tests reveal a signal fluctuation of about $\pm$ 15% due to photon "shot noise" (i.e., fluctuations due to changes in the number of photons in the test volume) and submicron particles in the air. It has been decided that this will not affect cross correlations because of the randomness of shot and submicron particle noise but will affect auto correlations. For auto correlations it will be necessary to deal with probability density functions which can be corrected by extracting the portion due to noise.

Vibrational Raman scattering has been selected for simultaneous concentration and temperature measurements in flows with combustion. The Candela Dye Laser and spectrometer have been ordered and a polychromator for mounting photomultipliers at the exit plane of the spectrometer is being designed. It is anticipated that considerable experience will be acquired with the Raman scattering system prior to the development of the combustion test facility.

3. Analysis. A computer code that uses the k-ϵ method to model turbulence has been acquired and used for numerical experiments which explored characteristics and capabilities of the k-ϵ approach for predicting flow details in the flame stabilization region with cold flow conditions. The code uses the usual conservation equations for the mean flow variables and two additional equations for evaluating the turbulent kinetic energy, k, and dissipation rate, ϵ, which are

employed as turbulence scales to establish a turbulent viscosity relating Reynolds stresses to mean flow strain rates. Also, a second computer code based on the same k-ϵ model has been written for the one-dimensional, asymptotic solution of fully developed channel flow. This code was developed as a simple method for assessing the other code at the asymptotic limit far downstream of the flame stabilization region.

It has been determined that at least 30 streamwise and 40 cross-stream grid points will be required for satisfactory convergence of the numerical computations in the flame stabilization region. This requires a CPU time of about 700 sec. on the CYBER 74. Also, it has been determined that the numerical solution must be extended to about 100 channel heights downstream of the step expansion before fully developed channel flow conditions are achieved. Because this asymptotic limit, which is easily specified, cannot be obtained in the test configuration it may be necessary to input downstream as well as upstream boundary conditions for accurate predictions in the flame stabilization region. Further studies are being made to determine the sensitivity of the results to the downstream conditions. The flowfield predictions by the two computer codes for the one-dimensional asymptotic limit were in excellent agreement. Also, these predictions agreed with available channel flow data.

Comparisons between predictions with the k-ϵ code and available experimental data for the cold flow version of the flame stabilization region have shown that predicted turbulent stresses and reattachment lengths are in serious error. However, substantial improvements in the predictions have been obtained by including a new velocity-pressure gradient correlation in the turbulent kinetic energy equation. Also it has been shown that additional improvements can be made by adjusting empirical constants in the k-ϵ equations. Justifications for changing constants are still being sought. It is anticipated that further improvements will be

made as the experimental data from the cold flow facility becomes available.

C. Publications

1. J. E. Hubbartt and W.C. Strahle, "External/Base Burning for Base Drag Reduction at Mach 3," AIAA Journal, 19, pp. 1502-1504, Nov., 1981.
2. W. C. Strahle, J.E. Hubbartt and R. E. Walterick, "Base Burning Performance at Mach 3," AIAA Journal, 20, pp. 986-991, July, 1982.

D. Personnel

Principal Investigators - Warren C. Strahle
James E. Hubbartt
Jechiel I. Jagoda

Research Engineers - Ronald E. Walterick

Graduate Research Assistant - Wilhemus A. DeGroot
William M. Grissom
William J. McNicoll
Johnny C. Richardson

E. Professional Activities

Strahle, W.C., "Base and External Burning for Propulsion," presented at JANNAF Combustion Meeting and AGARD Conference on Ramjets and Ramrockets for Military Applications, Oct., 1981.

Strahle, W.C., "Solid Propellant Airbreathing Combustion Phenomena," presented at AFOSR Contractors Meeting, Lancaster, CA, Feb., 1982.

TASK III
BEHAVIOR OF ALUMINUM IN SOLID PROPELLANT COMBUSTION

E. W. PRICE R. K. SIGMAN

A. Research Objectives

The objectives of this task were to gain understanding and improved control of combustion of the aluminum ingredient in solid propellant, and of the aluminum effect in overall propellant combustion. In practical terms, this relates to attainment and assurance of desired burning rate, combustion efficiency, combustor stability and resistance to detonation while striving for high propellant density and high specific impulse.

Specifically, the objectives were to clarify the accumulation processes that set the stage on the propellant burning surface for formation of "large" agglomerates of aluminum, and to clarify the conditions for ignition-agglomeration, the nature and combustion of agglomerates, and the nature of the oxide product population.

Six areas of investigation were described in the original proposal, and progress in these areas is summarized in the following.

B. Progress and Significant Accomplishments

General.

Because of the complex and varied nature of aluminum combustion behavior in propellants (Fig. 1), the present program has been designed to clarify the qualitative aspects of the combustion. This approach was based on the premise that a rigorous analytical description of the overall behavior would be intractable, and a simple analytical description would be naive. Accordingly, attention was addressed to clarification of the remaining controversial aspects of aluminum behavior.

A variety of experimental studies were undertaken and/or continued from earlier work, studies designed to establish the controlling mechanisms in the various sequential steps characteristic of aluminum behavior in combustion of ammonium perchlorate-aluminum-hydrocarbon binder propellants burning in quiescent atmospheres. In addition, it was proposed that studies be extended to propellants with other formulations, and to combustion with flow environments.

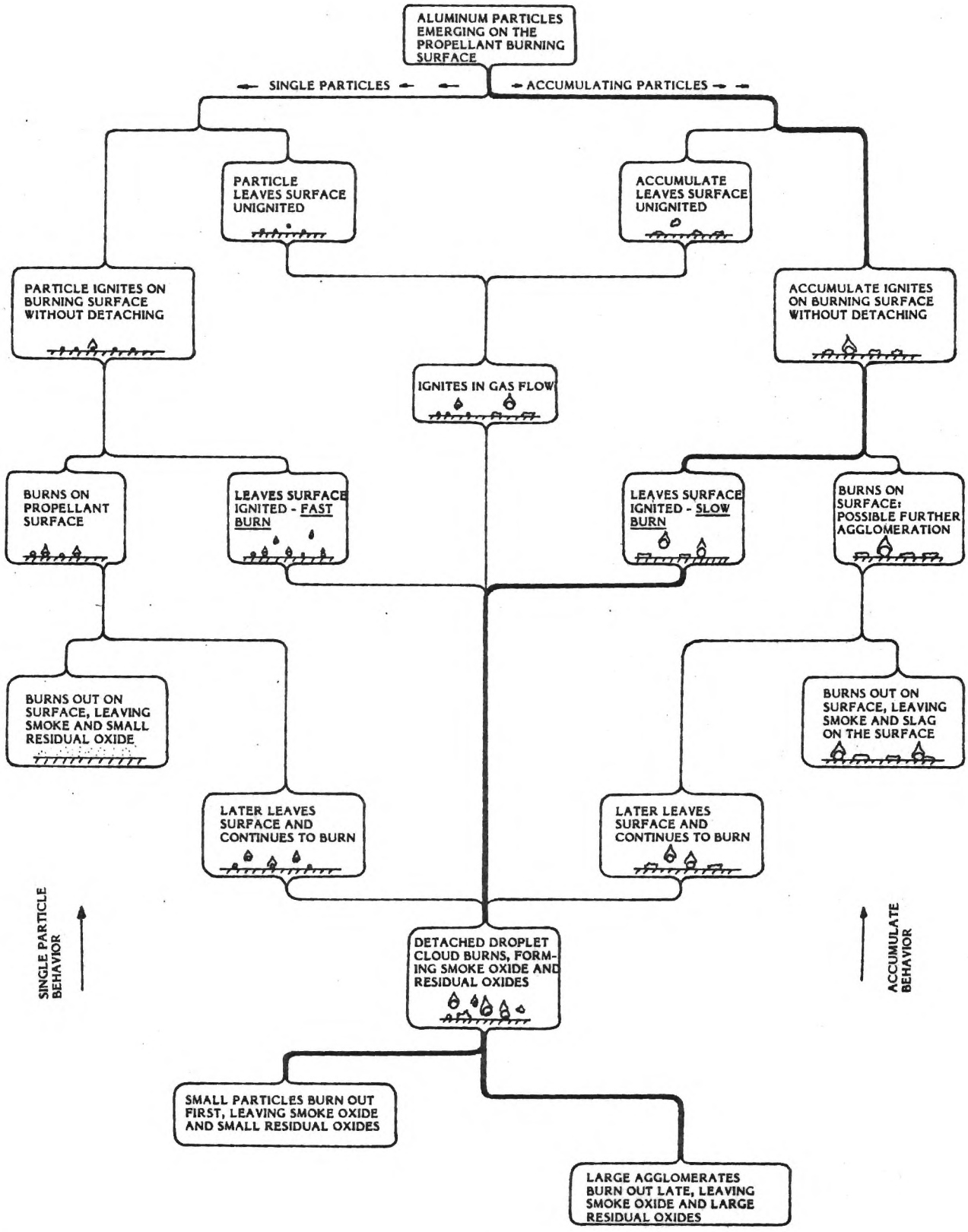

Fig. 1 Diagrammatic representation of the sequences of behavior of aluminum during propellant combustion.

Conditions Conducive to Inflamation of Accumulates.

A crucial aspect of aluminum behavior is the accumulation on the propellant burning surface, a process usually terminated upon local ignition of concentrations of aluminum called "accumulates". A variety of experiments were run that established that aluminum does not readily ignite in the environment of the deflagrating oxidizer alone. The experiments indicate that inflamation of accumulates is induced by exposure to local high temperature flamelets formed in the mixing interfaces between oxidizer and binder vapors. In addition to experiments reported earlier, this interpretation was used to predict the behavior of a series of propellants with bimodal oxidizer particle size distribution. Using particle sizes and pressures chosen specifically to control the availability of flamelets to ignite aluminum, the size of accumulates and resulting agglomerates was observed to follow closely the trends predicted on the basis of proximity of flamelets to terminate local accumulations. These results are partly reported in Ref. 1, and Fig. 2. Results now available indicate not only the dependence of inflamation on oxidizer-binder flamelets, but also a critical condition for existence of such flamelets near the burning surface (Ref. 1, 2). This critical condition was discovered on a companion project (Ref. 2), and explains also certain other singular aspects of propellant combustion such as burning rate trends of bimodal propellants (Ref. 3).

Nature of Agglomerates.

When an accumulate inflames, it usually coalesces into a single droplet called an "agglomerate", which detaches from the burning surface and burns in the combustor flow. These agglomerates often have rather complex structure that reflects the manner of their formation and affects their burning and the nature of the oxide products. In the present studies, agglomerates were quenched in a number of combustion systems, at various times during burning, and studied by a variety of methods. The collected results establish that a fully inflamed agglomerate is a spherical droplet of aluminum with a lobe of molten oxide. The droplet has from 5 to 15% void volume, the amount being dependent on pressure and agglomerate size, and the volume being in one or more unsymmetrically disposed voids that are not ordinarily open to the surface. The agglomerate also contains an irregular interior array of oxide films, remnants of the oxide skins on the original aluminum particles that coalesced into the agglomerate. These

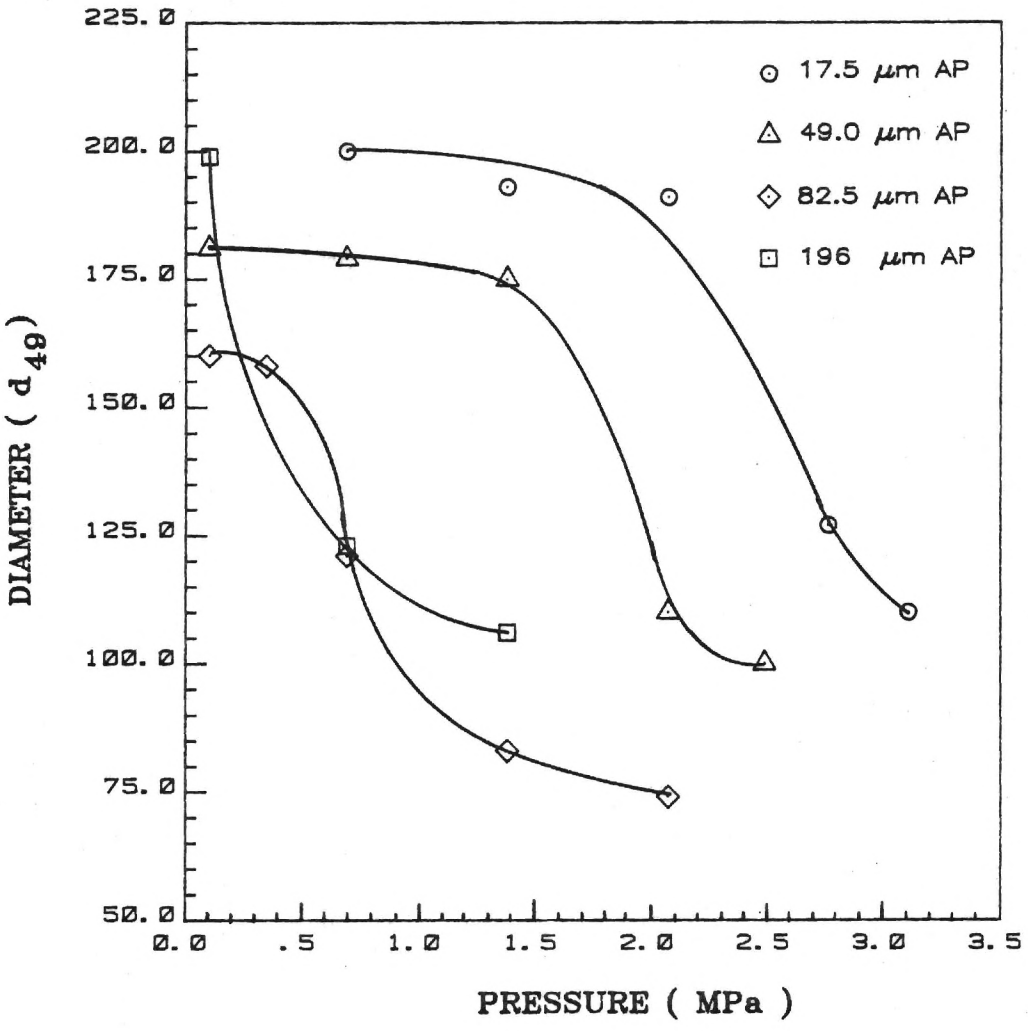

Fig. 2 Effect of pressure and oxidizer particle size on mass-average agglomerate size. Bimodal AP propellant with 4:1 ratio of coarse (400 μm) to fine AP. AP/Al/PBAN binder mass ratio 71/18/11. Transition to small agglomerate size corresponds to establishment of local oxidizer-binder flamelets on individual fine AP particles, and hence earlier ignition of aluminum.

features are revealed by microscopic examination of intact, cleaved, and acid-etched agglomerates, and are described more fully in Ref. 4 and 5.

Burning History of Agglomerates.

In addition to earlier studies by combustion photography, the present studies using quenching of agglomerates at various distances from the burning surface have permitted rather complete characterization of agglomerates and the entire plume as a function of time during burning. Fig. 3 shows the configurations of agglomerates at successively greater distance from the burning surface, and Fig. 4 shows the mass fraction of unreacted aluminum as a function of distance from the burning surface for a typical AP/Al/HC binder propellant. Results are described in greater detail in Ref. 4, 5, 6. Results establish that:

a) Most of the oxide (~ 85%) forms as fine smoke in a detached flame around the agglomerates.

b) Some of the oxide (0 - 5%) forms before agglomeration is complete and is present in and on the burning agglomerate.

c) Some oxide (0-10%) forms by either reaction or condensation on the agglomerate surface during burning.

d) The oxide increasingly dominates the agglomerate as the aluminum is burned away (Fig. 3c).

e) The aluminum droplet cloud is consumed very rapidly as it moves away from the burning surface (Fig. 4), but the consumption rate drops off rapidly, and the last 20% burns slowly enough to affect combustion efficiency in the motor. This problem is aggravated by heavy agglomeration and unusually fuel-rich stoichiometry.

Results to date do not determine the nature of the burnout phase of agglomerates, although they seem to exclude fragmentation events observed in some idealized laboratory experiments on single particle combustion (e.g., in air). Results also do not establish any burning rate law for individual agglomerates. This objective is being pursued, using a propellant that is formulated to form only one agglomerate size.

Oxide Product Populations.

It is generally recognized that, in addition to the fine oxide smoke formed in the flame envelope around the agglomerate, the final reaction products contain

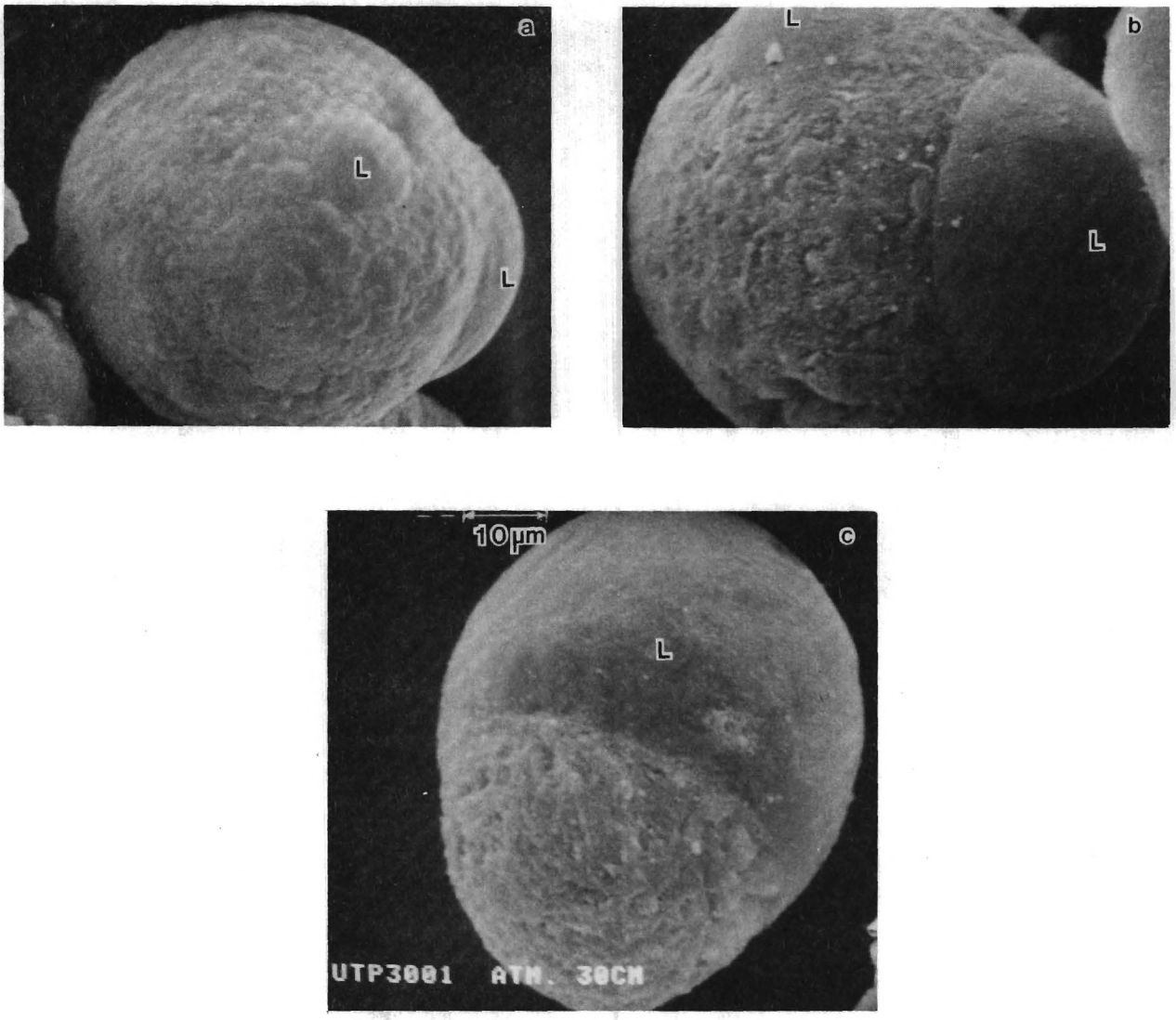

Fig. 3 Configuration of agglomerates at successively later times in burning. "L" designates oxide lobe.

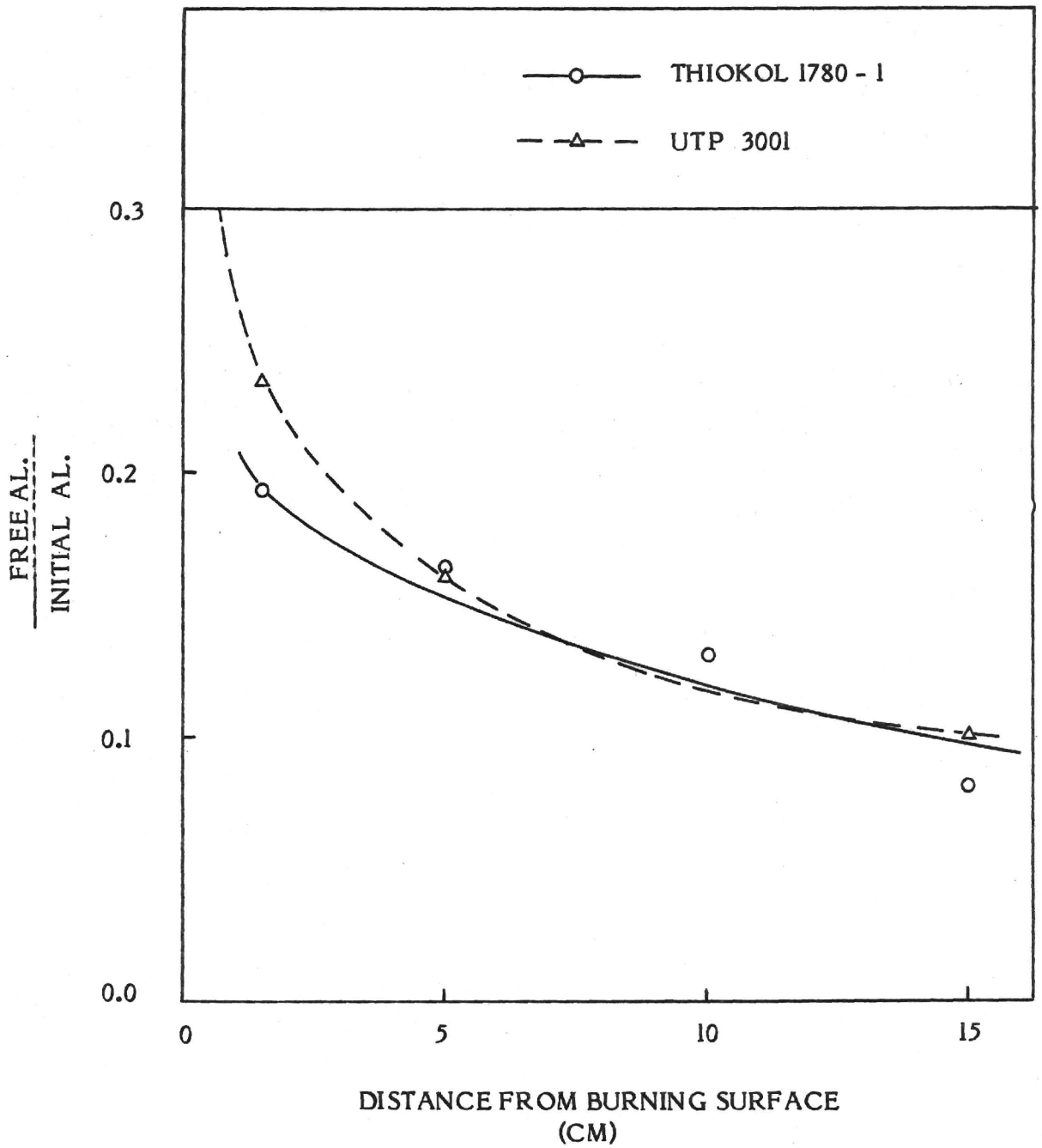

Fig. 4 Unburned aluminum vs quench distance. Tests at 0.7 MPa.

from 5 - 20% of coarser droplets. These are presumed to be the residual oxide left behind when agglomerates burn out. The present results of studies of quenched samples indicate that the size distribution is generally consistent with the trend of oxide accumulation on the parent agglomerates, implying that burnout is "noncatastrophic". However, this coarse fraction of the total oxide particle population (particles $> 5\ \mu m$) is made up of two different kinds of particles. One kind is relatively small in size (generally $< 35\ \mu m$) and is present in relatively small mass fraction. The particles are smooth, void-free, and nearly transparent. The second kind is relatively large ($> 30\ \mu m$), somewhat porous, white opaque, with surface (and sometimes interior) suggestive of crystallization patterns. The size distribution indicates that the coarse fraction represents the bulk of the residual agglomerate oxide. The smaller, transparent particles may be expelled from agglomerates during burnout. Details of the testing and results are reported in Ref. 4-6. The results account qualitatively for the observed oxide distribution in reaction products. Under convective flow conditions the size distribution in the combustion chamber would be modified to the extent that the agglomerate size distribution would be different (Ref. 7).

Combustion Behavior in Flow Environments.

Work on this subject has not been initiated yet. The current objective is to observe photographically the responsiveness of the behavior of aluminum on the burning surface to flow disturbances parallel to the burning surface.

Other Propellants.

It is considered to be important to apply the increased understanding and experimental methods to study of propellants other than the AP/Al/HC binder system. The rather limited efforts to obtain propellants with HMX and/or energetic binders have revealed that there are formidable difficulties in obtaining even very small quantities. The quantities required are so small that hazard can be reduced to zero, but shipping regulations are usually cited as the problem.

Plume quench tests were completed on an AP/Al/HTPB propellant containing 10% fine HMX. Results are reported in Ref. 5. The only visible effect of the HMX was the presence of tiny "blow holes" in the binder, indicating subsurface vaporization of the HMX.

Synthesis of Studies of AP/Al/HC Binder Systems.

A major effort was made to consolidate the results of the studies to date, which provide a fairly complete understanding of aluminum behavior in AP/Al/HCB systems burning under quiescent conditions. These efforts at consolidation are available in Ref. 5, and are reflected in Ref. 6 as well. In addition, much of the work is consolidated in the Ph.D. thesis (Ref. 7) that will be available in the near future.

Development of Experimental Methods.

Several new techniques were developed that have long-term usefulness.

1. A new method was developed for analysis of the content of unoxidized aluminum in quench samples; the method is relatively easy to use and gives accurate results.
2. A method of microscopic observation of the response of particles to heating was contrived using electrical heating of particles in the scanning electron microscope. Response of aluminum particles (in vacuum) was observed successfully.
3. A modification of the plume quench experiment was evaluated at atmospheric pressure. The method provides more precise knowledge of the distance from the propellant surface to quench point. The plume impinges perpendicularly on a porous plate flooded with transpired coolant (ethanol).

Summary.

The work during this year was primarily a continuation of studies of FY 1981 on agglomeration, ignition of accumulates, formation and nature of agglomerates, combustion of agglomerates, and formation and nature of product oxide droplets. Experimental methods (quiescent atmospheres) were improved and systematic tests were run to determine trends with pressure and propellant variables. The available understanding was organized into a qualitative theory, and the experimental results leading to that theory were assembled into a summary report. A family of propellants was devised to demonstrate certain critical features of the theory, and tested over a range of pressures. The observed agglomeration trends were consistent with trends predicted by the theory, and provide an explanation for previously unexplained results by other investigators.

References

1. Price, E. W., J. K. Sambamurthi, C. J. Park and R. K. Sigman, "Aluminum Agglomeration and Ignition in Propellants with Bimodal AP Size Distribution," 19th JANNAF Combustion Meeting, October 1982, to be published by CPIA.
2. Price, E. W., R. R. Panyam, J. K. Sambamurthi and R. K. Sigman, "Combustion of Ammonium Perchlorate-Polymer Sandwiches," 19th JANNAF Combustion Meeting, October 1982, to be published by CPIA.
3. Miller, R. R., "Effects of Particle Size on Reduced Smoke Propellant Ballistics," AIAA/SAE/ASME 18th Joint Propulsion Conference, June 1982, AIAA preprint AIAA-82-1096.
4. Price, E. W., C. J. Park, R. K. Sigman and J. K. Sambamurthi, "The Nature and Combustion of Agglomerates," 18th JANNAF Combustion Meeting, CPIA Publication 347, October 1981.
5. Price, E. W., R. K. Sigman, J. K. Sambamurthi and C. J. Park, "Behavior of Aluminum in Solid Propellant Combustion," Scientific Report on Contracts AFOSR F 49620-78-C-0003 and AFOSR F 49620-82-C-0013, Georgia Institute of Technology, June 1982.
6. Price, E. W., et al, "Rocket Research at Georgia Tech," Final Scientific Report on Contract AFOSR F 49620-78-C-0003, Georgia Institute of Technology, November 1981.
7. Sambamurthi, J. K., "Behavior of Aluminum on the Burning Surface of a Solid Propellant," Ph.D. Thesis in preparation at Georgia Institute of Technology.

C. Publications and Presentations

The following were published or presented during 1 October 1981 to 30 September 1982.

1. Price, E. W., C. J. Park, R. K. Sigman, and J. K. Sambamurthi, "The Nature and Combustion of Agglomerates," 18th JANNAF Combustion Meeting, CPIA Publication 347, October 1981.
2. Price, E. W., J. K. Sambamurthi, R. K. Sigman and C. J. Park, "Combustion of High Aluminum Content Solid Propellants, 18th JANNAF Combustion Meeting, CPIA Publication 347, October 1981.

3. Price, E. W., W. C. Strahle, B. T. Zinn, J. E. Hubbartt, R. K. Sigman and B. R. Daniel, "Rocket Research at Georgia Tech," Final Scientific Report on AFOSR Contract No. F49620-78-C-0003, Georgia Institute of Technology, November 1981.

4. Price, E. W., Behavior of Aluminum in Solid Propellant Combustion," presented at AFOSR/AFRPL Combustion Contractors Meeting, Lancaster, CA, March 1982.

5. Price, E. W., R. K. Sigman, J. K. Sambamurthi and C. J. Park, " Behavior of Aluminum in Solid Propellant Combustion," Scientific Report on Contracts AFOSR F 49620-78-C-0003 and AFOSR F 49620-82-C-0013, Georgia Institute of Technology, June 1982.

6. Price, E. W., J. K. Sambamurthi, C. J. Park and R. K. Sigman, "Aluminum Agglomeration and Ignition in Propellants with Bimodal AP Size Distribution," presented at 19th JANNAF Combustion Meeting, October 1982, to be published by CPIA.

7. Price, E. W., K. J. Kraeutle, J. L. Prentice, T. L. Boggs, J. E. Crump, and D. E. Zurn, "Behavior of Aluminum in Solid Propellant Combustion," NWC TP-6120, March 1982 (writing of this review was started by the first author in 1969, completed in 1980 under Naval Weapons Center and Georgia Institute of Technology sponsorship; publication completed in 1982).

D. Personnel

Principal Investigators -- E. W. Price, Professor, and R. K. Sigman, Senior Research Engineer.

Graduate Research Assistants -- J. K. Sambamurthi and C. J. Park.

E. Professional Activities

1. Participant, 18th JANNAF Combustion Meeting, presentation of papers 1. and 2. above, October 1981.
2. Organization, chair and report on JANNAF Workshop on Combustion Zone Microstructure, 1981-82.
3. Participant, AFOSR/AFRPL Combustion Contractors Meeting, March 1982.
4. Participant, AIAA Joint Propulsion Specialists Meeting, June 1982.
5. Member, AIAA National Publications Committee.

TASK IV

ROCKET MOTOR AEROACOUSTICS

WARREN C. STRAHLE

A. Research Objectives

The overall objective of this program is to show that a) if the turbulence structure is known within a rocket motor cavity flow and b) if the propellant response characteristics are known, then the pressure fluctuation level within a motor may be predicted with regard to its spectral content and amplitude. The specific goals for the past year have been redevelopment of the theory and addition to the data base.

B. Status of Research

Substantial progress has been made during the past year in meeting the program goal. The following paragraphs summarize the major accomplishments:

1. Hydrodynamic vs Acoustic Pressure. A breakthrough has occurred in prediction of the non-propagational, non-acoustic component of pressure away from the walls. It had previously been found that this component, significantly higher than wall-measured pressure fluctuations, could not be predicted. Moreover, the fact that it was so high was leading to serious doubts about the experimental procedure. A method was found during the past year to line-integrate the momentum equation in a manner to reveal this pressure component, and it is now predictable to within 10% accuracy. In conjunction with the fact that the acoustic component of wall pressure

fluctuations had already been proven predictable, it is now believed that the physics of pressure generation within flow cavities is now well-understood.

2. Theoretical Studies. In conjunction with the work above, the theory of both acoustic and non-acoustic pressure fluctuations has been reformulated to make it somewhat more understandable to the non-practitioner. Preliminary calculations have also been made in rocket motor environments where propellant response is important in determining the pressure level. It is being shown that any pressure level desired can be produced if the propellant and cavity combination is sufficiently near a stability limit.

3. Experimental Studies. Completion of data reduction and comparison of theory and experiment has now been completed on four set-ups. One has been a long pipe terminated with a choked nozzle. Three have been rocket motor simulators made of porous walls, taking in mass from the sides to simulate a center-perforated grain configuration. Variables have been length to diameter ratio and side wall impedance. A fifth configuration to be tested will vary internal velocity.

Agreement between calculated acoustic pressure and experiment have in general been good. A notable lack of agreement has been in the actual amplitude of the pressure fluctuation in the first longitudinal mode. It is believed that insufficient data have been taken on the velocity fluctuation spectrum for a good prediction here, and this deficiency is currently being rectified.

C. Publications

1. U. G. Hegde and W. C. Strahle, "Investigation of Turbulence Generated Pressure Fluctuation in Some Interior Flows" AIAA Paper No. 82-0175.

D. Personnel

Principal Investigator - Warren C. Strahle

Graduate Research Assistant - Uday G. Hegde

E. Professional Activities

Strahle, W. C., "Investigation of Turbulence Generated Pressure Fluctuations in Some Interior Flows", presented at AIAA 20th Aerospace Sciences Meeting, Orlando, FL, January 1982.

Strahle, W. C. "Rocket Motor Aeroacoustics" presented at AFOSR Contractors' Meeting, Lancaster, CA, March 1982.

AFOSR FINAL SCIENTIFIC REPORT

ROCKET RESEARCH AT GEORGIA TECH

Co-Principal Investigators

E. W. Price

W. C. Strahle

B. T. Zinn

J. E. Hubbartt

R. K. Sigman

B. R. Daniel

Prepared for

AIR FORCE OFFICE OF SCIENTIFIC RESEARCH

AEROSPACE SCIENCES DIRECTORATE

BOLLING AIR FORCE BASE, D. C.

Under

Contract No. F49620-82-C-0013

November 1983

GEORGIA INSTITUTE OF TECHNOLOGY

A UNIT OF THE UNIVERSITY SYSTEM OF GEORGI/

SCHOOL OF AEROSPACE ENGINEERING

ATLANTA, GEORGIA 30332

REPORT DOCUMENTATION PAGE

READ INSTRUCTIONS BEFORE COMPLETING FORM

1. REPORT NUMBER: AFOSR-TR-83
2. GOVT ACCESSION NO.:
3. RECIPIENT'S CATALOG NUMBER:

4. TITLE (and Subtitle): ROCKET RESEARCH AT GEORGIA TECH

5. TYPE OF REPORT & PERIOD COVERED: Final, 27 Nov. 81 - 30 Sept. 83

6. PERFORMING ORG. REPORT NUMBER:

7. AUTHOR(s): E. W. Price, W. C. Strahle, B. T. Zinn, J. E. Hubbartt, R. K. Sigman, B. R. Danile

8. CONTRACT OR GRANT NUMBER(s): AFOSR F49620-82-C-0013

9. PERFORMING ORGANIZATION NAME AND ADDRESS:
GEORGIA INSTITUTE OF TECHNOLOGY
SCHOOL OF AEROSPACE ENGINEERING
ATLANTA, GA 30332

10. PROGRAM ELEMENT, PROJECT, TASK AREA & WORK UNIT NUMBERS:

11. CONTROLLING OFFICE NAME AND ADDRESS:
AIR FORCE OFFICE OF SCIENTIFIC RESEARCH/NA
BLDG. 410
BOLLING AIR FORCE BASE, D.C. 20332

12. REPORT DATE: Nov. 1983

13. NUMBER OF PAGES:

14. MONITORING AGENCY NAME & ADDRESS (if different from Controlling Office):

15. SECURITY CLASS. (of this report): UNCLASSIFIED

15a. DECLASSIFICATION/DOWNGRADING SCHEDULE:

16. DISTRIBUTION STATEMENT (of this Report)

Approved for public release; distribution unlimited

17. DISTRIBUTION STATEMENT (of the abstract entered in Block 20, if different from Report)

18. SUPPLEMENTARY NOTES

19. KEY WORDS (Continue on reverse side if necessary and identify by block number)

SOLID PROPELLANT COMBUSTION, ALUMINUM AGGLOMERATION, ALUMINUM COMBUSTION, COMBUSTION INSTABILITY, COMBUSTION OSCILLATION, RESPONSE FUNCTION, IMPEDANCE TUBE, TURBULENCE NOISE, TURBULENT COMBUSTION, EXTERNAL BURNING PROPULSION, BASE FLOW, SUPERSONIC FLOW.

20. ABSTRACT (Continue on reverse side if necessary and identify by block number)

TASK I: Several investigations of phenomena related to the driving of combustible instabilities in solid propellant rocket motors were performed. A modified impedance tube setup for determining velocity coupled response functions of solid propellants was developed. Tests conducted in this facility showed that the characteristics of velocity coupled response functions depend upon the location of the propellant within the combustor. This

finding contradicts currently accepted notions that the velocity coupled response function is a propellant property. In addition, cold flow experimental studies of oscillatory flows in tubes with inflows through porous side walls and theoretical modelling of gas phase solid propellant flames were performed.

TASK II: Measurement and analysis of a simulated solid fueled ramjet combustion stabilization region. Flow field measurements were made using hot film, x-film, pitot-static and laser velocimeter instrumentation. Analysis was carried out using a k-ϵ methods.

TASK III: Studies continued on behavior of aluminum in the combustion zone of AP-hydrocarbon binder propellants, with further consolidation of past work into a qualitative theory, and conduct of a combustion study on specially formulated propellants designed as a test of the theory. Proposed studies of aluminum behavior in other propellant systems have not been conducted because of difficulties in obtaining samples. Studies were initiated on behavior of other nonvolatile ingredients that are used in propellants either as burning rate modifiers or combustion instability suppressants. Preliminary results are presented on combustion of ZrC in propellant flames, and several burning rate modifiers in AP-hydrocarbon binder sandwiches.

TASK IV: Turbulence generated noise in the interior flow of rocket motors. Measurements were made in cold flow simulators of solid rocket combustors, and results were compared with predictions based on adaptation of the Bernoulli enthalpy theory of aeroacoustics.

TABLE OF CONTENTS

GENERAL INTRODUCTION

Activities and progress are summarized for the 2 years of AFOSR Contract No. F49620-82-C-0013, with emphasis primarily on progress not reported in the previous annual reports and publications. The project consists of four interrelated tasks that are reported individually in this report and described below.

Task I has been concerned with the determination of the mechanisms of driving by solid propellants in unstable rocket motors. Special attention was paid to the determination of the response of the solid propellant burn rate to velocity oscillations parallel to the propellant surface. This phenomenon has been investigated in an impedance tube which has been developed for this purpose. Tests conducted to date showed that the driving provided by the solid propellant section depends upon its location within the combustor; an observation which contradicts current practices which assume that the velocity coupled response function is a propellant property. Additional studies conducted under this program included hot wire measurements of oscillatory velocity fields in tubes with porous walls and mass addition through these walls, and theoretical modelling of oscillatory solid propellant gas phase flames.

Task II is concerned with experiments and analysis on a reacting flow configuration which models the flame stabilization region of a solid-fueled ramjet. Current experiments have completed the facility development and cold flow testing. Conventional intrusive diagnostics have been used and initial results have been obtained with LDV, non-intrusively. The k-ϵ

method of turbulence analysis has been used with excellent results in the cold flow case. Primary interest is in the predictability of this complex flow field.

Task III is concerned with combustion behavior of relatively nonvolatile particulate ingredients in solid propellants, including metal fuel powders, burning rate modifiers, and combustion stabilizers. Behavior of such ingredients does not conform to usual combustion models, and is resistant to experimental observation because of the nonsteady, and microscopic scale of the relevant processes. A family of combustion experiments have been developed that permitted the combustion behavior of aluminum powder to be clarified and controlled. These methods are now being applied to other metals of interest (e.g., boron), to ballister modifiers (e.g., Fe_2O_3), and to combustion stabilizers (e.g., 2rc).

Task IV is concerned with prediction of turbulence-induced pressure fluctuations in rocket motors, particularly as they pertain to production of vibrations in motor structure. The approach combines analytical developments and cold flow experiments, using each as a means to validate or guide improvement of the others. The analysis indicates what measurements and data analysis are necessary to interpret the experiments, and the measurements indicate the ability of the theory to predict the real behavior. The experiments involved development of a suitable cold flow simulators for combustion chamber flow, and measurement of velocity and pressure fluctuations at appropriate locations.

TASK I

Driving of Combustion Instabilities by Solid Propellants

B. T. Zinn

B. R. Daniel

L. L. Narayanaswami

Y. P. Kwon

F. Chen

TASK I

Driving of Combustion Instabilities by Solid Propellants

B. T. Zinn, B. R. Daniel, L. L. Narayanaswami, Y. P. Kwon and F. Chen

A. Research Objectives

1. Develop an understanding of the mechanisms responsible for the driving of axial instabilities in rocket motors with tubular solid propellants. Specifically, identify the processes in the immediate vicinity of the burning propellant surface which exert the greatest influence upon the propellant driving.

2. Use a modified version of the impedance tube setup to determine the validity of using the so-called velocity response function in determining the stability of solid propellant rocket motors.

B. Results and Discussion

The following were accomplished under this research program.

1. Development of a modified impedance tube setup for the determination of the velocity coupled response functions of solid propellants under different oscillatory flow conditions was completed.

2. Linearized versions of the conservation equations were utilized to investigate the characteristics of the oscillatory flow inside the impedance tube and to develop a data reduction procedure for the developed impedance tube. The latter used measured standing wave data (i.e., amplitudes and phases) to determine the test propellant samples velocity coupled response functions.

3. The developed impedance tube setup and data reduction procedures were used to determine the velocity coupled response functions of a number of different propellants when they were placed at different locations relative to the standing wave minima. The measured data showed that one cannot assume, as has been done to date, that the velocity coupled response function is a propellant property which is space independent.

4. A cold flow experimental setup consisting of a tube with porous walls was designed and developed for the investigation of characteristics of oscillatory flows next to walls with mass addition. The objective of this study is to gain insight into the characteristics of the flow next to the propellant surface in unstable rocket motors.

5. The cold flow setup described under Item 4 above was used to determine the variation of the oscillatory flow component with distance from the porous wall. Variables investigated in this study included the porosity of the wall, the magnitude of the steady flow through the wall and the frequency and amplitude of the imposed flow

oscillations. This study pointed out serious limitations which are associated with the use of hot wires in oscillatory velocity measurements.

6. The modelling of the gas phase flame of a solid propellant burning in an unsteady rocket motor was initiated. The fundamental conservation equations are used as a starting point and viscous and heat conduction terms are retained in the model. A simpler version of the developed model is currently being programmed for the development of predictions which could be compared with cold flow experimental data.

7. The planning of a combustion experiment capable of simulating the oscillatory gas phase burning of solid propellants in unstable rocket motors was completed.

Some of the results obtained in the above described study are discussed in the following publications.

1. Chen, F. L., B. R. Daniel and B. T. Zinn, "Effect of Oscillations upon Velocity Distributions in Simulated Solid Propellant Flow Environments," to appear in the Proceedings of the 20th JANNAF Combustion Meeting.

2. Zinn, B. T., B. R. Daniel and L. L. Narayanaswami, "Investigation of the Driving and Gas Phase Losses Associated with Different Aluminized and Nonaluminized Propellants," CPIA Publ., No. 366, Vol. I, pp. 245-255, Oct. 1982.

3. Narayanaswami, L. L., B. R. Caniel and B. T. Zinn, "Experimental Investigation of Pressure and Velocity Coupled Response Functions of Aluminized and Nonaluminized Solid Propellants," AIAA Paper No. 83-0478, Jan. 1983.

4. Narayanaswami, L. L., B. T. Zinn and B. R. Daniel, "Investigation of the Characteristics of Velocity-Coupled Response Functions of Solid Propellants," submitted for publication in the 20th International Symposium on Combustion.

Papers 1, 3 and 4 are provided in Appendix A for further reference.

C. Publications

1. Chen, F. L., B. R. Daniel and B. T. Zinn, "Effect of Oscillations upon Velocity Distributions in Simulated Solid Propellant Flow Environments," to appear in the Proceedings of the 20th JANNAF Combustion Meeting.

2. Zinn, B. T., B. R. Daniel and L. L. Narayanaswami, "Investigation of the Driving and Gas Phase Losses Associated with Different Aluminized and Nonaluminized Propellants," CPIA Publ. No. 366, Vol. I, pp. 245-255, Oct. 1982.

3. Zinn, B.T., L. L. Narayanaswami, and B. R. Daniel, "Experimental Investigation of Pressure and Velocity Coupled Response Functions of Aluminized and Nonaluminized Solid Propellants," AIAA Paper No. 83-0478, Jan 1983.

4. Narayanaswami, L. L., B.T. Zinn and B. R. Daniel, "Investigation of the Characteristics of Velocity-Coupled Response Functions of Solid Propellants," submitted for publication in the 20th International Symposium on Combustion.

D. Personnel

Principal Investigators: Ben T. Zinn and Brady R. Daniel

Post Doctoral Fellow: Y. P. Kwon

Visiting Research Scholar: F. Chen

Graduate Research Assistant: L. L. Narayanaswami

E. Professional Activities/Interactions

1. Zinn, B. T., B. R. Daniel and L. L. Narayanaswami, "Investigation of the Driving and Gas Phase Losses Associated with Different Aluminized and Nonaluminized Propellants," presented at the 19th JANNAF Combustion Meeting, NASA/Goddard Space Flight Center, Greenbelt, Md., Oct. 4-7, 1982.

2. Zinn, B. T., B. R. Daniel and L. L. Narayanaswami, "Experimental Investigation of Pressure and Velocity Coupled Response Functions of Aluminized and Nonaluminized Solid Propellants," presented at the AIAA 21st Aerospace Sciences Meeting, Reno, Nevada, Jan. 10-13, 1983.

3. Zinn, B. T., "Determination of Admittances of Solid Propellants by the Impedance Tube Technique," Seminar presented at Northwestern Polytechnique Institute, Xian, China, April 1983.

4. Zinn, B. T., "Combustion Instability in Solid Propellant Rocket Motors," Seminar presented at Beijing Institute of Technology, Beijing, China, May 1983.

5. Zinn, B. T., "Theoretical and Experimental Determination of Nozzle Admittances," Seminar presented at Beijing Institute of Technology, Beijing, China, May 1983.

6. Zinn, B.T., F. Chen and B. R. Daniel, "Boundary Combustion and Flow Processes in Unstable Solid Propellant Rocket Motors," presented at the Eastern Section of The Combustion Institute 1983 Technical Meeting, Providence, R. I., Nov. 8-10, 1983.

7. Zinn, B. T., "Nozzle Effect upon Combustor Stability," presented at the ONR/AFOSR Workshop on Mechanisms of Instability in Liquid-Fueled Ramjets, Atlanta, March 16-18, 1983.

8. Zinn, B. T., Associate Editor for Combustion and Aeroacoustics; AIAA Journal.

9. Zinn, B. T., Member, Editorial Advisory Board for "Combustion Science and Technology" Journal.

10. Zinn, B. T., Member, U. S. Air Force Review Panel for the new Aero Propulsion Systems Test Facility (ASTF).

11. Zinn, B. T., Member, National Review Panel for DOE's Engine Combustion Technology Research Program.

APPENDIX A

Some of the Publications
Prepared under Task I

INVESTIGATION OF THE CHARACTERISTICS OF THE VELOCITY-COUPLED RESPONSE FUNCTIONS OF SOLID PROPELLANTS*

L. L. Narayanaswami*, B. T. Zinn**, and B. R. Daniel***

School of Aerospace Engineering

Georgia Institute of Technology

Atlanta, Georgia 30332

---

* Graduate Research Assistant

** Regents' Professor

*** Senior Research Engineer

Subject Matter

Solid Propellant Combustion Instability

Abstract

This paper describes the results of an experimental investigation which has been concerned with the validity of the state of the art approaches which use the so-called velocity-coupled response functions to determine the stability of solid propellant rocket motors. These approaches are based upon the fundamental assumption that the propellant velocity-coupled response function is a propellant property which is independent of location within the combustor. The validity of this assumption was investigated in a modified impedance tube setup specifically developed for this study. It consisted of a "driver" propellant sample at the upstream end of the tube and "test" propellant samples on the side walls at a desired location downstream of the "driver" propellant. An acoustic driver located at the downstream end of the tube was used to simulate conditions in an unstable motor by exciting a standing acoustic wave of desired properties in the tube. During a test, the driver was turned on, all the propellant samples were ignited and a series of pressure transducers attached to the tube wall were used to measure the resulting standing wave structure. These data together with a specially developed data reduction program were used to determine the velocity-coupled response functions of the "test" propellant samples. Tests were conducted with the "test" propellant samples at different locations along the impedance tube standing wave. The results of these tests clearly showed that the velocity-coupled response function is strongly dependent upon the propellant sample location relative to the impedance tube standing wave. These results also indicate that predictions

of existing solid propellant rocket motor stability programs are most likely invalid because they are based upon the erroneous assumption that the velocity-coupled response functions of the solid propellants are constant throughout the combustor. The paper points out the need for a reevaluation of current approaches for predicting the stability of solid propellant rocket motors.

Introduction

This paper describes the application of the impedance tube technique in the investigation of the validity of current practices which use the velocity-coupled response function to determine the stability of solid propellant rocket motors.[1] Combustion instabilities occur when energy supplied by the combustion process excites one or more of the natural acoustic modes of the combustor. This driving by the combustion process depends upon the characteristics of the space dependent flow oscillations in the vicinity of the propellant surface. For example, in a rocket motor experiencing an instability of its fundamental, longitudinal acoustic mode, the propellant sections at the two ends of the motor experience primarily pressure oscillations, the propellant section at the center of the motor experiences primarily velocity oscillations parallel to its surface and the remainder of the propellant grain experiences both velocity and pressure oscillations of varying amplitude and phase relationships. To determine the contribution of the entire propellant grain to the instability, the driving or damping provided by various sections of the propellant must be known. To date, this requirement has been interpreted as the need to know the propellant burn rate response to both pressure and velocity oscillations. These responses are generally referred to as the pressure- and velocity-coupled responses, respectively, and they are related to the pressure and velocity fluctuations through constant proportionality factors called the pressure- and velocity- coupled response functions.[1,2,3] While the existence of a pressure-coupled response function had been recognized earlier and it

has been the subject of a considerable number of investigations,[4,5,6] the higher complexity of the physico-chemical processes associated with the velocity-coupled response function has limited the number of investigations which have been concerned with the elucidation of its fundamental properties and applicability. The latter is the subject of this investigation.

It is well known that the steady burning rate of a solid propellant depends upon the properties of the flow next to its surface, which under certain conditions causes erosive burning.[7,8] Developing predictive capabilities of the steady burn rate and associated erosive burning of solid propellants would require detailed analysis of the complex, multidimensional mixing, heat transfer and chemical processes which occur next to the propellant surface. While such approaches have been pursued by several investigators[9-12], who have provided much insight into the causes of erosive burning, the complexity of the problem has, thus far, prevented the development of rigorous erosive burning models. In their absence, empirical models of erosive burning have been used to predict the performance of solid propellant rocket motors.

Experimental investigations of steady propellant burning indicate that there exists a threshold velocity u_t below which the burn rate is unaffected by the parallel flow[13-15] and above which the propellant burn rate is given by[16]

$$\frac{\bar{m}_b}{m_{bo}} = 1 + k(\bar{u} - u_t) \qquad (1)$$

where k and u_t are determined experimentally. While models of this type are useful in design, they do not provide fundamental understanding of the phenomenon at hand.

By now, there is ample evidence that solid propellant combustion processes are sensitive to the presence of velocity oscillations parallel to the propellant surface.[17-20] This sensitivity, which can be considered as the unsteady analog of steady state erosive burning, is termed velocity-coupling and the resulting burn rate oscillation, the velocity-coupled response. Considering the physics of the problem, one would expect that an oscillatory flow would produce oscillatory mixing, heat transfer and chemical processes next to the propellant surface which would result in an oscillatory propellant burn rate. When the proper phase relationship between the oscillatory propellant burn rate and the local pressure oscillations is established, driving of the flow oscillations occurs. Consequently, it is of utmost importance to develop dependable analytical capabilities which can predict such propellant combustion process-flow interactions. Again, as in the steady state case, the complexity of the problem has prevented the development of reliable solid propellant response models which are based upon fundamental principles and, consequently, all existing response models are heuristic in nature and they are merely extensions of the empirical steady state erosion model (see Eq. (1)) and concepts developed in pressure-coupling studies.

In modeling the velocity-coupled response it was argued that the combustion process is only responsive to the magnitude of the flow velocity and independent of the flow direction.[17,21,22] Then, following the steady

state erosion model, it was assumed that (1) there is a threshold velocity below which the propellant response is zero[1,23,24] and (2) when the magnitude of the total velocity (i.e., the vector sum of the steady and fluctuating velocities) is greater than the threshold velocity, the propellant response is proportional to the difference. Thus, the mass flux fluctuation due to a velocity oscillation parallel to the propellant surface was given by the following relationship

$$\frac{m_b'}{\bar{m}_b} = \frac{R_v}{\bar{a}} \left[(|\bar{u}+u'| - u_t) - (\bar{u} - u_t) \right], \quad |\bar{u}+u'| > u_t, \ \bar{u} > u_t \qquad (2)$$

where R_v is the velocity-coupled response function. Implicit in Eq. (2) is the assumption that R_v is a propellant property and thus independent of the propellant location within the combustor. While the validity of Eq. (2) has never been verified experimentally or theoretically, it has nevertheless served as a basis for a number of experimental investigations which were concerned with the determination of R_v[2,3,25-27] as a propellant property.

The manner in which a given propellant section responds to flow oscillations depends upon the structure of the steady state combustion zone next to its surface, as different steady state combustion zones may respond differently to oscillatory excitation. Since the local, steady state combustion zone is expected to depend upon the characteristics of the steady flow, it follows from the above discussion that both the steady and oscillatory components of the flow next to the propellant surface should affect the propellant response. Since the flow conditions within the combustor are space dependent, the effect of the flow upon the propellant

response is likely to be different at different combustor locations. Consequently, one would expect that the velocity-coupled response function R_v (see Eq. (2)), which is supposed to account for steady state flow and combustion effects, will also be space dependent;[28] a conjecture which contradicts the underlying assumption of Eq. (2) that R_v is strictly a propellant property. Since the clarification of this contradiction is of crucial importance to the development of analytical capabilities for predicting the stability of solid propellant rocket motors, both critical experimental and theoretical studies aimed at the resolution of this problem must be performed. This paper describes the results of an experimental investigation in which the impedance tube technique was used to explore this issue.

In what follows, a modification of the impedance tube technique, specifically developed for this study, is briefly discussed. This is followed by a description of the application of the modified impedance tube technique in the investigation of the velocity-coupled responses of solid propellants. The paper closes with a discussion of the measured data and their implications for solid propellant rocket motors stability analyses.

The Modified Impedance Tube Technique

This section describes the measurement technique developed for this study. The impedance tube technique was initially developed by acousticians who utilized it to measure the sound absorbing characteristics of various materials.[29,30] In these applications, the impedance tube consisted of a rigid wall tube with the tested material placed across one end and an

acoustic driver at the other. During a test, the driver was used to generate a train of acoustic waves of a desired frequency that propagated toward the tested material. These waves reflected off the tested sample with modified amplitude and phase and then combined with the incident wave train to form a standing wave in the tube. A traversing microphone was used to measure the structure of the resulting standing wave and this data together with appropriate analytical solutions were utilized to determine the amplitude and phase changes occuring at the tested sample surface; data which determine the sound absorbing characteristics of the tested material. Subsequently, this technique was modified to determine the admittances of choked nozzles,[31] acoustic liners,[32] and pressure coupled responses of burning solid propellants.[33,34] In this investigation, the impedance tube technique was further modified to investigate the velocity-coupled responses of solid propellants.

A schematic of the modified impedance tube setup used in this study is shown in Fig. 1. The objective of the experiment is to measure the velocity coupled response function of the "test" propellant samples. The "driver" propellant sample provides a stream of hot combustion products that flows past the "test" propellant samples in an attempt to simulate actual rocket motor flow conditions. In this configuration, the driver propellant experiences only pressure oscillations while the "test" propellant samples are subjected to both pressure and velocity oscillations. The experimental setup permits moving the "driver" propellant to different locations upstream of the "test" samples; a capability that enables the

investigation of the response of the "test" propellant samples at different acoustical environments along the standing wave.

In an experiment to determine the velocity-coupled response function, the acoustic driver is first used to setup a standing wave of a desired frequency in the impedance tube. Next, the propellant samples are ignited and a series of transducers mounted at preselected locations along the impedance tube walls are used to measure the continuously varying (due to the presence of ignition, quasi steady state and extinguishment periods) wave structure in the impedance tube. These pressure transducers are used in this setup because the short duration of a test (between one and three seconds) precludes the use of a traversing microphone for measuring the wave structure. While the test is in progress, a stepping motor is utilized to keep the "test" propellant surfaces flush with the adjacent impedance tube walls. The measured acoustic pressure data are used to determine the unknown velocity-coupled response function by utilizing a data reduction procedure specifically developed for this purpose.[35]

The issues raised in the previous section were investigated in this study by measuring the value of R_v in tests in which the "test" propellant samples were placed at different locations along the standing wave structure. If the same values (or close) for the response function R_v were obtained in all of these tests, then this would support the argument that R_v is a propellant property which is independent of location, and vice versa.

Theoretical Considerations

These theoretical studies were undertaken with the objective of developing an anlalytical methodology for determining the velocity-coupled response function from measured impedance tube pressure data. The system of conservation equations which is used to determine the axial, linear stability limits of solid propellant rocket motors also serves as the starting point for this study. It consists of the linearized, one-dimensional mass, momentum and energy conservation equations. Neglecting terms of $0(\bar{u}^2)$, and assuming periodic time dependence of the solutions, these wave equations can be expressed in the following form:[34,35]

Continuity:

$$i\omega\rho' + \frac{d}{dx}\left(\bar{\rho}u' + \bar{u}\rho'\right) = \frac{b}{A} m_b' \tag{3}$$

Momentum:

$$i\omega\bar{\rho}u' + \bar{\rho}\bar{u}\frac{du'}{dx} + \bar{\rho}\frac{d\bar{u}}{dx}u' + \frac{dp'}{dx} + \frac{b}{A}\bar{m}_b u' + Gu' = 0 \tag{4}$$

Energy:

$$i\omega p' + \bar{u}\frac{dp'}{dx} + \frac{d\bar{p}}{dx}u' + \gamma\bar{p}\frac{du'}{dx} + \gamma\frac{d\bar{u}}{dx}p' = \frac{b}{A}\bar{m}_b\bar{E}\left(\frac{E'}{\bar{E}} + \frac{m_b'}{\bar{m}_b}\right) \tag{5}$$

where

$$E = \gamma RT_F + \frac{R}{2C_v}\left(u^2 + u_b^2\right) \tag{6}$$

describes energy addition (and driving) at the propellant surface.

Examination of the above equations shows that the momentum and energy equations are decoupled from the continuity equation, since they contain only the dependent variables p' and u'. These equations can be solved provided the expression, $\frac{b}{A}\bar{m}_b\bar{E}\left(\frac{E'}{\bar{E}} + \frac{m_b'}{\bar{m}_b}\right)$ on the right hand side of the

energy equation is known. This expression describes the response of the propellant to disturbances in the flow field. To date, this term has been related heuristically to the acoustic pressure and velocity by the following expression

$$\frac{m_b'}{\bar{m}_b} + \frac{E'}{\bar{E}} = (R_p + \theta_p)\frac{p'}{\bar{p}} + (R_v + \theta_v)\frac{u'}{\bar{a}} \tag{7}$$

where

$$R_p + \theta_p = \frac{m_b/\bar{m}_b + E'/\bar{E}}{p'/\bar{p}} \quad \text{and} \quad R_v + \theta_v = \frac{m_b'/\bar{m}_b + E'/\bar{E}}{u'/\bar{a}} \tag{8}$$

where R_p and R_v are the pressure- and velocity-coupled response functions, respectively, and θ_p and θ_v relate E'/E, see Eq. (6), to p' and u'. It should be pointed out that in using Eq. (2) to obtain Eq. (7) it has been assumed that $u_t = 0$ and that $\bar{u} > |u'|$; a restriction which must be satisfied by the developed experiment. Furthermore, the distinction between R_v and R_p and θ_p and θ_v is purely academic, since currently there is no known way for distinguishing between these two sets of response functions. Consequently, it is customary[2] to consider the combination $(R_p + \theta_p)$ and $(R_v + \theta_v)$ as the pressure-and velocity-coupled response functions respectively; a practice which will be also followed in the remainder of this paper.

It is important to note that driving of oscillations in a combustor by velocity-coupling will occur if the latter has a component in phase with the local pressure oscillation. According to Eq. (7) the driving due to velocity oscillations is given by

$$\frac{m_b'}{\bar{m}_b} + \frac{E'}{\bar{E}} = (R_v + \theta_v) \frac{u'}{\bar{a}} \qquad (9)$$

Noting that the acoustic velocity oscillation u' is 90^o out of phase with the local pressure oscillation, it is clear from Eq. (9) that driving will occur only if the response function, $(R_v + \theta_v)$ will introduce a 90^o phase change that will result in the propellant response having a component in phase with the local pressure oscillation. Consequently, it is the imaginary part of the velocity-coupled response function which determines the contribution of velocity-coupling to rocket motor stability.[24]

When $R_p + \theta_p$ and $R_v + \theta_v$ are known, Eqs. (3) through (7) could be used to predict the characteristics of the standing wave inside the impedance tube or the stability of solid propellant rocket motors. Alternately, these equations provide a starting point for the determination of $R_v + \theta_v$ from measured impedance tube data. To optimize the planned impedance tube experiments, Eqs. (3) through (7) were used in a parametric study[35] which investigated if changes in the velocity-coupled response function $R_v + \theta_v$ produced measurable changes in the impedance tube wave structure. This study revealed that the largest changes in the impedance tube wave structure, due to changes in $R_v + \theta_v$, occur in the vicinity of the acoustic pressure minima. Consequently, accurate measurements of the wave structure near these minima would be required to accurately determine $R_v + \theta_v$.

The next step was the development of a suitable data reduction procedure to determine the velocity-coupled response function from the measured acoustic pressure data. Such a procedure was developed and it is discussed in detail in reference 35. It is based on the method of quasilinearization and it determines the value of $(R_v + \theta_v)$ which provides the "best" fit between the measured data and the solutions to the impedance tube wave equations. It should be noted, however, that the developed data reduction procedure presumes knowledge of the pressure-coupled response function. Consequently, the pressure-coupled response function has to be determined in a separate experiment or by the use of a reliable theory.

Experimental Efforts

The modified impedance tube developed for the investigation of the velocity-coupled response of solid propellants is shown in Fig. 2. It is approximately 6' long with a 4" x 1" rectangular cross-section and it has provisions for mounting 4" long "test" propellants samples on the sidewalls. Special adaptors for holding the Sunstrand pressure transducers, model No. 211B-5, which were used in this study are available at 0.3 inch intervals along the upper wall. An electro-pneumatic Ling EPT-94B acoustic driver is mounted a short distance upstream of the exhaust end and a spectral dynamic oscillator, model SD104A-5, is used to control the frequency and the amplitude of the oscillations generated by the driver. During an experiment, the entire setup is placed inside a high pressure tank to simulate actual rocket motor conditions.

The data acquisition system consists of a minicomputer equipped with a disc drive and an analog-to-digital converter. The analog data from the transducers are digitized and stored for post test analysis by this system. The test duration is divided into a series of data acquisition periods, separated from each other by periods of data transfer. Each data acquisition period, called a block, can be programmed to acquire data over a period whose duration is a multiple of 12 periods of the driven oscillations. Thus, data were collected over discrete periods of time (i.e., blocks) as no data was acquired during data-transfer periods. After the test, the stored data were numerically Fourier-analyzed to obtain the amplitudes and phases of the measured data at the test frequency. A study of the measured data (e.g., see Fig. (3)) showed the existence of ignition and extinguishment transients with a quasi-steady period in between. Data obtained during the quasi-steady period are input into the developed data reduction procedure[35] to determine the propellant velocity-coupled response function.

Results and Discussion

Several velocity-coupled response function determination tests which differed from one another by the location of the "test" propellant samples along the standing wave structure were performed. The same non-aluminized propellant was used in all of these experiments and the measured data are presented and discussed in this section.

As stated earlier, a reliable determination of the velocity-coupled response function requires a careful measurement of the standing wave

structure in the vicinity of the minimum point. Therefore, many of the pressure measurements had to be performed near the pressure node where the desired signal was masked by noise from other sources and signal averaging was required to reduce the effect of this noise. Since the available memory of the mini-computer limited the amount of data which could be recorded in a given block, an estimate of the minimum averaging time needed to sufficiently enhance the signal-to-noise ratio was required. This problem was investigated by comparing data averaged over different numbers of cycles of the test signal. The spatial amplitude and phase distributions obtained by averaging data measured during the quasi-steady burning period over 18, 36 and 72 cycles are compared in Figs. 4 and 5, respectively. Examination of these figures shows that the amplitude and phase data obtained as an "18 cycle average" exhibit considerable scatter about the "72 cycle average" while the "36 cycle average" data is consistent with the "72 cycle average" data. This indicates that averaging data over 36 cycles provides sufficient enhancement of the signal to noise ratio.

In the experiments to determine the velocity-coupled response functions, the spatial amplitude and phase distributions were obtained by averaging the measured signals over 36 cycles. The needed pressure-coupled response functions $R_p + \theta_p$ were measured by performing separate experiments with the same propellant in the impedance tube using a previously developed data reduction procedure.[34]

In the first of the velocity-coupled tests, the "test" samples were located upstream of the first pressure minimum and acoustic pressure data

measured around this minimum were used to determine $R_v + \theta_v$. In the second experiment, the "test" samples were located downstream of the first minimum and the acoustic pressure data measured around the second acoustic pressure minimum were used to determine $R_v + \theta_v$. The standing wave structures measured in these experiments are shown in Figs. 6 and 7. Also shown in these figures are the determined wave structures which provided the "best" agreement with the experimental data. The determined optimum values of Im $(R_v + \theta_v)$ which provided the "best" agreement are also presented in the figures.

An examination of Figs. 6 and 7 shows that there is satisfactory agreement between the measured and computed wave structures. However, the value of Im $(R_v + \theta_v)$ determined in the first experiment is considerably different from that obtained in the second; that is, the data indicate that Im $(R_v + \theta_v)$ of the propellant sample upstream of the pressure minimum is -3 and it equals 30 when the propellant sample is located downstream of the pressure minimum. Considerations of the physics of the problem together with the measured data indicate that in both tests the velocity coupled responses of the tested propellant samples attenuated the oscillations in the impedance tube. Qualitative support for this argument was provided by the observation that in both tests the amplitudes of the oscillation in the impedance tube decreased after propellant samples ignition.

The above reported data clearly show that the same propellant samples exhibit different velocity responses when positioned at different locations along a standing acoustic wave. Consequently, it must be

concluded that the velocity-coupled response function cannot be regarded as a propellant property and stability analyses which are based upon this notion are bound to yield erroneous rocket motor stability limits. Furthermore, while the results of this study clearly indicate that the propellant burn rate indeed responds to velocity oscillations parallel to the propellant surface, the nature of this response is currently not understood. Considering the importance of this type of response in solid propellant rocket motors stability analyses, it is strongly recommended that new endeavors aimed at the understanding of this type of propellant response be undertaken.

The results reported herein point out another misconception in current considerations of the contribution of velocity-coupling to motor stability. It has been argued that velocity-coupling does not contribute to the linear stability of the fundamental axial mode because the standing pressure wave undergoes a 180 degrees phase change between the fore and aft ends of the rocket motor. Consequently, if the assumption that the velocity-coupled response function is independent of location in the rocket motor holds, one half of the propellant will drive the oscillation and the remaining half will attenuate the oscillation with no net contribution to the driving of the combustor oscillation from velocity-coupling. The results of this investigation indicate that the velocity-coupled response function varies with location in the combustor and consequently velocity-coupling may contribute to the linear stability of the fundamental axial mode in a solid propellant rocket motor.

Nomenclature

a	speed of sound, m/s
A	cross-sectional area, m^2
b	perimeter of the sidewall propellant samples, m
C	heat transfer parameter, m
c_v	specific heat at constant volume J/kg-K
G	gas phase bulk loss coefficient, N-s/m^4
Im( )	imaginary part of ( )
m	mass burn rate per unit area, kg/m^2-s
p	pressure, N/m^2
R	specific gas constant, J/kg-K
R_p	pressure-coupled response function, nondimensional
R_v	velocity-coupled response function, nondimensional
t	time, s
T	temperature, K
u	velocity, m/s
u_t	threshold velocity, m/s
x	distance, m
γ	ratio of specific heats
ρ	density kg/m^3
θ_p, θ_v	defined in Equation (8)
ω	radian frequency, 1/s

Subscripts

b	properties at the sidewall propellant surface
F	flame property

Superscripts

′	fluctuating quantity
-	mean quantity

References

1. Culick, F. E. C., Comb. Sci. and Tech., 2, 179, 1970.

2. Micci, M. M., L. H. Caveny, and W. A. Sirignano, "Linear Analysis of Longitudinal Waves in Rocket Motor Chambers," AIAA Paper No. 79-1210, 1979.

3. Brown, R. S., R. C. Waugh, and V. L. Kelly, "Rotating Valve for Velocity-Coupled Combustion Response Measurements," AIAA Paper No. 81-1522, 1982.

4. Brown, R. S., F. E. C. Culick, and B. T. Zinn, "Experimental Methods for Combustion Admittance Measurements," In Boggs and Zinn (Ed.), Experimental Diagnostics in Combustion of Solids, AIAA Progress in Astronautics and Aeronautics, Vol. 63, pp. 191-220, 1978.

5. In Culick, F. E. C., "T-Burner Testing of Metallized Solid Propellants," AFRPL-TR-74-28, Final Report, 1974.

6. Perry, E. H., "Investigation of the T-Burner and its role in Combustion Instability Studies," Ph.D. Thesis, California Institute of Technology, 1970.

7. Kuo, K. K., and M. K. Razdan, "Review of Erosive Burning of Solid Propellants," 12th JANNAF Combustion Meeting, CPIA Publication 273, Vol. II, pp. 323-338, 1975.

8. Marklund, T., and A. Lake, ARS J., 3, 173, 1960.

9. Corner, J., "Theory of Internal Ballistics of Guns," John Wiley and Sons Inc., New York, 1950.

10. Tsuji, H., Ninth Symposium on Combustion, The Combustion Institute, p. 384, 1963.

11. Razdan, M. K., "Theoretical Studies of Erosive Burning of Double Base Solid Propellants," Master of Technology Thesis, Indian Institute of Technology, Kanpur, India, 1974.

12. Razdan, M. K., and K. Kuo, "Erosive Burning Studies of Composite Propellants by the Reacting Turbulent Boundary-Layer Approach," Final Report, AFOSR-76-2914, 1977.

13. Kreidler, J. W., "Erosive Burning - New Experimental Techniques and Methods of Analysis," AIAA Preprint 64, 155.

14. Zucrow, M. J., J. R. Osborn and J. M. Murphy, "An Experimental Investigation of the Erosive Burning Characteristics of a Non-homogeneous Solid," AIAA Preprint 64, 107.

15. Wimpress, R. N., "Internal Ballistics of Solid Fuel Rockets," McGraw-Hill, New York, pp. 129, 1950.

16. Heron, R., "Internal Ballistic Problems of Solid Propellant Rocket Technology," Vol. 1, Plenum Press, New York, 1961.

17. Hart, R. W., J. F. Bird, and F. T. McClure, Progress in Astronautics and Rocketry, 1, 423, 1960.

18. Bird, J. F., R. W. Hart and F. T. McClure, AIAA J., 3, 2248, 1965.

19. Price, E. W. and G. L. Dehority, "Velocity Coupled Axial Mode Combustion Instability in Solid Propellant Rocket Motors," ICRPG/AIAA, Second Propulsion Conference, Anaheim, California, pp. 213-217, 1967.

20. Price, E. W., "Evidence for Velocity Coupling," Presented at the First ICRPG Combustion Instability Conference, Orlando Air Force Base, 1964.

21. McClure, F. T., R. W. Hart and J. F. Bird, Progress in Astronautics and Rocketry, 1, 295, 1960.

22. McClure, F. T., J. F. Bird and R. W. Hart, ARS J., 32, 374, 1962.

23. Micheli, P., "Investigation of Velocity Coupled Combustion Instability," Interim Report, AFRPL-TR-75-54, 1975.

24. Culick, F. E. C., "Velocity Coupling Analysis," NWC TP 6363, 1983.

25. Stepp, E. E., AIAA J., 5, 945, 1967.

26. Beckstead, M. W., M. D. Horton, M. Krashin, and A. G. Butcher, "Velocity Coupling Combustion Instability," Final Technical Report, AFRPL-TR-, 1973.

27. Kuentzmann, P., and G. Lengelle, "Recent Research Activity at ONERA on Combustion Instability and Erosive Burning," Joint AFOSR/AFRPL Rocket Propulsion Meeting, Lancaster, CA, 1977.

28. Price, E. W., "Velocity-Coupling in Oscillatory Combustion of Solid Propellants," AIAA TN, 1979.

29. Scott, R. A., Proceedings of the Physical Society, 58, 253, 1946.

30. Lippert, W. K. R., Acustica, 3, 153, 1953.

31. Bell, W. A., "Experimental Determination of Three Dimensional Liquid Rocket Nozzle Admittances," Ph.D. Thesis, School of Aerospace Engineering, Georgia Institute of Technology, Atlanta, Georgia, 1972.

32. Zinn, B. T., B. R. Daniel, B. A. Janardan and A. J. Smith, Jr., "Damping of Axial Instabilities by Minuteman II, Stage III, Minuteman III, Stage III, Exhaust Nozzles," Air Force Rocket Propulsion Laboratory Interim Report, AFRPL-TR-72-71, 1972.

33. Salikuddin, M., "Application of the Impedance Tube Technique in the Measurement of Burning Solid Propellant Admittances," Ph.D. Thesis, School of Aerospace Engineering, Georgia Institute of Technology, Atlanta, Georgia, 1978.

34. Baum, J. D., "Experimental Determination of the Admittances of Solid Propellants by the Impedance Tube Technique," Ph.D. Thesis, Georgia Institute of Technology, Atlanta, Georgia, 1980.

35. Zinn, B. T. and L. Narayanaswami, Acta Astronautica, 9, 303, 1982.

Figure Captions

Fig. 1. A Schematic of the Impedance Tube Modified for Velocity-Coupled Response Measurements.

Fig. 2. An Isometric View of the Developed Impedance Tube Setup.

Fig. 3. Typical Time Variations of Measured Pressure Amplitudes and Phases for Two Tube Locations. Note the Various Test Periods.

Fig. 4. Comparison of Spatial Amplitude Distributions Obtained by Averaging the Pressures Measured During the Quasi-Steady Burning Period Over 18, 36 and 72 Cycles.

Fig. 5. Comparison of Spatial Phase Distributions Obtained by Averaging the Pressures Measured During the Quasi-Steady Burning Period Over 18, 36 and 72 Cycles.

Fig. 6. A Comparison of the Experimental and Theoretically Determined Axial Variations of the Amplitude and Phase of the Impedance Tube Standing Wave when the "Test" Samples were Located Upstream of the First Pressure Minimum.

Fig. 7. A Comparison of the Experimental and Theoretically Determined Axial Variations of the Amplitude and Phase of the Impedance Tube Standing Wave with the "Test" Samples Located Downstream of the First Pressure Minimum.

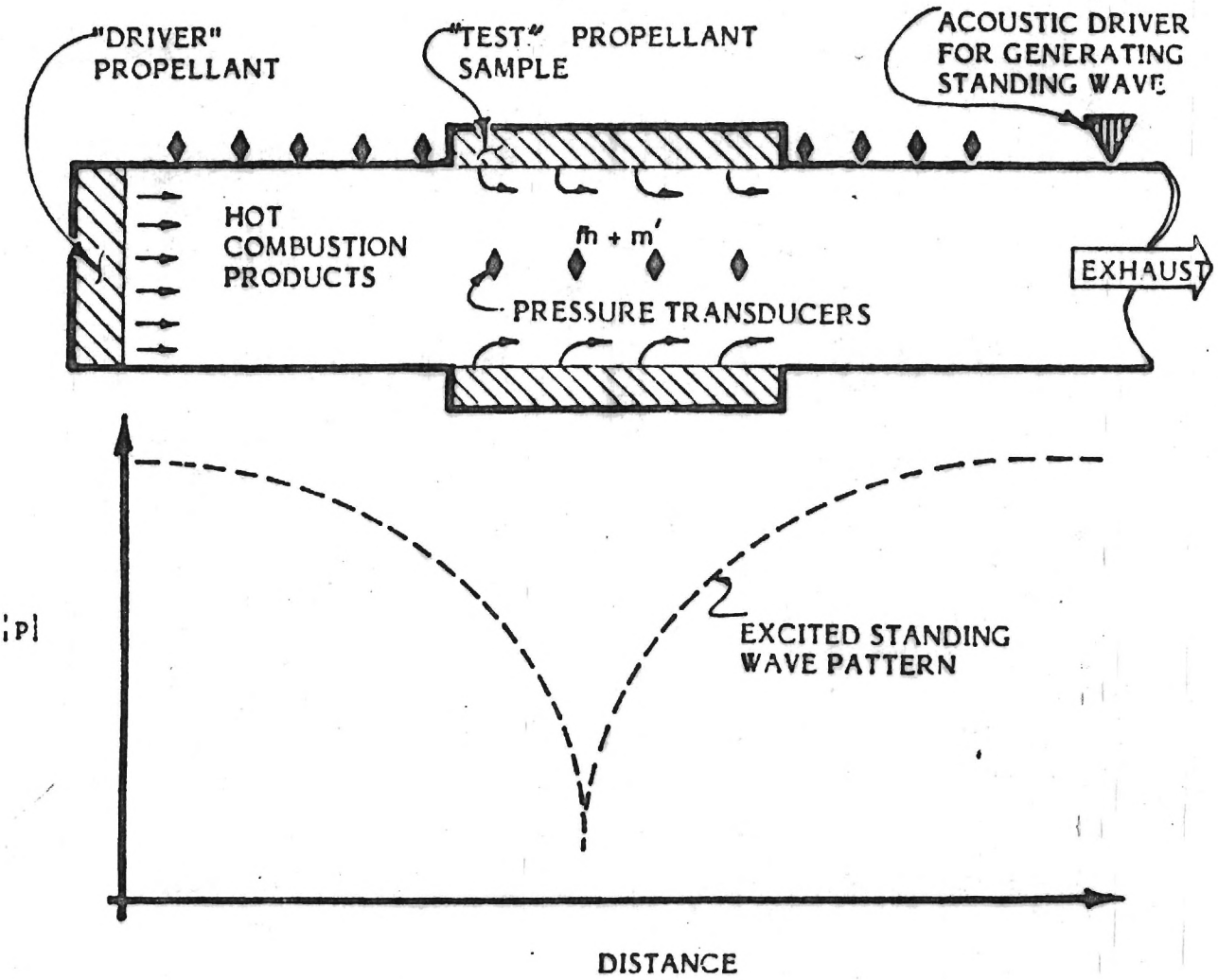
"DRIVER" PROPELLANT
"TEST" PROPELLANT SAMPLE
ACOUSTIC DRIVER FOR GENERATING STANDING WAVE
HOT COMBUSTION PRODUCTS
fn + m'
PRESSURE TRANSDUCERS
EXHAUST
|P|
EXCITED STANDING WAVE PATTERN
DISTANCE

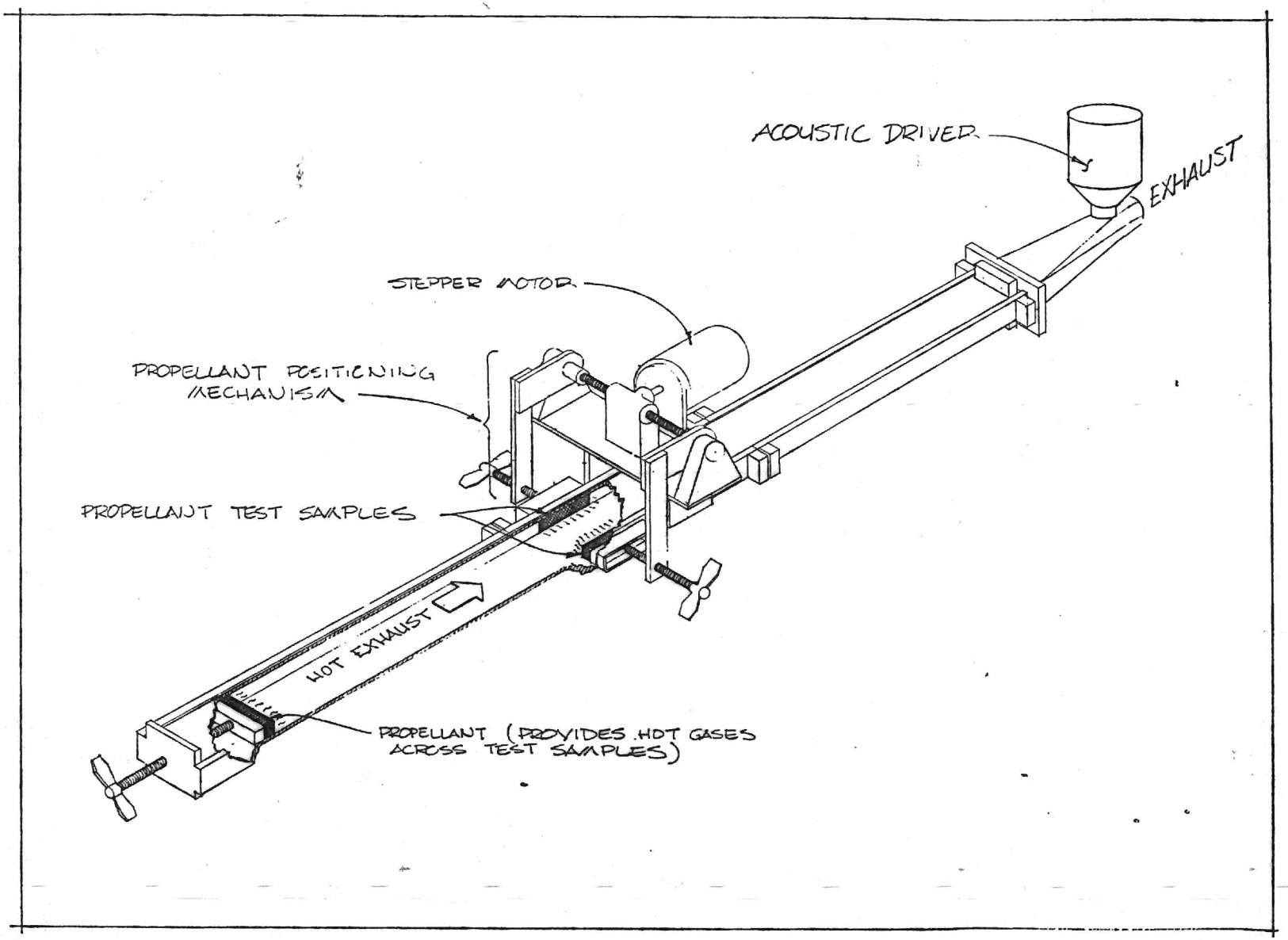
ACOUSTIC DRIVER
EXHAUST
STEPPER MOTOR
PROPELLANT POSITIONING MECHANISM
PROPELLANT TEST SAMPLES
HOT EXHAUST
PROPELLANT (PROVIDES HOT GASES ACROSS TEST SAMPLES)

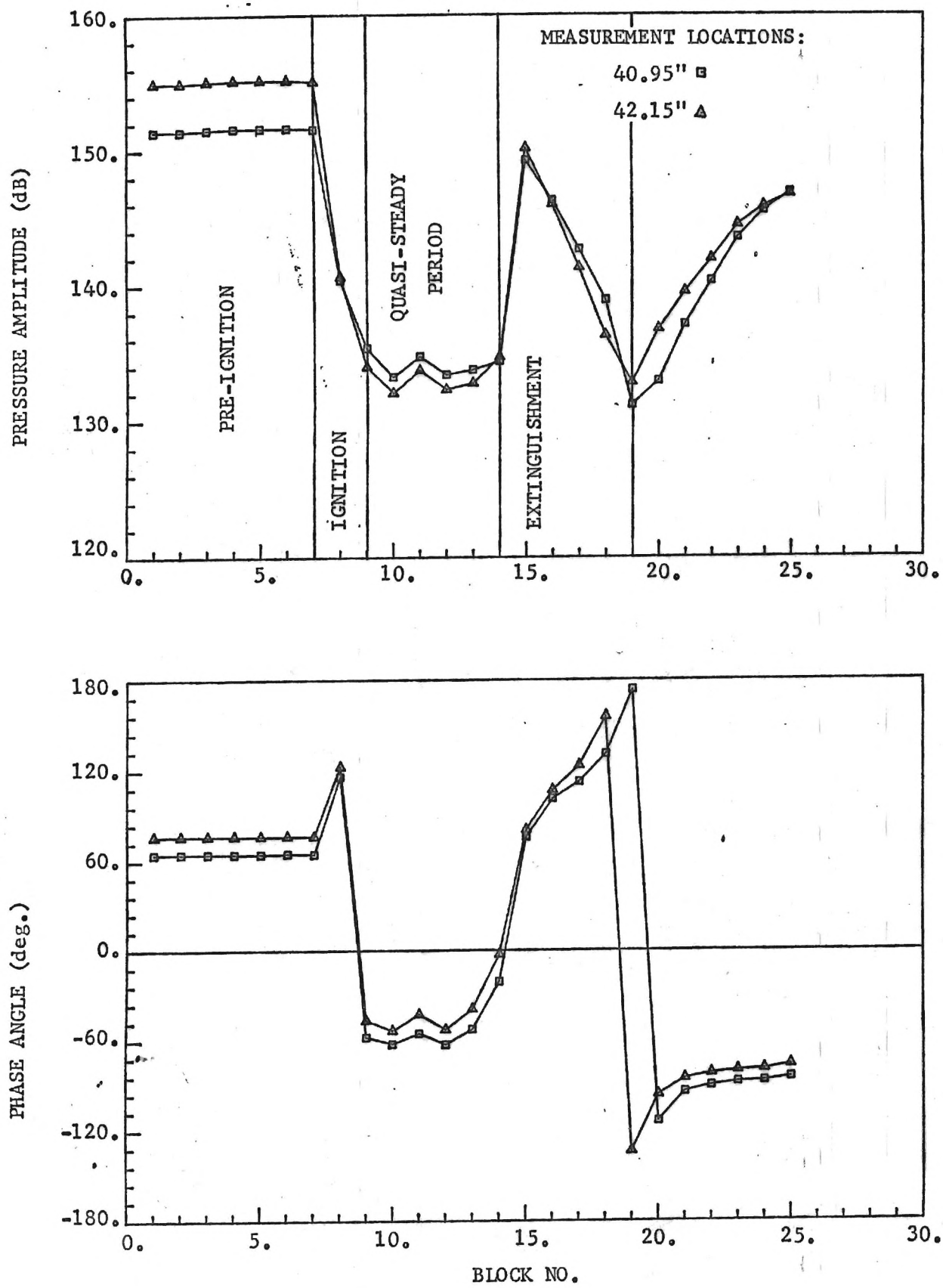
MEASUREMENT LOCATIONS:
40.95"
42.15"
PRE-IGNITION
IGNITION
QUASI-STEADY PERIOD
EXTINGUISHMENT
PRESSURE AMPLITUDE (dB)
160.
150.
140.
130.
120.
0.
5.
10.
15.
20.
25.
30.
PHASE ANGLE (deg.)
180.
120.
60.
0.
-60.
-120.
-180.
BLOCK NO.

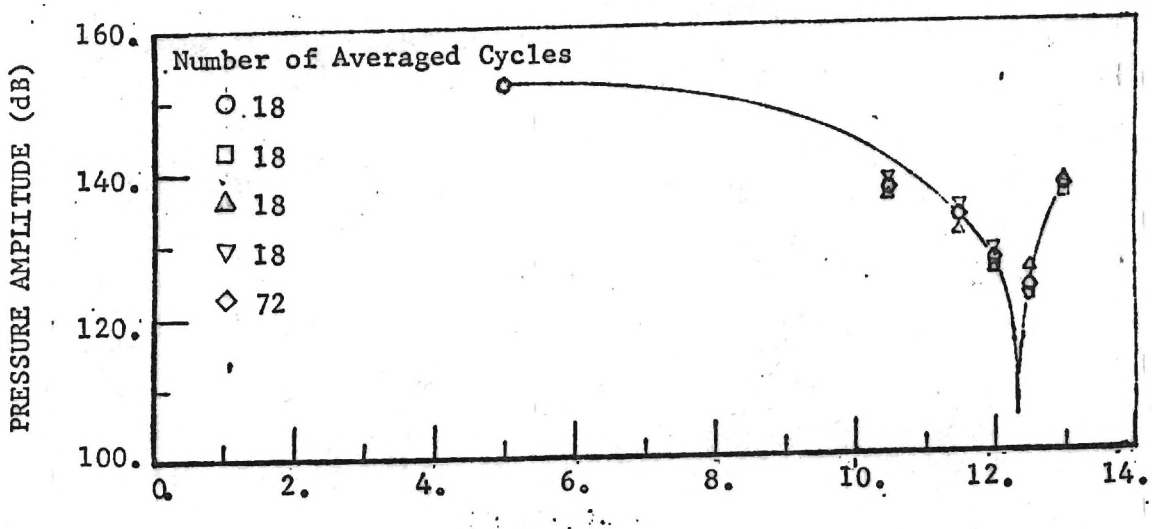
Number of Averaged Cycles
18
18
18
18
72
PRESSURE AMPLITUDE (dB)
160.
140.
120.
100.
0.
2.
4.
6.
8.
10.
12.
14.

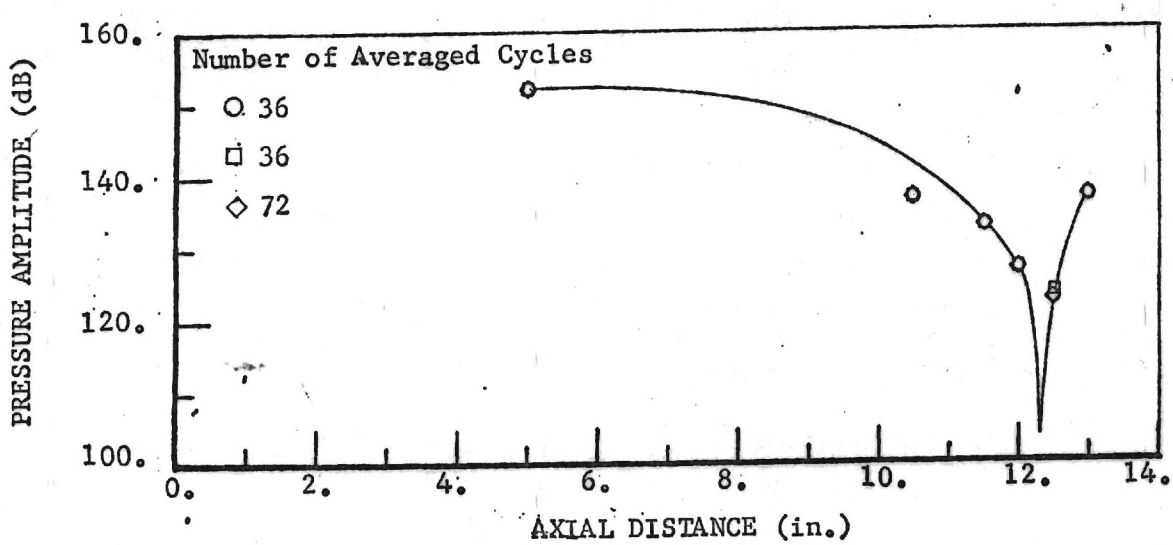
Number of Averaged Cycles
36
36
72
PRESSURE AMPLITUDE (dB)
160.
140.
120.
100.
0.
2.
4.
6.
8.
10.
12.
14.
AXIAL DISTANCE (in.)

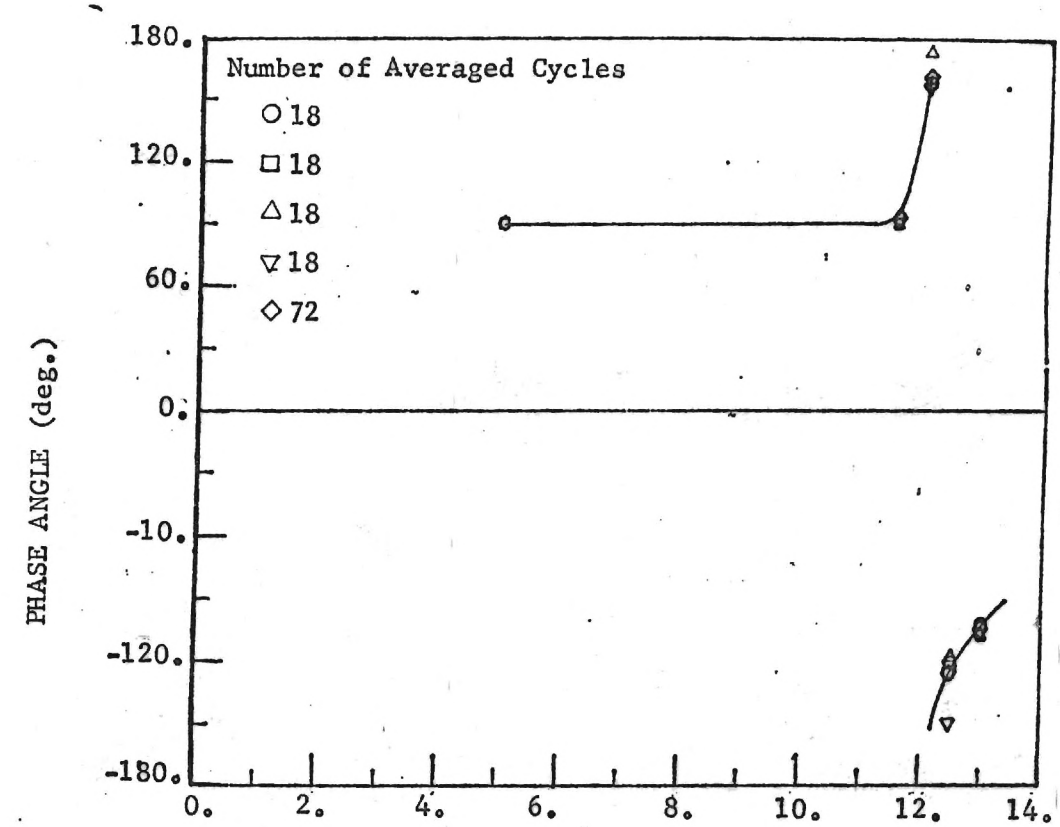
Number of Averaged Cycles
○ 18
□ 18
△ 18
▽ 18
◇ 72
PHASE ANGLE (deg.)
180.
120.
60.
0.
-10.
-120.
-180.
0.
2.
4.
6.
8.
10.
12.
14.

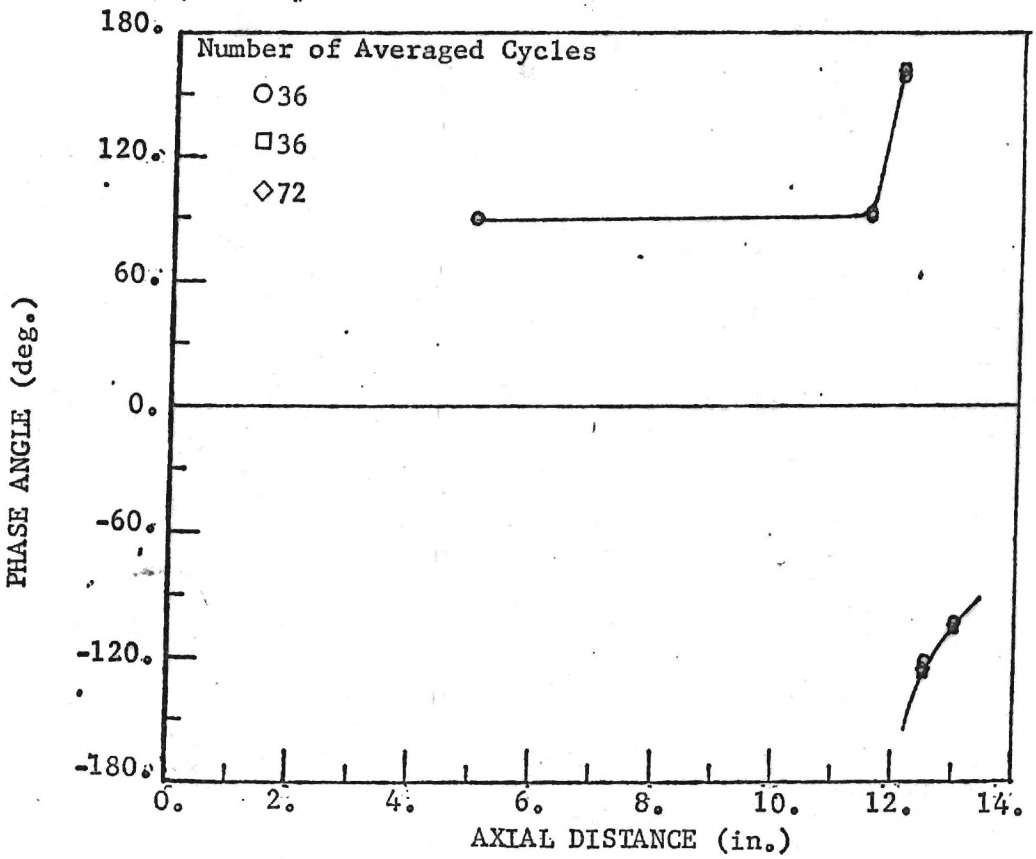
Number of Averaged Cycles
○ 36
□ 36
◇ 72
PHASE ANGLE (deg.)
180.
120.
60.
0.
-60.
-120.
-180.
0.
2.
4.
6.
8.
10.
12.
14.
AXIAL DISTANCE (in.)

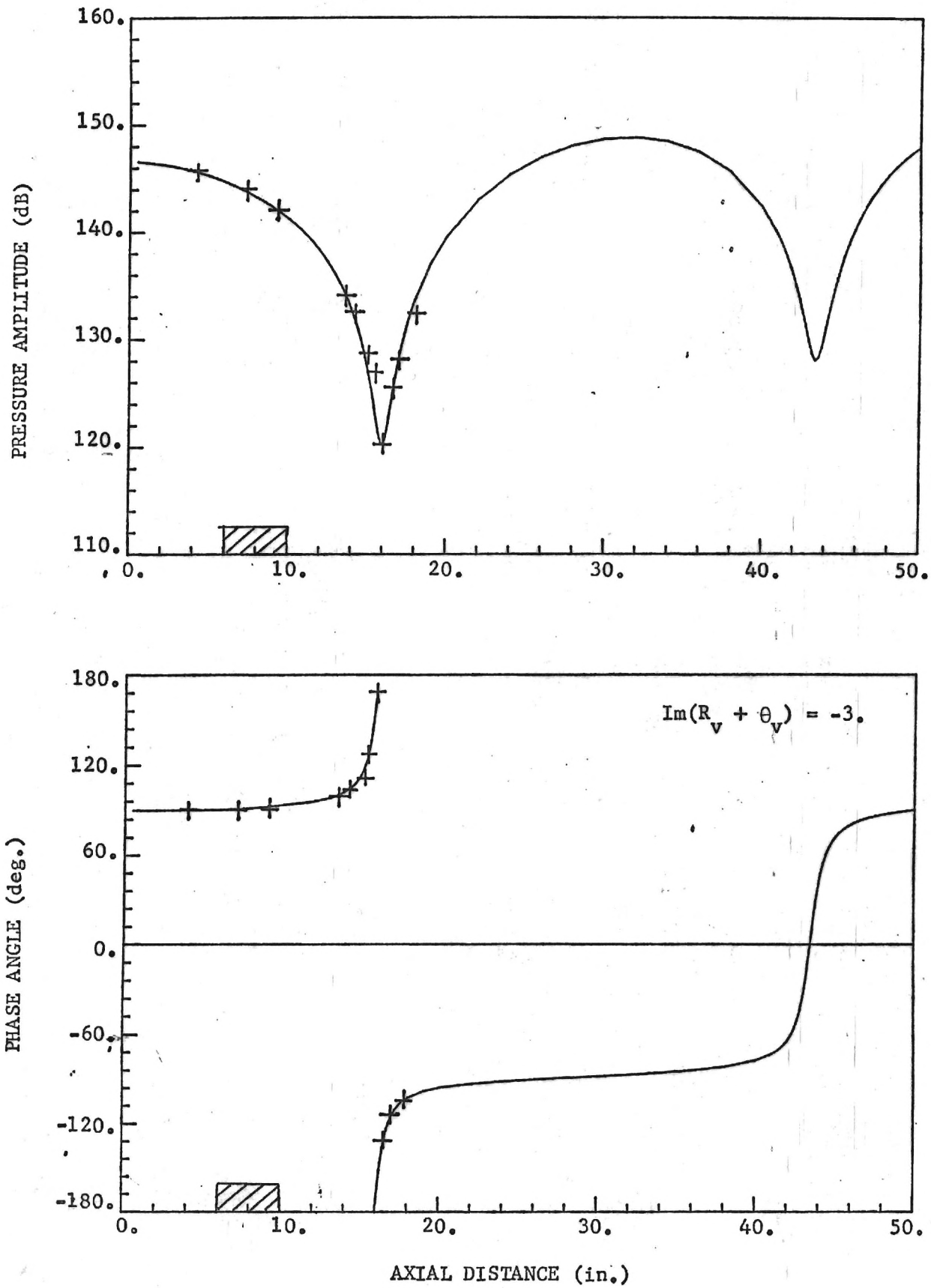
160.
150.
140.
130.
120.
110.
PRESSURE AMPLITUDE (dB)
0.
10.
20.
30.
40.
50.
180.
120.
60.
0.
-60.
-120.
-180.
PHASE ANGLE (deg.)
Im(R_v + θ_v) = -3.
AXIAL DISTANCE (in.)

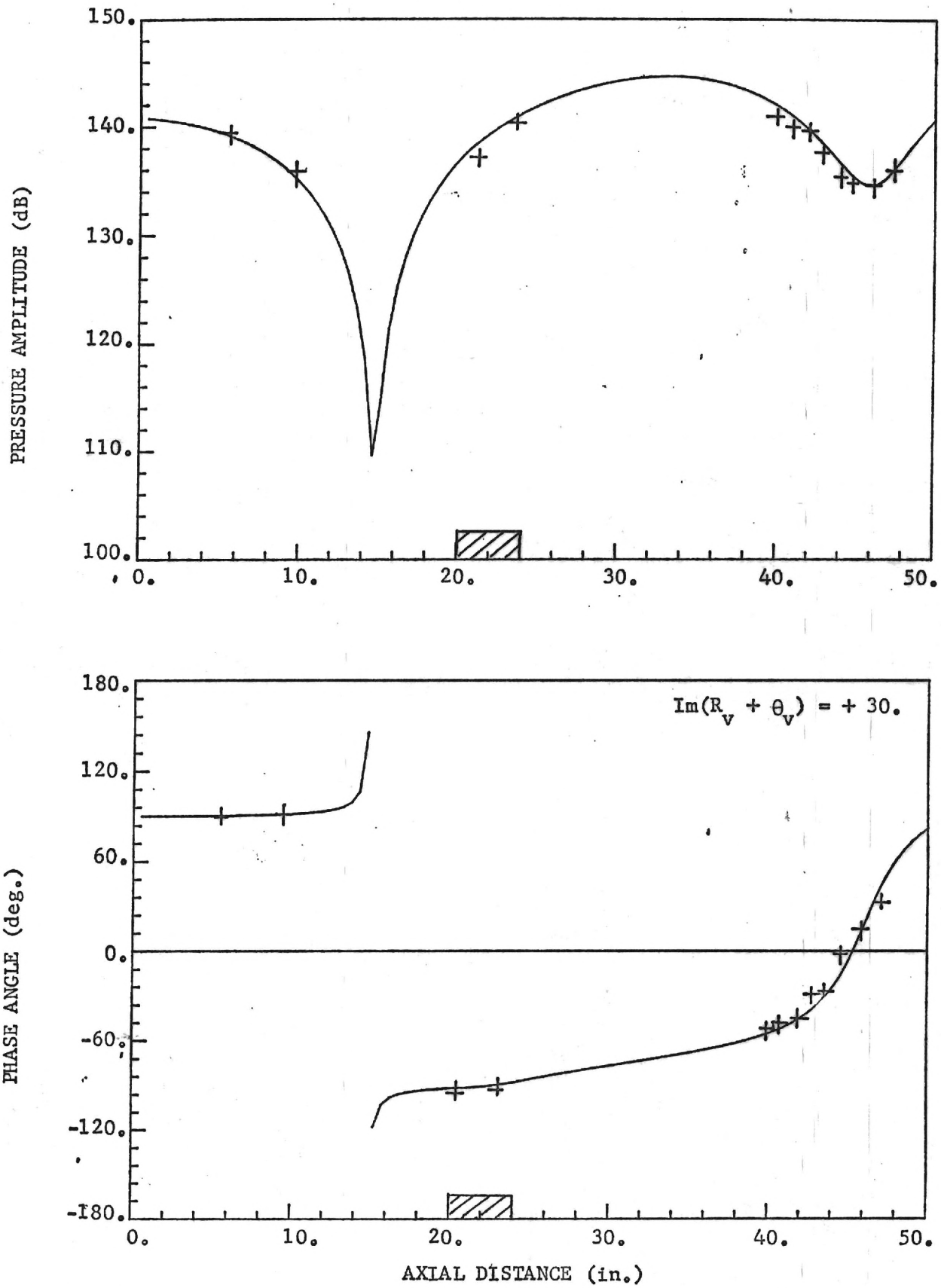
150.
140.
130.
120.
110.
100.
PRESSURE AMPLITUDE (dB)
0.
10.
20.
30.
40.
50.
180.
120.
60.
0.
-60.
-120.
-180.
PHASE ANGLE (deg.)
Im(R_v + θ_v) = + 30.
AXIAL DISTANCE (in.)

AIAA'83

AIAA-83-0478

Experimental Investigation of Pressure and Velocity Coupled Response Functions of Aluminized and non-Aluminized Solid Propellants

L.L. Narayanaswami, B.R. Daniel and B.T. Zinn,
Georgia Institute of Technology,
Atlanta, GA

AIAA 21st Aerospace Sciences Meeting

January 10-13, 1983/Reno, Nevada

EXPERIMENTAL INVESTIGATION OF PRESSURE AND VELOCITY COUPLED RESPONSE FUNCTIONS OF ALUMINIZED AND NON-ALUMINIZED SOLID PROPELLANTS

L. L. Narayanaswami*, B. R. Daniel** and B. T. Zinn***
School of Aerospace Engineering
Georgia Institute of Technology
Atlanta, Ga. 30332

Abstract

This paper describes investigations of the characteristics of the response functions of different aluminized and nonaluminized propellants. The results of an investigation of the dependence of propellant driving and damping characteristics upon its aluminum content indicate that aluminum addition increases both the propellant driving and the gas phase losses. This paper also discusses the status of an ongoing experimental investigation of the "so-called" velocity coupled response function of solid propellants. A modified impedance tube was developed for this study and comparison between measured data and corresponding theoretical predictions are presented and discussed.

Nomenclature

English

- A cross sectional area of the tube, $m^2(ft^2)$
- b perimeter of the side wall propellant samples, m(ft)
- C_v specific heat at constant volume, J/kg-K(Btu/slug-^oR)
- F drag force experienced by the flow per unit volume, $N/m^3(lb/ft^3)$
- G gas phase bulk loss coefficient, $N\text{-}s/m^4(lb\text{-}s/ft^4)$
- m_b mass injection rate per unit area, $kg/m^2\text{-}s(slug/ft^2\text{-}s)$
- p pressure, $N/m^2(lb/ft^2)$
- R specific gas constant, J/kg-K(Btu/slug-^oR)
- R_p pressure coupled response function
- R_v velocity coupled response function
- T temperature, K(^oR)
- ΔT non-isentropic temperature perturbation at the combustion zone, K(^oR)
- u velocity, m/s(ft/s)
- x distance, m(ft)
- Y propellant admittance

Subscripts

- b properties at the side wall propellant surface
- F properties at the flame

Superscripts

- $'$ fluctuating quantity
- $-$ mean quantity

Greek

- γ ratio of specific heats
- ρ density, $kg/m^3(slug/ft^3)$
- ω radian frequency, (1/s)

Research sponsored under AFOSR Contract No. F49620-82-C-0013.

* Graduate Research Assistant
** Senior Research Engineer
*** Regents' Professor, Associate Fellow, AIAA.

Introduction

Combustion instability is a serious problem that has hindered the development of solid rocket motors since their early days. Combustion instability occurs when the interaction between a combustion disturbance and the combustion processes at the propellant's surface results in a positive energy feedback between the two that is larger than the energy losses experienced by the disturbance due to viscous effects, heat transfer, nozzle damping and so on. Since the growth or decay of a given disturbance in a rocket motor depends upon its interaction with the entire length of the burning propellant grain, it is important to understand how this interaction depends upon the location of the burning propellant section within the combustor. For example, in a rocket motor experiencing an axial instability of its fundamental acoustic mode, the propellant grains at the two ends of the motor experience primarily pressure oscillations, the propellant grain at the center experiences primarily velocity oscillations, and the remainder of the propellant grain experiences both pressure and velocity oscillations. Therefore, to predict the stability of this rocket motor, it is important that data describing the propellant's burn rate response to pressure and velocity oscillations, be available. These burn rate responses to pressure and velocity oscillations are referred to as pressure and velocity coupled response functions, respectively. This paper describes recent progress made in a research program that is concerned with the experimental determination of the response functions of various solid propellants under different excitation conditions.

The first part of the paper describes the results of an investigation of the effect of aluminum addition upon the response functions and gas phase losses associated with aluminized propellants. This study had been undertaken because of indications[1] that aluminum addition to a propellant may worsen the stability of a given rocket motor; a situation that may arise when the overall increase in propellant driving due to aluminum addition is larger than the corresponding overall increase in damping due to the presence of aluminum oxide particles in the gas phase. To investigate the possible occurence of such a situation, it is necessary to determine the dependence of the propellant driving and its associated gas phase losses upon its aluminum contents. In this study, the previously developed impedance tube set-up[2,3] has been utilized to investigate the dependence of the pressure coupled response function and associated gas phase losses of a given propellant formulation upon its aluminum content. The second part of the paper describes some recent results obtained in an experimental study that is concerned with the determination of the velocity coupled response functions of solid propellants in a modified impedance tube set-up specifically developed for this purpose[4].

Response Functions and Damping of Aluminized Propellants

This section describes the results of the investigation of the effect of aluminum addition upon the pressure coupled response functions and gas phase losses of a specific solid propellant formulation. The pressure coupled response function, R_p, of a solid propellant is defined as[5]

$$R_p = \frac{m'/\bar{m}}{p'/\bar{p}} = \frac{(\rho'\bar{u} + \bar{\rho}u')/\bar{\rho}\bar{u}}{p'/\bar{p}} = \frac{u'/\bar{u} + \rho'/\bar{\rho}}{p'/\bar{p}} = \frac{Y}{\gamma \bar{M}_b} + \frac{\rho'/\bar{\rho}}{p'/\bar{p}} \quad (1)$$

where $\bar{M}_b = \bar{u}/\bar{a}$ is the Mach number of the mean flow at the propellant surface and Y is the non-dimensional, complex, propellant admittance. The real part of the admittance, Y_r, is a measure of the driving provided by the propellant. When the oscillations at the propellant surface are isentropic, Eq. (1) reduces to

$$R_p = \frac{1}{\gamma}\left(\frac{Y}{\bar{M}_b} + 1\right) \quad (2)$$

Equation (2) shows that in the isentropic case R_p can be determined once Y and $\bar{M}_b$ are known. In the present study Y and $\bar{M}_b$ were determined experimentally and then substituted into Eq. (2) to determine R_p.

A schematic of the experimental set-up, utilized to measure the admittance Y of the tested solid propellants and the associated gas phase losses is shown in Fig. 1. It consists of a tube with the tested, disc-shaped solid propellant sample placed at one end and an acoustic driver at the other end. The need to test at high pressures resulted in the placement of the impedance tube in a pressurized tank that kept the pressure differences across the transducers' diaphragms around 25 psig, allowing the utilization of more sensitive, low impedance pressure transducers, which increased the accuracy of the measured acoustic pressure data. During an experiment, the acoustic driver was utilized to generate a standing wave of a desired frequency in the impedance tube and an array of pressure transducers mounted at pre-selected locations along the impedance tube walls was used to measure the continuously varying acoustic wave structure inside the impedance tube. The measured acoustic pressure data were continuously fed, via an analog-to-digital converter, into a minicomputer-disc system for storage. After the test, the stored data were Fourier analyzed to obtain the spatial distribution of the amplitudes and phases in the impedance tube. These data were then used together with solutions of the impedance tube wave equations to determine the propellant admittance and gas phase losses[6].

The capability for simultaneous measurements of the propellant response functions and the gas phase acoustic losses makes the above described impedance tube facility suitable for a study of the influence of propellant aluminum content on the propellant's driving and damping characteristics. Such a study was undertaken using propellants that were supplied by AFRPL. To isolate the effect of aluminum content, three different propellant formulations differing only in their aluminum content were to be tested; that is, the formulation of the nonaluminized fraction of each of the tested propellants was to be the same. Such propellant formulations could be obtained ideally by replacing different weight fractions of a given propellant formulation with an equivalent weight of aluminum. In the planned tests, the three propellant formulations were going to have zero, five, and eighteen percent of aluminum by weight. Unfortunately, propellant processing difficulties resulted in variations of the developed propellant compositions from those that had been desired. The discrepancy is described in Table I where the actual and "desired" formulation of the three propellants are compared. It indicates that the amount of binder remained constant in all three formulations and that the added aluminum replaced some of the AP particles. Thus, the three propellants varied from one another both in their aluminum content and in the formulation of their nonaluminized fractions.

The three propellants were tested in the impedance tube over the frequency range of 400 to 1200 Hz and typical results are presented in Fig. 2 where the frequency dependence of the propellants' driving (i.e., Y_r) and their gas phase damping (i.e., G) are presented. Examination of this figure shows (1) the existence of maxima in the response function curves and that the frequency at which these occur changes with the aluminum content of the propellant; and (2) that the propellant driving and associated gas phase damping increase with an increase in the propellant aluminum content. Since increasing both the propellant driving and the gas phase damping would exert countering effects on the stability of a rocket motor, one cannot determine the effect of aluminum addition upon a given rocket stability without conducting an analysis capable of properly accounting for the above indicated effects. Finally, it remains to establish that the observed effects are due to the aluminum addition only and not due to the differences in the compositions of the nonaluminized fractions of the tested propellants.

Velocity Coupled Response Measurements

In this section, recent progress made in the experimental investigations of the so called velocity coupled response functions of solid propellants, is reported. The experimental configuration of the modified impedance tube facility utilized in this study is shown in Fig. 3, along with the impedance tube wave equations[6,7]. The "driver" propellant sample provides a stream of hot combustion products that moves past the two test propellant samples in an attempt to simulate actual rocket flow conditions. In this configuration, the driver propellant "experiences" only pressure oscillations while the test propellant samples are subjected to both pressure and velocity oscillations. The experimental set-up permits moving the "driver" propellant to different locations upstream of the test propellant samples; a capability that provides an opportunity for investigating the response of the test propellants at different acoustical environments along the standing wave. During a test, a stepping motor is utilized to feed the test propellant samples inward at the propellant burn rate. This is done in order to maintain the burning test propellant surfaces flush with the adjacent impedance tube walls.

The wave equations presented in Fig. 3 are those utilized in this study to determine the unknown velocity coupled response function R_v and they represent an "accepted" formulation of the axial instability problem[8]. It should be pointed out, however, that the definitions of R_p and R_v utilized herein differ from those used by other investigators. (See for example, Eq. 1). Furthermore, it appears that the introduction of these definitions was motivated by the need to simplify the mathematical formulation of the combustion instability problem and not by any sound theoretical and/or experimental justification.

A new data reduction program has been developed for the determination of the unknown velocity coupled response function, R_v, from the measured acoustic pressure data. The data reduction procedure is based on the method of quasi-linearization[9] and has been discussed in detail in reference 4. The method requires that the acoustic pressure data used in the estimation of R_v be measured in that region of the impedance tube where the test propellant samples are located. It should also be noted that the data reduction program presumes a knowledge of the pressure coupled response function and it determines only the velocity coupled response function. Consequently, the pressure coupled response function needs to be determined in a separate experiment or by the use of a reliable theory.

During an experiment to determine the velocity coupled response function, the impedance tube is placed inside a pressurized tank for the reasons mentioned in the previous section. Next, the acoustic driver is turned on to set up a standing wave of a desired frequency inside the impedance tube and pressure transducers mounted at preselected locations along the impedance tube walls are used to measure the continuously varying wave structure in the impedance tube. As in the pressure coupled case, the acoustic pressure data are continuously fed, via an analog-to-digital converter, into a minicomputer-disc system for storage. The test duration is divided into a series of data acquisition periods, separated from each other by periods of data transfer. Each data acquisition period, called a block, can be programmed to acquire data over a period whose duration is a multiple of 12 periods of the test oscillation. It is to be noted that data taken during a test is discrete since no data is acquired during data-transfer periods. After the test, the stored data are Fourier-analyzed to obtain the amplitudes and phases of the measured data at the test frequency. A study of the analyzed data shows the existence of ignition and extinguishment transients with a quasi-steady burning period in between. Data obtained during this quasi-steady period is used, along with the solutions of the impedance tube wave equations, to evaluate the propellant response.

In what follows, some recent results obtained in the experimental determination of the velocity coupled response functions of solid propellants are presented. A non-aluminized propellant was used in this investigation and the presented results are for an excitation frequency of 750 Hz.

In the experiments conducted to date, the test propellant samples were located near a pressure node where the velocity oscillations are maximum. Since, as mentioned earlier, the pressure measurements need to be performed in the region of the impedance tube where the test propellant samples are located, some of the acoustic pressure measurements had to be performed near a pressure node. Consequently, the desired signal was often buried in noise from other sources. Signal averaging can be used to separate the signal from the noise. Since the available memory of the minicomputer limited the amount of data that could be recorded in a given block, an estimate of the minimum number of periods of the test signal over which the data should be averaged to sufficiently enhance the signal-to-noise ratio was required. This problem was investigated by comparing data averaged over different numbers of cycles of the test signal.

The spatial amplitude and phase distributions, obtained before propellant ignition by averaging data over 12, 18 and 36 cycles, are compared in Figs. 4 and 5, respectively. Examination of these figures shows that while the amplitude distribution agrees in all cases, the "12 cycle average" phase data exhibits considerable scatter about the "36 cycle average" and the "18 cycle average" phase data exhibits almost no scatter. This indicates that averaging over 18 cycles is probably enough for a sufficient enhancement of the signal prior to ignition.

However, examination of the data measured during the quasi steady burning period, showed that averaging the data over 18 cycles does not suppress the noise sufficiently. This is illustrated in Figs. 6 and 7 which compare the spatial amplitude and phase distributions obtained by averaging data measured during the quasi-steady burning period over 18, 36 and 72 cycles. Examination of these figures shows that the amplitude and phase data obtained as an "18 cycle average" exhibits a considerable scatter about the "72 cycle average". However, it can also be seen from these figures that the "36 cycle average" presents almost no scatter. This indicates that, during the quasi-steady burning period, a "36 cycle average" would be required to increase sufficiently the signal to noise ratio.

Consequently, the spatial amplitude and phase distributions used to evaluate the velocity coupled response functions were obtained by averaging the measured signals over 36 cycles. The needed pressure coupled response functions were measured by the experimental procedure described in the previous section. A comparison between the computed standing wave pattern (i.e., a solution of the wave equations presented in Fig. 3) that provided the "best" agreement, and the experimental data is presented in Fig. 8. The determined optimum value of R_v and the measured value of R_p that were used to predict the standing wave pattern are also indicated in the figure.

Examination of Fig. 8 indicates a reasonable agreement between the predicted and measured amplitude distributions. In contrast, some disagreement is noted in the compared phase distributions. These discrepencies could be due to errors in measurements and/or the data reduction procedure or due to shortcomings in the wave equations that are currently utilized (See Fig. 3) to model the axial instability problem. Specifically, the model for the axial instability problem utilized in this study assumes that the driving due to velocity coupling is directly related to the acoustic velocity itself. However, other functional relationships may be more appropriate as, for example, has been noted by Culick[8], who argued that the burn rate response to the velocity fluctuations should only depend upon the amplitudes of the velocity oscillation and not its direction. Also, there exists no proof that the utilized "one-dimensional" formulation is indeed capable of accounting for the multi-dimensional aspects of the problem where driving of the axial oscillations occurs on the side walls.

Summary

In this study, the impedance tube developed to measure the pressure coupled response functions of solid propellants was used to investigate the dependence of a propellant's driving and damping characteristics upon its aluminum content. The results of this study indicate that aluminum addition increases both the propellant "pressure-coupled" driving and the associated gas phase acoustic losses . Depending on which of these effects is dominant, the addition of aluminum may stabilize or destabilize a given rocket motor. The development of a modified impedance tube for the measurement of velocity coupled response function has also been described. Some recent results obtained in this investigation are presented and discussed.

References

1. Price, E. W., Personal Communication.

2. Baum, J. D., Daniel, B. R., and Zinn, B. T., "Application of the Impedance Tube Technique to the Measurement of the Admittances of Aluminized Solid Propellants. AIAA Paper No. 81-0122, 1981.

3. Baum, J. D., Daniel, B. R., Zinn, B. T., "Determination of Solid Propellant Admittances by the Impedance Tube Method," AIAA Paper No. 81-0281, Feb. 1981.

4. Zinn, B. T., Narayanaswami, L., "Application of the Impedance Tube Technique in the Measurement of the Driving Provided by Solid Propellants During Combustion Instabilities," Acta Astronautica, , Vol. 9, No. 5, pp. 303-315, May 1982.

5. Perry, E. H., "Investigations of the T-Burner and its Role in Combustion Instability Studies," Ph.D. Thesis, California Institute of Technology, May 1970.

6. Baum, J. D., "Experimental Determination of the Admittances of Solid Propellants by the Impedance Tube Technique," Ph.D. Thesis, School of Aerospace Engineering, Georgia Institute of Technology, May 1980.

7. Micci, H. M., Caveny, L. H., and Summerfield, M., "Linear Analysis of Forced Longitudinal Waves in Rocket Motor Chambers," AIAA Paper No. 79-1210, June 1979.

8. Culick, F. E. C., "Stability of Longitudinal Oscillations with Pressure and Velocity Coupling in a Solid Propellant Rocket," Comb. Sci. and Tech., Vol. 2, No. 2, pp. 179-201, 1970.

9. Seinfeld, J. H. and Lapidus, L., "Mathematical Methods in Chemical Engineering," Prentice-Hall International Series in the Physical and Chemical Engineering Sciences, Vol. 3, Chap. 7, pp. 389-398, 1974.

PROPELLANT COMPOSITION (%)

	UZ-7: Non-aluminized		UZ-8: 5% Aluminum		UZ-9: 18% Aluminum	
INGREDIENT	ACTUAL	DESIRED	ACTUAL	DESIRED	ACTUAL	DESIRED
R-45m	9.34	9.34	9.34	8.573	9.34	7.6588
INDOPOL	1.85	1.85	1.85	1.7575	1.85	1.517
TEPANOL	0.15	0.15	0.15	0.1425	0.15	0.123
AP-200 μ	51.00	51.00	51.00	48.45	33.00	41.82
AP-50 μ	15.00	15.00	12.00	14.25	13.00	12.3
AP-8 μ	22.00	22.00	20.00	20.90	19.00	18.04
ALUMINUM: 4.5 μ	0.00	0.00	5.00	5.00	18.00	18.
IDPI	0.66	0.66	0.66	0.627	0.66	0.5412

Table I. Comparison of desired and actual compositions of tested propellants.

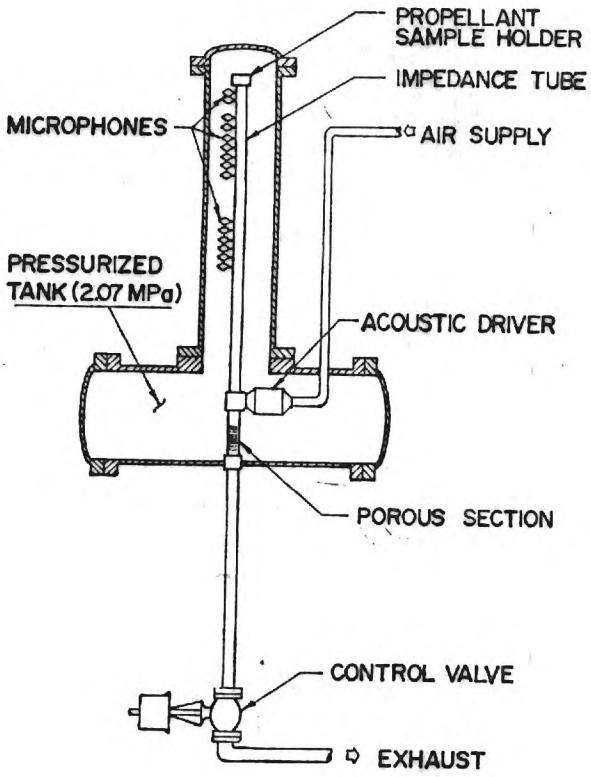

Fig. 1. Schematic Diagram of the Impedance Tube Facility.

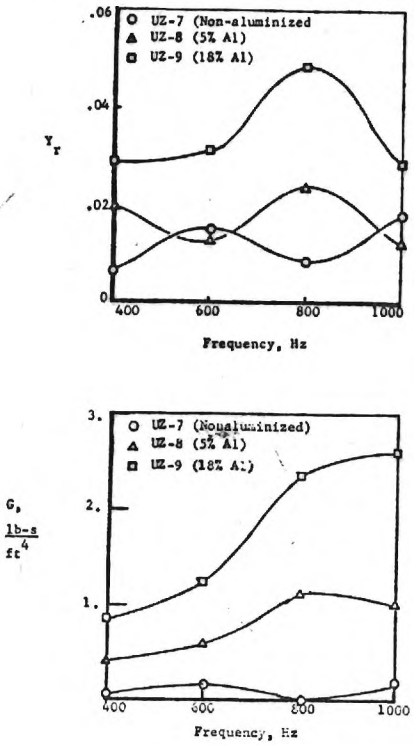

Fig. 2. Dependence of Propellant Driving, Y_r, and Associated Gas Phase Losses, G, upon Frequency and Propellant Aluminum Content.

IMPEDANCE TUBE WAVE EQUATIONS

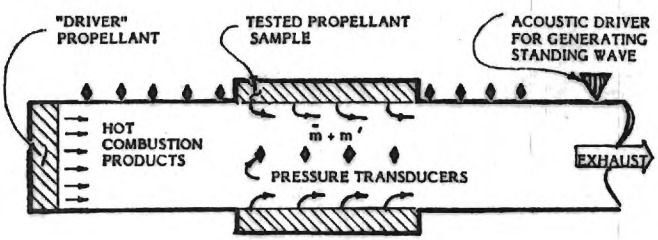

CONTINUITY: $$i\omega\rho' + \frac{d}{dx}(\bar{u}\rho' + \bar{\rho}u') = \frac{b}{A}m_b'$$

MOMENTUM: $$i\omega\bar{\rho}u' + \bar{\rho}\bar{u}\frac{du'}{dx} + \bar{\rho}\frac{d\bar{u}}{dx}u' + \frac{dp'}{dx} + \frac{b}{A}\bar{m}_b u' + F' = 0$$

ENERGY: $$i\omega p' + \bar{u}\frac{dp'}{dx} + \frac{d\bar{p}}{dx}u' + \gamma\bar{p}\frac{du'}{dx} + \gamma\frac{d\bar{u}}{dx}p' = \frac{b}{A}\bar{m}_b\bar{E}\left(\frac{E'}{\bar{E}} + \frac{m_b'}{\bar{m}_b}\right) + (\gamma-1)\,C\bar{u}u'$$

WHERE $$E = \gamma RT_F + \gamma R\Delta T + (R/2C_v)(u^2 + u_b^2)$$

THE VELOCITY AND PRESSURE COUPLED RESPONSE FUNCTIONS ARE INTRODUCED BY LETTING

$$R_p = \frac{\left(\frac{E'}{\bar{E}} + \frac{m_b'}{\bar{m}_b}\right)}{\left(\frac{p'}{\bar{p}}\right)} \quad ; \quad R_v = \frac{\left(\frac{E'}{\bar{E}} + \frac{m_b'}{\bar{m}_b}\right)}{(u'/\bar{a})}$$

OR

$$\frac{m_b'}{\bar{m}_b} + \frac{E'}{\bar{E}} = R_p\frac{p'}{\bar{p}} + R_v\frac{u'}{\bar{a}}$$

Fig. 3. Set-up and Equations Utilized for the Determination of Velocity Coupled Response Functions.

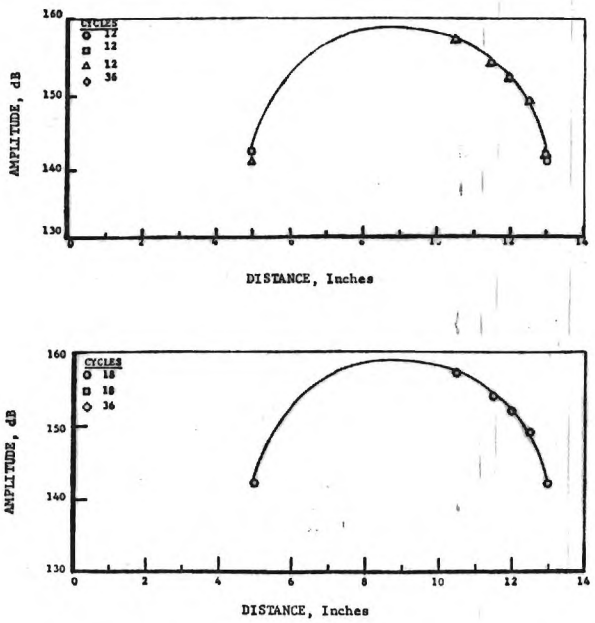

Fig.4. Comparison of Spatial Amplitude Distributions Obtained by Averaging the Pressure Measured Prior to Ignition over 12, 18 and 36 Cycles.

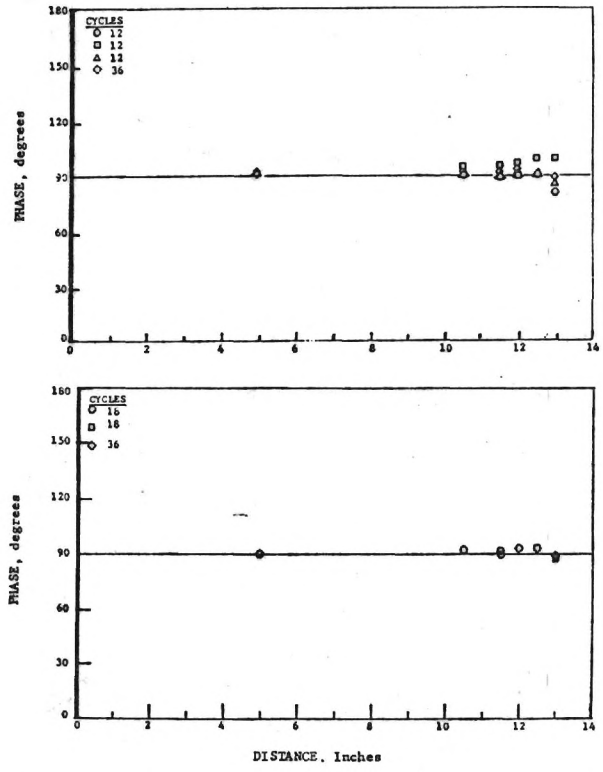

Fig. 5. Comparison of Spatial Phase Distributions Obtained by Averaging the Pressures Measured Prior to Ignition over 12, 18 and 36 Cycles.

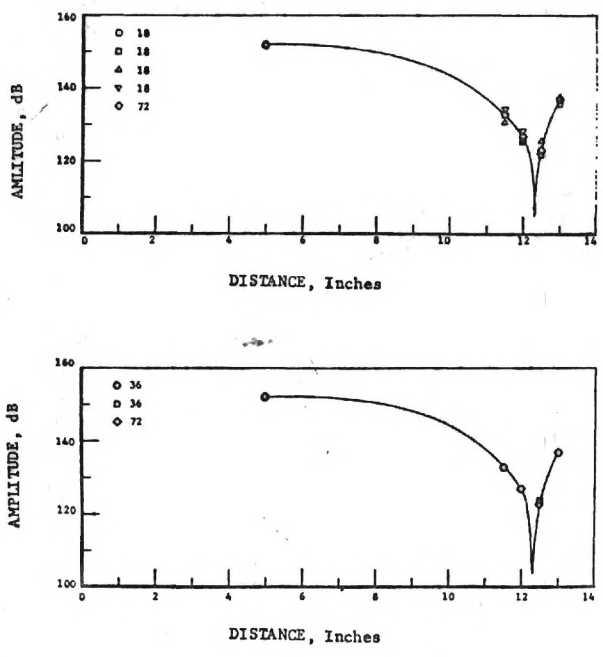

Fig. 6. Comparison of Spatial Amplitude Distributions Obtained by Averaging the Pressures Measured during the Quasi-Steady Burning Period over 18, 36 and 72 Cycles.

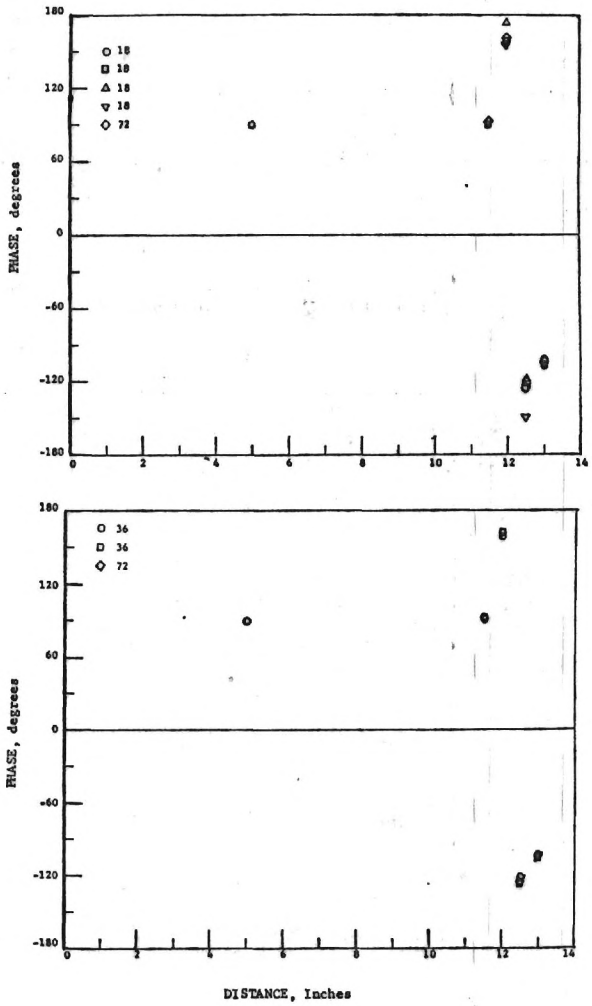

Fig. 7. Comparison of Spatial Phase Distributions Obtained by Averaging the Pressures Measured during the Quasi-Steady Burning Period over 18, 36 and 72 Cycles.

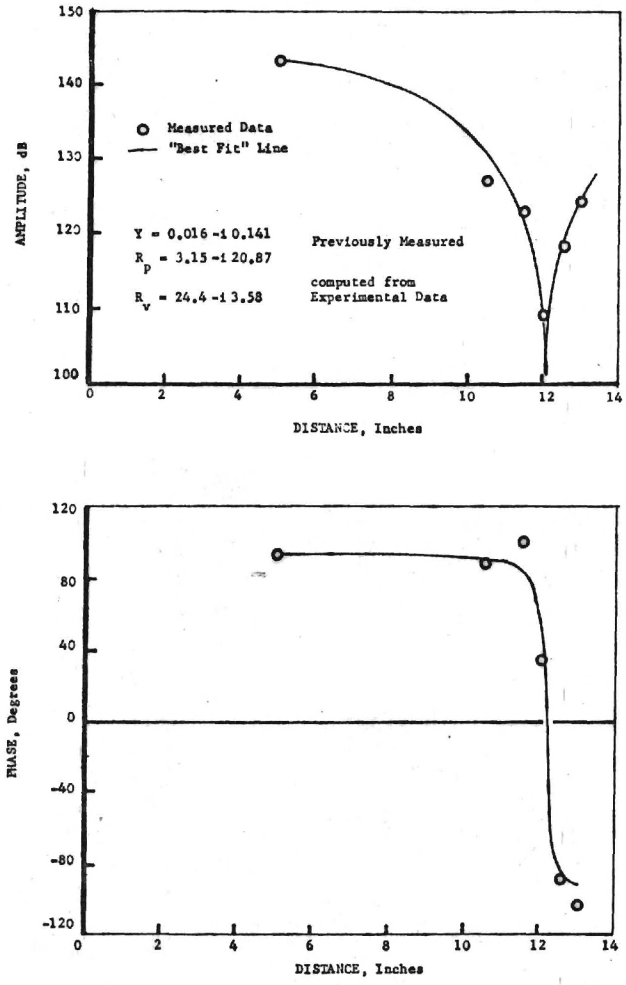

Fig. 8. Axial Variation of Amplitude and Phase of the Standing Wave in the Impedance Tube; A Comparison Between Theory and Experiment.

EFFECT OF OSCILLATIONS UPON VELOCITY DISTRIBUTIONS IN SIMULATED SOLID PROPELLANT FLOW ENVIRONMENTS*

F. L. Chen,** B. R. Daniel# and B. T. Zinn##
School of Aerospace Engineering
Georgia Institute of Technology
Atlanta, Georgia 30332

INTRODUCTION

This paper describes the status of an investigation which has been concerned with the determination of the flow characteristics inside solid propellant rocket motors experiencing axial instabilities. When the instability drives one of the longitudinal modes of the combustor, different sections of the propellant are exposed to different oscillatory flow conditions; that is, portions of the propellant near pressure nodes are subjected primarily to axial velocity oscillations parallel to their surfaces, propellant sections near velocity nodes experience primarily acoustic pressure oscillations and the remaining propellant sections experience both pressure and velocity oscillations. The interactions of these oscillations with the propellant combustion processes are responsible for the observed axial instabilities and they involve complex fluid mechanical, heat transfer and chemical mechanisms. In general, these interactions occur near the burning propellant surface and they produce velocity oscillations v' at the propellant surface which are normal to the direction of the core flow oscillations. Consequently, both the steady state and oscillatory flow fields are multidimensional and their velocities change direction, from radial to axial, somewhere between the propellant surface and the combustor centerline. This observation also indicates that while axial instabilities are generally treated as one dimensional problems (e.g., see Refs. 1-3) these phenomena are actually multidimensional and they should be treated as such.

A propellant exhibits an unsteady burn rate during an instability because the presence of flow oscillations probably results in periodic mixing, diffusion, heat transfer and chemical processes next to its surface. The manner in which a given propellant section responds to flow oscillations depends upon the structure of the steady state combustion zone next to its surface, as "different" steady state combustion zones may respond differently to oscillatory excitation. Since the structure of the local, steady state combustion zone is expected to depend upon the characteristics of the steady flow, it follows from the above comments that both the steady and oscillatory components of the flow next to the propellant surface affect the propellant response. In addition, one should keep in mind that (1) the characteristics of the oscillatory flow field are known to depend upon the steady flow properties; (2) the presence of oscillations may affect the characteristics of the steady flow by causing early transition to turbulent flow, modifying the turbulence structure and the introduction of acoustic streaming; and (3) the processes described under (2) above may be amplitude dependent.

It follows from the above discussion that there is a need to develop an understanding of the flow fields in unstable rocket motors. Ideally, one would want to acquire such knowledge by performing specific diagnostics in unstable rocket motor. However, difficulties associated with performing the needed measurements inside rocket combustors and the high cost of firing actual rocket motors render such an approach impractical. Also, considerations of the complexities of the problem when chemical reactions occur in the combustor strongly suggest that as a first step towards the solution of the problem at hand one should investigate, both experimentally and theoretically, the characteristics of the flow in a "cold flow" rocket-like facility capable of simulating the flow conditions inside solid propellant rocket motors experiencing axial instabilities. One such possibility is to use a channel in which the propellant burning is simulated by mass addition through porous side walls.

Steady flows in channels with porous walls have been investigated experimentally by Yagodkin[4], Yamada et al[5], Taylor[6] Heusman and Eckert[7], Dunlap et al[8] and others. These studies show that the following occur in a closed end porous tube with mass injection through the wall: (a) the axial velocity distribution is self similar over substantial axial distances; (2) turbulence begins forming while the velocity profile remains self similar; (3) transition of the self similar laminar profile to a turbulent profile occurs at large distances from the closed end; and (4) maximum turbulence intensity occurs in an annular region between the wall and the centerline and the downstream development of the turbulence profile is not similar.

Keeping the above flow characteristcs in mind, one is faced with the following questions when considering the combustion instability problem: (1) does the presence of flow oscillations in the motor affect the above-mentioned steady flow characteristics and under what conditions? and (2) how do these steady flow characteristics affect the acoustic flow field and unsteady propellant response? With the exception of the recent study of Brown[9], it does not appear that these questions were addressed in studies of flows in channels with mass addition from the side walls. On the other hand, related questions were considered in studies of oscillatory flows in tubes with solid walls. These[10-13] indicate that the presence of pulsations in the flow may (1) change the turbulence structure of the flow; (2) enhance

---

* Research supported under AFOSR Contract No. F49620-82-C-0013; Dr. Len Caveny Contract Monitor.
** Visiting Scholar from NPU, Xian, Peoples Republic of China
# Senior Research Engineer
Regents' Professor

transition to turbulence; (3) augment and sometimes inhibit heat transfer to the walls; (4) cause flow reversal during some portion of the cycle; and (5) result in maximum velocity occuring someplace between the centerline and the wall. While these results were observed in pipes with solid walls, it is also possible that similar behavior also occurs in flows originating through side-wall mass addition. Since, as discussed above, both the steady and unsteady flow fields affect the propellant response during instabilities, it is of utmost importance that the characteristics of these flow fields in channels with side-wall mass addition under both oscillatory and steady flow conditions be studied. This paper presents results obtained during early phases of an investigation which has been concerned with this problem.

EXPERIMENTAL SETUP

The experimental setup is shown in Fig. 1. It consists of a 1.9 inch I.D. porous wall tube whose ends are connected to solid wall tubes. The tube on the right is connected to a large vacuum tank and its flow rate is controlled by a valve located upstream of the vacuum tank. An acoustic driver attached to the opposite end of the tube was used to excite a standing acoustic wave of desired amplitude and frequency in the tube. The hot wire probe was used to obtain radial distributions of the velocity at the indicated location and the microphone to measure the amplitude of the sound wave.

Tests were conducted with different steady state flow rates and different excitation conditions. In addition, in an effort to check the validity of the hot wire measurements under oscillatory flow conditions, the hot wire probe was used to measure centerline velocities at different locations of a solid wall tube in which a standing acoustic wave was driven by means of an acoustic driver in the absence of a steady flow.

RESULTS AND DISCUSSION

This section presents radial dependence of the velocity distributions measured with the hot wire probe shown in Fig. 1. Figure 2 presents a comparison of the steady state, velocity profiles in the presence and absence of a 291 Hz standing acoustic wave in the tube. In the absence of acoustic oscillations, the magnitude of the velocity varied between 2.5 m/sec near the centerline, where the velocity was axial, to 0.3 m/sec near the wall where the velocity was radial. Since the hot wire traverse was performed with the hot wire perpendicular to both the axial and radial components of the velocity, the hot wire probe responded to both the axial and radial velocity components and its signal was proportional to the magnitude of the velocity vector. Figure 2 shows that when sound is present, the hot wire probe indicates that the magnitude of the steady velocity increases near the wall and decreases near the centerline. These effects increase as the wave amplitude increases from 141 dB to 146 dB.

Before discussing the data presented in Fig. 2, it should be pointed out that an examination of the hot wire output on an oscilloscope as the radial traverse was carried out revealed that it remained nearly sinusoidal between the centerline of the tube and a short distance (of the order of a fraction of an inch) from the wall where the signal became partially rectified. The probe output became fully rectified when the probe traverse was completed at a distance of approximately .01 inches away from the wall, where the steady (radial) velocity is very low. To elucidate the causes of the observed increase in steady velocity near the wall in the presence of sound (see Fig. 2), the hot wire was used to measure the centerline velocity in a tube closed at both ends (with no steady flow) in which a standing acoustic wave was excited by means of an acoustic driver. As expected, the probe waveform output (on an oscilloscope) was fully rectified throughout the tube and it's voltmeter output indicated the presence of both steady and oscillatory flow components.

The probe indications of the presence of a steady flow component in a situation where such a flow was absent is sympotomatic of the difficulties that such probes experience when used in flow situations where the magnitude of the oscillatory component of the velocity is larger than the magnitude of steady component of the velocity. These problems are discussed in detail in Ref. 13 and they are caused by flow reversal and the inability of the probe to respond to the rapid changes in flow direction when the magnitude of the velocity is very low. In view of these comments, it is not clear whether the observed increase in the magnitude of the steady component of the velocity near the wall in the presence of an acoustic field is indeed due to a fluid mechanical phenomenon (such as nonlinear acoustic effect) or due to the peculiarities of the hot wire probe when used in an oscillating flow field, or both.

Next, the observed reduction (see Fig. 2) in the magnitude of the steady velocity component near the center line of the tube in the presence of sound is considered. Again, it could be a fluid mechanical phenomenon but most likely it is caused by the nonlinearity of the hot wire response whose output voltage is proportional to the square root of the magnitude of the velocity. For the data presented in Fig. 2, the magnitude of the steady component of the velocity is larger than the magnitude of the oscillatory velocity component outside the steady state velocity boundary layer. Consequently, one can argue (qualitatively) that in the presencce of an acoustic field the hot wire output near the tube centerline is given by

$$E = \frac{1}{2}\left\{\sqrt{\bar{u} + |u'|} + \sqrt{\bar{u} - |u'|}\right\} < \sqrt{\bar{u}} \qquad (1)$$

where u' and $\bar{u}$ are the oscillatory and steady state components of the velocity, respectively. Equation (1) indicates that the presence of an oscillatory velocity component would tend to reduce the hot wire voltage output, as shown in Fig. 2, even though the steady state velocity remains unchanged.

Finally, it should be pointed out that the bands which are used in Fig. 2 to describe the steady velocities inside the tube represent the ranges of measured variations of the steady velocity components at the indicated locations.

The test conditions described in Figure 3 differ from those considered in Figure 2 by the fact that they involve a lower steady state velocity; that is, the maximum centerline velocity of the data in Fig. 3 is approximately 1.5 m/sec while it is 2.5 m/sec in the case considered in Fig. 2. For the data presented in Fig. 3 the magnitude of the oscillatory component of the velocity was comparable to that of the steady velocity component all along the radius when the dB level was 146. As a result, the hot wire output was partially rectified near the tube centerline and fully rectified near the wall. Thus, using the arguments presented above, it is believed that this rectification effect was the cause of the observed increase in the magnitudes of the steady state velocity when 146 dB oscillations were present in the tube. In contrast, the steady velocity distribution measured with 141 dB oscillations in the tube resembles those presented in Fig. 2 and the reasons for its deviation from the steady velocity distribution measured in the absence of sound are probably due to the effects considered in the discussion of the data presented in Fig. 2.

Figure 4 contains a comparison of steady state velocity distributions measured when standing waves of different frequencies and the same amplitudes were excited inside the experimental setup. In each of the tests, the DC and AC outputs of the hot wire probe were the same at the centerline of the tube. When this condition was satisfied, the measured steady state velocity distributions lie within the band shown in Fig. 4 for frequencies of 291, 392, 581, 600, 866 and 1470 Hertz. This result indicates that if the presence of an oscillatory velocity in the tube has any effect upon the steady velocity distribution, then this effect is independent of frequency at least for the conditions investigated under this study.

Figure 5 presents a comparision of the radial distributions of the AC components of the hot wire outputs in the presence and absence of a 291 Hz sound wave. The variation of the measured AC voltage at each radial location is described by the indicated band. An examination of Figure 5 reveals that both distributions have a maximum between the centerline and the wall at a distance of approximately .06 inches from the wall. When no sound is present in tube, the AC voltage describes the turbulence level of the flow and its magnitude drops rapidly when one moves away from the location of maximum turbulence. Figure 5 also indicates that when 291 Hz sound is excited in the tube the AC output of the hot film increases considerably throughout the tube cross sectional area. This increase in the AC signal output is due to the presence of sound in the tube. It is interesting to note that when the hot wire signal was observed on an oscilloscope during tests with sound excitation, it became difficult to "see" (on the oscilloscope) the oscillatory velocity signal as the region of maximum AC output was traversed. This was caused by the masking of the acoustic wave signal by the random, high intensity turbulence in this region.

The observed existence of a region of maximum fluctuating velocities (i.e.,turbulence and acoustic velocity) between the centerline and the wall is consistent with the findings in related studies[11]. Reference 11, which investigated the effect of sound upon convective heat transfer, referred to such a region as "abnormal turbulence" and it argues that this phenomenon is most likely responsible for the observed increase in convective heat transfer between the flow and the wall. If this assertion is indeed correct, then the increase in the magnitude of the fluctuating velocity observed in the present study may cause propellant driving in unstable rocket motors by modifying heat transfer, mixing and chemical processes near the propellant surface. As a matter of fact, this phenomenon may be one of the major causes of the so-called velocity coupling which is believed to be a major contributor to the driving of axial instabilities in solid propellant rocket motors.

Before leaving this section a few comments regarding the hot wire measurements are in order. First, as indicated above, the hot wire data presented in this paper only describes magnitude variations of the velocity vector which changes direction from being radial at the wall to being axial near the tube centerline. To check for possible wall effects upon the hot wire measurements, the hot wire output was monitored as the hot wire probe was moved from the centerline towards the wall with no flow or sound present in the tube. In this case the probe output remained at zero level until it reached a distance of approximately 0.04 inches from the wall. At this point the DC output of the probe started increasing and it further increased as the probe was moved from this point towards the wall in spite of the fact that there was no sound or flow in the tube. It is believed that this voltage increase was caused by heat transfer from the hot wire to the wall. This phenomenon could affect the accuracy of the velocity measurements near the wall where the magnitudes of the measured velocities are small. Another phenomenon which can affect the accuracy of the hot wire measurements is free convection from the wire which was shown[14] to be important when the magnitude of the measured velocity is less than, approximately, 25 cm/sec. Finally, Ref. 15 reports that the orientation of the hot wire supports relative to the steady component of the velocity can also affect the accuracy of the hot wire measurements. These studies indicate that while the shape of the measured velocity profiles are not affected by the orientation of the hot wire supports, their magnitudes can differ by as much as 75 percent with the highest and lowest accuracies obtained when the hot wire supports are aligned along or perpendicular to the direction of the steady flow, respectively. Unfortunately, the supports of the hot wire used in this study were perpendicular to direction of the mean flow which according to Ref. 15 may have resulted in some errors in the measured velocities. However, since the orientation of the wire supports does not affect the shapes of the measured velocity profiles, then the velocity distributions presented herein should at least provide a correct qualitative descriptions of the investigated flows.

SUMMARY

This paper describes the status of an ongoing study in which a hot wire is used to investigate the effect of acoustic oscillations upon the radial distribution of the velocity in a tube simulating the flow conditions in solid propellant rocket motors. While the data indicates that the presence of oscillations may strongly influence the velocity field near the wall, where mass addition occurs, there are also indications that the measured hot wire velocities are in error in flow regions where the magnitudes of the steady velocity components are of the same order as the magnitudes of the oscillatory velocity components. Hence, utmost caution should be exercised in the interpretation of these data, especially in the wall region where the largest errors in the hot wire measurements most likely occur.

REFERENCES

1. Culick, F. E. C., "The Stability of One-Dimensional Motions in a Rocket Motor," Combustion Science and Technology, Vol. 7, 19, 73, pp. 165-175.

2. Culick, F. E. C., "Interactions Between the Flow Field, Combustion, and Wave Motions in Rocket Motors," NWC TP 5349, June 1972.

3. Micci, M. M., L. H. Caveny and W. A. Sirignano, "Linear Analysis of Forced Longitudinal Waves in Rocket Motor Chambers," AIAA Paper 79-1210, AIAA/SAE/ASME 15th Joint Propulsion Conference, June 18-20, 1979, Las Vegas, Nevada.

4. Yagodkin, V. I., "Use of Channels with Porous Walls for Studying Flows which Occur During Combustion of Solid Propellants," Proceedings of the 18th Astronautics Congress, Vol. 3, 1967, pp. 69-79.

5. Yamada, K., Goto, M., and Ishikawa, N., "Simulative Study on the Erosive Burning of Solid Rocket Motors," AIAA Journal, Vol. 14, No. 9, September 1976, pp. 1170-1176.

6. Taylor, Sir Geoffrey, "Fluid Flow in Regions Bounded by Porous Surfaces," Proceedings of Royal Society, London 234A 1199, 1956, pp. 456-475.

7. Huesmann, K. and Eckert, E. R. G., "Untersuchungen ueber die Laminare Stroemung und den Umschlag zur Einblasung durch die Rohrwand," Waerme-und Stoffubertragung, Bd. 1, 52, 1968.

8. Dunlap, R., Willoughby, P. G., and Hermsen, R. W., "Flowfield in the Combustion Chamber of a Solid Propellant Rocket Motor," AIAA Journal, Vol. 12, No. 10, October 1974, pp. 1440-1412.

9. Brown, R. S., Waugh, R. C., Willoughby, P. G., and Dunlap, R., "Coupling Between Velocity Oscillations and Solid Propellant Combustion," United Technology Center presentation at the Working Session on Combustion Instability/Flow Interactions, AFOSR Contractors Meeting, February 11, 1983, Lancaster, California.

10. Feiler, C. E., "Experimental Heat-Transfer and Boundary-Layer Behavior with 100-CPS Flow Oscillations," NASA TN D-2521, December 1964.

11. Bogdonoff, D. W., "A Study of the Mechanisms of Heat Transfer in Oscillating Flow," Ph.D. Thesis, Department of Aerospace and Mechanical Sciences, Princeton University, 1967.

12. Clamen, M. and Minton, P., "An Experimental Investigation of Flow in an Oscillating Pipe," Journal of Fluid Mechanics, Vol. 81, Part 3, July 13, 1977.

13. Richardson, P. D., "Effects of Sound and Vibrations on Heat Transfer," Applied Mechanics Reviews, Vol. 20, No. 3, March 1967.

14. Rasmussen, C. G., "The Air Jet Hot-Wire Microphone: Application of Hot-Wire Techniques to the Measurement of Steady and Alternating Particle Velocity in Air at Velocities below 2 m/sec.," DISA Information, pp. 5-13.

15. Van Thinh, Nguyen, "On Some Measurements Made by Means of a Hot Wire in a Turbulent Flow Near a Wall," DISA Information, pp. 13-18, taken out of Thinh, N. Van: C. R. Acad. Sc. Paris, t. 264, pp. 1150-1152 (June 19, 1967). Series A.

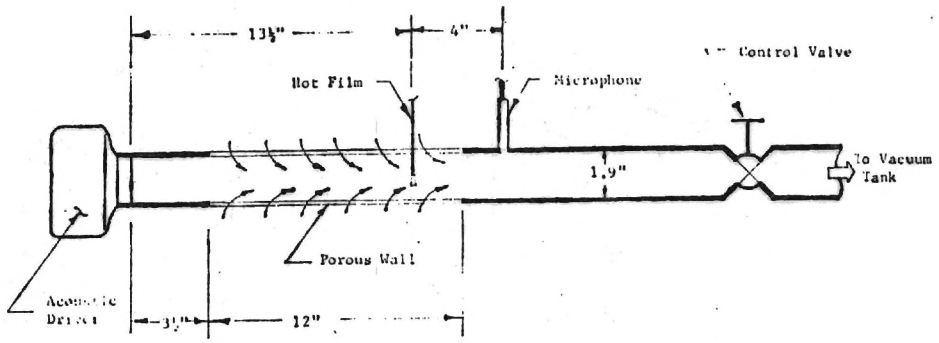

Figure 1. A Schematic of the Experimental Setup.

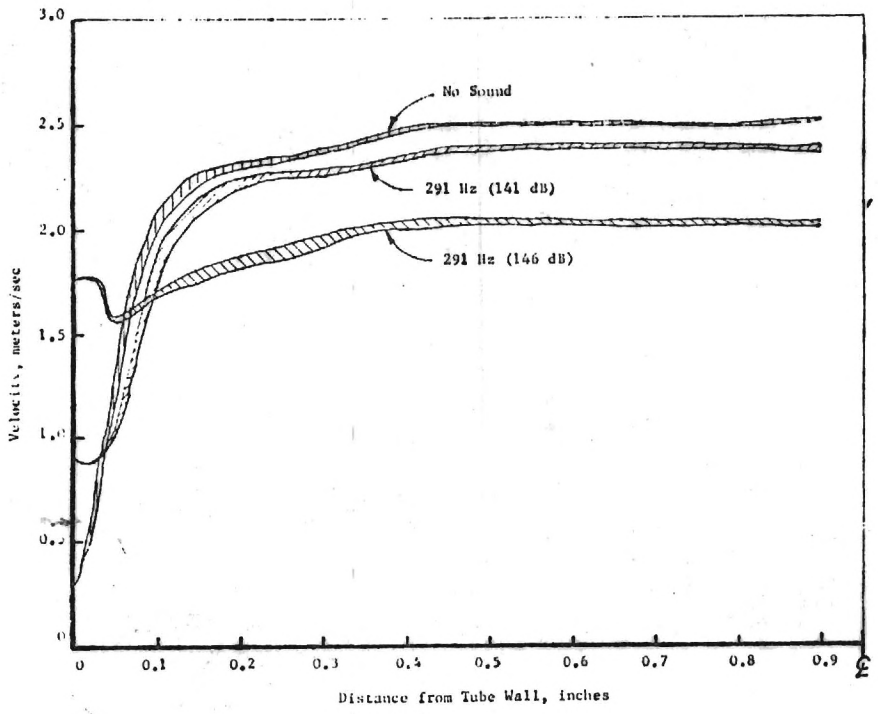

Figure 2. A Comparison of the Steady State, Radial Distributions of Velocities Measured in the Presence and Absence of Sound Fields of the Same Frequency and Different Amplitudes.

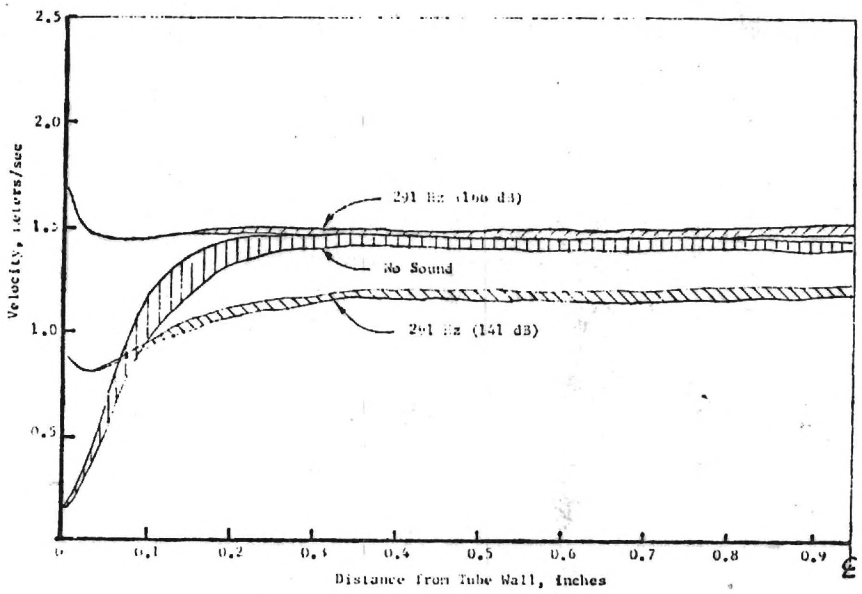

Figure 3. A Comparison of the Steady State, Radial Distributions of Velocities Measured in the Presence and Absence of Sound Fields of the Same Frequency and Different Amplitudes.

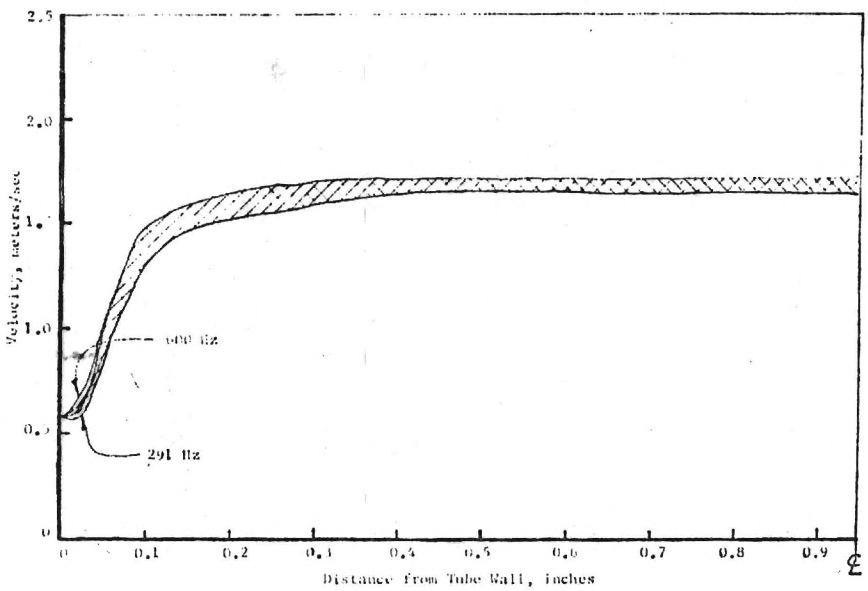

Figure 4. Dependence of the Radial Distributions of the Steady State Velocities upon the Frequency of the Excited Acoustic Wave.

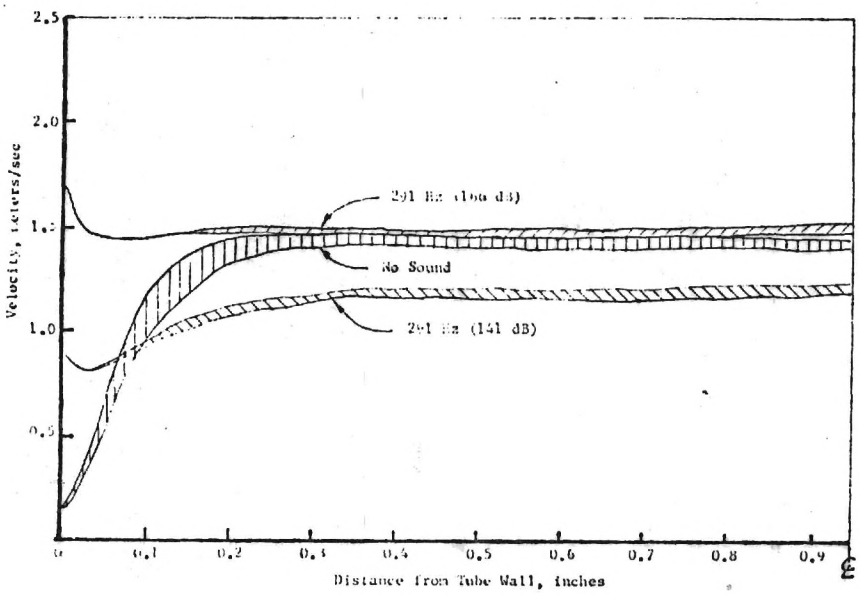

Figure 3. A Comparison of the Steady State, Radial Distributions of Velocities Measured in the Presence and Absence of Sound Fields of the Same Frequency and Different Amplitudes.

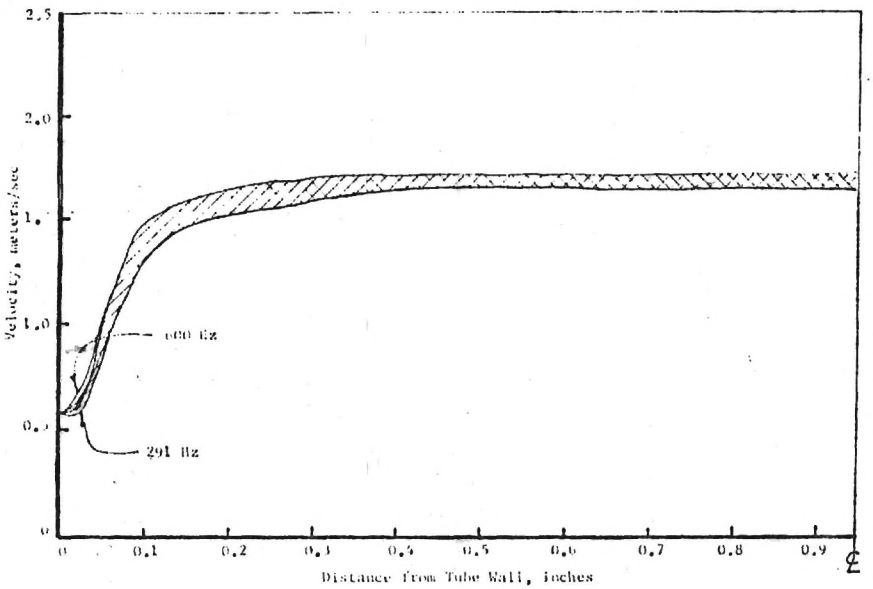

Figure 4. Dependence of the Radial Distributions of the Steady State Velocities upon the Frequency of the Excited Acoustic Wave.

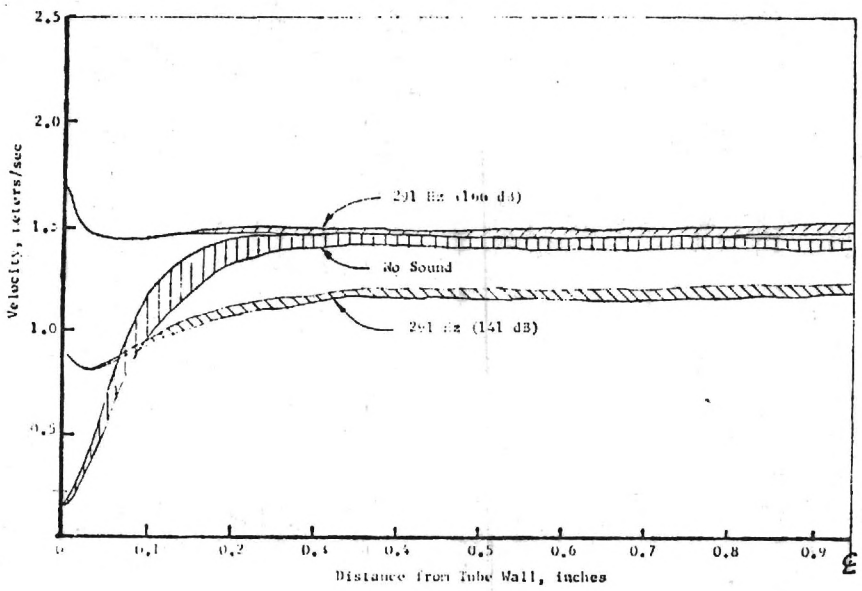

Figure 3. A Comparison of the Steady State, Radial Distributions of Velocities Measured in the Presence and Absence of Sound Fields of the Same Frequency and Different Amplitudes.

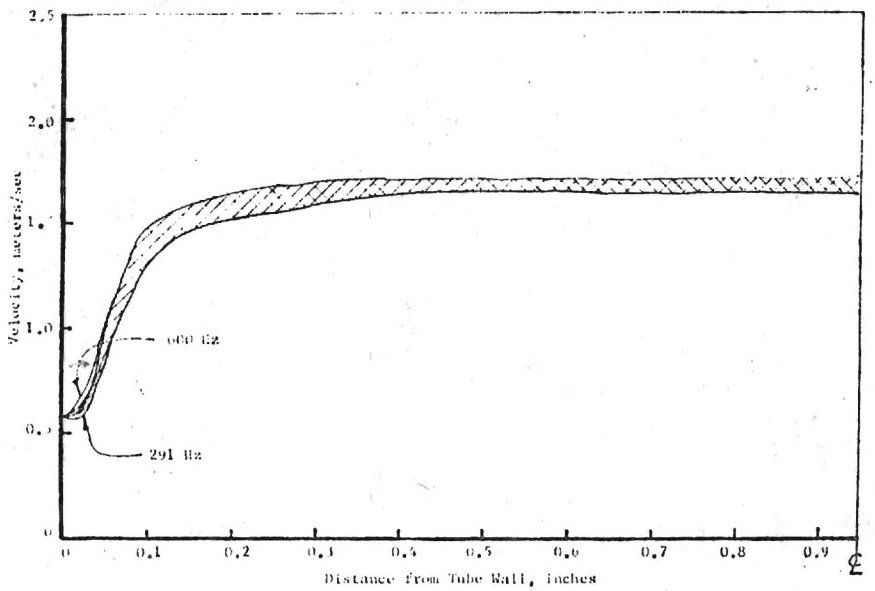

Figure 4. Dependence of the Radial Distributions of the Steady State Velocities upon the Frequency of the Excited Acoustic Wave.

TASK II

Heterogeneous Diffusion Flame Stabilization

J. E. Hubbartt

J. I. Jagoda

W. C. Strahle

TASK II

Heterogeneous Diffusion Flame Stabilization

J. E. Hubbartt, J. I. Jagoda, W. C. Strahle

A. Research Objectives

This program utilizes a facility which models the flame anchoring region of a solid fueled ramjet. The major objective is to ensure predictability of this kind of a flow through computation which is supported by an adequate data base.

B. Results and Discussion

The following tasks were completed under this research program

1. Design, development, construction and checkout of a wind tunnel system which models the flame stabilization region of a solid fueled ramjet.
2. Acquisition and set-up of a two component laser velocimeter and construction of a three component actuation system for the velocimeter.
3. Cold flow tests using hot film, x-film and laser velocimetry together with pitot-static testing.
4. Set-up and development testing with laser Rayleigh scattering.

The results are described in AIAA Paper No. 84-0013 which will be given in Reno, Nevada at the 22nd AIAA Aerospace Sciences Meeting. That paper follows, since it properly describes the program.

C. Publications

Walterick, R. E., Jagoda, J. I., Richardson, C. R. J., deGroot, W. A., Strahle, W. C., Hubbartt, J. E., "Experiments and Computation on Two-Dimensional Turbulent Flow over a Backward Facing Step," submitted to the AIAA Journal.

D. Personnel

Principal Investigators: James E. Hubbartt, Warren C. Strahle and Jechiel I. Jagoda

Research Engineer: R. E. Walterick

Graduate Research Assistants: C. R. J. Richardson, W. A. deGroot W. Grissom, W. I. McNicoll

E. Professional Activities/Interactions:

1) Walterick, R. E., Richardson, C. R. J., de Groot, W. A., Strahle, W. C., Hubbartt, J. E. and Jagoda, J. I., "Heterogeneous Diffusion Flame Stabilization: Constant Density Results," accepted for presentation at the 20th JANNAF Combustion Meeting, Monterey, CA, Oct. 1983.

2) Walterick, J. E., Jagoda, J. I., Richardson, C. R. J., de Groot, W. A., Strahle, W. C., and Hubbartt, J. E., "Experiment and Computation on Two-Dimensional Turbulent Flow over a Backward Facing Step," AIAA Paper No. 84-0013, 22nd AIAA Aerospace Sciences Meeting, Reno, NV, Jan. 1984.

EXPERIMENTS AND COMPUTATION ON TWO-DIMENSIONAL TURBULENT FLOW OVER A BACKWARD FACING STEP

R. E. Walterick*, J. I. Jagoda†, C. R. J. Richardson°
W. A. De Groot**, W. C. Strahle††, and J. E. Hubbartt°°
School of Aerospace Engineering, Georgia Institute of Technology
Atlanta, Georgia

Abstract

Measurements are made of two components of velocity and shear stress on a turbulent incompressible two-dimensional flow over a backward facing step in a confining channel. A k-ε method of calculation was developed which produces good agreement with experiment for both time mean and turbulence quantities. Reattachment length is particularly well predicted. Sensitivity of this flow to geometrical details and initial conditions has been numerically investigated and found to be high; consequently comparison with other data sets is difficult. Fluctuations of the order of 2% were found in a region of the flow which should not have been vortical, and acoustic motions due to an unsteady recirculatory flow are suspected.

List of Symbols

a	coefficient in the finite difference equation
b,c	coefficients in the linearized source term
C_μ, C_1, C_2	turbulence model constants
E	empirical constant in 'law of the wall' equation
F_o	shear force at the solid boundary
G	production term in the turbulent kinetic energy equation
H	step height
k	turbulent kinetic energy
p	pressure
S_Φ	'source' term in the governing equation for 'Φ'
U	mean axial velocity
U_∞	mean freestream axial velocity at the inlet
u	turbulent fluctuating velocity in the axial direction
$\overline{u^2}$	Reynolds normal stress in the axial direction
V	mean transverse velocity
v	turbulent fluctuating velocity in the transverse direction
$\overline{v^2}$	Reynolds normal stress in the transverse direction
$\overline{uv}$	Reynolds shear stress
x,X	axial coordinate
y,Y	transverse coordinate
α	empirical constant in the velocity - pressure gradient correlation model
Γ_Φ	effective turbulent exchange coefficient for 'Φ'
ε	dissipation rate of turbulence energy
κ	von Karman constant
μ	molecular (laminar) viscosity
μ_{eff}	effective viscosity
μ_t	turbulent viscosity
ν	laminar kinematic viscosity
ρ	density
$\sigma_k, \sigma_\varepsilon$	turbulent Prandtl numbers for diffusion of k and ε
τ	shear stress
Φ	dependent variable (U,V, k,ε etc.)
δ_{ij}	Kronecker delta
δVol	elemental volume corresponding to a given cell

Subscripts

i,j	tensor notation
p	node at which calculations take place
E,N,S,W	nodes surrounding the 'p' node
t	turbulent value
$\bar{\Phi}$	values pertaining to the dependent variable 'Φ'
o	value at solid boundary
1	value at near-wall node
rms	root mean square

Introduction

Solid-fueled ramjets operate by ingestion of air and subsequent combustion with a solid fuel.[1] A low velocity region of flow near the head end of the fuel grain is imperative for flame stabilization. This may be achieved by creating a backward facing step at the flow boundary thereby forcing a recirculation zone behind the step. In practice the flow field is highly turbulent, and, even without combustion, is highly complex.

A goal at this laboratory is to be able to compute the solid-fueled ramjet flowfield to an accuracy commensurate with providing scaling laws for quantities such as the flame blowoff limit and fuel regression rate. To this end a facility is under development to simulate a solid fueled ramjet flame stabilization region. The first phase of this development has yielded the cold flow facility of Fig. 1. The first phase tests of a backward facing step in a cold flow have been completed and are the subject of this paper.

Incompressible two dimensional turbulent flow over a backward facing step has received considerable work from several investigators and a recent review article[2] summarizes this work. This flow was labeled as a standard flow with a number 0420 assigned to it in Ref. 3. Consequently, the work here adds to the data base of such flows. It should be noted that this flow is highly complex, there are discrepancies in the results of several investigators, and truly satisfactory calculability of the flow has not been demonstrated.[3] A calculation method is developed here which gives somewhat better predictability of the flow than has been heretofore demonstrated, especially with regard to reattachment length. Comparisons are given between calculations and the experimental results of several workers together with the experimental work at this laboratory.

---

* Research Engineer. Member, AIAA
† Assistant Professor. Member, AIAA
o Graduate Research Assistant
** Graduate Research Assistant
†† Regents' Professor. Associate Fellow, AIAA
°° Professor, Member, AIAA

Facility

Tunnel

The tests described in this paper were carried out ina specifically designed suction type open tunnel. In this facility, shown in Fig. 1, air is drawn in directly from the room through a bellmouth (8.5 cm radius of curvature) into a rectangular boundary layer development section, 7 cm high, 41.9 cm wide and 61.6 cm long. At the end of this section the flow passes over a 3.47 cm high backward facing step into the test section which is 43.2 cm long, 10.47 cm high and 41.9 cm wide. A ratio of step height to width of 12 was selected to eliminate possible wall effects near the axis of the test section, Ref.[2]. This section is followed by a transition section consisting of a 30 cm long constant area duct joined to a 61 cm long small angle diffuser of expansion ratio 2:1, which dumps into a large plenum chamber. The diffuser and plenum chamber are separated by a thin, fine mesh screen.

A 60 HP centrifugal blower draws the air from the other end of the plenum through a 1 cm honeycomb structure followed by a screen. The plenum chamber, honeycomb and screens serve to prevent flow disturbances created in the blower from passing back up into the test section. The exhaust from the blower is ducted through a throttling orifice to a port in an external wall of the building through which the flow is discharged.

The side walls of the test section consist of broadband anti-reflection coated, optical quality glass plates which permit optical diagnostics of the flow to be carried out. The tunnel is fitted with a row of static pressure taps in the streamwise direction, displaced 1.27 cm from the center line, for determining local static pressures as well as the axial static pressure distribution. Seven and six such ports, equally spaced, are fitted into the floor of the boundary layer development section and the constant area connecting duct, respectively. Both the ceiling and the floor of the test section are instrumented with 23 static pressure taps. The separation between these ports in the test section is 2.54 cm, except near the reattachment point of the flow, where this spacing has been halved.

Lateral rows of five static pressure taps were also incorporated into the tunnel at selected positions in the boundary layer development section, the step itself, the test section, and beyond, in order to monitor the two dimensionality of the flow. All static pressures were measured by a Scanivalue system using variable-capacitance, precision pressure transducers. The Mach number in the test section is about 0.2 and the flow was observed to be almost perfectly two dimensional. Furthermore, smoke and tufts attached to all tunnel walls were used to verify the quality of the flow.

A second row of access parts was incorporated in the test section ceiling, parallel to the static pressure parts on the opposite side of the tunnel center line, in order to permit diagnostic probes to be introduced into the flow. An actuator fitted to the top of the tunnel facilitates a remotely controlled vertical traversing of the probes, while the streamwise translation in discrete steps corresponding to the position of the probe access ports was carried out manually. The stagnation temperature of the flow was determined with a thermocouple placed just downstream of the test section.

Diagnostics

Probe measurements of velocities were carried out using single hot-films (TSI 1210-20), x-films (TSI 1243-10) of length/diameter = 20, single hot wires (TSI 1210-T 1.5) and pitot probes. Some preliminary laser Doppler velocimeter (LDV) results will also be reported here.

The hot film and x-film probes were calibrated in a uniform nonturbulent flow using 15 discrete velocities over a range from 45 to 260 ft/sec. At each velocity the probe output signal was periodically sampled, digitized and a mean output voltage determined. These mean voltages for the fifteen sampled velocities were fitted to King's law using the least square technique in order to establish the calibration coefficients. These calibrations were carried out before and after each run. In general, it was found that the discrepancy between the calibration carried out before and after three complete vertical traverses was less than 1.5%. Single and x-film measurements were carried out at each measurement station in the tunnel. The x-films were placed in the vertical plane, normal to the tunnel floor with each film at an angle of 45° to it. The single film was positioned normal to the plane of the x-films. Mean velocities in the streamwise and the vertical directions were determined from the mean voltages. The mean squares of the fluctuating components of the signal of each of the three films were used to determine the mean squares of the fluctuating components of velocity as well as the Reynolds shear stresses. All values were normalized with respect to the steady component of the streamwise velocity upstream of the step. The effects of the normal and binormal velocity components on the films were taken as equal while the effects of velocities tangential to the films were neglected.

Mean stagnation pressure distributions throughout the flow in the test section were determined using a traversable pitot probe connected to a 100 mm Hg pressure transducer. These stagnation pressures were referenced to the static pressures as determined at the tunnel ceiling for the relevant downstream locations in order to determine the mean streamwise velocity distributions.

Both hot wire and pitot probe techniques have problems in areas of high turbulence superimposed on low velocities as well as in reverse flow regions of the flow field. Hot wire probes, which generally permit the determination of mean velocities and turbulent intensities, are unable to differentiate between forward and reverse flow. This makes them unsuitable in locations where the peak velocity fluctuations exceed the mean flow velocity. Furthermore, the linearization techniques used become inaccurate at local turbulence intensities larger than about 30%. The pitot probes and pressure transducers exhibit too slow a response for turbulence intensity measurements. The probes further suffer for having to be reversed for backward flows. They are, therefore, again inaccurate in regions where the velocity fluctuations exceed the mean flow velocity.

In order to overcome these problems the position of flow reversal (the recirculation region zero velocity line) as obtained using laser Doppler velocimetry is also being reported here. The velocimeter used is a two-component system (TSI 9100-7) fitted with a 4 watt argon ion laser (Spectra Physics 165-08) and operates in the back-scatter mode using two counter type signal processors (TSI 1990 A). Bragg cell frequency shifters (TSI 9108) in one beam of each of the two beam pairs permit a detection of reverse flow. The frequency shift introduced by the Bragg cells is adjusted to local flow conditions to permit acceptance of the entire velocity related signal with maximum accuracy. Filter bandwidths are adjusted simultaneously to yield a maximum signal to noise ratio without loss in extreme velocity fluctuations. The system is mounted on an actuator which is remotely controlled in three degrees of linear translation and manually adjustable in tilt. The

digital counter outputs are analysed in the form of velocity probability density functions which permits the determination of mean velocities and turbulence intensities.

Analysis

Governing Equations

A two-equation turbulence model (k-ε) is used for the prediction and analysis of the two-dimensional, steady, turbulent flow over a backward facing step.[4,5] In this model, transport equations for the turbulent kinetic energy and its dissipation rate are employed along with the conservation equations for mass and momentum and an equation for the turbulent viscosity.

For a two-dimensional, steady, turbulent flow, the governing equations can be written in the general form[6,7]

$$\frac{\partial}{\partial x}(\rho U\Phi) + \frac{\partial}{\partial y}(\rho V\Phi) = \frac{\partial}{\partial x}\left[\Gamma_\Phi \frac{\partial \Phi}{\partial x}\right] + \frac{\partial}{\partial y}\left[\Gamma_\Phi \frac{\partial \Phi}{\partial y}\right] + S_\Phi \qquad (1)$$

where Φ represents the dependent variable (U,V,k,ε etc.) being considered (Φ = 1 for the continuity equation), Γ_Φ is the appropriate effective exchange coefficient for the turbulent flow and S_Φ is the "source" term. This model assumes isotropic diffusion with the diffusion coefficient (Γ_Φ) given as

$$\Gamma_\Phi = (\Gamma_\Phi)_{laminar} + (\Gamma_\Phi)_t$$

The definitions of Γ_Φ and S_Φ for the various dependent variables (Φ) are listed in Table 1. These definitions are similar to those given in Ref. (7) except those for the turbulent kinetic energy equation.

The turbulent kinetic energy equation for a steady flow can be written as

$$\frac{\partial}{\partial x_j}(\rho U_j k) = -\overline{\rho u_i u_j}\frac{\partial U_i}{\partial x_j} - \rho\varepsilon + \frac{\partial}{\partial x_j}\left[\Gamma_k \frac{\partial k}{\partial x_j}\right] - \overline{u_i \frac{\partial p}{\partial x_i}} \qquad (2)$$

Usually the velocity-pressure gradient correlation term, which is the last term on the right hand side of Eq. (2), is lumped into the diffusion term, the third term on the right side of Eq. (2). Based on independent work done at the Georgia Institute of Technology,[8] it was decided to include this correlation term explicitly in the turbulent kinetic energy equations. This velocity–pressure gradient correlation term is modelled as

$$\overline{u_i \frac{\partial p}{\partial x_i}} = -\frac{2}{3}\alpha\rho\,\overline{u_i u_j}\frac{\partial U_i}{\partial x_j} \qquad (3)$$

where α is an empirical constant. This correlation term is added to the source term in the turbulent kinetic energy equation (see Table 1).

The following equation for the Reynolds stresses has been used in this analysis.

$$\rho\,\overline{u_i u_j} = \frac{2}{3}\rho k\,\delta_{ij} - \mu_\varepsilon\left(\frac{\partial U_i}{\partial x_j} + \frac{\partial U_j}{\partial x_i}\right) \qquad (4)$$

Wall functions which link the flow variables at solid boundaries to those in the near-wall region are employed.

Solution Technique

A numerical code called TEACH,[6] originally developed at Imperial College, is used to solve the elliptic partial differential equations given by Eq. (1) and Table 1 along with the appropriate boundary conditions. This code was modified to include the velocity-pressure gradient correlation term and the modified version of the numerical code is referred to as TEACH-GT in the present work.

In the numerical code, the flow domain is overlaid with a rectangular grid. The grid is arranged such that the flow boundaries lie along the control volume boundaries. All the dependent variables except the velocities are calculated at the intersection points or "nodes" of the grid. The velocities are calculated at locations midway between these nodes.[6,7]

A finite difference counterpart of Eq. (1) is derived by supposing that each variable is enclosed in its own control volume or "cell" formed by the grid liner. Equation (1) is integrated (microintegration) over the control volume corresponding to each node. A hybrid differencing scheme is used. The source term is linearized as

$$\int_{Volume} S_\Phi \, dVol = b\,\Phi_p + c$$

where the subscript 'p' denotes the node at which calculations take place.

The continuity and momentum equation are combined to derive an equation which relates the changes in the pressure field to those in the mean velocity field.[7] The pressure changes obtained from this equation are used to adjust the velocity field thus satisfying the continuity equation.

The finite difference equations are assembled to yield the general equation

$$(a_p - b)\,\Phi_p = a_N\Phi_N + a_S\Phi_S + a_E\Phi_E + a_W\Phi_W + C \qquad (5)$$

where N, S, E and W denote the nodes surrounding the node 'p' and

$$a_p \equiv a_N + a_S + a_W + a_E \qquad (6)$$

These equations are solved with appropriate modifications made to account for the boundary conditions.

Boundary Conditions

The conditions at the outlet are seldom known. The practice employed here is to locate the outlet boundary in a region where the flow is strongly outwards directed and hence insensitive to downstream conditions. The upwind differencing scheme used here helps in this respect.

The variables at the solid boundaries (denoted by the subscript o) are linked to those at the first grid node near the wall (denoted by the subscript '1') by algebraic relations which are consistent with the logarithmic "law of the wall" (wall functions).[7] Use of these wall functions minimizes computer storage and run times.

Table 1. Definitions of Terms

Conserved property	Φ	Γ_Φ	S_Φ
Mass	1	0	0
x momentum	U	μ_{eff}	$\frac{\partial}{\partial x}\left[\mu_{eff}\frac{\partial U}{\partial x}\right] + \frac{\partial}{\partial y}\left[\mu_{eff}\frac{\partial V}{\partial x}\right] - \frac{\partial p}{\partial x}$
y momentum	V	μ_{eff}	$\frac{\partial}{\partial x}\left[\mu_{eff}\frac{\partial U}{\partial y}\right] + \frac{\partial}{\partial y}\left[\mu_{eff}\frac{\partial V}{\partial y}\right] - \frac{\partial p}{\partial y}$
Turbulent energy	k	$\frac{\mu_{eff}}{\sigma_k}$	$\left(1+\frac{2}{3}\alpha\right) G - \rho\varepsilon$
Dissipation rate	ε	$\frac{\mu_{eff}}{\sigma_\varepsilon}$	$\frac{\varepsilon}{k}\left(C_1 G - C_2\rho\varepsilon\right)$

where $G = -\rho\,\overline{u_i u_j}\,\frac{\partial U_i}{\partial x_j}$

$\mu_{eff} = \mu_t + \mu$

$\mu_t = C_\mu\,\rho\,\frac{k^2}{\varepsilon}$

and

C_μ	C_1	C_2	σ_k	σ	α
0.09	1.44	1.92	1.0	1.217	0.067

The wall function for the momentum equation is,

$$U_1^+ = \frac{1}{\kappa}\,\ell n(Ey_1^+) \qquad (7)$$

where

$$U_1^+ = \frac{U_1 C_\mu^{\frac{1}{4}} k_1^{\frac{1}{2}}}{(\tau/\rho)_o} \qquad (8)$$

$$Y_1^+ = \frac{Y_1 C_\mu^{\frac{1}{4}} k_1^{\frac{1}{2}}}{\nu} \qquad (9)$$

$E = 9.79$ and $\kappa = 0.4187$

The quantity k_1 is calculated from the regular balance equation for the cell corresponding to the near-wall node. While calculating k_1, an average value is assigned to the dissipation term in the turbulent kinetic energy equation which is deduced from the assumption [9]

$$\int_o^{Y_1} \varepsilon\, dy = \frac{C_\mu\, k_1^{3/2}}{\kappa}\,\ell n(Ey_1^+) \qquad (10)$$

The production term in the turbulent kinetic energy equation is approximated as

$$G \simeq \frac{\tau_o (U_1 - U_o)}{Y_1} \qquad (11)$$

The boundary condition along the solid boundary for the momentum equation is applied in the form of a shear force (F_o) given as

$$F_o = \tau_o\,\delta X_{EW} = -\frac{\rho_1 C_\mu^{\frac{1}{4}} k_{PW}^{\frac{1}{2}} (U_1 - U_o)}{U_1^+}\,\delta Vol \qquad (12)$$

where $k_{pw} = \frac{1}{2}(k_p + k_w)$ for the near wall node. The τ_o in Eq. (11) is deduced by inverting the logarithmic law of the wall given by Eq. (7). The dissipation rate at the near wall node is calculated directly from the expression.

$$\varepsilon_1 = \frac{C_\mu^{3/4} k_1^{3/2}}{\kappa y_1} \qquad (13)$$

Predictions

Grid dependency tests were carried out and a 31 x 41 grid was chosen for the analysis. A grid spacing which is expanding in the axial direction has been used. The grid spacing is constant in the transverse direction. The outlet boundary is located at a distance of twenty four stepheights from the inlet (step).

Preliminary calculations with plug flow conditions at the inlet and $\alpha = 0$ (Eq. (3)) yielded a reattachment length of 5.86 stepheights. This is lower than the experimentally observed reattachment length of 7 ± 1 stepheights.[2,10,11] The reattachment length measured at the experimental facility at Georgia Institute of Technology was 7.33 stepheights. Inclusion of the velocity-pressure gradient correlation term given by Eq. (3) improved the prediction of reattachment length. With $\alpha = 0.067$ and plug flow conditions at the inlet, the reattachment length was predicted to be 6.22 stepheights.

Inlet conditions are important in this analysis. The inlet location coincides with the stepface in this analysis. Since the calculations in the TEACH-GT code start at the grid just downstream of the stepface, it is important to have accurate inlet conditions. Specifically, the mean axial velocity profile at the inlet must be accurate. Calculations were carried out with different mean velocity profiles at the inlet. The most accurate among these profiles was the one measured at the experimental facility mentioned in the present work using hot-wire anemometry. With this profile at the inlet and $\alpha = 0.067$, the reattachment length was predicted to be 7.26 step heights which compares very well with the experimentally measured reattachment length. The computer execution time for a typical calculation was about 1200 CPU seconds on a CYBER 835 computer.

Use of Eq. (4) in the analysis implies that the normal turbulent stresses are nearly equal which is inaccurate, especially in the high turbulence regions. With this equation, the streamwise turbulence intensities are underpredicted and the transverse turbulence intensities are overpredicted. Any comparison of the turbulence intensities evaluated from Eq. (4) with experimental data must therefore be inaccurate. For this reason the following empirical relations for plane shear layers[12] were used to calculate the turbulence intensities after obtaining the converged solution using the numerical code TEACH-GT.

$$\left.\begin{aligned} \frac{\overline{u^2}}{k} - \frac{2}{3} &= 0.3 \\ \frac{\overline{v^2}}{k} - \frac{2}{3} &= -0.18 \end{aligned}\right\} \qquad (14)$$

Results

The experimental results presented here are primarily from hot-film anemometry. Some pitot probe data and preliminary laser velocimeter data are included for the purpose of comparison. In all cases the probe measurements in the vertical plane are terminated above $y/H = 2.0$ due to physical restrictions between the probes and the test facility.

Figure 2 shows the development downstream of the step of the longitudinal component of the mean velocity, the longitudinal and vertical components of the turbulence intensity and the shear stress. The freestream velocity, which nominally is 74.0 meters per second, is used to normalize the results. Pitot probe derived mean velocities are included for comparison with hot-film data at six x/H locations that bracket the shear layer mean reattachment point. The mean reattachment point is shown from the pitot data to occur at an x/H of 7.33, which is in excellent agreement with the TEACH-GT prediction of x/H = 7.26. The characteristic reverse flow in the recirculation region is seen at locations x/H = 4.4 and x/H = 5.13. Pitot data in the reverse flow of the recirculation region was obtained with the probe reversed. Pitot measurements upstream and downstream of the six presented here are available, but only those that coincide exactly with the hot-film x/H locations are shown. Note that the hot-film measurement presentation is terminated prior to entry into the recirculation region. The longitudinal turbulence intensity based on local mean velocity approaches 50 percent at the termination point. Inaccurate probe readings result beyond this point because the signal is rectified. In the freestream above the shear layer the comparison of pitot and hot-film data yields acceptable agreement; however, disagreement between the pitot and hot-film data at x/H = 7.33 and x/H = 8.06 as the test section floor is approached can be attributed to the above mentioned signal rectifying problems and truncation of the voltage-velocity relation. Finally, a freestream flow acceleration of approximately 2.5 percent is seen at x/H = 1.1 and x/H = 2.56. This fact is confirmed by pitot measurements.

Turbulence intensities are shown for x/H = 1.47 to x/H = 10.99 in the second portion of Fig. 2. For this case values of u_{rms} have been determined from single film measurements and values of v_{rms} from x-film measurements of $\left(\frac{\overline{u^2} + \overline{v^2}}{V_\infty^2}\right)$ with single film data of $\frac{\overline{u^2}}{V_\infty^2}$ subtracted to determine $\frac{\overline{v^2}}{V_\infty^2}$. Hence v_{rms} data are presented at only six x/H locations where single film and x-film measurements are coincident. Freestream turbulence intensity at the step location has been measured at 1.5 percent. This value is higher than normally found in a potential flow core. As noted in this investigation and as reported by other investigators[10] there appears to be a low frequency flow oscillation indicated by the reattachment point wandering about a mean location by $\pm$ one stepheight. This oscillation could be seen as contributing to the velocity fluctuations. In the freestream u_{rms} levels are the same, as is to be expected. Within the shear layer v_{rms} is lower than u_{rms} and shows more scatter in the data. Again measurements are not presented in the recirculation region. Finally, the characteristic broadening of the shear layer accompanied by a drop in maximum u_{rms} values as the flow proceeds downstream is evident. The lower portion of Fig. 2 presents shear stress levels in the flow. Values are essentially zero in the freestream and grow as the shear layer is entered. A maximum is reached prior to reattachment followed by a gradual broadening and drop in levels. The return to values of zero at the wall for x/H = 7.33 is expected since it is the mean reattachment point. However, proceeding downstream at the wall one would expect the levels to increase toward those typical of a turbulent boundary layer. No such increase occurs with the levels remaining at zero. However, in this region the lower mean velocities coupled with high local turbulence intensity causes the x-film results to be inaccurate.

Figure 3 provides a mapping of the extent of the recirculation region. Shown is a comparison of pitot probe

data with the preliminary laser velocimeter data and the computation of TEACH-GT of the zero velocity streamline. The pitot derived zero velocity line was determined from exptrapolation of pressure data from the pitot probe. Due to probe inaccuracies in low mean velocity, high turbulence regions (i.e. high flow angularity at the measurement point) accurate pitot data was not obtained in a band centered on the actual zero velocity point at each station measured. Hence, the exptrapolation of the data outside of this band was required. The agreement of the pitot data with the computation is quite good from x/H = 2.2 downstream to the reattachment point. As stated previously the mean reattachment point is accurately predicted for this case. The inaccurate behavior of TEACH-GT in the vicinity of the step is due to the large grid spacing in the computational scheme. The pitot data indicates an initial drop in the recirculation region height in the region from x/H = 0.0 to x/H = 2.2 followed by a plateau between x/H = 2.2 and x/H = 5.5 and a final drop until x/H = 7.33. The preliminary laser data indicates a higher recirculation region between x/H = 2.2 and x/H = 3.66 and between x/H = 6.59 and x/H = 7.33. Further testing is required to verify this trend.

The recirculation region flow details as computed by TEACH-GT are shown in Fig. 4. Each arrow indicates the velocity magnitude and direction at a point. The magnitude and direction of U_∞ is shown for reference. The vector plot indicates the existence of one large recirculation region terminating at reattachment. There is no evidence of a second smaller opposite rotation recirculation region at the step test section floor juncture as reported in some investigations.[13] This is probably due to the grid spacing being too large to pick up this small scale recirculation zone.

A more detailed comparison between several experiments and the TEACH-GT computation for local mean velocity is shown in Fig. 5 for an x/H of 7.33 (i.e. at reattachment).* The pitot data agrees well with the computation except in the freestream where TEACH-GT overpredicts by four to five percent. In this case hot film data are included that confirm the pitot measurements except in the low mean velocity, high turbulence region near the wall where the hot-film data is inaccurate. The data of Kim et al.[10] differs significantly with TEACH-GT in the shear layer with better agreement in the freestream. The data of Eaton & Johnston[2] are obtained with a pulsed wire anemometer and are in excellent agreement with the hot film results.

Profiles of u_{rms} are presented in Fig. 6 for the downstream location x/H = 7.33 (i.e., reattachment) and x/H = 10.99. At reattachment both sets of data display higher freestream values than those computed by TEACH-GT. This is a reflection of the higher overall freestream u_{rms} values first shown in the initial conditions at the step. Above y/H = 1.0 the experimental data are in close agreement and indicate a thicker shear layer than TEACH-GT, as also indicated in Fig. 5. It should be noted that the TEACH-GT computations have been modified in this case to account for anisotropic turbulence conditions.[12] Below y/H = 1.0 the data bracket the computation indicating good prediction of the maximum value and location of u_{rms}.

In the second portion of Fig. 6 (x/H = 10.99) freestream values of u_{rms} are again higher than those computed and the shear layer is thicker. The data profiles are similar except that the single film data indicate a shear layer displaced slightly further from the floor than that of Kim et al. Maximum values of u_{rms} are predicted well with just a slight discrepancy in the y/H location of the maximum. Here, TEACH-GT incorrectly shows u_{rms} values going to zero at higher y/H values than found in turbulent boundary layers. The plot has been terminated at y/H = 0.0385, the last computed point at the floor. The single film data more accurately shows the actual trend of higher levels closer to the floor.

A plot of the maximum value of $\frac{\overline{u^2}}{V_\infty 2}$ for each measurement station is shown in Fig. 7. Here again the results of TEACH-GT have been adjusted for anisotropic turbulence conditions.[12] The single film data are slightly underpredicted but the agreement is quite acceptable. Despite more scatter in the single wire data it too brackets the prediction and agrees with the single film data. All the data sets except those of Kim et al. predict a maximum of the maximum values of $\frac{u^2}{V_\infty 2}$ slightly downstream of x/H = 5.0. Kim et al. indicates maximum values nearer the reattachment point. Values computed by TEACH-GT have been eliminated in the vicinity of the step due to grid generated inaccuracies.

A similar presentation for the maximum values of $\frac{\overline{v^2}}{V_\infty 2}$ is given in Fig. 8. TEACH-GT values are again adjusted for anisotropic turbulence conditions. Agreement between experiment and theory is fair. Kim's data levels are in better agreement with the theory except that the maximum is again predicted to occur at values closer to reattachment. x-film data were not obtained upstream of x/H = 4.4 nor downstream of x/H = 8.06. Therefore, it is not known if at least the maximum point is correctly predicted by the x-film. The Bremmer et al.[14] data show large scatter and disagreement with theory.

Reynolds shear stress profiles at two different x/H locations are shown in Fig. 9, one at reattachment and one further downstream at the last x-film measurement location. Both Kim's data and the x-film data indicate a thicker shear layer at these locations than predicted by TEACH-GT. For y/H greater than about 1.0 the data are comparable but below y/H = 1.0 the x-film data are below those of Kim. At the reattachment location the data of Kim et al. show a maximum value which agrees well with that predicted by TEACH-GT. However, the y/H location of this maximum is higher than predicted. The x-film data, though lower in magnitude more nearly defines the maximum y/H location according to the theory. The stresses at reattachment as determined by TEACH-GT and the hot-film go to zero at the floor as they should. At x/H $\approx$11 TEACH-GT and Kim's data are in good agreement as to magnitudes and maximum location. The x-film data maximum location is also in agreement. As previously stated the stresses should not go to zero at the floor so rapidly for this downstream location.

Figure 10 presents the streamwise development of the maximum value of Reynolds shear stress. The TEACH-GT computation is included as well as a curve computed for $-\overline{uv}$ = 0.3 based on the work of Ref. (12). The data of Bremmer et al.[16], though sparse, are in good agreement with the unadjusted TEACH-GT computation. For x/H $\geq$ 7 levels of Kim et al. are in excellent agreement with the three-tenths turbulent kinetic energy approximation. However, the maximum value is again measured at reattachment whereas the x-film data from this experiment provides a better correspondence with the results from TEACH-GT as to location of the maximum.

---

* Note that the data from Kim et al. and Eaton and Johnston have been faired through for purposes of clarity.

In the preceeding presentation of results from several different investigations there exist discrepancies among the various data sets and the TEACH-GT computations. In an effort to determine causes for these differences it was decided to investigate the influence of two factors using results from TEACH-GT. One of these factors was the effect of varying initial conditions in longitudinal mean velocity profile and longitudinal turbulence intensity at the step (i.e., x/H = 0.0). The other was a variation of test section height to step height (see Fig. 1). The sensitivity to initial flow conditions is shown in Fig. 11 which presents u_{rms} profiles at reattachment. Looking first at the two results with a uniform velocity profile (plug flow) the effect of varying initial u_{rms} levels is negligible except in the freestream region. Even in the freestream the differences are nearly damped out. Changing to the single wire measured initial velocity profile as input together with a turbulence intensity of one percent, there is a growth of the shear layer in height and maximum values that more closely approaches the experimental single film values at reattachment. Calculations of reattachment length give x/H = 6.3 for the uniform flow case and x/H = 7.26 for the experimental case. Therefore the recirculation region has experienced an overall enlargement. Apparently any differences amongst investigations as to initial conditions would contribute to further differences throughout the flow. It should be noted that all TEACH-GT computations presented to this point use the experimentally generated velocity profile as input for initial conditions. The effect of varying the test section height to step height is the second influential factor checked and is presented in Fig. 12 with area ratio as a parameter. Again a u_{rms} profile at x/H = 7.33 is depicted. The area ratio is determined by keeping the test section height constant and varying the height of the step. Several important trends become evident First, with increasing area ratio the shear layer becomes thicker. This is a consequence of a larger pressure rise and an overall increase in the extent of the recirculation region. At an area ratio of 1.33 the computed reattachment length is 5.8 step heights and at an area ratio of 2.0 the reattachment has grown to 7.94 step heights. Secondly, along with the growth in the recirculation region there occurs a movement away from the test section floor of the maximum u_{rms} values, again a consequence of an enlarging recirculation region. Finally, after reattachment u_{rms} values typically decline rapidly so that as the reattachment length decreases the u_{rms} values at x/H = 7.33 should decrease also. Differences of area ratio between investigators is another source of discrepancies in data sets.

Discussions

The contributions of this work are to a) add to the data base of two dimensional turbulent flow over a backward facing step and b) put forth a computational method based upon k-ε technique which will adequately predict the results. By adjustment of the usual method of treatment of the velocity-pressure gradient correlation in the turbulent kinetic energy equation, it has been found possible to obtain overall good agreement with experiment. This agreement comes about in both time mean and turbulence quantities. The primary deficiency in the calculation appears to be an underprediction of the width of the shear layer.

Neglect of the parallel velocity effect on the x-film has resulted in a somewhat low measurement of the magnitude of v_{rms} and uv. This deficiency will be corrected with the future laser velocimetry measurements. However, the data are in general agreement with the body of data collected from other workers. The calculations have suggested that such comparisons must be made with care since the flow field is sensitive to initial conditions and the exact geometry.

A primary finding is that the freestream is turbulent in regions where no vorticity should be present. This can only be an unsteady low frequency potential motion set up by the unsteady, confined flow. Such unsteadiness has been reported by other workers.

Acknowledgements

This work was supported by the Air Force Office of Scientific Research under Contract No. F49620-82-C-0013.

References

1. Netzer, D. W., "Modeling Solid-Fuel Ramjet Combustion." J. Spacecraft and Rockets, 14, 762-766 (1977).

2. Eaton, J. K. and Johnston, J. P., "A Review of Research on Subsonic Turbulent Flow Reattachment," AIAA Journal, 19, 1093-1100 (1981).

3. Kline, S. J., Cantwell, B. J. and Lilley, G. M.," 1980-81 AFOSR-HTTM- Stanford Conference on Complex Turbulent Flows" Vol. 1. Stanford University, Stanford, 1981, p. 297.

4. Jones, W. P. and Launder, B. E., "The Prediction of Laminarization with a Two-Equation Model of Turbulence," International Journal of Heat Mass Transfer, 15, pp. 301-313 (1972).

5. Launder, B. E. and Spalding, D. B., Lectures in Mathematical Models of Turbulence, Academic Press, London, 1972.

6. Grosman, A. D., Khalil, E. E. and Whitelaw, J. H., "The Calculation of Two-Dimensional Turbulent Recirculating Flows," Turbulent Shear Flows I (1977), Springer-Verlag 1979, pp. 237-255.

7. Pope, S. B. and Whitelaw, J. H., "The Calculation of Near-Wake Flows," Journal of Fluid Mechanics, 73, pt. 1, pp. 9-32 (1976).

8. Strahle, W. C., "Velocity-Pressure Gradient Correlation in Reactive Turbulent Flows," Combustion Science and Technology, 32, pp. 289-305 (1983).

9. Launder, B. E. and Spalding, D. B., "The Numerical Computation of Turbulent Flows," Computer Methods in Applied Mechanics and Engineering, Vol. 3, 1974, pp. 269-289.

10. Kim, J., Kline, S. J. and Johnston, J. P., "Investigation of Separation and Reattachment of a Turbulent Boundary Layer: Flow Over A Backward Facing Step," Report MD-37, Thermosciences Division, Department of Mechanical Engineering, Stanford University, April, 1978.

11. Abbott, D. E. and Kline, S. J., "Experimental Investigation of Subsonic Turbulent Flow Over Single and Double Backward Facing Steps," Transactions of The ASME Journal of Basic Engineering, 84, pp. 317-325 (1962).

12. Launder, B. E., Reece, G. J. and Rodi, W., "Progress in the Development of a Reynolds-Stress Turbulence Closure," Journal of Fluid Mechanics, 68, pt. 3, pp. 537-566 (1975).

13. Abott, D. E. and Kline, S. J., "Experimental Investigation of Subsonic Turbulent Flow Over Single and Double Backward Facing Steps," Journal of Basic Engineering, 84, p. 317 (1962).

14. Bremmer, R., Thompson, H. D. and Stevenson, W. H., "An Experimental and Numerical Comparison of Turbulent Flow Over A Step," AFWAL-TR-80-2108, December, 1980.

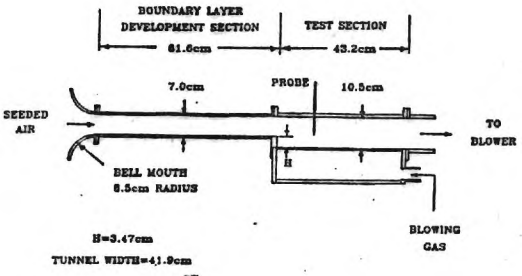

Figure 1. Test Section Details.

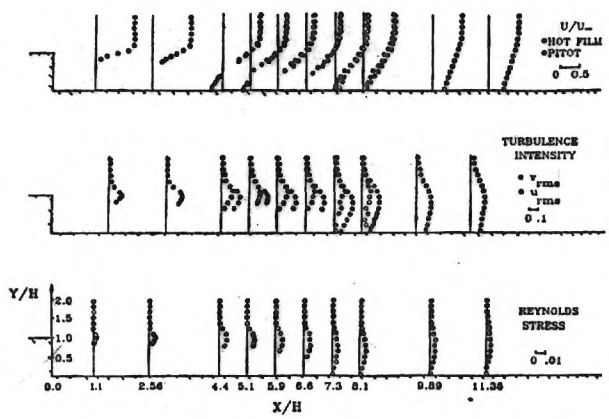

Figure 2. Mean Velocity, Turbulence Intensity and Shear Stress Profiles.

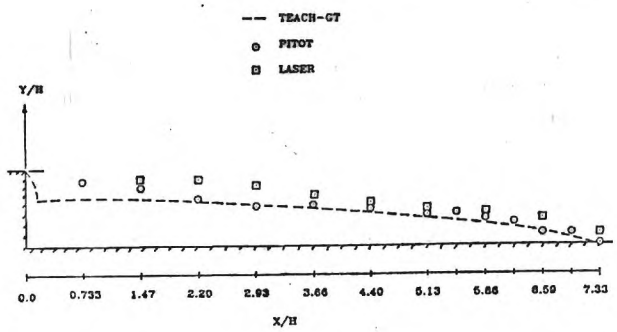

Figure 3. Recirculation Region Zero Velocity Line.

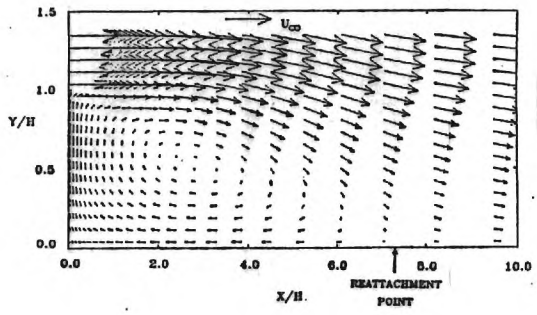

Figure 4. Recirculation Region Velocity Vector Diagram.

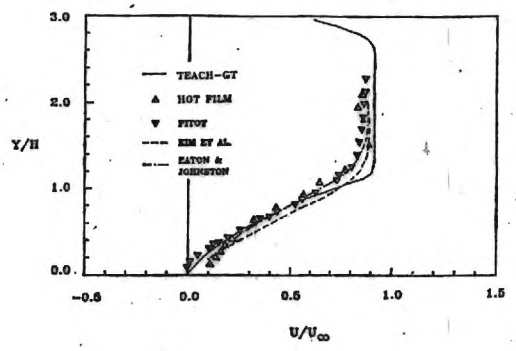

Figure 5. Comparison of Longitudinal Mean Velocity.

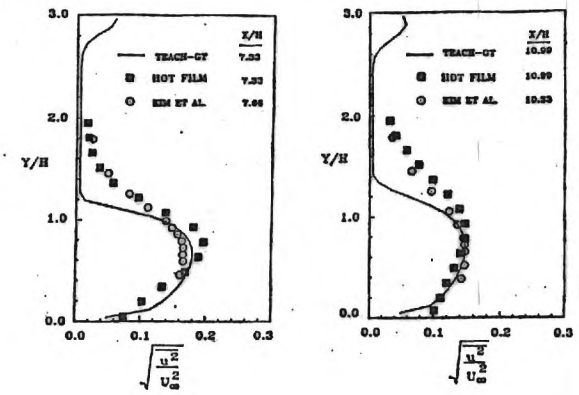

Figure 6. Comparison of Longitudinal Turbulence Intensity Profiles.

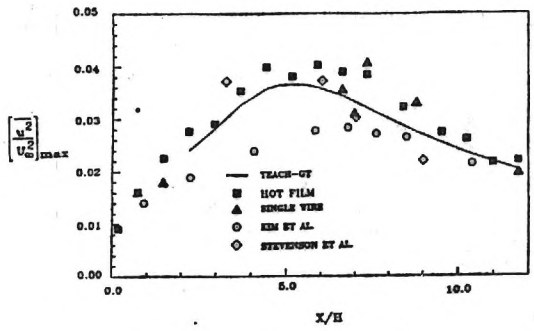

Figure 7. Maximum of Longitudinal Turbulence Intensity Squared.

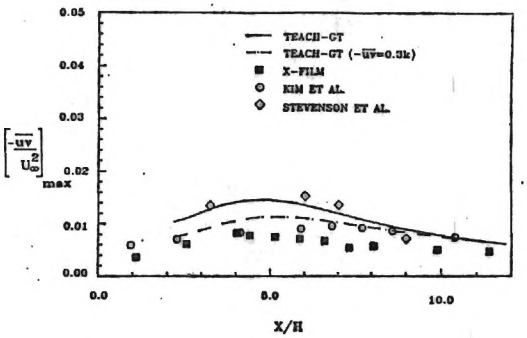

Figure 10. Maximum Reynolds Shear Stress.

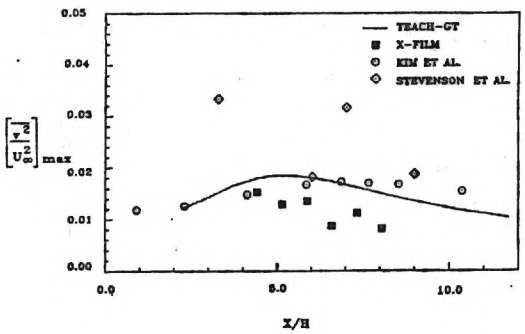

Figure 8. Maximum of Vertical Turbulence Intensity Squared.

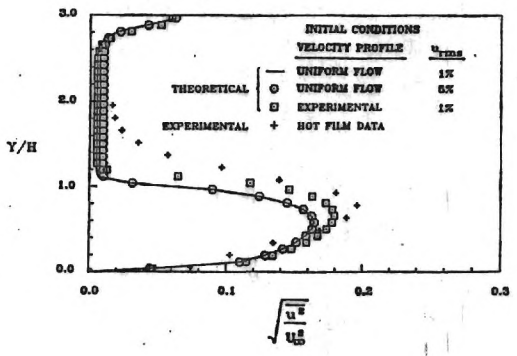

Figure 11. Sensitivity at Reattachment to Initial Flow Conditions.

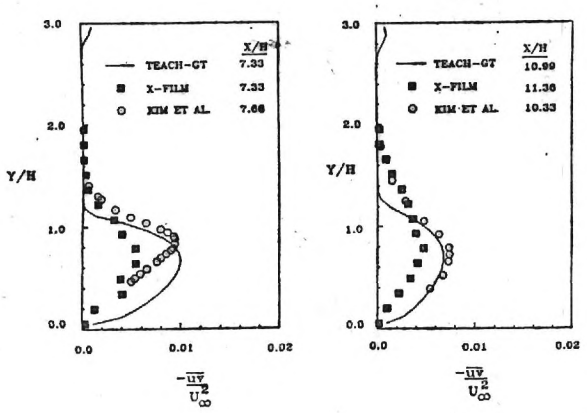

Figure 9. Comparison of Shear Stress Profiles.

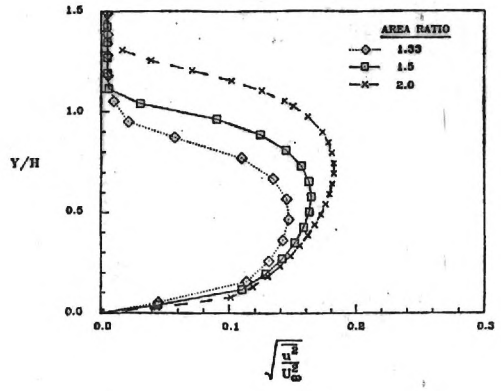

Figure 12. Sensitivity to Area Ratio.

Strahle, W. C.: Associate Editor for Combustion and Aeroacoustics, AIAA Journal

Strahle, W. C.: Organizer of ONR/AFOSR Workshop on Instability of Liquid Fueled Ramjets.

Jagoda, J. I.: Member of the AIAA Propellants and Combustion T. C.

TASK III

BEHAVIOR OF ALUMINUM IN SOLID PROPELLANT COMBUSTION

E. W. PRICE R. K. SIGMAN

A. Research Objectives

The objectives of this task are to gain understanding and improved control of combustion of the aluminum ingredient in solid propellant, and of the effect of aluminum on overall propellant combustion. In practical terms, this relates to attainment and assurance of desired burning rate, combustion efficiency, combustor stability and resistance to detonation, while striving for high propellant density and high specific impulse.

During the present year, the above objective has been extended to study of the behavior of other particulate propellant ingredients that, like aluminum, have relatively low volatility and hence tend to concentrate on the burning surface. Such ingredients include other metals, additives to modify burning rate, and additives to control combustion stability.

Specifically, the objectives for FY 1983 were: 1) to clarify the detailed behavior of aluminum in AP/HC binder/Al propellants; 2) to assemble the detailed behavior of aluminum into a systematic qualitative theory; 3) to develop an experiment for controlled perturbation of the burning surface of aluminized propellants by flow disturbances; 4) to carry out a screening study of aluminum behavior with propellants other than AP/HC/Al formulations; and 5) to start studies on other low volatility ingredients.

B. Status of Research

Detailed Behavior of Aluminum and Qualitative Theory

The primary emphasis for the year has been on consolidation of accumulated results into a qualitative theory for aluminum behavior and completing tests to evaluate critical features of the theory. Most effort has been on ammonium perchlorate-hydrocarbon binder-aluminum (AP/HC/Al) systems, with attention directed to the behavior of aluminum prior to and during detachment from the burning surface. This includes the ignition-agglomeration step.

Specific progress includes:

a) Exploration of a method for study of the response of aluminum particles during heating, using a scanning electron microscope. Single and interacting particles are located on an electrically heated element in the SEM and observed at high magnification during heating. The method holds promise for understanding (and modifying) the breakdown of the oxide skin that leads to sintering and/or coalescence of hot particles.

b) Completion of a qualitative theory for aluminum behavior in combustion of AP/HC/Al systems. This consists of a "scenario" for the complex sequence of processes that control behavior. That portion of the theory covering events on the propellant burning surface (up to and including agglomeration and ignition) is summarized in Ref. 1.

c) Because of a diversity of views regarding the conditions that precipitate ignition of accumulative aluminum on the burning surface (and because of the critical importance of ignition to overall behavior), the accumulated evidence regarding ignition was assembled into a single report (Ref. 2). As contended in the qualitative theory, ignition of agglomerate-forming aluminum is

a propagative inflamation of sintered particle arrays, precipitated locally by exposure to oxidizer-binder flamelets. This behavior cannot be described accurately without consideration of the multidimensional features of the combustion zone.

d) The qualitative theory was tested by evaluation of its predictive capability. A special series of propellants was prepared, and tendency towards aluminum agglomeration was measured in combustion plume quench tests. The test series was designed to verify a theoretically predicted transition in agglomeration behavior as a function of pressure and oxidizer particle size. Preliminary results were presented in last year's report (Ref. 3). Further quench tests and combustion photography have confirmed and extended the results, which clearly show the predicted transitions in agglomeration behavior (Fig. 1). Details are reported in Ref. 1, 4-7. It should be stressed that the experiment is a test of several aspects of the theory, including the criterion for ignition of aluminum noted above, and the requirement that this criterion be applied in terms of a multidimensional view of the combustion zone microstructure.

Experiment for Perturbation of the Burning Surface

The objective of this experiment is to learn more about the response of aluminum behavior to the gas flow environment, with particular emphasis on response of accumulation-agglomeration-ignition-detachment processes. In particular, the objective is to determine the response to transient and periodic disturbances. Such response is considered to be critical to understanding combustion instability of aluminized propellants, but has thus far received only minimal study. Our improved understanding of aluminum behavior in general should greatly facilitate interpretation of results of perturbation response tests.

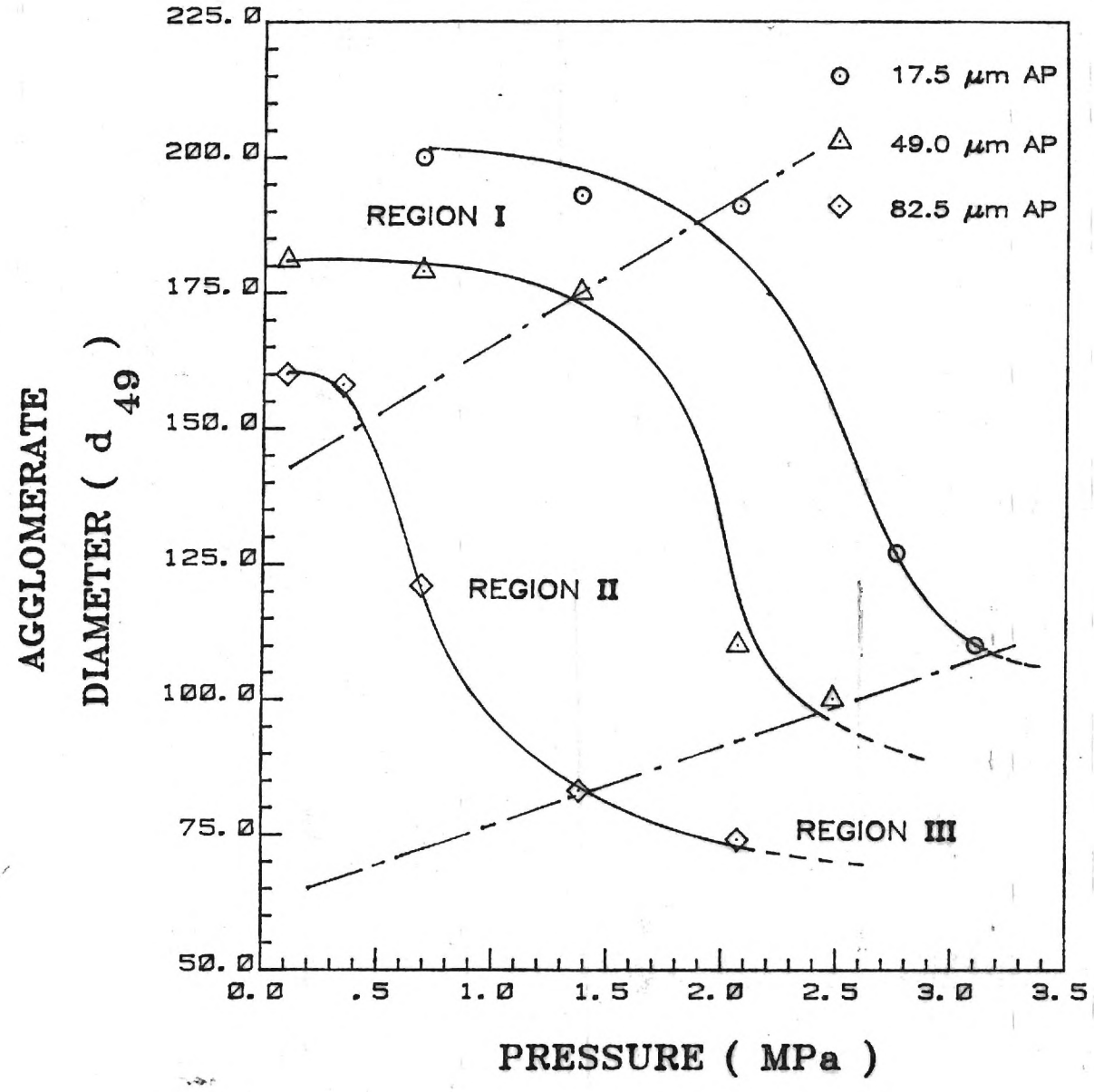

Fig. 1 Experimental verification of aluminum accumulation-ignition-agglomeration theory using propellants with bimodal oxidizer particle size and three different sizes for fine component.

Region I: Aluminum concentration continues until ignited by AP-binder flamelets of coarse oxidizer.

Region II: Transition region.

Region III: Aluminum concentration is limited by presence of AP-binder flamelets on all AP particles.

Preliminary design was made of a pulsating jet adaptation to the combustion window bomb, which would permit time-resolved observation of burning surface behavior during jet impingement. This phase of the work was not otherwise pursued during this fiscal year.

Aluminum Behavior with "Other" Propellants

Combined experience of various laboratories has shown that aluminum behavior is significantly different with propellants other than the AP/HC/Al system, and the theory clearly indicates why this should be. However, studies of other systems have been much less systematic, and some of the newer propellant systems have received almost no attention relative to aluminum behavior. In view of improved understanding of the detailed mechanisms of aluminum behavior, it is now timely to examine other propellant systems for application, extension and exploitation of the theory.

The intent expressed in the proposal for the present studies was to obtain propellant samples from ongoing programs in other laboratories and carry out screening tests by combustion photography and plume quenching. A number of efforts were made to obtain samples, but government restrictions on release and transport of samples has thus far frustrated these efforts. In view of the very small amount of propellant required, it does not seem that these difficulties should be insurmountable, but it seems likely that some initative from AFOSR will be required.

Behavior of Other Nonvolatile Ingredients

In addition to aluminum, there are a variety of other particulate ingredients used in propellants that accumulate on the burning surface without

gassification. These include burning rate modifiers such as iron, chromium and copper oxides, and instability suppressants such as zirconium carbide. The mechanisms by which these ingredients act are matters of speculation, and the search for new ballistic modifiers is largely empirical. However, the experimental methods and background of observational data now available on behavior of low volatility ingredients offer improved opportunity to clarify the combustion mechanisms that make these ingredients useful. In the present program, two studies have been started on additives, one on the combustion of ZrC particles in propellant combustion, and the other on combustion of AP/HC binder sandwiches with ballistic modifiers in the binder or oxidizer laminae.

a) Combustion of ZrC was studied by hot stage microscopy, and by combustion photography and plume quench tests on propellant samples. In the hot stage microscope, particles exhibited no change during heating to 1500°C in CO or Ar atmospheres. In an O_2 atmosphere, the particles formed a white oxide coating at about 1350°C.

Combustion photography of propellant samples with 1% ZrC showed particles burning vigorously above the burning surface. No agglomeration on the burning surface was evident, and the small particles burned very rapidly. Quench tests showed that the particles burned in a very complex fashion, with oxide accumulation on the surface and burning in fissures. This is consistent with the high melting point of ZrC and the high boiling point of ZrO_2. The presence of CO as a reaction product appears to play a role in preventing ZrO_2 from blocking diffusion of oxidizing species to the particle surface. Judging from the apparent fissure-burning, the interplay of accumulating ZrO_2, escaping CO, and inward-diffusing oxidizing species is a very complex process. At this point it is too soon to tell how ZrC might stabilize combustion, and the state of the oxide product

droplets after burnout has not yet been determined. Future tests will address this latter question, and tests will be concentrated on ZrC samples with demonstrated effect on oscillatory combustion at known frequency (so that the possible role of particulate damping by ZrO_2 can be evaluated).

b) Combustion of AP-polymer sandwiches has been pursued in great detail on a companion project, with the goal of relating observable features with the structural details of the flame complex. The results of this research provide a framework of experimental methods, observational results, and mechanistic interpretation that offer the opportunity of elucidating the mechanisms by which burning rate modifiers act in the combustion zone.

A series of quench tests were conducted on AP-PBAN sandwiches with 10% ballistic modifier (by weight) in the PBAN lamina. For those initial tests, a burning pressure of 3.45 MPa was chosen. PBAN lamina thickness was 50 μm. Ballistic modifiers were ZrC, Al_2O_3, Fe_2O_3, B_4C, $Cu_2Cr_2O_4$, CuO, Iron Blue and Ferrocene. In this series of tests, two classes of results were obtained, illustrated by the two quenched samples in Fig. 2. In part a of the figure, the sample looks very much like the ones with pure PBAN laminae. Such samples resulted with Al_2O_3, ZrC, and B_4C additives. Part b of the figure is typical of samples with $Cu_2Cr_2O_4$, Fe_2O_3, Iron Blue and Ferrocene. In all these cases the additive accumulated on the surface of the binder lamina. The burning rate was enhanced. The surface profile of the quenched sample showed characteristic changes that have been interpreted as resulting from approach of the kinetically limited leading edge of the oxidizer-binder flame closer to the surface. It seems likely that this is a result of catalytic "cracking" of large fuel vapor molecules in the filigree of accumulated additive above the binder. Concentration of catalytically active additives on the binder surface appears to be necessary to produce burning rate

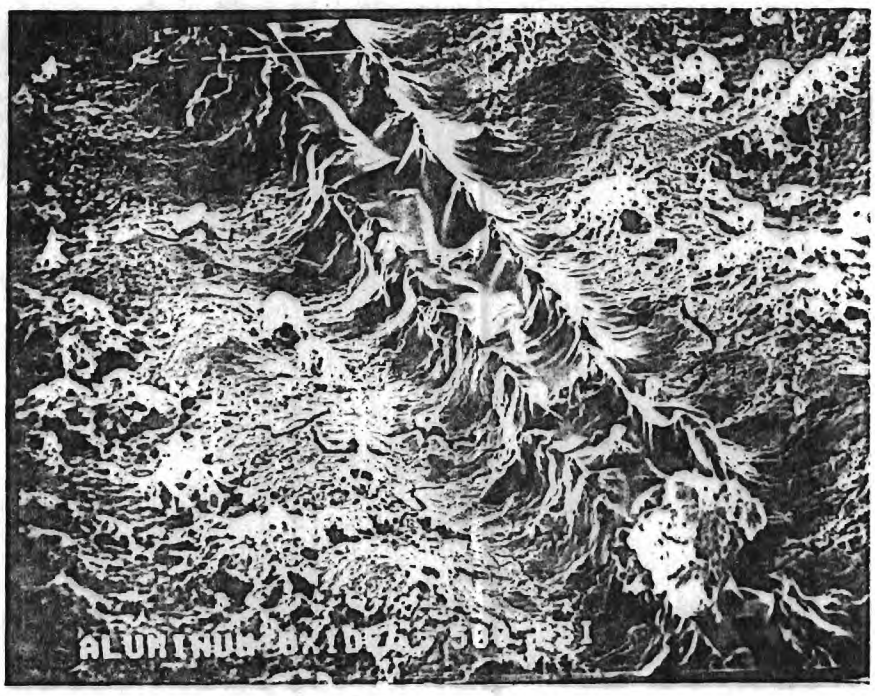

a

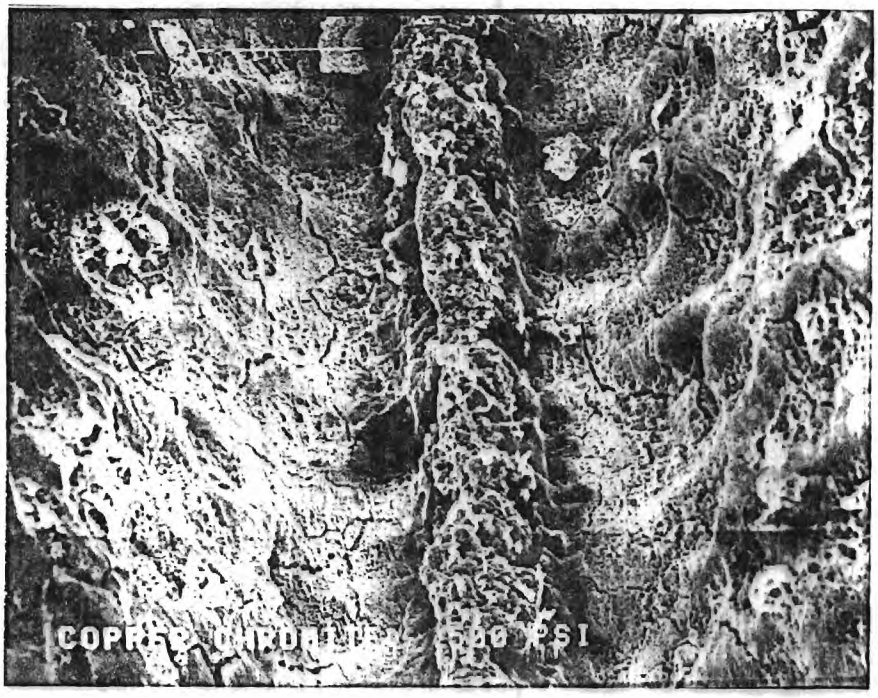

b

Fig. 2 Scanning electron microscope pictures of quenched sandwiches.
a) Example of surface with non-accumulating additive (Al_2O_3) that did not modify burning.
b) Example of surface with ballistically active, accumulating additive (Cr_2O_3) (dull appearance of surface compared to part a is due to imaging technique).

Fig. 2c Explanation of Figure 2a.

A) Area of AP self-deflagration, unaffected by AP-binder flame.
B) Burning-rate controlling regions, where AP deflagration and AP-binder flames in combination yield maximum surface heating (high rate results in a "Vee"-shaped overall surface profile as in 2b).
C) "Smooth band," where heat flow into the endothermic binder retards AP regression and AP surface decomposition is shifted to dissociative sublimation.
D) Binder lamina (recessed under these test conditions unless additive accumulates).

change. These issues will be more fully elucidated when tests are made with other binders and at other pressures.

References

1. Sambamurthi, J. K., "Behavior of Aluminum on the Burning Surface of a Solid Propellant," Ph.D. Thesis, Georgia Institute of Technology, Atlanta, GA, March 1983.
2. Price, E. W., J. K. Sambamurthi, R. K. Sigman and T. S. Sheshadri, "Conditions for Inflammation of Accumulated Aluminum in the Propellant Combustion Zone," 20th JANNAF Combustion Meeting, October 1983, to be published by CPIA.
3. Daniel, B. R., et al, "Combustion Dynamics in Rockets," Interim Scientific Report on AFOSR Contract No. F49620-82-C-0013, Georgia Institute of Technology, Atlanta, GA, November 1982.
4. Sambamurthi, J. K., " Aluminum Agglomeration in Solid Propellant Combustion," presented at AIAA 21st Aerospace Sciences Meeting, Reno, NV, January 1983, AIAA Paper No. 83-0479.
5. Price, E. W., "Behavior of Aluminum in Solid Propellant Combustion," presentation at the AFOSR/AFRPL Rocket Propulsion Research Meeting, Lancaster, CA, March 1983.
6. Sambamurthi, J. K., and E. W. Price, "Aluminum Agglomeration in Solid Propellant Combustion," accepted for publication in AIAA Journal.
7. Price, E. W., J. K. Sambamurthi, C. J. Park and R. K. Sigman, "Aluminum Agglomeration and Ignition in Propellants with Bimodal AP Size Distribution," 19th JANNAF Combustion Meeting, Chemical

Propulsion Information Agency, CPIA Pub. 366, Vol. I, October 1982, p.23.

C. Publications and Presentations

The following were published or presented during 1 October 1982 to 30 September 1983.

1. Sambamurthi, J. K., "Behavior of Aluminum on the Burning Surface of a Solid Propellant," Ph.D. Thesis, Georgia Institute of Technology, Atlanta, GA, March 1983.

2. Price, E. W., J. K. Sambamurthi, R. K. Sigman and T. S. Sheshadri, "Conditions for Inflammation of Accumulated Aluminum in the Propellant Combustion Zone," 20th JANNAF Combustion Meeting, October 1983, to be published by CPIA.

3. Daniel, B. R., et al, "Combustion Dynamics in Rockets," Interim Scientific Report on AFOSR Contract No. F49620-82-C-0013, Georgia Institute of Technology, Atlanta, GA, November 1982.

4. Sambamurthi, J. K., " Aluminum Agglomeration in Solid Propellant Combustion," presented at AIAA 21st Aerospace Sciences Meeting, Reno, NV, January 1983, AIAA Paper No. 83-0479.

5. Price, E. W., "Behavior of Aluminum in Solid Propellant Combustion," presentation at the AFOSR/AFRPL Rocket Propulsion Research Meeting, Lancaster, CA, March 1983.

6. Sambamurthi, J. K., and E. W. Price, "Aluminum Agglomeration in Solid Propellant Combustion," accepted for publication in AIAA Journal.

7. Price, E. W., J. K. Sambamurthi, C. J. Park and R. K. Sigman, "Aluminum Agglomeration and Ignition in Propellants with Bimodal AP

Size Distribution," 19th JANNAF Combustion Meeting, Chemical Propulsion Information Agency, CPIA Pub. 366, Vol. I, October 1982, p.23.

D. Personnel

Principal Investigators -- E. W. Price, Professor, and R. K. Sigman, Senior Research Engineer.

Post Doctoral Fellow -- J. K. Sambamurthi.

Graduate Research Assistant -- B. B. Lieber.

E. Professional Activities

1. Participant, 19th JANNAF Combustion Meeting, presentation of Ref. 7 above, October 1982.
2. Participant, AFOSR/AFRPL Rocket Propulsion Research Meeting, presentation of Ref. 5 above, March 1983.
3. Participant, AIAA 21st Aerospace Sciences Meeting, presentation of Ref. 4 above, January 1983.
4. Area organizer for ONR/AFOSR Workshop on Mechanics of Instability in Liquid Fueled Ramjets (organized session on Instability Phenomenon in Other Systems, and prepared and presented introductory paper), March 1983.
5. Member, AIAA National Publications Committee, Editorial Board of AIAA Educational Book Series.

TASK IV

Rocket Motor Aeroaouustics

W. C. Strahle

TASK IV

ROCKET MOTOR AEROACOUSTICS

A. Research Objective

The fundamental objective was to demonstrate that the fluctuating pressure field in a rocket motor may be calculated if the state of the turbulence of the interior flow is known.

B. Results and Discussion

The overall results of this program are documented in AIAA Paper No.84-0287 which will be presented at the 22nd Aerospace Sciences Meeting. This paper follows as a proper summary of the program.

C. Publications

Hegde, U. G. and Strahle, W. C., "Sound Generation by Turbulence in Simulated Rocket Motor Cavities," submitted to AIAA Journal.

D. Personnel

Principal Investigator: Warren C. Strahle

Graduate Research Assistant: Uday G. Hegde

E. Professional Activities/Interaction

Hegde, U. G. and Strahle, W. C., "Investigation of Turbulence Generated Pressure Fluctuations in Some Interior Flows," AIAA Paper No. 82-0175 presented at 20th AIAA Aerospace Sciences Meeting, Orlando, FL, Jan., 1982.

SOUND GENERATION BY TURBULENCE IN SIMULATED ROCKET MOTOR CAVITIES

U. G. Hegde* and W. C. Strahle**
Georgia Institute of Technology
Atlanta, Georgia 30332

Abstract

The present investigation is motivated by vibration problems in solid propellant rocket motors. A class of interior flows modelled to simulate flow conditions inside rocket motor cavities is considered. The turbulence generated pressure fluctuation consists of two components - acoustic and hydrodynamic. The Bernoulli enthalpy theory of aeroacoustics is employed to extract acoustic pressure spectra from experimentally obtained turbulence data and acoustic impedance values at flow boundaries. The effects of turbulence intensities, sidewall acoustic impedance, length to diameter ratio of the cavity and different mass flux on the acoustic pressure level are investigated in experimental configurations. Typical pressure levels inside rocket motor environments are calculated utilizing the A-B representation for propellant response.

Nomenclature

a	tube radius
A	tube cross section area, parameter in Eq. (18)
B	parameter in Eq. (18)
c	isentropic speed of sound
f	quantity defined by Eq. (5)
$F(\omega)$	frequency correction factor
g_o	Green's function for the Bernoulli enthalpy problem
g_ω	Green's function for the acoustics problem
g_T	inverse Fourier transform of $k^2 g_\omega$
h	specific enthalpy
H	Bernoulli enthalpy
H_o	cross section average of Bernoulli enthalpy fluctuations
k	wave number
k_{oo}	modified wave number
ℓ	duct length
l_{corA}	correlation length in axial direction
$\bar{M}_e$	mean Mach number at nozzle entrance plane
$\bar{M}_o$	mean Mach number at head end
$\bar{M}_r$	mean radial Mach number at propellant surface
n	index in burning rate law
p	pressure
p_H	hydrodynamic pressure fluctuation
p_Φ	acoustic pressure fluctuation
$Q(x)$	factor in Eq. (15)
r	radial coordinate, propellant burning rate
$\vec{r}$	two dimensional polar coordinate
R	defined by Eq. (20)
R_T	inverse Fourier transform of R
s	specific entropy
S_{oo}	defined by Eq. (13)
$S_{\Phi\Phi}$	acoustic pressure auto spectrum
S_{ij}	cross power spectrum between signal i and signal j
t	time
T_ω	defined by Eq. (12)
$\vec{u}$	incompressible field velocity vector
$\bar{U}_l$	mean axial velocity
$\bar{U}_{lc}$	cross section averaged axial velocity
$\vec{v}$	total velocity vector
$\vec{v}_a$	acoustic velocity vector
V	tube volume
x, x_o	axial coordinate
z	axial separation coordinate
α_s	thermal diffusivity of propellant
β	side wall/propellant specific acoustic admittance
β_{crit}	critical β for stability analysis
γ	ratio of specific heats
δ	Dirac delta function
χ	wall loss factor
Φ	acoustic potential, azimuthal coordinate in Fig. 6
Λ	defined by Eq. (18)
ρ	density, radial coordinate in Fig. 6
ρ_o	reference state density
$\bar{\rho}_g$	mean density of gaseous products from combustion
$\bar{\rho}_s$	mean density of solid propellant
λ	acoustic wavelength
λ_{oo}	modified acoustic wavelength
ζ_e	specific acoustic impedance at nozzle entrance plane
ζ_o	specific acoustic impedance at head end
ω	angular frequency
$\vec{\omega}$	vorticity vector

Superscripts

$\bar{\ }$	mean or ensemble or cross section average
$'$	fluctuation
$*$	complex conjugate
$\rightarrow$	vector quantity

Subscripts

i	quantity in i^{th} direction
ω	discrete Fourier transform

Introduction

The issue of pressure fluctuations in interior flows has attracted the attention of the propulsion community due to its relevance to vibration and instability problems in solid propellant rocket motors.[1] Under normal operating conditions these fluctuations can be of the order of 1-2% of the mean chamber pressure, and usually these fluctuations are random (Fig. 1). However, fluctuations near the acoustic resonant frequencies of the chamber may develop a nearly stationary phase relationship and aggravate the vibration problem.

---

* Graduate Research Assistant, Student Member, AIAA

** Regents' Professor, Aerospace Engineering, Associate Fellow, AIAA.

One source of pressure fluctuations inside rocket motors is the turbulence present within the chamber. Pressure fluctuations associated with the turbulent eddies arise to balance the local, unsteady acceleration. A small part of the turbulence energy can, however, escape in the form of acoustic radiation (Fig. 2). Modification of the acoustic radiation takes place due to reflections from the nozzle and at the propellant surface, and a standing wave may be set up in the chamber. The prediction of the pressure levels associated with this standing wave, given sufficient data about the turbulence field and the acoustic properties at the flow boundaries, is the objective of this paper.

The Bernoulli enthalpy approach of Yates[2] will be used. The fluctuating pressure field is specified by two scalar fields - the Bernoulli enthalpy and the acoustic potential. The resulting equations resemble the formalism proposed by Ribner[3] who distinguished between the fluctuating pressure field (labelled pseudosound) associated with the incompressible motion of eddies and the pressure field (acoustic) associated with the compressible motion of the fluid. Investigation of the acoustic field in cold flow simulations of rocket motors will be described here.

Analysis

The configurations of Figs. 3 and 4 are considered. Figure 3(a) depicts a pipe flow terminated by a choked nozzle and Fig. 3(b) shows a simulation of a rocket cavity by means of a porous tube with the entire mass injected from the side walls. Two other versions of the porous tube are shown in Fig. 4. Figure 4(a) shows a modified version of the porous tube that has acoustically stiffer walls due to sections of the tube being taped. Figure 4(b) shows a shortened version of the porous tube. The majority of the pipe (Fig. 3(a)) is filled with fully developed turbulent flow. The pressure drop across the walls of the porous tube is, on the average, about 4500 N/m^2 and is much lower than the pressure drop across the nozzles under choked conditions. This ensures that the net mass flux through the nozzle is determined purely by its area ratio. In all the cases considered the exit Mach number was about 0.1. A version of the shortened porous tube having an average exit Mach number of 0.07 was also investigated.

Due to the low Mach numbers considered, the primary flow in the configurations may be taken to be incompressible. Following Yates[2], the fluid velocity is split into two components, one associated with the incompressible field and the other being the acoustic velocity.

$$\vec{v} = \vec{u} + \vec{v}_a \quad , \quad \nabla\cdot\vec{u} = 0 \qquad (1)$$

$$\vec{v}_a = \nabla\Phi \quad , \quad \vec{\omega} = \nabla \times \vec{u}$$

The governing equations are

$$\frac{1}{c^2}\frac{D^2\Phi}{Dt^2} - \nabla^2\Phi = \frac{1}{c^2}\frac{DH}{Dt} \qquad (2)$$

$$\nabla H = -\frac{D\vec{u}}{Dt} \qquad (3)$$

where the Bernoulli enthalpy, H, is given by

$$H = h + \frac{D\Phi}{Dt} + \frac{|\nabla\Phi|^2}{2}$$

and the operator

$$\frac{D}{Dt} = \frac{\partial}{\partial t} + \vec{u}\cdot\nabla$$

is the substantial derivative following the non acoustic motion of the fluid.

Entropy variations have been neglected because it is the larger energy containing eddies that are responsible for sound generation and these are inviscid to a good approximation. Acoustic velocities have been neglected compared to the velocities associated with the incompressible field. Magnitude estimates show this to be an excellent approximation. Moreover, Eq. (2) has been linearized with respect to the acoustic potential Φ.

Fluctuations in the pressure field are obtained from the isentropic equation of state

$$dh = \frac{dp}{\rho}$$

In terms of H and Φ, this becomes

$$p' = \rho_o\left(H' - \frac{\partial\Phi}{\partial t}\right)$$

where under the linear approximation the density is replaced by the reference state density ρ_o. The pressure fluctuation therefore consists of two parts, one being associated with the unsteady, compressible motion of the fluid, and therefore the acoustic pressure

$$p_\Phi = -\rho_o\frac{\partial\Phi}{\partial t} \qquad (4)$$

The other is associated with H and the incompressible motion, and hence is the hydrodynamic pressure fluctuation

$$p_H = \rho_o H'$$

It will be the acoustic pressure p_Φ that is of interest in the following development.

The nonhomogeneous wave equation, Eq. (2), is to be solved. This requires a knowledge of the H field. The solution for H is obtained by taking the divergence of Eq. (3) and solving the resultant Poisson's equation

$$\nabla^2 H = -\frac{\partial^2 u_i u_j}{\partial x_i \partial x_j} = -f(x_i,t) \qquad (5)$$

The boundary condition $\nabla H\cdot\vec{n}$ is specified from Eq. (3) at the head end, the side walls and the nozzle entrance plane.

Only plane wave acoustic motion will be considered since it is readily shown that the turbulence energy is negligible at transverse mode frequencies. Thus, the cross section average of Eq. (2) representing plane wave motion is investigated with H being replaced by its cross section

averaged fluctuation H_o on the right hand side of Eq. (2). The solution for H_o may be written in terms of the Green's function g_o for the equation

$$\frac{d^2 g_o}{dx^2} = -\frac{1}{A}\,\delta(x - x_o)$$

with $g_o = 0$ at the head end

and $\frac{dg_o}{dx} = 0$ at the nozzle entrance plane

The solution is

$$g_o(x,x_o) = \frac{x_o}{A} \qquad x \geq x_o$$
$$= \frac{x}{A} \qquad x \leq x_o$$

and H_o is given in terms of g_o by

$$H_o = \int_{V_o} g_o\, f'(x_{oi},t)\, dV_o + \int_{A_{surface}} g_o (\nabla H \cdot \vec{n})'\, dA_o \qquad (6)$$

Simplification of Eq. (6) is facilitated by noting that $\nabla \cdot \vec{u} = 0$, and that turbulent velocity fluctuations vanish at the entrance plane and on the side walls in all the configurations. For the pipe flow, the inlet flow is a potential flow and all velocities vanish on the walls. For the porous tube flows, there is no flow in at the head end and the low Reynolds number of the flow through the pores of the tube (pore velocity and pore diameter are of the order of 1m/sec and 10^{-6}m) indicates that turbulent velocity fluctuations are absent at the tube walls. The solution for H_o may then be expressed as

$$H_o(x) = -\frac{1}{A}\int (u_1^2)'\, dA \qquad (7)$$

where the integral is over the local cross section area.

Velocity fluctuations in the experimental configurations are an order of magnitude below the mean velocity. This enables the linearization of Eq. (7)

$$H_o(x) = -\frac{2}{A}\int \bar{U}_1\, u_1'\, dA$$

Now $\bar{U}_1 = \bar{U}_{1c} + (\bar{U}_1 - \bar{U}_{1c})$ where $\bar{U}_{1c}$ is constant over the cross section. Substituting into Eq. (7), the term $\int \bar{U}_{1c}\, u_1'\, dA = \bar{U}_{1c}\int \nabla \cdot \vec{u}'\, dV = 0$ because $\nabla \cdot \vec{u}' = 0$. Hence,

$$H_o(x) = -\frac{2}{A}\int (\bar{U}_1 - \bar{U}_{1c})\, u_1'\, dA \qquad (8)$$

The acoustic field is obtained from Eq. (2). As mentioned previously, H is replaced by H_o on the right hand side of Eq. (2). A further simplification occurs by noting that the axial length scale of H_o is that of g_o and is ℓ, the length of the duct, while its time scale is $a/\bar{U}_1$ where a, the duct radius, is a typical vortical length scale[4]. Accordingly, the partial time derivative of H_o dominates the convective acceleration term in DH_o/Dt for large ℓ/a as in the cases under consideration. Therefore DH_o/Dt is approximated by simply $\partial H_o/\partial t$. Then, for low Mach numbers, the cross section averaged Fourier transform of Eq. (2) becomes

$$\frac{d^2\bar{\Phi}_\omega}{dx^2} + k_{oo}^2\,\bar{\Phi}_\omega = \frac{i\omega}{c^2} H_{o\omega} \qquad (9)$$

where the modified wave numbers k_{oo} is given by

$$k_{oo}^2 = k^2 - i\,\frac{2k\beta}{a}$$

and may be approximated by

$$k_{oo} = k - i\pi\chi$$

with $k = \omega/c$

The boundary conditions on $\bar{\Phi}_\omega$ are[5]

$$\frac{d\bar{\Phi}_\omega}{dx} + \frac{ik}{\zeta_o + \bar{M}_o}\,\bar{\Phi}_\omega = 0 \quad \text{at} \quad x = 0$$

$$\frac{d\bar{\Phi}_\omega}{dx} + \frac{ik}{\zeta_e + \bar{M}_e}\,\bar{\Phi}_\omega = 0 \quad \text{at} \quad x = \ell$$

The solution is obtained by using the Green's function g_ω satisfying

$$\frac{d^2 g_\omega}{dx^2} + k_{oo}^2\, g_\omega = -\delta(x - x_o)$$

which has the same boundary conditions as $\bar{\Phi}_\omega$. The function g_ω is obtained by standard methods. For example, for the porous tube cases which have $\bar{M}_o = 0$, g_ω at the head end (x = 0) is given by,

$$g_\omega(o,x_o) = -\left[k_{oo}\cos k_{oo}(\ell - x_o) + \frac{ik}{\zeta_e + \bar{M}_e}\sin k_{oo}(\ell - x_o)\right] \Bigg/$$
$$\left\{k_{oo}\left[\left(k_{oo} - \frac{k^2}{\zeta_o k_{oo}(\zeta_e + \bar{M}_e)}\right)\sin k_{oo}\ell\right.\right.$$
$$\left.\left. - ik\left(\frac{\zeta_o - \zeta_e - \bar{M}_e}{(\zeta_e + \bar{M}_e)\zeta_o}\right)\cos k_{oo}\ell\right]\right\} \qquad (10)$$

The acoustic potential $\bar{\Phi}_\omega$ is then given by

$$\bar{\Phi}_\omega(x) = -\frac{2i\omega}{Ac^2}\int_{V_o} (\bar{U}_1 - \bar{U}_{1c})\, u_{1\omega}\, g_\omega(x,x_o)\, dV_o$$

and the acoustic pressure transform by

$$P_{\Phi\omega}(x) = -\frac{2\rho_o k^2}{A} \int_{V_o} (\bar{U}_1 - \bar{U}_{1c})\, u_{1\omega}\, g_\omega\,(x,x_o)\, dV_o \qquad (11)$$

The autospectrum, $S_{\Phi\Phi}$, of the acoustic pressure is obtained by multiplying $P_{\Phi\omega}$ by its complex conjugate and taking an ensemble average

$$S_{\Phi\Phi}(x) = \frac{\rho_o 2k4}{A^2} \times \iint_{V_1 V_2} g_\omega^*(x,x_1)\, g_\omega(x,x_2)\, \overline{T_\omega^*(\vec{x}_1) T_\omega(\vec{x}_2)}\, dV_1 dV_2$$

where

$$T_\omega(\vec{x}) = 2(\bar{U}_1 - \bar{U}_{1c})\, u_{1\omega}(\vec{x}) \qquad (12)$$

To estimate $S_{\Phi\Phi}$, the axial correlation length is introduced

$$l_{corA} = \frac{1}{S_{11}} \int_{-\infty}^{+\infty} S_{12}\, dz$$

where S_{11} is the autospectrum of T_ω and S_{12} is given by

$$S_{12} = \text{Real } \overline{T_\omega^*(x_o,\vec{r})\, T_\omega(x_o+z,\vec{r})}$$

and is the real part of the cross spectrum of T_ω with respect to axial separation z. Typical values of $l_{cor\,A}$ at the half radius, obtained experimentally, are plotted in Fig. 5.

The Green's function g_ω has a length scale of λ, the acoustic wavelength. For frequencies under consideration, $\lambda \gg l_{cor\,A}$ so that g_ω varies slowly over the distance scale where the axial correlation of T_ω falls to zero. Introducing

$$S_{oo}(x) = \left(\frac{\rho_o}{A}\right)^2 \int dA(\vec{r}_1) \int dA(\vec{r}_2)\, \overline{T_\omega^*(x,\vec{r}_1)\, T_\omega(x,\vec{r}_2)} \qquad (13)$$

the expression for $S_{\Phi\Phi}$ is approximated by

$$S_{\Phi\Phi}(x) \simeq k^4 \left[\int_o^{\ell} S_{oo}(x_o)\, |\, g_\omega(x,x_o)\,|^2\, dx_o\right] l_{corA} \qquad (14)$$

For purposes of estimation, it is assumed that

$$S_{oo}(x) = S_{oo}(\ell)\, Q(x)\, F(\omega) \qquad (15)$$

For pipe flow, since the majority of the pipe is filled with fully developed turbulent flow both Q(x) and F(ω) are taken to be unity. For the porous tube cases, Q (x) is taken to be a second degree polynomial and is constructed by noting that $S_{oo}(0) = 0$, $\left.\frac{dS_{oo}}{dx_o}\right]_{x=0} = 0$ and that $Q(\ell) = 1$. The frequency correction F(ω) that has been used here is obtained by considering the autospectrum, S_{11}, of the fluctuating axial velocity at several axial stations at half radius,

$$F(\omega) = \frac{\frac{1}{n}\sum_{i=1}^{n} S_{11}(x_i)}{S_{11}(\ell)}, \quad x_N = \ell$$

Typically, n = 2 or 3 has been used with the autospectra being measured near the head end and at half the length of the tube.

Finally, $S_{oo}(\ell)$ has to be estimated. Using the coordinate system of Fig. 6, and following Ref. 6, the approximation is used

$$S_{oo}(\ell) \approx \frac{2\rho_o^2 \pi}{A} \left[\int_o^{a/2} S_{12})_{\Phi=\pi/2}\, \rho d\rho + \int_o^{3a2} S_{12})_{\Phi=3\pi/2}\, \rho d\rho\right] \qquad (16)$$

where

$$S_{12} = \text{Real } T_\omega^*(\ell, a/2, o) \cdot T_\omega(\ell,\rho,o)$$

This requires fixing an anemometer at half the radius and carrying out a traverse of another anemometer along the diameter defined by the reference probe and the tube center (Fig. 6).

Experimental

The pipe in Fig. 3(a) is 6m. long and 5 cm. in diameter. The tubes in Figs. 3(b) and 4 are constructed of porous sleeves made of sintered steel and are also 5 cm. in diameter. The setups are instrumented with flush mounted microphones and hot film anemometers. The wall microphones are used to measure wall pressure spectra and cross spectra. The hot films are used to obtain necessary axial velocity correlations.

Wall pressure spectra and cross spectra associated with the modified porous tubes are shown in Fig. 7. At the head end, where there is no turbulence, the spectrum shows peaks at the resonant acoustic frequencies of the tube. In the nozzle end spectrum, the acoustic peaks are lost in the broadband background level. The head to nozzle end cross spectrum reveals only the acoustic part. A comparison of the head end spectrum with the head to nozzle end cross spectrum shows both to be of the same level. This strengthens the belief that the head end spectrum is mainly acoustic whereas the nozzle end spectrum is dominated by flow noise (pseudo sound) which is local in nature[7]. Investigations of flow noise for the case of fully developed turbulent pipe flow are reported in Ref. 7.

The real part of the axial velocity cross spectra at the nozzle entrance plane at a frequency of 100 Hz referred to a point at half radius is plotted in Fig. 8 for the pipe and porous tube configurations having an average Mach number of 0.1 at the nozzle entrance plane. The value for zero separation corresponds to the autospectrum at 100 Hz. Clearly, turbulence levels in the porous tube configurations are higher as compared to those in the pipe. Also, the turbulence levels are highest for the modified porous tube configuration.

Acoustic impedance measurements were carried out using the classical impedance tube technique. Figure 9 shows the measured impedance at the bellmouth inlet for the pipe and its side wall loss factor. Figure 10 plots the wall loss factor for the porous tube configurations (M_e =

0.1). The wall loss factors for the porous tubes are an order of magnitude higher than those for the pipe indicating that the side walls of the tube act as acoustic dampers. Among the porous tube configurations, the loss factor for the modified porous tube is lowest since those sections of the tube that were taped tended to acoustically stiffen the side walls. It should be noted that it is the quantity $\pi\chi$ that has been plotted in the figures.

The specific acoustic impedance, ζ_e, at the nozzle entrance plane was theoretically obtained using the short nozzle approximation. The expression for ζ_e for low Mach numbers is

$$\zeta_e = \frac{2}{\bar{M}_e(\gamma-1)} \qquad (17)$$

Comparisons of the predicted acoustic spectra with wall measured pressure spectra are shown in Fig. 11 through Fig. 15. For the pipe flow, the comparison is at the nozzle end where the wall measured spectrum contains both hydrodynamic and acoustic components. However, the resonant peaks are clear and definite and a valid comparison can be made. For the porous tube cases, the comparison is at the head end where the wall measured spectrum is mainly acoustic.

It is seen in all cases the resonant frequencies are well predicted and the magnitude of the spectra is predicted to within a factor of three. Since only limited turbulence data was used in the prediction this factor is acceptable. The most serious discrepancy is with regard to the relative magnitude of the first mode as compared to the other modes for the porous tube cases. The experimental spectra show the level at the first mode to be much higher than the levels at the other modes. The predicted spectra for the porous tubes does not show this behavior to the degree present in the experimental spectra. Two reasons for this discrepancy may be advanced. First, by using the impedance tube technique, wall loss factors can be measured only near to and above the second natural frequency. Values at lower frequencies were obtained by linear extrapolation and may have been in error to some extent. Secondly, the frequency correction factor $F(\omega)$ may not be sufficient. In particular, a better estimate of $S_{oo}(\ell)$ may be obtained by measuring cross spectra of velocity fluctuations with respect to radial separation for more than one representative point. In other words, the limited amount of turbulence data used could also be responsible for the discrepancy. Considering the fact, however, that it is certainly not feasible to map the entire turbulence field in the setups, the predicted spectra are in good agreement, overall, with the measured spectra.

An understanding of the effects of different aspects of the flow configuration on the acoustic pressure level may be obtained from the spectra in the porous tubes. From Fig. 8 and Fig. 10, it is clear that turbulence intensities are higher and wall loss factors lower for the modified porous tube as compared to the basic porous tube. This is reflected in the higher pressure levels in the modified porous tube. Considering the basic and the shortened porous tube, both have approximately the same wall loss factors (Fig. 10), but at the common resonant modes, the levels in the shortened porous tube are higher (Fig. 12 and Fig. 14). When the side walls tend to damp the acoustic motion, a lower ℓ/d ratio results in higher pressure levels. When the side walls drive the acoustic motion, as is generally true in rocket motors, the effect is reversed. As far as exit Mach number is concerned higher pressure levels are associated with higher exit Mach numbers (see Figs. 14 and 15). The velocity terms in Eq. (11) provide a M^2 scaling for the pressure fluctuation while the denominator of the Green's function, g_w, contains ζ_e which varies inversely as the Mach number (Eq. (17)). The net effect, then, is a scaling of the pressure fluctuation with the exit Mach number $\bar{M}_e$ and therefore of the pressure level with $\bar{M}_e^2$. This scaling is also evident in both the measured and predicted spectra for the two versions of the shortened porous tube.

Application to Rocket Motors

The present theory may be extended to center perforated rocket motors by identifying β, the side wall specific acoustic admittance with the propellant admittance. The propellant admittance has been modelled here by the A-B representation of propellant response[8]. For simplicity, it is assumed that fluctuations at the burning surface of the propellant are isentropic. Then, in terms of the A-B model

$$\beta = -\bar{M}_r\left[\frac{\gamma n\, AB}{\Lambda + (A/\Lambda) - (1+A) + AB} - 1\right] \qquad (18)$$

where

$$\Lambda = \frac{1}{2} + \left[\frac{1}{4} + \frac{i\alpha_s\omega}{r^2}\right]^{1/2}$$

and r is the burning rate of the solid propellant.

The criterion for linear instability of a rocket motor is obtained by setting the denominater of the Green's function, g_w, to zero. For small $\bar{M}_e$, terms of the order of $\bar{M}_e^2$ and higher may be neglected. Then, using Eqns. (10) and (17) the criterion for instability becomes,

$$k_{oo}\sin k_{oo}\ell - \frac{ik(\gamma-1)\bar{M}_e}{2}\cos k_{oo}\ell = 0 \qquad (19)$$

The effect of β is felt through the modified wave number k_{oo} according to Eq. (9).

For a given rocket geometry and exit Mach number the value of β, denoted by β_{crit}, may be obtained that makes the rocket unstable. It is then possible to specify the parameters A and B that yield β_{crit}, given the thermal diffusivity of the propellant and the burning rate law. An example of the stability curve in terms of the parameters A and B is shown in Fig. 16. The calculation assumes the following values

$$\ell/a = 30,\quad n = 0.65,\quad r = 1\text{cm/sec},\ \gamma = 1.2,$$

$$\bar{M}_e = 0.2,\ \frac{\alpha_s}{ca} = 7.2\times10^{-7} \text{ and } \bar{\rho}_s/\bar{\rho}_g = 150$$

As the parameters A and B are varied in a suitable manner (e.g., in the direction of the arrow in Fig. 16), the propellant becomes more driving and the acoustic pressure level in the chamber increases. Typical variations in the pressure level may be estimated by scaling the turbulence quantites obtained experimentally.

The scaling is done by assuming that $A^2 S_{oo}(x)$ varies as $\rho_o^2 \bar{U}_{1c}^4$ and evaluating the density ρ_o in terms of the mean pressure and temperature in the rocket chamber

via the perfect gas equation. Further, it is assumed that l_{corA}/a remains constant.

A sample calculation is shown in Fig. 17. The mean pressure and temperature inside the rocket motor were taken as $13.8 \times 10^6 N/m^2$ and $2500^\circ K$. The radius of the motor was taken as 0.05 m. Turbulence levels were scaled from the shortened porous tube ($\bar{M}_e = 0.1$) configuration. The rocket motor was assumed to have $\bar{M}_e = 0.2$ and $\ell/a = 30$. It is seen that the pressure level becomes significant only very near to a stability limit. Away from the stability limit the rise in pressure level is not steep but gradual as the propellant becomes more driving. But very near to the stability limit there is a steep increase in the pressure level.

Another interesting result is obtained by considering the nature of the Green's function g_ω. The acoustic pressure transform (Eq. (11)), under the assumption leading to Eq. (14), may be approximated as

$$p_{\hat{Q}_\omega} \approx - \frac{2\rho_o \, l_{corA}}{A} \sum_{n=0}^{N} k^2 g_\omega(x,x_n) \, R(\omega,x_n)$$

where $x_n = n \, l_{corA}$, $x_N \approx \ell$ and

$$R(\omega,x_n) = \int_{A_{(x_n)}} (\bar{U}_1 - \bar{U}_{1c}) \, u_{1\omega} \, dA \qquad (20)$$

The inverse Fourier transform of Eq. (20) is

$$p_{\hat{Q}}(x\ t) \approx - \frac{2\rho_o \, l_{corA}}{A} \sum_{n=0}^{N} g_T * R_T \, . \qquad (21)$$

where the * symbol denotes the convolution operation.

As a simple exercise one term of Eq. (21) corresponding to $x = 0$ and $x_N = \ell$ was chosen. The function $g_\omega(0,\ell)$ for a 0.5% pressure level (Fig. 17) was calculated as a function of frequency. The signal from a white noise generator simulated R_T. The inverse Fourier transform of $k^2 g_\omega(0,\ell)$ was convoluted with a sample R_T over a time of 0.25 seconds. The result is shown in Fig. 18. The signal R_T is the source strength for the pressure fluctuations and is a random signal. But when it is operated upon by g_T a periodic signal of nearly constant amplitude results. This occurs because g_T acts like a bandpass filter such that signals at or near the resonant frequencies of the motor are passed unhindered whereas fluctuations at other frequencies are suppressed. In this numerical experiment, the amplitude of the resulting signal will depend upon the content of the white noise sample chosen. For an actual rocket motor, the pressure fluctuation according to Eq. (21) is given by a sum of convolutions which will depend on the frequency content of the turbulence over the entire volume of the rocket chamber. For statistically stationary turbulence, the net frequency content of the turbulence over the entire chamber should not vary appreciably with time. Hence, in this case also the pressure fluctuation will be nearly periodic and of nearly constant amplitude.

Conclusion

The generation of sound by turbulence in simulated rocket motor interior flows has been investigated analytically and experimentally. The entire volume of turbulence within the motor cavity is responsible for the generation of acoustic pressure fluctuations. However, it is possible to estimate the pressure spectra from limited data on the turbulence field and from knowledge of the acoustic impedance at flow boundaries. Higher turbulence levels increase the pressure level. If the energy in the turbulence spectrum is high in frequency bands containing resonant frequencies of the motor, the problem may become severe. Increase in pressure level with increase in propellant driving characteristics is very gradual away from a stability limit. Significant pressure levels are generated only extremely close to a stability limit where for all practical purposes the motor may be deemed unstable. However, an interesting result is that while the driving turbulence is band limited noise the resulting pressure oscillation is nearly periodic in character.

Acknowledgements

This work was supported by the Air Force Office of Scientific Research under Contract No. F49620-78-C-0003.

References

1. Derr, R. L., Mathes, H. B. and Crump, J. E., "Application of Combustion Instability Research to Solid Propellant Rocket Motor Problems", AGARD Conference Proceedings No. 259, April 1979.

2. Yates, J. E., "Application of the Bernoulli Enthalpy Concept to the Study of Vortex Noise and Jet Impingement Noise," NASA CR 2987, April 1978.

3. Ribner, H. S., "The Generation of Sound by Turbulent Jets," Advances in Applied Mechanics (Editors: H. L. Dryden and Th. von Karman), Academic Press, New York, 1964, pp. 103-182.

4. Laufer, J., "The Structure of Turbulence in Fully Developed Pipe Flow," NACA Tech. Report, No. 1174, 1954.

5. Hegde, U. G., "Turbulence Generated Pressure Fluctuations in a Class of Interior Flows," Ph.D. Thesis, Georgia Institute of Technology, 1983.

6. Strahle, W. C. and Neale, D. H., "Turbulence Generated Pressure Fluctuations in a Rocket-Like Cavity," AIAA Journal, Vol. 19, 1981, pp. 360-365.

7. Komerath, N. M., Hegde, U. G. and Strahle, W. C., "Turbulent Static Pressure Fluctuations Away from Flow Boundaries," Paper No. 83-0754, AIAA 8th Aeroacoustics Conference, April 1983.

8. Culick, F. E. C., "A Review of Calculations for Unsteady Burning of a Solid Propellant," AIAA Journal, Vol. 6, 1968, p. 2241.

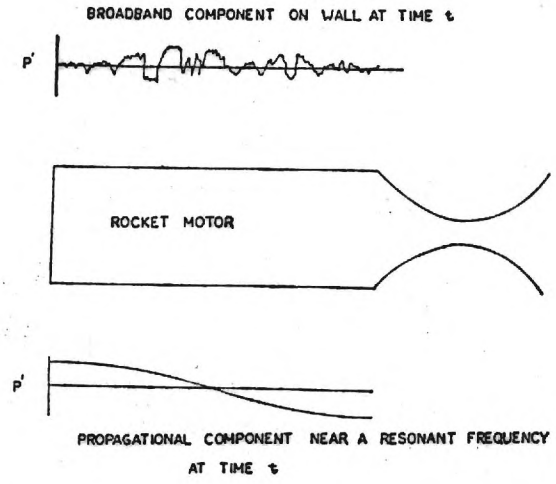

Figure 1. Fluctuating pressure components inside a rocket motor.

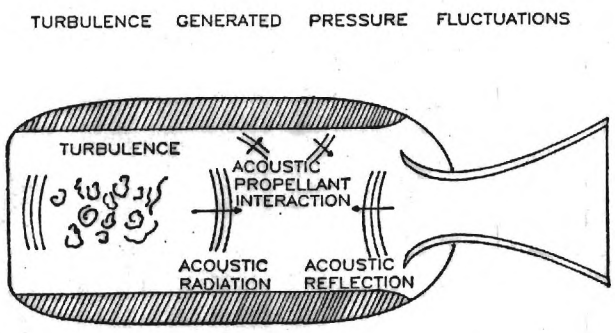

Figure 2. Turbulence generated pressure fluctuations.

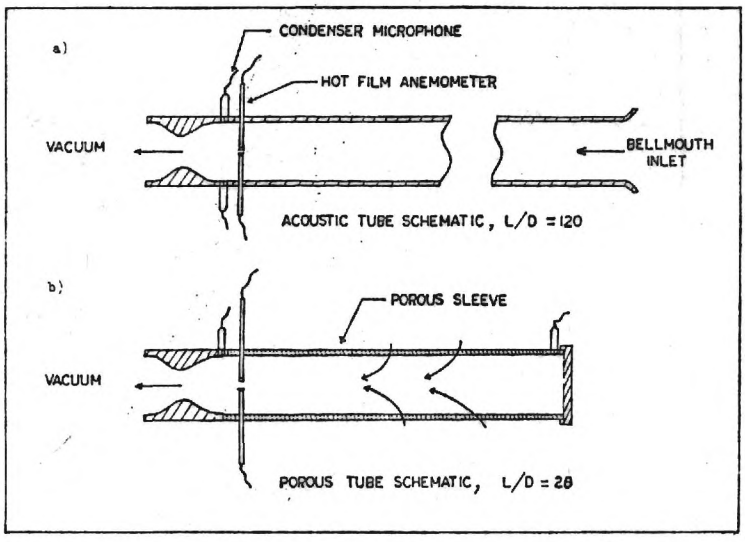

Figure 3. Schematic diagram of the experimental configurations (I).

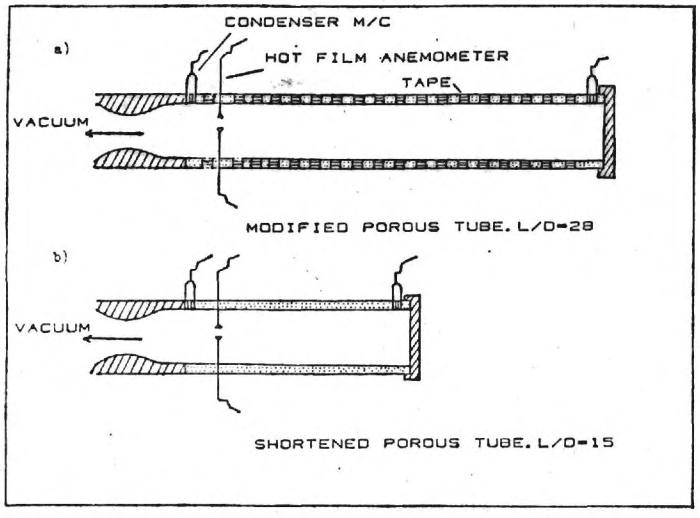

Figure 4. Schematic diagram of the experimental configurations (II).

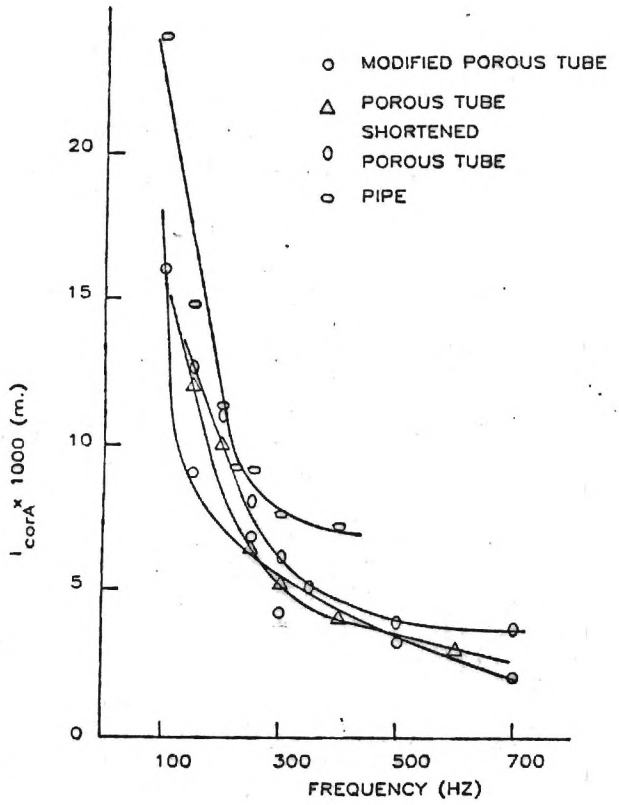

Figure 5. Axial correlation lengths as a function of frequency ($\bar{M}_e$ = 0.1).

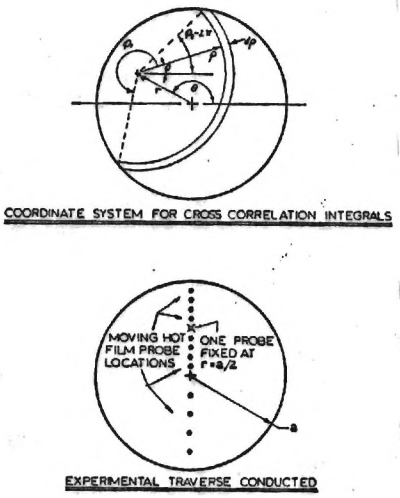

Figure 6. Coordinate system for cross correlation integrals.

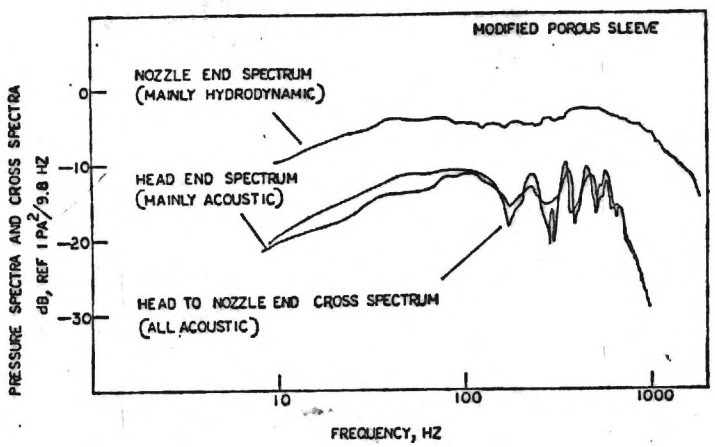

Figure 7. Wall pressure spectra and cross spectra in modified porous tube.

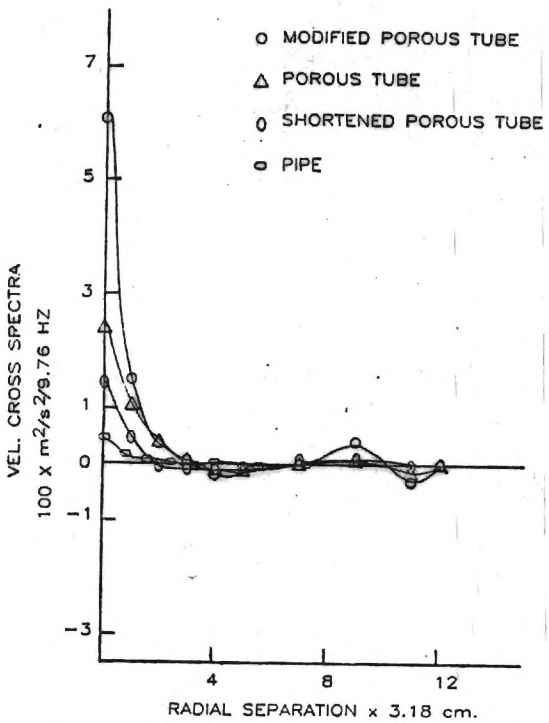

Figure. 8. Cross spectra of axial velocity fluctuations at 100 Hz. with respect to radial separation ($\bar{M}_e$ = 0.1).

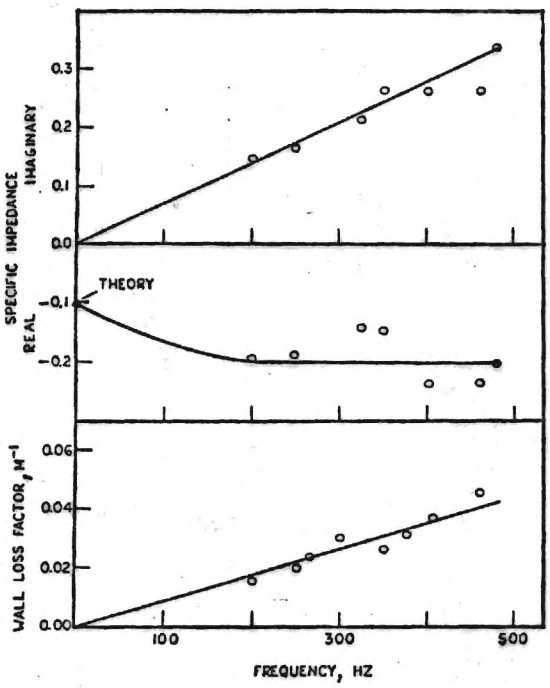

Figure 9. Measured acoustic impedances for the pipe.

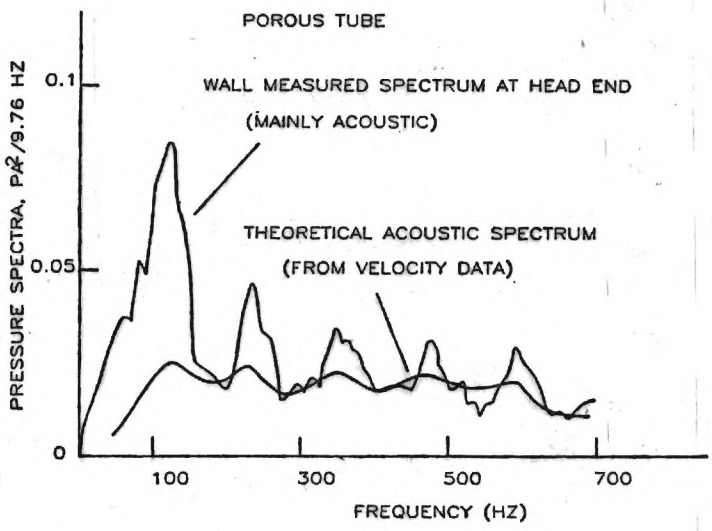

Figure 12. Pressure spectra at head end for basic porous tube.

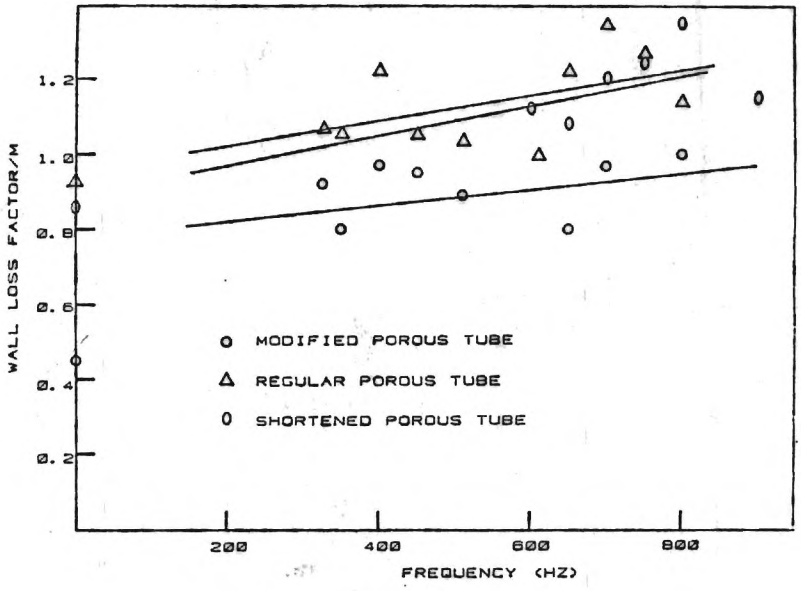

Figure 10. Measured wall loss factors for porous tube configurations ($\bar{M}_e = 0.1$).

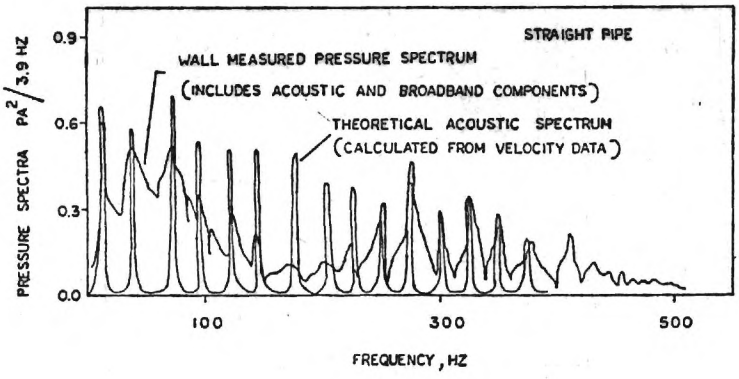

Figure 11. Pressure spectra at nozzle entrance plane for pipe flow.

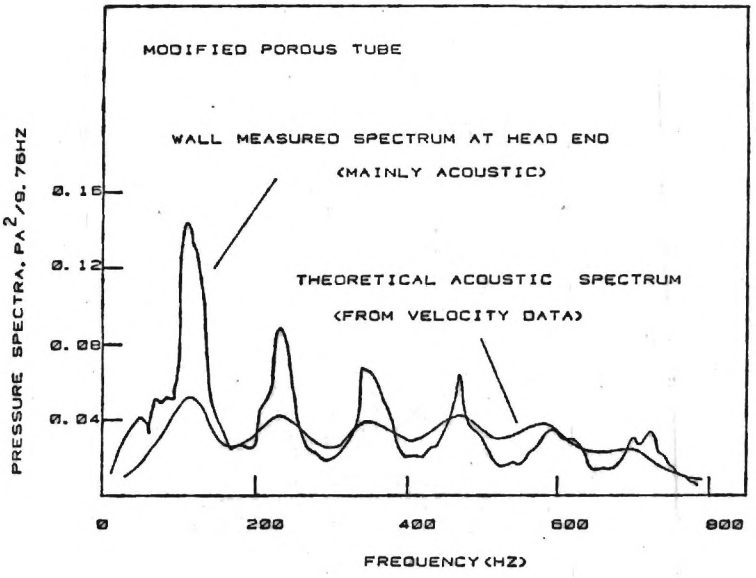

Figure. 13. Pressure spectra at head end for modified porous tube.

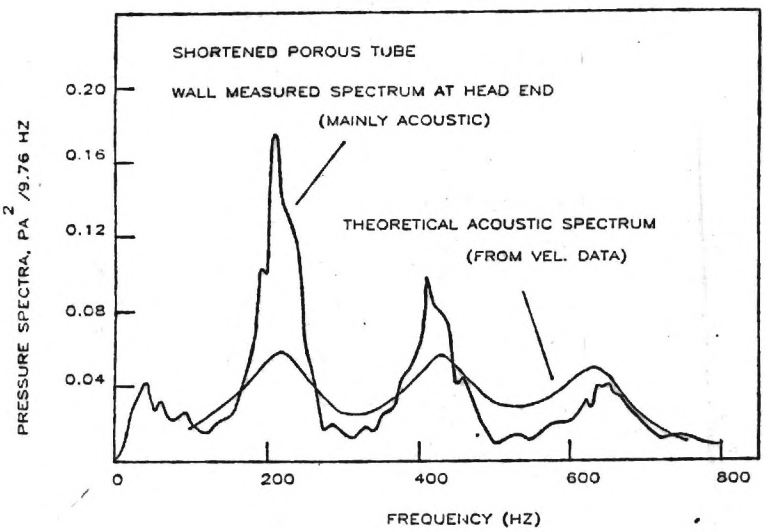

Figure 14. Pressure spectra at head end for shortened porous tube ($\bar{M}_e$ = 0.1).

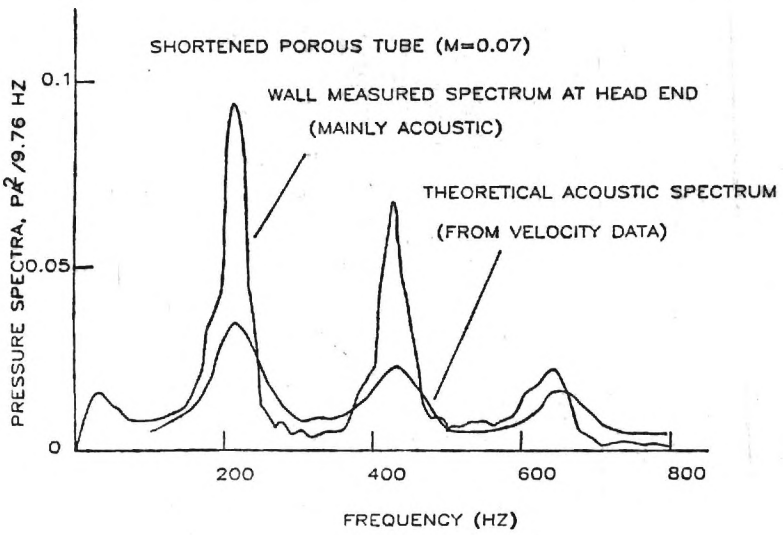

Figure 15. Pressure spectra at head end for shortened porous tube (M_e = 0.07).

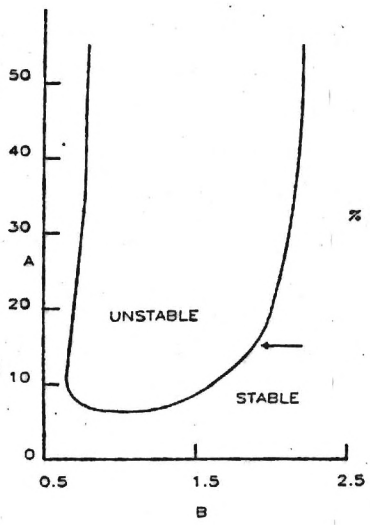

Figure 16. Typical stability limit in terms of the parameters A and B.

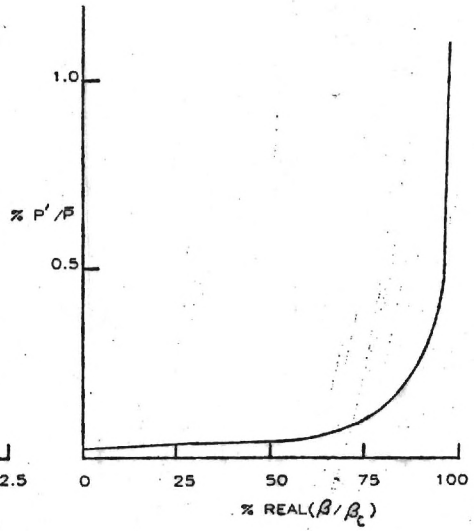

Figure 17. Typical pressure levels as a function of (β/β_{crit}).

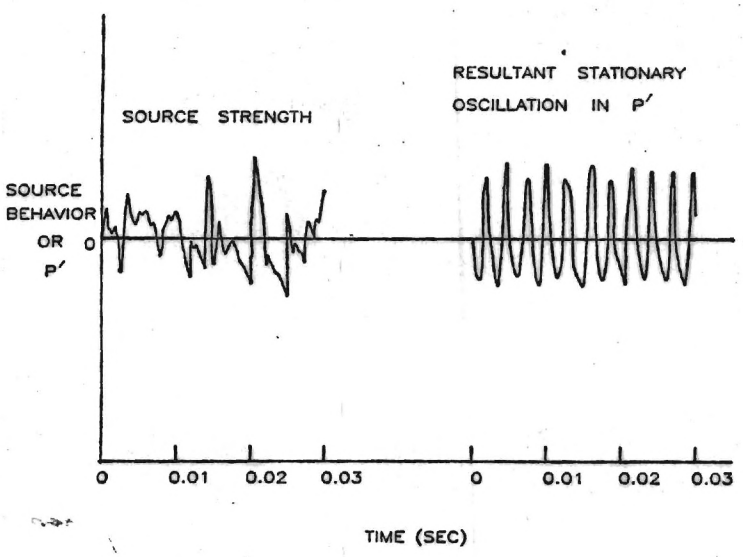

Figure 18. Action of the Green's function g_ω as a filter.

Hegde, U. G. and Strahle, W. C., "Sound Generation by Turbulence in Simulated Rocket Motor Cavities" AIAA Paper No. 84-0287 to be presented at 22nd AIAA Aerospace Sciences Meeting, Reno, NV, Jan. 1984.

Strahle, W. C., "Turbulence Generated Pressure Fluctuations in Some Interior Flows," invited remain at Carnegie-Mellon University, April, 1983.

Strahle, W. C.: Associate Editor for Combustion and Aeroacoustics, AIAA Journal.